A combination of apatite fission track and (U-Th)/He thermochronometers to constrain the escarpment evolution in south eastern Australia: a case study of high elevation passive margins

A thesis submitted for the Degree of

Doctor of Philosophy

At the University of Glasgow

Cristina Persano

Department of Geography and Geomatics,
University of Glasgow
G12 8QQ Glasgow, United Kingdom

September 2003

Mi ci e' voluto un anno per farlo piu' corto

[It took me one year to make it shorter]
(L. Sciascia, Preface to "La civetta"; 1956)

Acknowledgements

Numerous people contributed encouragement, guidance and help during this work.

First of all, I would like to thank my supervisors, Prof. Paul Bishop, Dr. Tim Dempster and Dr. Finlay Stuart, here listed in strictly alphabetical order. During the last years I have appreciated their perceptive understanding, guidance and friendship. I would like to thank them for the opportunity they gave me and for their patience, crucial to the successful completion of this thesis. I would also like to thank all the academic and technical staff in the department of Geography and Geomatics, in the division of Earth Science at the University of Glasgow and at SUERC: thanks for your help and your moral support. Here I want to remember just few of them, who more than others suffered my questions and my continuous requests for help. Dr. Colin Braithwaite, apart from letting me using his cathodoluminesce microscope, lent me a stereoscopic microscope, saving me from picking apatites using a petrographic, non stereoscopic microscope: to him it will go my eternal gratitude. I want to thank Dr. Rob Ellam and Dr. Valerie Olive at SUERC for the use of the ICPMS and for the time they have dedicated to me, trying to reveal the secrets of isotopic dilution and analytical chemistry. Thanks also to Dr. Sorcha Diskin for her help with the analyses and Dr. Dan Barfod for the frequent fruitful discussions. Thanks to Bill Higgison and John Gilleece for their help with the samples preparation and to Kenny Roberts for all the times he helped me with the computer. Thanks are also due to my fellow students: thanks for having encouraged me when I was depressed and convinced I could not make it, and also for all the times you pretended my English was perfectly understandable. In

particular I would like to thank Alison (now Dr. Bowdler-Hicks), Kathy, Liam and Simon.

Prof Andy Gleadow, Dr. Rod Brown, Dr. Barry Kohn and Dr. Asaf Raza provided guidance and supervision during my three months visit at the University of Melbourne, Australia. Vicki-Ann Dimas was a most appreciated field assistance during my second trip to collect samples in eastern Australia. I would like to thank Dr. Finlay Stuart and Dr. Susan Waldron for the collections of some of the samples.

I would like also to thank Dr. Peter van der Beek and Dr. Brian Bell for their constructive comments.

Financial assistance was provided by the University of Glasgow with the award of a post-graduate research scholarship and a MacRobertson scholarship that funded the second of my field trips to Australia.

However, none contributed more to this work than Carlo: his patience, intelligence, sensibility and, not least financial support, made the completion of this thesis possible. To him this work is dedicated.

Statement of authorship

Except where reference is made in the text, this thesis does not contain material published elsewhere or extracted in whole or in part from a thesis presented by me for any other degree or diploma.

No other person's work has been used without clearly quoting the source in the text of the thesis.

This thesis differs substantially from any work that has been, or is being, submitted to any other university for any degree, diploma or any other qualification.

Thesis summary

Escarpments are first order topographical features, which characterise the morphology of high elevation passive margins. Their erosional nature and correlation with continental breakup are well established, but the timing of formation and evolution of the escarpments are still poorly constrained. The unique sensitivity of apatite fission track and apatite (U-Th)/He thermochronometers to temperatures between 120 and 40°C make them ideal techniques to study the cooling history of rock in the shallow crust (less than 5 km).

In this project apatite fission track and (U-Th)/He thermochronometers are used to determine the cooling history of rocks from the coastal (south eastern New South Wales) and the interior (Bathurst area) regions of the eastern Australia high elevation passive margin. Two traverses across the coastal lowlands, escarpment and plateau top are used to determine the tempo and styles of response of the landscape to the continental breakup and sea-floor spreading of the Tasman Sea (85 Ma). The three prevailing models of escarpment evolution, namely retreat into a downwarped rift shoulder, escarpment retreat and excavation in place on a high elevation rift shoulder with flexural rebound are described and tested using a previously untested combination of apatite fission track and (U-Th)/He data. The thermochronological data indicate that the coast was affected by a denudational pulse that peaked around 120-100 Ma and that was extinguished by the time of sea-floor spreading. The rapid denudational event caused the removal of 3-4.5 km (depending on the geothermal gradient) of crust at the coast and of approximately 2 km at the present base of the escarpment. The

thermochronological data are inconsistent with the downwarped rift shoulder model and the apatite (U-Th)/He data indicate that, while the coast was denuded very rapidly, the coastal lowlands were excavated in place at a much lower pace, and the escarpment reached its present position no later than 60 Ma. This suggests that during continental extension and breakup, rates of denudation at the coast were approximately 80-30m/Myr (depending on the geothermal gradient), whereas at the base of the present escarpment they were about 10-5 m/Myr. The period after sea-floor spreading was characterised by stability and low rates of erosion. The pre-breakup topography, reconstructed using the backstacking technique, is characterised by a considerable relief in the area of the present escarpment. This result confirms the hypothesis that the escarpment evolved pinned to its present position.

On the plateau apatite fission track and (U-Th)/He ages are in excess of 200 Ma, either side of the Drainage Divide, suggesting that the area inland of the escarpment was not affected by the continental breakup. However, at the Bathurst area, across the Continental Drainage Divide, ~100 Ma He ages are found. Combined with the existing apatite fission track record, the He data suggest that the Bathurst region has been tectonically active in the Late Mesozoic and possibly in more recent times. However, such tectonic activity may have been a local feature that did not affect the first order, long wavelength topography of the Continental Drainage Divide.

Table of contents

List of figures

List of Tables

CHAPTER ONE

INTRODUCTION

How many years can a mountain exist
Before it's washed to the sea?
Yes, 'n' how many years can some people exist
Before they're allowed to be free?
Yes, 'n' how many times can a man turn his head,
Pretending he just doesn't see?
The answer, my friend, is blowin' in the wind,
the answer is blowin' in the wind.
(Bob Dylan, 1963)

1.1 Introduction

Geomorphology is a historical science, which studies in the origin and evolution of landforms. Attention is focused on causes, effects and time over which the processes that control the landscape act. The interest in geomorphology of the Earth's surface goes back to the "natural philosophers" like Leonardo da Vinci (possibly the first to deny the theory of the Genesis Flood) and Charles Darwin, amongst others. Hutton (1726-1797) argued that currently active surface processes, i.e. denudation, were responsible for shaping the Earth's surface throughout geological time. He found no reason to invoke catastrophes (rapid, large, or unusual events) to explain what he observed in the rock record. This interpretation required that Earth history must have been "immense with no vestige of a beginning and no prospect of an end" (Hutton, 1788; p.212). Lyell (1797-1875) fleshed out an extreme version of Hutton's views known as uniformitarianism, according to which most geological processes act slowly and constantly over long time scales (Lyell, 1830). The issue of time became fundamental. The suggestion of Darwin that the Earth was at least 300 Myr old

particularly captivated these "geomorphologists", although they had to face the severe criticisms of physicists like Lord Kelvin, who, having based their theories upon mathematical calculations, were perceived as more credible (Darwin, 1859; Kelvin, 1862).

With the discovery of radioactivity at the beginning of the 20th century and the subsequent development of radiometric dating methods (see Chapter 2), the disagreement about the age of the Earth, which had characterised the previous fifty years, was soon replaced by the consensus that exists today. However, although geological processes now had all the time they needed to shape the Earth's surface, there was little agreement about how the landscape had evolved. When in the 1960s the theory of plate tectonic was first proposed, "it seemed to have all the answers" (Ollier, 1985; p.2). Plate tectonics could account for the formation of the primary topographic features of the Earth's surface, such as the division between continents and oceans, the locations of mountain belts and ocean ridges (Seyfert & Sirkit, 1973). With the maturing of the concept of plate tectonics, attention turned to the mesoscale features and to issues such as the detailed tectonic and geomorphic evolution of plate boundaries and the feedback effects of denudation and sedimentation on the primary tectonic processes at these boundaries (e.g. England & Molnar, 1990). A special publication on tectonics and topography of the Journal of Geophysical Research (1994) distilled thirty years of studies in this field and represents the base upon which long term landscape evolution studies have been built. The development and incorporation of new tools, such as 3-D numerical process models (e.g. van der Beek *et al.*, 2002), sensitive low temperature thermochronology (e.g. Kohn *et al.*, 2002; Persano *et al.*, 2002) and cosmogenic isotope

studies (e.g. Cockburn *et al.*, 2000) is now providing the possibility of constraining landform evolution at a regional to continental scale.

The study presented here aims to generate new, empirical data with which to test the new ideas resulting from modelling studies of passive margins evolution, and ultimately to provide a better understanding of tempos and styles of landscape evolution (e.g. Kooi & Beaumont, 1994; Beaumont *et al.*, 2000, van der Beek *et al.*, 2002). In particular, this research is focused on reconstructing the syn- and post-breakup history of high elevation passive margins, taking eastern Australia as a case study. A combination of apatite fission track and apatite (U-Th)/He thermochronometers is used to quantify the denudation of the margin and, in particular, to determine the evolution of first order topographical features such as the escarpments that typify high elevation passive margins. The sensitivity of these two radiometric systems to low temperatures (<120°C and <80°C, respectively; Chapter 2) provides the ability to constrain the small amounts and rates of denudation that are characteristic of passive margins and to test predictions made by numerical models.

The rest of this chapter (i) describes the geomorphological characteristics of high elevation passive margins and describes the role of plate tectonics in their generation; (ii) describes the existing models of landscape development at passive margins and outlines the difficulties experienced in integrating the classical theories of landscape evolution with empirical data, especially in eastern Australia (e.g. Bishop, 1988); (iii) introduces the study area and the observations used to constrain the chronology of denudation in the region.

The analytical aspects of apatite fission track and (U-Th)/He thermochronology are described in Chapter 2, along with an explanation of how low temperature thermochronological data are applied and interpreted. Chapters 3 and 4 describe and interpret new apatite fission track (Chapter 3) and (U-Th)/He (Chapter 4) data from the south eastern Australian continental margin. The results are compared with numerical models to identify the syn- and post-breakup evolution of the landscape and, in particular, to determine the rates and modes of escarpment development. Chapter 5 is a detailed study of the Bathurst region, in the interior of the eastern Australian highlands, in order to determine the evolutionary history of this part of the plateau. The key aim of Chapter 5 is to investigate the role of local scale geological and geomorphological features to constrain the evolution of long-wavelength, first order topography. In Chapter 6 the relationship between the various tectonic and geomorphic processes that have contributed to forming the present eastern Australia landscape is discussed and some speculations on a general scenario of landscape evolution common to all high elevation passive margins are presented.

1.2 The high elevation passive margins

Passive margins are first order structures that develop during continental breakup, rifting and ocean basin formation. The breakup of Pangea generated many of the high elevation oceanic margins observed today (Figure 1.1) and the palaeomagnetic record from the ocean floor has constrained the timing of most of these riftings (McElhinny, 1973). Passive margins exhibit a wide range of morphologies, but they can be broadly distinguished as either high elevation or low elevation margins (Gilchrist & Summerfield, 1990). High elevation passive margins are characterised by the presence

of an escarpment, a macro-geomorphological feature that abruptly divides a low relief upland plateau from low altitude coastal plain. Well-studied examples include eastern Brazil (Gallagher *et al.*, 1995), the Red Sea (Steckler & Omar, 1994), southern Africa (King, 1950), western India (Gunnell & Fleitout, 1998) and eastern Australia (Ollier, 1982). The escarpments are characteristically over 1 km in elevation and are commonly between 60 and 200 km inland of the continent-ocean boundary. The erosional nature of these escarpments and their correlation with continental breakup are now well established (King, 1950; Ollier, 1982), but the interaction between tectonic and denudational processes and the feedback effects that the two processes can cause are poorly constrained (Gilchrist & Summerfield, 1990; Gilchrist & Summerfield, 1994; Pazzaglia & Gardner, 1994; Ollier & Pain, 1994; Seidl *et al.*, 1996; Ollier & Pain, 1997).

Conceptual models of passive margins evolution date back to the early 20th century when Suess (1904) identified the escarpment of southern Africa as a denudational feature, unrelated to faulting. King (1950) embraced the theory of continental drift and was the first to suggest an origin for the series of scarps he observed across the southern African margin, as escarpment retreat coupled with denudational isostatic rebound to account for the evolution of the coastal plain (King, 1955; Pugh, 1955). Ollier (1982) proposed that the escarpment in eastern Australia was related to continental breakup, suggesting that it retreated inland from the new continental edge. Although these models are historically very important, they are all qualitative, as they lacked a way to quantify the processes responsible for escarpment formation and evolution. Apatite fission track analysis was the first low temperature thermochronometer to provide quantitative constraints on amount and rates of denudation. In the early 1980s, the first

studies in eastern Australia (Morley *et al.*, 1981) and the Red Sea (Kohn & Eyal, 1981) showed that apatite fission track ages along the present coastline are usually the same as, or younger than, the age of the onset of sea-floor spreading. These studies also demonstrated that the ages become progressively older inland toward the escarpment and onto the high elevation plateau. The fission track ages indicate several km of post-breakup denudation at the present coastline, whereas the plateau was essentially unaffected by the opening of the new ocean. This continental-scale pattern has been confirmed in all high elevation passive margins (Moore *et al.*, 1986; Brown *et al.*, 1990; Gallagher *et al.*, 1995; Gunnell & Fleitout, 1998; Abbate et al., 2002). Locally, however, fission track studies have shown that plateau regions can have undergone significant amounts of syn-rift denudation (e.g. Dumitru *et al.*, 1991; O'Sullivan *et al.*, 1995; Kohn *et al.*, 2002), whereas the coastal plain may have endured little denudation (Moore *et al.*, 1986). Fission tracks in apatite record the time and amount of cooling (e.g. Brown *et al.*, 1994), but the extent to which this cooling is a reflection of uplift-driven denudation remains a matter of debate and the notion that increased denudation may occur without significant uplift is now being considered (van der Beek, 2002).

Despite the abundant literature discussed above about high elevation passive margins, key aspects of their evolution remain poorly constrained and several fundamental questions about origin and development of the escarpment are still open (Kooi & Beaumont, 1994).

For instance, the kilometric-scale denudation suggested by the fission track data is inconsistent with passive margin formation by the *downwarped rift shoulder model* (e.g. Ollier & Pain, 1997). This model predicts minimum erosion at the present coastline (up to 500 m) and constant escarpment retreat rates of the order of 1-2 km/Myr (Ollier,

1982; Seidl *et al.*, 1996). The processes responsible for the erosion, and in particular, the escarpment evolution still remain to be clarified. Numerical models have suggested that the pre-rift topography exerts a fundamental control on the evolution of the margin. "If the initial topography is a horizontal plateau, the margins evolve through escarpment retreat; if the pre-rift topography included an inland drainage divide, the initial plateau seaward of this divide will be rapidly degraded and a new escarpment develops at the location of the initial divide" (van der Beek, 2002; p.7). 3-D numerical models predict that the two mechanisms, usually referred as *escarpment retreat* and *excavation in place*, produce different rates of denudation across the newly formed coastal plain (van der Beek *et al.*, 2002). In the case of escarpment retreat, rates of denudation will exceed 1 km/Myr in the first 10 Myr after breakup and then rapidly decrease by at least an order of magnitude, as the wave of denudation migrates toward the interior of the continent. Conversely, in the excavation-in-place scenario, syn-rift rates of denudation may only exceed a few hundreds metres per Myr and then rapidly decay to the present low values (10-5 m/Myr) soon after breakup (van der Beek *et al.*, 2002).

These numerical models highlight the importance of precisely constraining amounts and rates of denudation taking in consideration their spatial and temporal variations and, as it will be shown for the south eastern Australian passive margin, this task can be achieved by combining apatite fission track and (U-Th)/He data.

This project aims to address two fundamental issues:

(i) constraining the amount and rate of syn- and post-breakup erosion at a typical high elevation passive margin, with the ultimate aim of determining the tectonic mechanisms driving denudation, and

(ii) determining the styles of escarpment formation and evolution.

1.3 The south eastern Australian passive margin

The east Australian high elevation passive margin is over 3000 km long (Figure 1.2) and in the southern part is characterised by an undulating upland plateau surface – the South Eastern Highlands – that is separated from a low relief lowland coastal zone by a steep escarpment or, in places, a broad escarpment zone (Ollier, 1982). The Highlands take two general forms: north of approximately 18°S and south of 26°S they consist of a broad asymmetrical arch that rises gradually from the inland sedimentary basins in the west to the area of the Continental Drainage Divide (CDD; Bishop, 1988). The highlands in the intervening parts are more symmetrical, their crest is up to 400 km from the continental margin and the continental shelf is wider. The elevation of the highlands either side of the CDD is generally less than 1 km in Queensland and less than 2 km elsewhere, except in the New South Wales and Victorian Alps. The contours of Figure 1.2 highlight the fact the highlands are not a topographic continuum but are characterised by alternating higher regions separated by lower saddles (Bishop, 1988). In New South Wales, the greatest elevations are on areas of Palaeozoic rocks, whereas the Permian-Triassic Sydney Basin constitutes an area of generally low altitude, with the exception of the Blue Mountains region.

The greatest relief always corresponds to the escarpment. Its abrupt edge is obvious on a topographic map and, at first order approximation, it can be followed along the entire margin from the contour maps (Figure 1.2). At a more local scale the escarpment has gaps in areas where the scarp cannot be drawn with confidence such as in the region

inland of Sydney (Ollier, 1982), (Figure 1.2). The escarpment always lies seaward of the CDD; in some places they are separated by hundreds of kilometres, elsewhere by only 15 km (Ollier, 1982). This contrasts with all other high elevation passive margins (eastern Brazil, south Africa, the Red Sea and western India) where the escarpment corresponds to the CDD (Figure 1.3). For this reason the eastern Australian margin is often not incorporated into the numerical models of passive margin formation and escarpment evolution (e.g. Kooi & Beaumont, 1994).

The eastern Australian margin formed during Cretaceous continental extension, rifting and formation of the Tasman Sea (sea-floor spreading 85-62 Ma; Weissel & Hayes, 1977). According to one hypothesis, espressed by Ollier & Pain (1997), "the continental margin is basically a former land surface – the palaeoplain – which has been warped, producing the basal unconformity offshore where is it down-warped, and the marginal swell where it is upwarped" (p.2). High altitude (up to 500 m) surfaces that are present across the coastal plain are considered to be remnants of the palaeoplain (e.g. Seidl *et al.*, 1996). The presence of palaeosols dating from Late Mesozoic times (Bird & Chivas, 1993) is also taken as evidence that the coastal plain experienced little syn- and post-breakup denudation (Ollier & Pain, 1994). The issue of the downwarped palaeoplain is considered again in Chapter 3 and 4.

The minimum age of the escarpment in south eastern Australia can be established locally by its relationship with basalts found above, below or on the escarpment. In southern New South Wales, Oligocene basalts on the coastal plain near Ulladulla (Figure 3.2) are considered to be an indication that, at least at that locality, escarpment erosion predated lava extrusion (Young & McDougall, 1985). These basalts constrain

maximum Neogene escarpment retreat rates to 150 m/Myr (Nott *et al.*, 1996), an order of magnitude lower than the escarpment retreat rates calculated from the age of breakup and the distance of the major escarpment-forming knickpoints inland of the continental edge (2 km/Myr, Seidl *et al.*, 1996; 1km/Myr, Weissel & Seidl, 1998).

The minimum amount of erosion of the coastal plain predicted by the downwarped rift shoulder model contrasts with the interpretation of the apatite fission track data (Kohn *et al.*, 2002). The youngest fission track ages on the south eastern Australian margin are between 70 and 100 Ma and usually occur no more than a few km inland of the present coastline (e.g. Moore *et al.*, 1986). These late Mesozoic ages and their long mean track lengths are consistent with the removal of 3-4 km (depending on the palaeogeothermal gradient) of crustal section during breakup (Dimitru *et al.*, 1991).

The obvious controversy between the erosional history defined by the fission track data and the downwarped rift shoulder scenario may be resolvable using new information. For example, a combination of apatite fission track and cosmogenic isotope exposure chronology study of the Namibian sector of the southwest African margin has demonstrated that post-breakup denudation rates have been temporally variable (Cockburn *et al.*, 2000). Fission track data reveal an initial phase of rapid denudation rates of the order of 40 m/Myr, with escarpment retreat rates of about 1 km/Myr, between 130 and 36 Ma. Cosmogenic isotope analyses indicate that recent erosion rates have been only about 5 m/Myr and the retreat rates about 10m/Myr. Consequently the simple model of constant escarpment retreat across the coastal plain can be ruled out. A compilation of denudation rates of the eastern Australian margin using different methods is presented in Figure 1.4. The different methods span different time scales

and their results are difficult to integrate. The combination of apatite fission track and cosmogenic isotopes techniques used in southern Africa presents a similar problem, as the two methods are sensitive to different time scales (10^6-10^8 Myr versus <5 Myr) and crustal depths (2-5 km versus 1-2 m). Apatite (U-Th)/He thermochronology is effective at the same time scale as fission track and is sensitive to 80 to 40°C (crustal depths of 1-3 km). This thermal range partly overlaps the range at which fission tracks are annealed in apatite (section 2.2) and consequently combining the two techniques has the potential to provide better quantitative constraints on the processes that determine the formation and evolution of major topographical features.

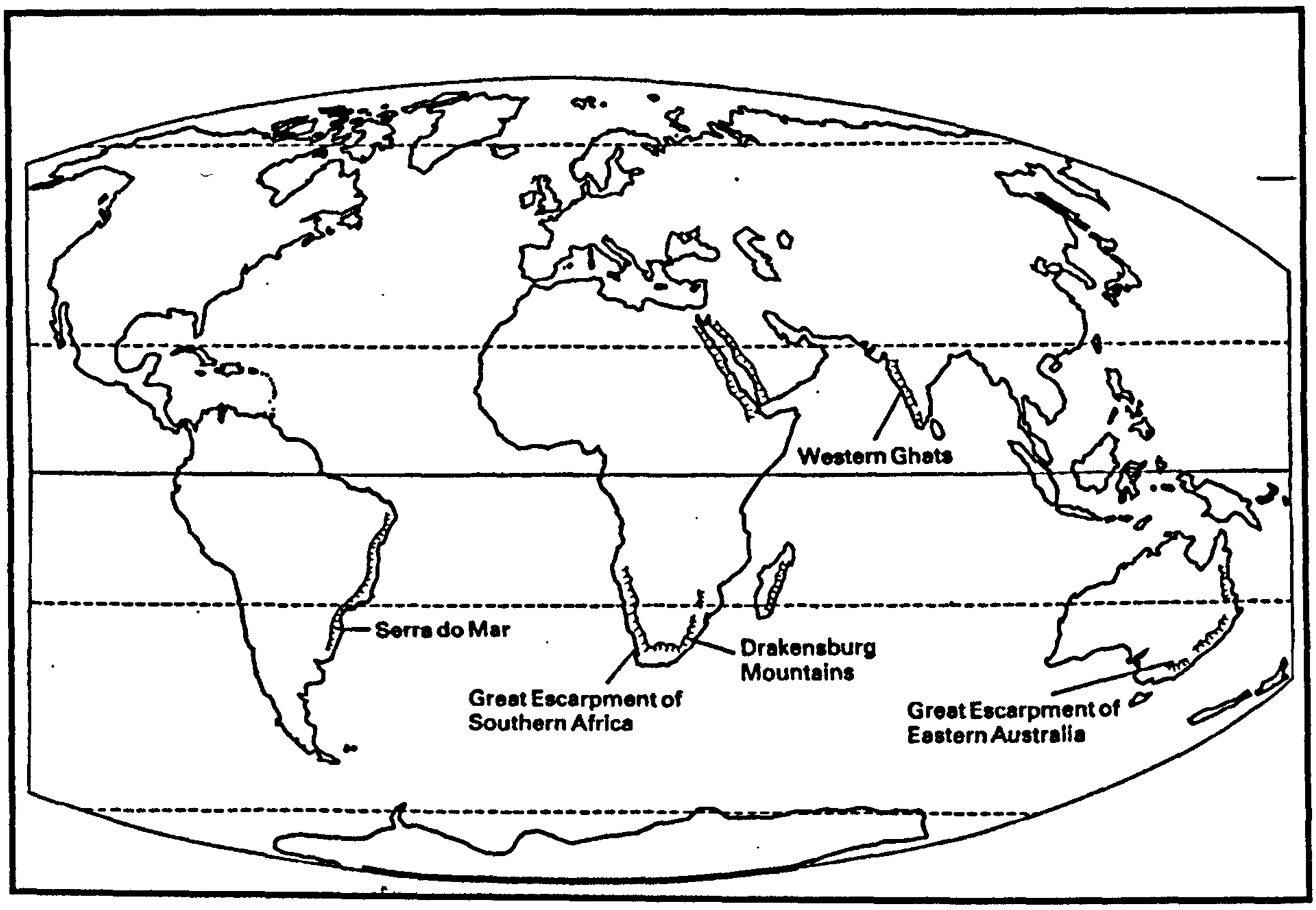

Figure 1.1: High elevation passive margins around the world. Escarpments are shown running parallel to the margin defining a narrow coastal plain (from Summerfield, 1990)

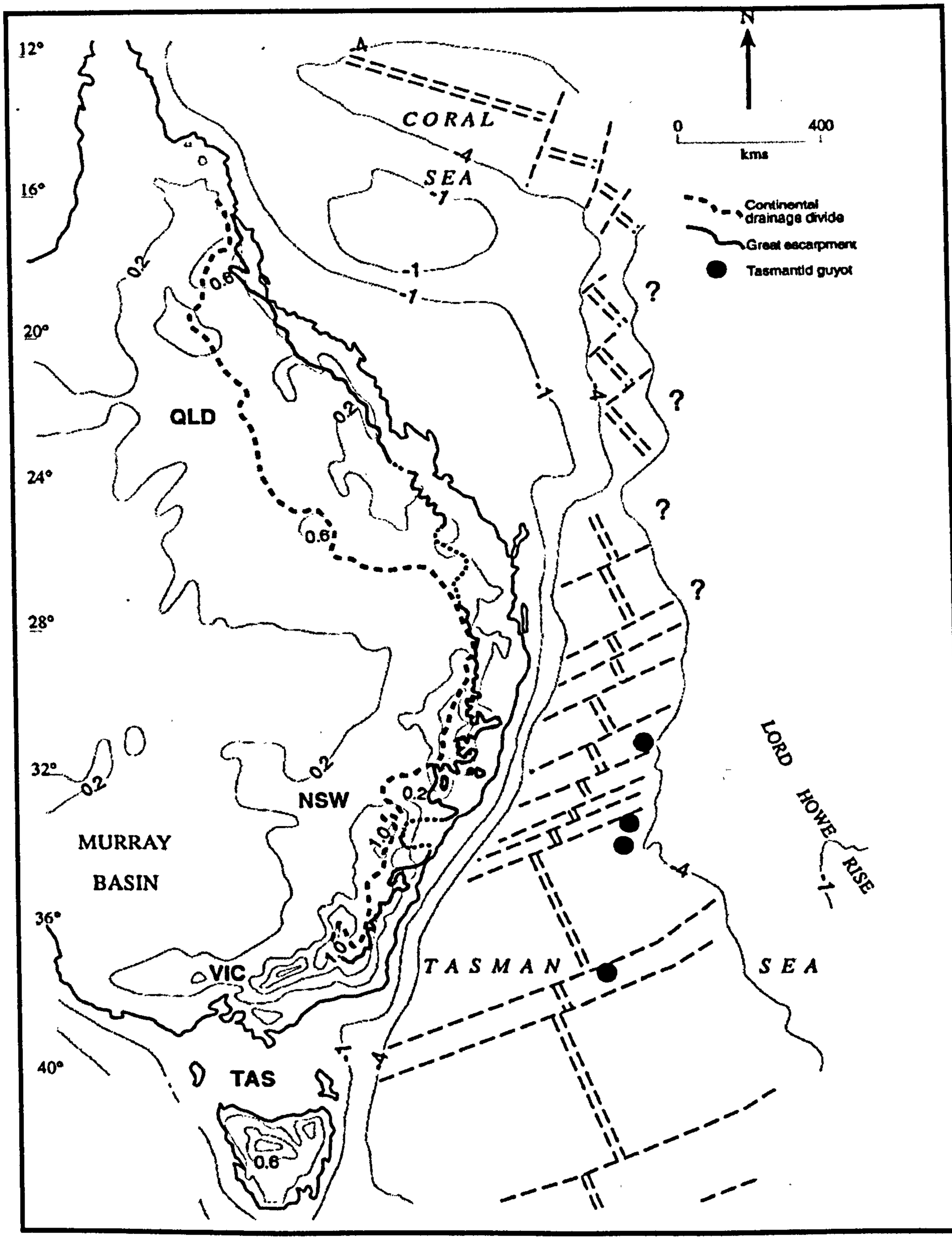

Figure 1.2: Map of eastern Australia showing the Continental Drainage Divide (thick dashed line) and the escarpment (thick line) (from Ollier, 1982). The sea-floor spreading ridges and transform faults are also shown, along with four guyots in the Tasman Sea (from Bishop & Goldrick, 2000).

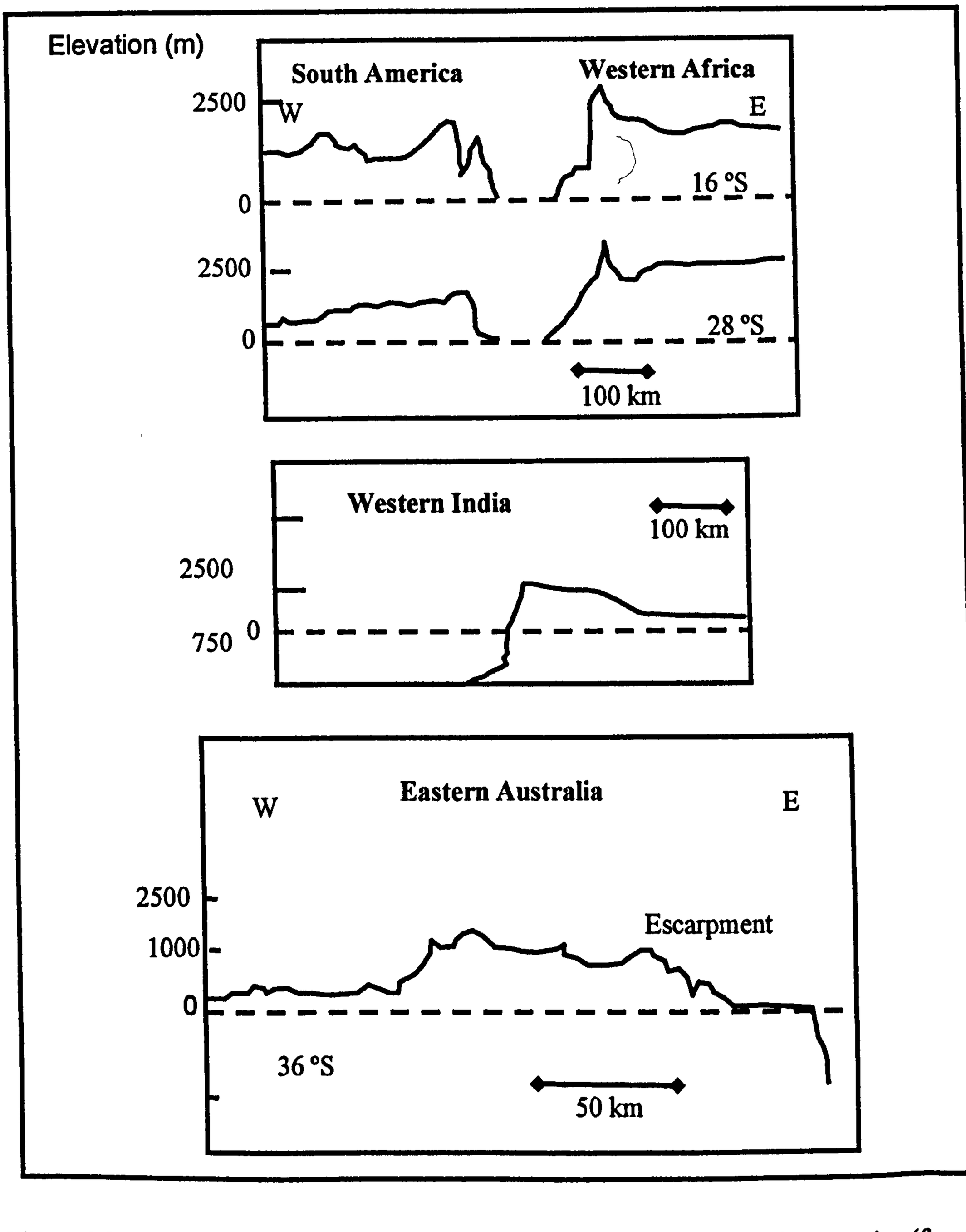

Figure 1.3: Topographic profiles across some of the high elevation passive margins (from Gilchrist & Summerfield, 1994; Gunnell & Fleitout, 2000). In eastern Australia the escarpment does not coincide with the Continental Drainage Divide, as happens in all the other case (see text for discussion).

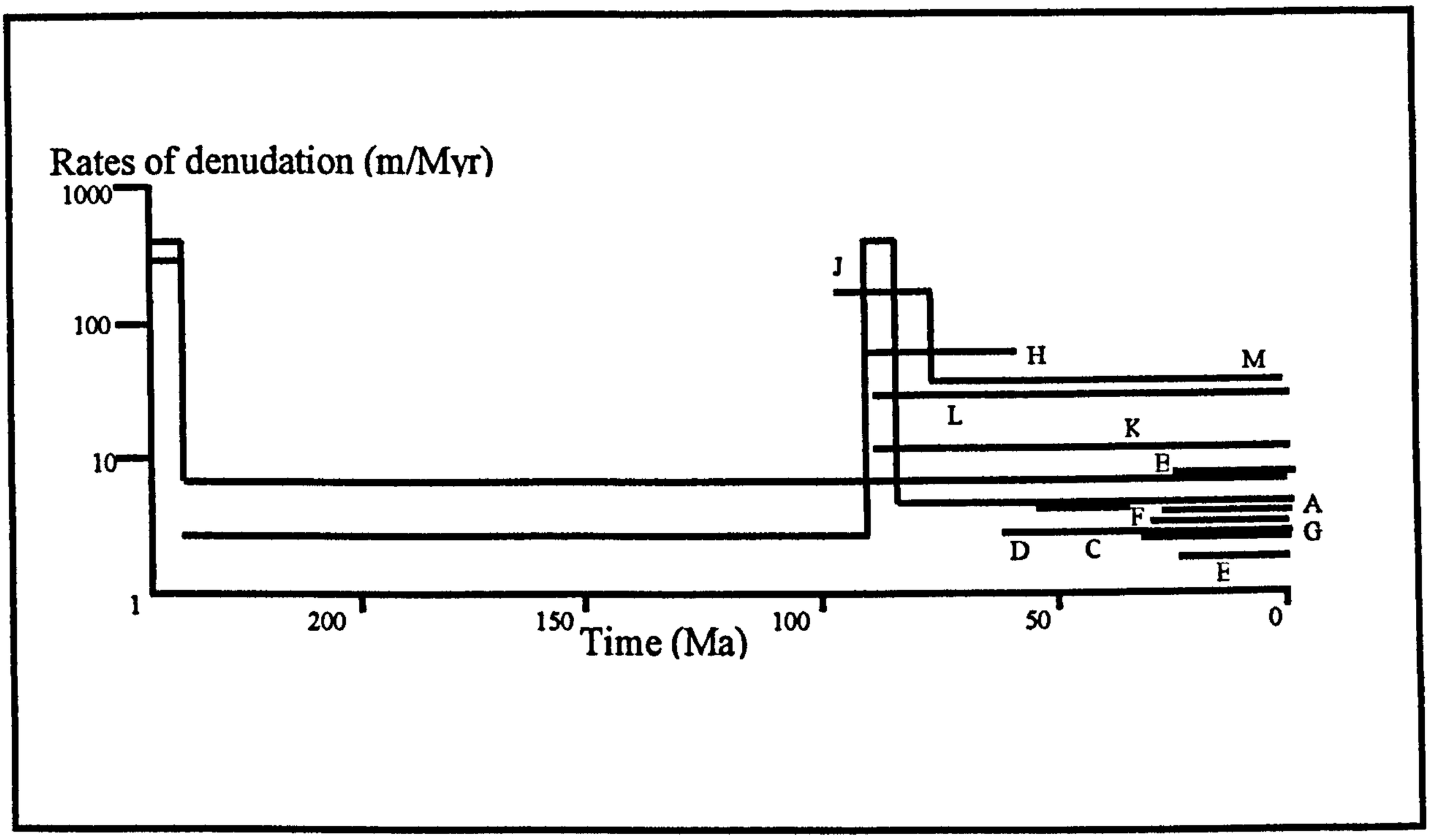

Figure 1.4: Rates of denudation and river incision in eastern Australia. A, B, C, D and E represent Cenozoic rates of river incision derived from the ages of basalt lava flows. F, G and H represent rates of denudation derived from basin sedimentation. I, J, K, L and M represent rates of denudation derived from apatite fission track analyses (from Bishop & Goldrick, 2000).

CHAPTER TWO

LOW TEMPERATURE THERMOCHRONOLOGY: THEORY AND APPLICATIONS

Indeed, it appears probable that it [the He system] will prove one of the most reliable methods of determining the age of the various geological formations

(Rutherford, 1906)

2.1 Introduction

In 1969 Clarke and Jäger published the first attempt to reconstruct rates of denudation using geochronological data (Clarke & Jäger, 1969). These estimates were derived by correlating the closure temperatures of several radiometric dating schemes (Dodson, 1973) to specific crustal depths, using an estimated palaeogeothermal gradient (Clarke & Jäger, 1969). The closure temperature common for most mineral geochronometers is greater than 200°C, thereby restricting the usefulness of these methods to orogenic settings characterised by high rates of denudation that have brought rock to the surface from significant depth (usually greater than 5 km). Apatite fission track and apatite (U-Th)/He are sensitive to temperatures of less than 120°C and they have the potential for estimating rates and amount of rock denudation to many geomorphological problems. In the next sections the theoretical and technical aspects that are important for their application to the evolution of rifted margins are introduced.

2.2 Apatite fission track thermochronology

Although the fission track method has been applied widely in the last three decades (e.g. Wagner, 1968; Naeser, 1979; Gleadow, 1981; Green *et al.* 1989), Baumhauer first identified anomalous etched pits on apatite crystals in 1894 (Baumhauer, 1894). The difficulty of observing the pits on the surface of crystals remained until the chemical etching method was implemented (Young, 1958). Fleischer *et al.* (1975) described the detection, observation and interpretation of nuclear tracks in solids. Since then, the fission track technique has been applied as a dating tool in many fields including archaeology, nuclear physics, extraterrestrial physics and biology (e.g. Bellot-Gurlet *et al.*, 1999; Ciubotariu, 2001; Li *et al.*, 2001; Perelygin *et al.*, 2003; for a review of earlier works: Wagner & van der Haute, 1992). The sensitivity of track annealing in apatite to 60° to 120°C has resulted in the development of apatite fission track thermochronology (AFTT), which is widely used in geomorphology to constrain the cooling history of rock masses in the shallow crust (less than 5 km).

2.2.1 Formation of fission tracks

Spontaneous fission of ^{238}U produces two positively charged nuclei of approximately equal mass, which are propelled in opposite directions away from the site of fission. As they move through the mineral, the two nuclei damage the crystal structure, removing electrons from within the mineral atoms that become positively charged, repelling each other. A disrupted track is formed in the crystal (Fleischer *et al.*, 1975). When chemically etched, the fission tracks appear as randomly oriented tubes, about 0.5 μm wide and 16-17 μm long in apatite (Figure 2.1). Although FTT considers only the

fission tracks left by the fission of ^{238}U, other elements such as ^{235}U and ^{232} Th may be present in at least ppb levels and produce similar effects in the mineral lattice. For instance, ^{235}U, which always represents approximately 0.7% of the total natural uranium in apatite, may be artificially induced to fission by bombardment with thermal neutrons (Hurford & Green, 1982). However, fission of ^{232}Th and ^{238}U is not induced by thermal neutrons and this characteristic is exploited to obtain the quantity of U present in the sample in order to calculate its fission track age (see below). The contribution of ^{232}Th to the spontaneous fission tracks observed in a crystal is negligible as the decay constant is $\sim 2 \times 10^{-21}$ y^{-1} (Wieler & Eikenberg, 1998), approximately four order of magnitude lower than the ^{238}U (Hurford & Green, 1983).

In summary, the number of fission tracks in a mineral is proportional to the U concentration, the rate at which the atoms of U undergo fission and the time since mineral cooled below the temperature at which fission tracks are preserved. Fission track are annealed (repaired) with increasing temperature (Fleischer *et al.*, 1965). The probability that a randomly oriented fission track intersects a randomly cut crystal surface on which the tracks are counted is dependent on the length of the etchable portion of the fission track. The temperature controlled shortening of fission tracks in mineral is exploited as a chronometer of the thermal history of rock masses (Wagner, 1972)

2.2.2 Thermal annealing of the fission tracks

Fission tracks in a mineral lattice are gradually annealed with time, according to a rate that primarily depends on the temperature and the chemical composition of the mineral.

Laboratory experiments (e.g. Laslett *et al.*, 1987; Donelick *et al.*, 1990; Crowley *et al.*, 1991) and data from boreholes where temperature had been independently measured (e.g. Gleadow & Duddy, 1981; Hammerschmidt *et al.*, 1984) have been used to understand the kinetics of the annealing process. These studies show that over geological time scales fission track annealing at temperatures greater than 120°C is so efficient that fission tracks are repaired as soon as they are formed. Track annealing occur by track shortening and becomes measurable outside the uncertainties of the method above approximately 60°C for a holding time of 10^6-10^8 years (Donelick *et al.*, 1990). The temperature range over which annealing occurs is called the Partial Annealing Zone (PAZ) (Gleadow & Fitzgerald, 1987). The rate of annealing does not vary linearly with temperature and holding time, and complex mathematical models have been developed to predict fission track annealing rates for different time-temperatures paths (Laslett *et al.*, 1987; Crowley *et al.*, 1991; Ketcham *et al.*, 1999). Differences amongst these models include the procedure used to etch the crystals and the rate at which annealing is considered to occur at a given temperature range, but perhaps the major factor influencing rates of annealing, is the apatite chemical composition. Laboratory experiments have demonstrated that Fluorine-rich apatites are characterised by higher rates of annealing than Chlorine-rich apatites (Brown *et al.*, 1994). Many annealing models (e.g. Laslett *et al.*, 1987; Crowley *et al.*, 1991) assume that apatites have a composition similar to Durango apatite (a F-rich apatite, chosen as a standard mineral (Young *et al.*, 1969). As F-rich apatites are compositionally the most abundant in magmatic and many metamorphic rocks, the simplification introduced by these models produces results that are qualitatively acceptable. However, Ketcham *et al.* (1999) have proposed a formulation that takes account of the compositional control

on annealing behaviour using constraints from laboratory experiments and boreholes samples (Green *et al.*, 1989). The dependence of the annealing process upon chemical composition is complex, with parameters such as cation substitution of Ca for rare earth elements (REE), abundance of U and Th and radiation damage being possible controls of the kinetics of annealing (Ketcham *et al.*, 1999). The effect of all these parameters on the annealing process is considered by measuring the maximum diameter of the etch pits parallel to the crystallographic *c*-axis – the Dpar - on the polished surface of the sample (Donelick, 1993). Laboratory experiments and data from geological samples suggest that when etching conditions are tightly controlled the Dpar is a reliable indicator of the annealing process in apatites (Ketcham *et al.*, 1999).

2.2.3 Apatite fission track ages

The total production of spontaneous fission tracks (F_s) per unit of volume is:

$$F_S = \frac{\lambda_{fission}}{\lambda} {}^{238}U\left(e^{\lambda t} - 1\right) \qquad 2.1$$

where λ is the total decay constant (1.552×10^{-10} y^{-1}; Hurford & Green, 1983), $\lambda_{fission}$ is the fission decay constant (about 7×10^{-17} y^{-1}; Hurford & Green, 1983) and t is the age.

After polishing and etching a surface of the apatite sample (see Appendix 2), a proportion (q) of the total tracks is visible at the surface. Therefore, the counted spontaneous fission track density (ρ_s) is:

$$\rho_s = qF_s = \frac{\lambda_{fission}}{\lambda} {}^{238}U\left(e^{\lambda t} - 1\right) \qquad 2.2$$

ρ_s can be directly counted on the mineral section and the amount of ^{238}U can be deduced using the "external detector method" (Hurford & Green, 1982). In this technique a mica with no (or only ppb levels) of U concentration is placed over the apatite grain mount (see Appendix 2) and subjected to irradiation with thermal neutrons. Fission tracks are induced throughout the apatite crystals and those within 12 μm of the surface may leave the crystal and penetrate the mica. After irradiation, the mica is etched and the induced fission tracks (ρ_i) are counted. The amount of ^{235}U in the apatite is calculated as follows:

$$\rho_i = q^{235}U\phi\sigma \qquad 2.3$$

where ϕ is the thermal neutron flux per unit volume and σ is the cross-section of ^{235}U for induced fission. Equations 2.2 and 2.3 can be combined:

$$\frac{\rho_s}{\rho_i} = \frac{\lambda_{fission}}{\lambda\phi\sigma Ig}(e^{\lambda t} - 1) \qquad 2.4$$

where I is the $^{235}U/^{238}U$ (1/137.8), g is a geometry factor that takes into account the fact that the spontaneous tracks were also produced by ^{238}U atoms that were in the apatite crystal that had been polished away, whereas the induced tracks are only produced by the ^{235}U atoms in the section of the apatite crystal left after polishing. Equation 2.4 can be rearranged to calculate t (Price & Walker, 1963):

$$t = \frac{1}{\lambda}\ln\left(1 + \frac{\lambda\phi\sigma Ig\rho_s}{\rho_i\lambda_{fission}}\right) \qquad 2.5$$

ϕ and σ can be calibrated using metal activation monitors of Au, Co or Cu. These types of flux monitors, however, can react differently to geological materials and therefore, a standard material, usually a silicate glass with a known U concentration, is placed in the reactor alongside the sample (Hurford & Green, 1982). After irradiation, the tracks induced by fission on a mica attached to the glass standard are counted (ρ_D).

Using a standard glass, the amount of ^{238}U of the sample can be calculated as follows (e.g. Duddy & Kelly, 1999):

$$^{235}U_{sample} = \frac{\rho_t {}^{235}U_{glass}}{\rho_D} \qquad 2.6$$

Using 2.6, equation 2.5 can be rearranged to solve for *t*:

$$t = \frac{1}{\lambda}\ln(1+\frac{\lambda Ig\rho_D\rho_s}{\rho_i\lambda_{fission}}) \qquad 2.7$$

However, the uncertainty of the $\lambda_{fission}$ value remains (Bigazzi, 1981). To eliminate the fission decay constant term, Hurford and Green (1981, 1982, 1983) suggested including a standard mineral in the same irradiation and, by comparing directly the track ratio of the standard and the unknown sample, removing the uncertainty of $\lambda_{fission}$. They introduced the "zeta calibration method", where:

$$\zeta = \frac{(e^{\lambda_{std}} - 1)}{\lambda(\rho_s/\rho_i)_{std}g} \qquad 2.8$$

Hence, equation 2.7 can be rewritten:

$$t = 1/\lambda[1+\lambda\zeta(\rho_s/\rho_i)g\rho_D] \qquad 2.9$$

ζ depends on the glass and the reactor used and is derived from the calculation of ages of standard samples, usually Durango, Fish Canyon Tuff and Mt. Dromedary apatites (see Appendix 1). The term ζ also takes into account systematic errors in counting tracks by operators.

2.2.4 Fission track length distribution

Fission track lengths must be measured in tracks that are parallel to the polished surface and completely confined within the host mineral. If possible, about 100 confined, horizontal tracks are recorded for each sample. They become etched by the acid penetrating through an intersecting crack (Track-IN-CLEavage) or track (Track-IN-Track) that crosses the polished surface. Identifying fission tracks as either TINCLE or TINT may be important, as TINT may be underetched and their full length not revealed (Laslett *et al.*, 1982).

Although biased against measuring short tracks (Laslett *et al.*, 1982), the track length distribution provides a powerful method of identifying a sample's thermal history. Confined track length distributions for three different thermal histories are shown in Figure 2.2. Rocks that have experienced rapid cooling and have not been reheated (thermal history (a)) show a unimodal track length distribution, clustered toward long track lengths that approximate the original length of tracks. The small discrepancy between the mean length of tracks induced in the laboratory (16.3 ± 0.9 μm) and the mean track length in rapidly cooled rocks (14-15 ± 1 μm) is not completely understood

and it may be due to a different behaviour between spontaneous and induced tracks (Wagner & van der Haute, 1992) or to partial annealing occurring over geological times at surface temperatures (e.g. Donelick *et al.*, 1990). Usually it is considered that over geological times track shortening occurs between 120 and 60°C and only tracks formed after the sample has cooled below 60°C are not affected by annealing. Slowly cooled samples are characterised by a wide, negative skewed track length distribution with a significant number of shorter track lengths (especially if the sample has left the PAZ quite recently) and a larger standard deviation on the mean (thermal history (c)). If the rock has experienced a more complex thermal history, the track length distribution is also more complex. In case (b), the sample has experienced two phases of rapid cooling; thus, the track length distribution is bimodal with the shorter tracks representing the time spent in the PAZ, before the last cooling episode (Brown, 1991).

In addition to temperature, time and chemical composition, the rate of annealing (and hence track length distribution) is also affected by track orientation to the *c*-axis (Green *et al.*, 1986; Crowley *et al.*, 1991). Although tracks parallel to the *c*-axis are longer than tracks oriented at high angles, especially at high rates of annealing, the probability of seeing a confined track is greatest when the track is oriented about 65-75° from the *c*-axis (Carlson *et al.*, 1999). This bias seems to be due to the anisotropic etching characteristic of the apatite which gives rise to narrow widths of etched tracks at very low and very high angles to the *c*-axis and a consequent lack of fully etched fission tracks in those orientations (Donelick *et al.*, 1999).

In order to account for anisotropic crystallographic effects, only those horizontal confined fission tracks parallel to the *c*-axis (± 10°) are generally measured. Donelick *et*

al. (1999) have suggested a method to convert the length of a track with a random orientation into an equivalent track length parallel to the *c*-axis, increasing the number of usable track length measurements. Although simple, this correction requires the determination of the angle between a specific track and the *c*-axis, a capability that is not yet routinely available for most fission track microscopes. For this work, only fission tracks that looked parallel or sub-parallel to the *c*-axis were measured, at the expenses of a larger number of data.

As the rate of annealing increases, the probability of a single track intersecting the polished surface of the host mineral decreases. Therefore, a relationship between mean track length reduction (l/l_0) and track density reduction (ρ/ρ_0) is expected. Green (1988) found that in apatites with similar chemical composition the relationship between l/l_0 and ρ/ρ_0 is linear and one-to-one for $l/l_0 > 0.65$, but that for more strongly annealed grains, l/l_0 is greater than ρ/ρ_0 (Figure 2.3). An apatite crystal that has experienced track shortening has a fission track age that is younger than a hypothetical sample that had entered the PAZ at the same time, but has been rapidly cooled. By dividing the fission track age by the track length reduction (l/l_0), an indication of when the sample entered the PAZ is obtained (Green, 1988).

2.2.5 Interpretation of apatite fission track data

The limited stability of fission tracks in apatite when exposed to temperatures characteristic of the upper few kilometres of the crust results in a systematic variation of rate of annealing and hence track length distribution and fission track age with depth. The form of such depth profiles reflects the distribution of temperature with depth in the

shallow crust, providing crucial information to constrain the thermal history experienced by the crustal section in that particular area. Figure 2.4 shows a typical fission track data profile derived from a borehole in a tectonically stable area (Brown, 1991). The form of the profile is controlled by the increase of temperature with depth, so that mean track length and apparent ages are progressively reduced with depth. The concave-up section of the fission track age-depth profile defines the PAZ (Figure 2.4). Below this zone apparent ages approach zero, as all fission tracks are rapidly annealed at temperatures greater than 120°C. Above the PAZ, the ages are constant, suggesting that the rate of annealing is very low.

The shape of the apparent age profile is sensitive to the rate of denudation. Brown *et al.* (1994) demonstrated that the initial concave-up profile is smoothed to an almost straight line for denudation rates greater than 30 m/Myr, sustained over a period of at least 100 Myr (the required holding time is shorter for higher rates of denudation). In this case, the gradient of the linear apparent age profiles approaches the rate of denudation, with the age of single samples approximating the time at which they cooled below about 100°C.

More complicated cooling histories produce more complex fission track age profiles. If, for example, a tectonically stable region is successively rapidly denuded, the base of the (fossil) PAZ will be shifted upwards toward the new surface. Samples that before the rapid cooling event were at more than 120°C and, therefore, had a zero fission track age, start to accumulate fission tracks as denudation commences. A new apparent age profile is developed below the earlier one and the transition between the two will be marked by a pronounced inflection, usually referred to as a "break in slope" (e.g.

Brown, 1991). In a borehole or vertical profile showing this particular trend the fission track ages corresponding to the break in slope indicate the time when the rapid denudational event occurred.

2.2.6 Forward and inverse modelling of fission track data

Annealing models produced in the last eight years or so are able to predict fission track ages and track length distributions for given time – temperature paths (forward model). These models also provide possible time-temperature paths for given fission track data (inverse model) (Gallagher, 1995; Ketcham *et al.*, 2000). The nature of fission track annealing in apatite is such that all the predictive models are non-linear with temperature, and so conventional inverse methods, such as least squares, are not appropriate (Gallagher, 1995). Models have been developed to incorporate geological information and to produce numerous time-temperature paths, as uncertainties in the fission track data preclude the possibility of identifying a unique thermal history. Gallagher (1995) proposed a Monte Carlo-based genetic algorithm (Monte Trax) that is able to define, on an initial stochastic search, the region of good-fit solutions, and a subsequent refinement stage to find the best solution. However, the annealing models incorporated by Monte Trax assume a Durango composition, and, so far, the software does not allow the chemical composition and/or the track orientations to be incorporated. AFTSolve (Ketcham *et al.*, 1999) allows the operator to use the annealing models contained in Monte Trax, but also to take in account the kinetic variability among different chemical apatite compositions by including the measurements of the Dpar. AFTSolve is also able to incorporate information about the orientation of the confined tracks with respect to the *c*-axis, variation in initial track length, and the

biasing effect of using ^{252}Cf irradiation to increase the number of confined fission tracks in young samples (Donelick *et al.*, 1999). The program can be used as a forward or as an inverse model and the thermal histories that best fit the data (the value of the χ^2 test can be changed by the operator) are saved in an "Excel" worksheet where they can be easily plotted or used for other softwares (like DECOMP, see below).

2.3 (U-Th)/He geochronology

The discovery that the α particles produced by the radioactive decay of Th and U isotopes are nuclei of helium (^4He) marked the beginning of geochrononology (Rutherford, 1904). As Rutherford stated in 1906, "if the rate of production of helium from known weights of the different radioelements were experimentally known, it should be possible to determine the interval required for the production of the amount of helium observed in radioactive minerals, or, in other words, to determine the age of the mineral" (p. 191). Although the (U-Th)/He system was the first radiometric scheme ever applied to dating rock crystallisation, it was soon clear that only very dense and compact radioactive minerals are able to retain a large portion of helium trapped in their structure (Rutherford, 1906). Rutherford himself stated that helium will escape from the mineral lattice and the "helium age" will be younger than the actual age of the rock.

Keevil (1941) subsequently found an average helium retentivity of 25% in granitic rocks and 44% in basic igneous rocks. Hurley (1950) claimed that the low retentivity of helium is due to its superficial location in a rock sample and so helium is easily lost. Hurley (1950) demonstrated that magnetite retains helium, and later experiments

showed that non-metamict zircons have (U-Th)/He ages similar to their U/Pb age (Damon and Green, 1963). The search for dense minerals that could trap helium led to the investigation of the potential applications of the radiometric system to aragonitic fossils. Fanale and Schaeffer (1965) and Bender (1973) demonstrated that the U/He system provides ages on fossils and corals in agreement with independent age estimates. Bender (1973) was the first to consider a correction for the α-particles ejected outside the mineral lattice during decay (α-recoil correction).

Zeitler *et al.* (1987) refreshed interest in the technique by demonstrating that (U-Th)/He ages of gem-quality apatites provided an age of cooling through about 100°C. They also demonstrated that loss of helium through the mineral lattice was consistent with volume diffusion from a spherical mineral grain. Their results were confirmed by Lippolt *et al.* (1994) who analysed samples from different geological environments and obtained helium ages younger than those computed with other radiometric systems, but similar to the fission track ages, confirming a closure temperature of around 100°C. These studies are of fundamental importance as they demonstrate that helium is sensitive to low temperatures. In the 1990s, a series of experimental determinations of helium diffusion in apatites, notably by Prof Ken Farley's research group at California Institute of Technology, demonstrated that the He diffusion in F-rich apatite grains occurs by volume diffusion and is consistent with a closure temperature of 75±7°C (for cooling rate of 10°C/Myr), (Farley *et al.*, 1996; Wolf *et al.*, 1996a; Warnock *et al.*, 1997; House *et al.*, 1999; Farley, 2002). The procedure used to obtain (U-Th)/He ages varies slightly between laboratories but, in all variants of the technique, parent and daughter elements are measured on the same apatite crystals, as individual apatite

crystals from the same rock often have highly variable U and Th concentration, as well as heterogeneous distribution (Meester and Dunai, 2002b). In the following sections an overview of the (U-Th)/He thermochronological method is provided, along with a description of the technique used to prepare samples (section 2.4). The analytical equipment for He, U and Th analysis are then described, along with estimates of the precision and accuracy of the measurements (sections 2.4, 2.5 and 2.6). The analytical procedure is described in Appendix 2.

2.3.1 Apatite (U-Th)/He thermochronology

^{4}He nuclei (α particles) are produced by the radioactive decay of heavy nuclei that have an unstable proton to neutron ratio. The helium present in nature is almost completely produced by the decay of ^{238}U, ^{235}U, ^{232}Th and ^{147}Sm, following:

$$^{238}U \Rightarrow \quad ^{206}Pb + 8\,^{4}He + 6\beta^{-} + Q \qquad \lambda_{238} = 1.552 \times 10^{-10}\ y^{-1} \qquad (2.10)$$

$$^{235}U \Rightarrow \quad ^{207}Pb + 7\,^{4}He + 4\beta^{-} + Q \qquad \lambda_{235} = 9.848 \times 10^{-10}\ y^{-1} \qquad (2.11)$$

$$^{232}Th \Rightarrow \quad ^{208}Pb + 6\,^{4}He + 4\beta^{-} + Q \qquad \lambda_{232} = 4.947 \times 10^{-11}\ y^{-1} \qquad (2.12)$$

$$^{147}Sm \Rightarrow \quad ^{143}Nd + 1\,^{4}He + Q \qquad \lambda_{147} = 6.538 \times 10^{-12}\ y^{-1} \qquad (2.13)$$

where Q is the sum of the decay energies (MeV) for the entire series and λ is the decay constant for each element. Equation 2.13 shows that the decay constant of Sm is two orders of magnitude lower than the decay constant of U. For a typical Durango composition (Table 2.1), where the concentration of Sm is about 14 times higher than

that of U and 0.8 times lower than Th, the contribution of ^{4}He from the decay of Sm is 100 times less than the amount of He produced by the decay of U and Th. Thus, only U and Th are considered as parent elements for the production of ^{4}He.

Durango samples (1 mg)								
Element (ppm)	D1	D2	D3	D4	D5	D6	Average	1σ (%)
As	700.0	678.8	702.4	771.2	744.2	754.8	725.3	1.9
Sr	453.7	462.8	498.8	490.0	474.7	480.9	476.8	1.6
Nd	1004.8	1015.2	1046.3	1083.5	1035.2	1053.0	1039.7	2.3
Sm	129.1	127.9	131.9	128.6	125.0	126.1	128.1	1.4
Th	154.1	152.4	159.1	171.1	163.5	165.9	161.0	2.4
U	9.1	8.6	9.2	8.9	8.5	8.8	8.9	2.3

Table 2.1: Six samples from the same Durango gem quality crystal were analysed at SUERC to determine their contents of U, Th and other trace elements (the analytical uncertainty is 1%; 1σ in the Table represents the stardard deviation of the mean). Each aliquot weights 1 mg and consists of pure apatite fragments (100-300 μm). The samples were dissolved in 10 ml 5% nitric acid and analysed by ICP-MS.

The Helium production in a mineral is defined by the following equation:

$$^4He = 8^{238}U\left(e^{\lambda_{238}t}-1\right)+7^{235}U\left(e^{\lambda_{235}t}-1\right)+6^{232}Th\left(e^{\lambda_{232}t}-1\right) \qquad 2.14$$

where ^{4}He, ^{238}U, ^{235}U and ^{232}Th are the present-day concentrations expressed in numbers of atoms and t is the accumulation time or the He age. This equation cannot be solved directly for the time t and it must be solved using an iterative method. As the

$^{235}U/^{238}U$ ratio is constant and equal to 1/137.88, there is no need to measure ^{235}U, and so equation 2.5 can be written as follows:

$$^{4}He = {}^{238}U\left[\left[8\left(e^{\lambda_{238}t}-1\right)+\frac{7}{137.88}\right]^{238}U\left(e^{\lambda_{238}t}-1\right)\right]+6^{232}Th\left(e^{\lambda_{232}t}-1\right) \qquad 2.15$$

Using this equation to determine (U-Th)/He ages requires the following assumptions to be met:

i) *Secular equilibrium between all the daughter decay elements.* Secular equilibrium is reached when the decay rate of each daughter nuclide in the chain is equal to that of the parent, i.e.:

$$\lambda_0 n_0 = \lambda_1 n_1 = \lambda_2 n_2 = \lambda_i n_i \qquad 2.16$$

where λ_0 is the decay constant and n_0 is the number of atoms of the original parent element, λ_1 and n_1 are the decay constant and the number of atoms of the first daughter, and so on. Regardless of initial conditions, secular equilibrium is reached within approximately 5 half-lives of the longest-lived intermediate nuclide experiencing fractionation, in this case ^{234}U, which has a half-life of 2.4×10^5 years. Therefore, the necessity of reaching secular equilibrium limits the application of (U-Th)/He geochronology to samples older than one million years (Farley *et al.*, 2002). Attempts at using helium to date volcanic samples 350,000 yrs old revealed the complexity of making a correction as secular equilibrium is not reached and the number of daughter elements atoms should be known *a priori* (Farley *et al.*, 2002).

ii) *No significant ^{4}He is present in the crystal initially.* Atmospheric ^{4}He contamination is insignificant as the concentration of ^{4}He in the atmosphere is 5 ppm. However fluid inclusions may carry crustal or mantle ^{4}He, which, when extracted along with the radiogenic ^{4}He from the crystal lattice, leads to spuriously old He ages. (U-Th)/He ages older than the crystallisation age of the rock have been considered to be due to the presence of such inclusions (Stockli *et al.*, 2000; Persano *et al.*, 2002). Fluid inclusions are usually only a few microns in size and are often difficult to identify when the apatite crystals are selected for analysis (see below). Such fluid inclusions may represent a first order source of errors.

The quantity of cosmogenic and fluid inclusion ^{3}He is negligible with respect to the amount of ^{3}He spike introduced in the extraction line with each sample (see section 2.3.5.4).

iii) *^{4}He is produced only by the U and Th present in the mineral lattice.* This assumption is particularly important in the case of apatite. Apatite usually contains between 10 and 100 ppm of U whereas zircons and monazite, for example, can contain up to 1000 ppm of U (Wedepehl, 1978). Small zircon and monazite inclusions are very common in apatite. The ^{4}He extracted from the apatite can include ^{4}He produced by radiogenic decay in the zircon. However, only the U and Th hosted in the apatite are typically analysed. The helium released by the zircon inclusion is parentless and produces a spuriously old (U-Th)/He age. Many authors have stressed the necessity of analysing apatite crystals that are completely free of inclusions if reasonable He ages are to be produced (House *et al.*, 1997; House *et al.*, 1999; Crowley *et al.*, 2002; Persano *et al.*, 2002). During this project, attempts have been made in the SUERC

laboratory to dissolve the inclusions along with the apatites, but non-reproducible data were obtained. However, these are preliminary results and further work is needed to assess the experimental procedure and the treatment of the data.

^{4}He atoms can also be implanted in a crystal from a neighbour host mineral. α particles can travel across the mineral lattice for a distance that depends on the host mineral (about 15 μm in zircon and 20 μm in apatite). However, this effect is in most cases insignificant as a large number of atoms of He must be implanted in the crystal to affect its (U-Th)/He age.

iv) *There has been no loss and/or addition of U and Th since the formation of the crystal.* U and Th can diffuse out of the mineral lattice at high temperatures. In the case of apatite, a loss of U and Th has been detected during melting of the crystals by laser heating (see section 2.3.8). For this reason, as the (U-Th)/He data presented here were the first to be produced at SUERC, a series of experiments were carried out before routine analyses were performed, in order to determine the correct holding time and temperature range to extract all the helium in apatite crystals without causing loss of U and Th (see section 2.3.5.1). Loss of U and Th can also occur through alpha recoil of the parent elements. When an α particle is produced, the parent element is recoiled by 30-100 nm (stopping distance in flogopite) and if it is close to the of the crystal edge it may be ejected outside the grain (Gögen & Wagner , 2000). This is most likely to affect (U-Th)/He ages only if the parent elements are concentrated in the outermost part of the crystal.

v) *There has been no loss of He after the sample has cooled below the closure temperature.* Helium loss may occur through cracks present in the mineral, especially for apatite rather than zircon, given the latter's brittleness. For this reason, apatite crystals with fractures are not used for (U-Th)/He analysis.

Two transport processes operate simultaneously to affect the retention of radiogenic helium produced in the mineral lattice: diffusion and recoil. In the following sections (2.3.2 and 2.3.3) the two processes are described, focusing on the case of apatite.

2.3.2 Diffusion of helium in apatite

Diffusion describes the process of atomic migration. The rate of diffusion of a particle in a solid depends primarily on the temperature, but also on the lattice geometry, vibrational frequency of the atoms and the activation energy necessary to be overcome for the process to occur (e.g. Dodson, 1973; Crank, 1975). Isothermal heating of Durango apatite for increasing periods of time shows that the He loss follows a linear relationship with the square root of time, suggesting that He is lost by volume diffusion through the mineral lattice (Zeitler at al., 1987; Farley, 2002). The data fit best if spherical or cylindrical mineral geometries are assumed. Experiments with slabs of Durango apatite cut parallel and perpendicular to the *c*-axis suggest weak preferential He diffusion along the *c* axis (Warnock *et al.*, 1997). Thus, the most appropriate geometry for modelling He diffusion from apatite is an infinite cylinder, rather than a sphere (Farley, 2002).

Step heating extraction of He from Durango apatite (Zeitler *et al.*, 1987; Farley, 2002) and other apatite samples (Lippolt *et al.*, 1994; Wolf *et al.*, 1996; Warnock *et al.*, 1997)

have demonstrated that diffusion of He is often linear on an Arrhenius plot (Figure 2.5). In this diagram, He loss is represented by D/a^2 where D is the diffusion rate at temperature T (K) and a (μm) is the half width of the apatite prism. For a given grain size, diffusion rates increase exponentially with temperature. At a given temperature, diffusive loss of He decreases with grain size, which is indicative of a single domain diffusion, i.e. that the crystal fragment is the domain size for He diffusion.

The slope of the linear trend (Figure 2.5) for temperatures lower than ~400°C represents the activation energy (E_a) and the intersection with the y-axis is the diffusion coefficient at infinite temperature (D_0). These values can be used to compute the closure temperature (T_c) of He in apatite (Dodson, 1973). As the diffusion domain should be the whole grain, the closure temperature depends on grain size. By definition, T_c is the temperature at which a dynamic equilibrium between daughter isotope production by radioactive decay and retention by the crystal is achieved (Dodson, 1973). The time when T_c is achieved is the apparent age. Durango apatite fragments of 100 μm radii have a closure temperature of 68°C (for a cooling rate of 10°C/Myr) and, varying the radius from 50 to 150 μm changes T_c by ± 5°C (Figure 2.6).

The diffusion process does not stop after cooling below the closure temperature. Experiments using the $^{40}Ar/^{39}Ar$ technique have demonstrated that a maximum of 42% of the daughter element is retained by the crystal at closure temperature (Lee, 2000). To investigate the temperature range at which He is retained by the apatite crystal, Wolf *et al.* (1998) have solved the production-diffusion equation of He for apatites kept at constant temperature for different durations. They demonstrated that He starts to accumulate in the apatite crystal at approximately 80°C and stops diffusing out of the

crystal at approximately 40°C (Figure 2.7). The temperature range over which 5-95% of the total He is retained by the crystal is called the Partial Retention Zone (PRZ).

Helium ages of apatites from boreholes in the Otway Basin, Victoria, Australia, provide a test of the modelled position of the PRZ (House *et al.*, 1999). The He ages decrease to zero with depth and although they show significant variations within a given temperature interval, they are consistent with the temperature range of the PRZ defined by Wolf *et al.* (1998).

As the PRZ depends on the rate of cooling and crystal size, the He concentration in an apatite crystal is a function of the cooling history and crystal dimensions. A forward model can be used to predict the He age of an apatite crystal with a defined cooling history. However, any (U-Th)/He age can be obtained for numerous time-temperature paths (Wolf *et al.*, 1998). These finding highlights the importance of multiple analyses and the integration of (U-Th)/He with other thermochronometers, in particular the apatite fission track system.

Diffusion rate varies also with crystal size. At any given temperature within the PRZ, larger crystals will retain more He than smaller ones (Reiners and Farley, 2001). The influence of crystal size is more pronounced the longer the samples are held in the PRZ (Figure 2.8). The size effect is most important in the cooler part of the He PRZ and in small crystals (approximately 60 μm in diameter) the lower limit of the PRZ can be as low as 30°C. The influence of crystal size on apatite He ages can be turned to an advantage as it is possible to model the size-age correlation to better constrain the cooling history of slowly cooled samples (Reiners & Farley, 2001, Chapter 5). For fully

exploiting this possibility, size variations in single aliquots should be minimised and, for best results, single grain analyses should be performed.

2.3.3 Recoil of ^4He

Recoil (ejection) is the process whereby the ^4He nucleus (α-particle) is ejected from the mineral lattice during decay of the parent isotope. The ejection distance depends on the radioactive isotope and on the mineral structure. In apatite the average stopping-distance for α-particles produced by radioactive decay of ^{238}U, ^{235}U and ^{232}Th are 22.46, 19.68 and 22.83 μm respectively (Farley *et al.*, 1996). If the radioactive parent nucleus lies within one stopping-distance of the edge of the crystal, then the ^4He nucleus could be ejected. The ejection probability is maximum (50%) if the parent nucleus is situated on the planar edge of the crystal. It is also possible that α-particles ejected from neighbouring crystals could be implanted in an adjacent apatite (see section 2.3; Farley *et al.*, 1996) (Figure 2.9). Only the outermost 20 μm of the crystal is affected by the recoil phenomenon. The distribution of the parent isotopes in the mineral lattice is a primary factor in controlling the amount of He lost by recoil. If the parent isotopes are uniformly distributed throughout the mineral the diffusion of He toward the exterior produces a gradient within the grain so that the He concentration in the rim of the crystal is less than in the core. Consequently physically removing the outer part of the crystal would bias He ages towards older values (Farley, 2002). Farley *et al.* (1996) have suggested an analytical solution to the problem. They "correct" (U-Th)/He ages using a recoil correction factor (F_t), which represents the total fraction of He nuclei retained by the crystal and is based on the measured grain geometry and size. For the

calculation, the apatite crystal is approximated to a hexagonal prism and F_t can be obtained as follows:

$$Ft = 1 + a_1 \beta + a_2 \beta^2 \qquad 2.17$$

where:

$$\beta = (2.31L + 2R)/(RL) \qquad 2.18$$

where L is the length and R is the radius of the apatite crystal. a_1 and a_2 are numerical factors depending on the parent element:

for the ^{238}U and ^{235}U series $a_1 = -5.13$ and $a_2 = 6.78$

for the ^{232}Th series $a_1 = -5.90$ and $a_2 = 8.99$

Typically the recoil correction is calculated for each grain in the aliquot and for each parent element. The aggregate recoil correction used to correct the measured He age is a weighted mean of the contribution from each grain by mass. In practise the recoil correction can vary between 0.9 and 0.65 and decreases with increasing crystal size (Figure 2.10).

This correction is based on three important assumptions:

i) *Implantation is negligible and only the α-ejection is taken in account.* Usually the content of U and Th of other minerals in contact with the apatite crystal (generally biotites and other mafic phases) is low and the contribution of He is negligible.

ii) *The recoil correction does not affect the diffusion process.* As diffusion is a function of the spatial distribution of the He produced by the radioactive decay, the diffusion gradient diminishes in the outer 20 μm, where He is depleted by α-recoil. As a result, the conventionally corrected ages are generally over-corrected if diffusion has occurred over a long period of time, i.e. if the sample has resided in the PRZ for more than several millions years (Meesters and Dunai, 2002b). In practice, the recoil factor as calculated by the Farley *et al.* (1996) approach is applicable to rapidly cooled samples and it may overcorrect the (U-Th)/He ages of slowly cooled samples.

iii) *U and Th distribution in each apatite is homogeneous.* A uniform U and Th distribution is assumed. However, U-zoning in apatite crystals is well documented by fission track observations (e.g. Galbraith, 1990; Wagner & van der Haute, 1992). If the spatial distribution of the parent isotope is known, a correction can be applied (describe in section 4.3 and Appendix 1). Meesters and Dunai (2002b) have recently demonstrated that retentivity of He in the mineral lattice is strongly dependent on zoning. Retention is lower if the parent nuclides are concentrated in the outer part of the grain. The dependence on U and Th zoning becomes stronger the longer the grain has resided in the PRZ and simple heterogeneities can produce variations in (U-Th)/He ages of up to 33% when compared to ages derived from a homogeneous distribution (Meesters and Dunai, 2002b). Meesters and Dunai (2002b) have developed a forward model for He ages that accounts for diffusion, α-recoil and zoning (section 4.4).

2.3.4 Sample preparation

Apatite is present in many types of rocks as an accessory mineral, forming usually less than 1% abundance. In the following sections the methods used to separate apatites from the bulk of the rock are described.

2.3.4.1 The use of thin sections and the cathodo-luminescence microscope

Three to ten kilograms of sample were collected. For every sample, a polished thin section was prepared and observed using a cathodo-luminescence (CL) microscope (courtesy of Dr. Braithwaite). The electron beam directed on the surface of the thin section causes apatite to emit a easily visible bright orange colour, enabling the size and content of apatite in the rock to be quickly assessed. Besides being an inexpensive method, CL allows observation of zonations in REE. Dempster *et al.* (2003) have suggested that REE distribution reflects the U, and possibly Th, distribution within the apatite crystal.

2.3.4.2 Mineral separation

Apatite-bearing samples were disaggregated into cm-sized fragments using a jaw crusher and ground to less than 500 μm diameter using a roller mill. The ground material was then sieved into four fractions: 500 to 355 μm, 355 to 250 μm, 250 to 64 μm and less than 64 μm. The 355-64 μm fractions were washed and a heavy mineral concentrate was obtained using a Wilfley table. This concentrate was dried in the laboratory at room temperature. Diffusion experiments have demonstrated that He loss

occurs even if samples are kept at 250°C for only 30 minutes (experiments conducted at SUERC and Zeitler *et al.*, 1987). This characteristic makes the use of ovens for drying samples inappropriate as He loss may occur.

The highly magnetic fraction was removed using a hand magnet and the remaining sample was passed through a Frantz magnetic separator using the following settings: 7°/20° (vertical and forward tilting, respectively) and 0.5 Amp., 7°/20° and 1.0 Amp. From the non-magnetic fraction the heavy-mineral fraction was isolated using conventional heavy-liquid mineral separation procedures. Tetrabromoethane (TBE) was used initially for separation of the "light" fraction (<2.9 $g.cm^{-3}$) but was replaced later in this study by a concentrated solution of sodium polytungstate (SPT), which is less toxic than TBE. The heavy fraction (> 2.9 $g.cm^{-3}$) containing apatites, zircons and titanites was immersed in Di-iodomethane and the less dense fraction (< 3.32 $g.cm^{-3}$) further purified using magnetic techniques, when necessary.

2.3.4.3 Handpicking the apatite crystals

Individual crystals were handpicked from the apatite concentrate under a binocular polarised light microscope at 218x magnification (courtesy of Dr. Braithwaite). Near-surface zircon inclusions, even only a few microns in diameter can be spotted using polarised light because of their bright interference colours. Apatite crystals were carefully observed in order to avoid He-bearing inclusions and grains with cracks, which could represent preferential pathways of He diffusion through the mineral lattice. The length and diameter of inclusion-free apatite crystals were then measured using a 10x10 μm graticule. Presence or absence of the pyramidal terminations was also noted

and each apatite crystal sketched. Apatites were selected to minimise the total variation in grain diameter in order that the standard deviation of the recoil correction (calculated a priori, assuming a U/Th ratio of 2) in each aliquot was ± 0.5%.

2.3.5 The ^{4}He analysis

In this section the analytical equipment used to extract and analyse He concentrations in minerals is described along with precision and accuracy of the data.

2.3.5.1 Extraction and clean-up system

Figure 2.11 shows the system used to extract He from the samples. In the early phases of this study, apatites were loaded in copper foil packets, but this was later replaced by re-usable stainless steel capsules that allow easy retrieval of the crystal after He analysis. Nine to twelve capsules were inserted into a Monax glass "tree" with nine branches located above a resistance-heated double-walled vacuum furnace with a Mo crucible. Each sample was dropped into the furnace (Figure 2.11). After the loading, the furnace and tree were pumped using a turbo-membrane pump system; an all-bakeable valve between the pump and the line allowed it to be isolated. During normal clean-up procedures (after each extraction) ultra-vacuum conditions (~10^{-9} torr) were maintained by a 30 l/second-triode ion pump.

The furnace temperature has been calibrated using an optical pyrometer. During the early stages of this project, many analyses were performed to calibrate the system. Helium extraction for more than 20 Durango aliquots demonstrated that heating the sample for 40 minutes at 950°C releases all the He in the crystal without parents loss.

The extraction line is constructed of 0.625 cm diameter stainless steel piping connected via Conflat flanges with Cu-gasket seals, and is bolted directly onto the mass-spectrometer bench. Bakeable all-metal Varian valves are used throughout. Active gases (N_2, O_2, CO_2, ect) extracted during heating react with a Zr-Al alloy getter, kept at approximately 550°C. A metal finger, containing approximately 1 g of activated charcoal held at -172°C by liquid N_2, was used to condense Ar, Kr, Xe and the remaining active gases. A second liquid N_2-cooled charcoal finger was mounted close to the mass-spectrometer (Figure 2.11) in order to minimise the partial pressure of Ar during the determination of He. A second getter at room temperature is mounted directly below the mass-spectrometer to remove H from the residual gases. The removal of H is important because: (1) H may suppress the ionisation of the He in the source, and (2) H_3-HD (mass 3) may contribute to the ^{3}He peak.

2.3.5.2 The ^{4}He mass-spectrometer

^{4}He analysis was made using a quadrupole mass spectrometer (Hiden HAL3F Analytical System, Warrington, England). The mass spectrometer was interfaced to a control computer through a rack-mounted mass spectrometer interface unit. The quadrupole mass analyser is configured for a 0-50 amu using a radio frequency head mounted on the mass spectrometer. The mass spectrometer was fitted with a conventional electron-impact ion source which was operated at an emission current of ~ 1 mA and an electron energy of 70 eV. The mass spectrometer is fitted with a Faraday cup and electron multiplier collector. During this study the Faraday cup was used to attain flat-topped peaks at the expense of sensitivity.

2.3.5.3 Isotope dilution and calibration

The system sensitivity (2×10^{-6} A/cc for ^{4}He) was calibrated on a daily basis using a manometrically determined ^{4}He standard from a 1 l reservoir. The gas standard delivered $1.83 \pm 0.003 \times 10^{-7}$ cc of ^{4}He (STP) per 0.105 cc aliquot. Standard ^{4}He abundances were measured within each run to $\pm$ 0.1% (1σ) and between runs to $\pm$ 0.2% (1σ).

Sample ^{4}He abundances were determined by isotopic dilution with a constant volume of ^{3}He. The reproducibility of the ^{3}He was determined from twice daily measurements against the ^{4}He standard. The volume of ^{3}He was calculated as a spike to standard ratio (^{3}He/^{4}He); its variation within each run was $\pm$ 0.05% (1σ).

The uncertainty of the He concentration measurements is dominated by the uncertainty of the ^{3}He spike volume. The ^{3}He isotope dilution was not corrected for depletion because all the analyses for this study were performed in the first 700 runs, when the depletion effect was insignificant.

2.3.5.4 Blanks for ^{4}He analysis

The ^{4}He of unspiked cold and hot furnace blanks was below the detection limit of the mass spectrometer ($< 0.02 \pm 0.02$ ncc). The primary source of ^{4}He in the blank is from the ^{3}He reservoir. The ^{3}He/^{4}He ratio of the ^{3}He reservoir (~1300) meant that 1-2 ncc ^{4}He were introduced with each delivery of ^{3}He. Re-extractions of He from samples were performed for every sample and were repeated until the ^{3}He/^{4}He was> 1200. In

this way, the blank levels were always less than 0.1% of the total ^{4}He released by the samples.

The abundance of H_2 was measured routinely to determine the contribution of ^{3}H and HD isotope to the ^{3}He spike. Levels of H were constant throughout the measurements, ranging from 0.2 to 0.4 ncc. The contribution of ^{3}H-HD was negligible.

2.3.6 U and Th analysis

After He extraction the capsules containing the apatite crystals were retrieved from the furnace. U and Th were analysed in aqueous solution using an Inductively Coupled Plasma Mass Spectrometer (ICPMS). The quantities of U and Th were determined as the ratio of their concentrations ($[^{238}U]/[^{232}Th]$) using isotopic dilution. In the following section the analytical procedures and the equipment used to perform the analyses are described.

2.3.6.1 Apatite dissolution and isotopic dilution

During the initial stages of this project the apatite crystals were loaded in copper packets, but this procedure was later replaced by loading into stainless steel capsules. The steel capsules were wrapped in copper foil that was removed and the capsules opened after He analysis. The apatite crystals in the capsule were transferred into a teflon beaker with 2 ml of 5% nitric acid and approximately 1.3 ng of ^{235}U and 3 ng of ^{230}Th spikes. The spikes were prepared by dissolving certified standard (courtesy of Dr. Ellam) ^{235}U and ^{230}Th powder in nitric acid and diluting to obtain a concentration of 15

ppb. Fractionation in the mass spectrometer was corrected using the U500 standard with a certified value $^{235}U/^{238}U = 0.9997$.

Copper packets were dissolved in U and Th-spiked nitric acid along with the apatites. U and Th were purified using conventional cation exchange chemistry (Luo *et al.*, 1997). After equilibration, the solution was brought to 5 ml using 5% nitric acid and transferred in plastic tubes for ICPMS analysis.

2.3.6.2 ICPMS analysis

U and Th concentrations were determined by VG PlasmaQuad PQ2 plus ICPMS (VG Elemental, Cheshire, England) fitted with a Meinhard nebulizer and a Scott, double pass, water-cooled glass spray chamber. Instrumental parameters are given in Table 2.2 (Olive *et al.*, 2001). The limits of detection in a quadrupole ICPMS are best presented in terms of detector noise (cps) rather than concentrations (Olive *et al.*, 2001). The instrumental background level reported in Table 2.2 represents the mean of fifty 90s aspirations of the 5% nitric acid solution used to "purge" the instrument between samples. In order to monitor instrumental mass fractionation, repeated analyses of U500 standard were performed. Each sample run began with two U500 aliquots and subsequent analyses interspersed to bracket every three samples. The reproducibility of measuring 5 ppb U500 solution was approximately 0.15%. U and Th concentrations in the samples were accurate to ± 2.5% (1σ).

Sample uptake rate	0.8 ml min^{-1}
Washout time	180 s
Uptake time	90 s
Acquisition time	90 s
Data acquisition mode	Peak jumping
Dwell time	10.24 ms
Points per peak	3
No. of replicates	3
Blank (cps) for U	<100
Blank (cps) for Th	<100

Table 2.2: ICPMS acquisition parameters

2.3.7 Precision and accuracy of the measurements

The uncertainty associated with (U-Th)/He data derives from the uncertainties in the measurements of U, Th and He and was dominated by the accuracy of the ^{3}He, ^{235}U and ^{230}Th spikes. Repetitive analyses conducted in the early stages of this project showed that the ^{3}He-spike/^{4}He-standard ratio was known to better than 0.5% (n = 10) and the uncertainty on the ^{230}Th and ^{235}U spike concentration was approximately 1%. Figure 2.12 that shows empirical data obtained in the early stages of this work and it indicates that, when the concentrations of U and Th are known with a precision of 1%, the error on the He ages is dominated by the He determination. A better precision on the U and

Th measurements (i.e. 0.5% in Figure 2.12) does not improve significantly the error on the He ages. Given the errors on He, U and Th determinations at the SUERC laboratory, the overall uncertainty was about 3% (1 σ).

To determine the accuracy of the data produced, a mineral standard was repeatedly analysed. As He ages commonly represent cooling ages, the mineral standard needs to have cooled through the He closure temperature and the closure temperature of a second chronometer at the same time. Conventional mineral standards tend to be those that have cooled to surface temperatures very rapidly. Volcanic rocks best fulfil this requirement. We have followed the California Institute of Technology (CIT) laboratory procedure and have used the Durango apatite. Durango is a fluoroapatite that occurs in pyrothermal or volcanogenic deposits at Cerro de Mercado (Mexico). The crystals used as a mineral standard have a certified composition (Young *et al.*, 1969). Fission track dating of Durango apatite gives an age of 31.4 ± 0.5 Ma (McDowell & Keizer, 1977), and the K/Ar age of feldspars from volcanic rocks bracketing the apatite deposits is 31.4 ± 0.5 (Green, 1985). Repeated analysis of the CIT laboratory Durango apatite standard over the period of this project yielded an age of 32.8 ± 2.3 Ma (n = 48) (Table 2.3). This was in excellent agreement with the 32.0 ± 1.0 Ma age measured in the CIT laboratory (Farley, 2002).

Six replicates of the 99OZ13 sample collected for this project (Chapter 3 and 4) were analysed in order to determine the reproducibility of the analytical technique. The sample yielded a 8% variation (1σ) in age that is used throughout this study as a measure of the uncertainty in the mean age of all samples. This compares to a reproducibility of 6% for the CIT laboratory (Farley, 2003). The slightly poorer

Durango types	date	Age (Ma)
Durango 2	N/A	34.7
Durango 2	N/A	28
Durango 2	N/A	29.2
Durango 2	N/A	28.3
Durango CIT	13/06/00	31.9
Durango CIT	20/06/00	30.32
Durango CIT	20/06/00	29.78
Durango CIT	21/06/00	28.72
Durango CIT	22/06/00	30.04
Durango CIT	22/06/00	30.81
Durango CIT	22/06/00	32.67
Durango CIT	12/07/00	31.8
Durango CIT	22/08/00	33.4
Durango CIT	24/08/00	33.3
Durango CIT	14/09/00	40.3
Durango CIT	14/09/00	33.69
Introduction of steel capsules		
Durango CIT	20/10/00	34.08
Durango CIT	25/10/00	31.6
Durango CIT	30/10/00	27.5
Durango CIT	25/11/00	33
Durango CIT	06/02/01	33.1
Durango CIT	02/07/01	36.1
Durango CIT	23/02/01	34
Durango CIT	26/02/01	39.3
Durango CIT	03/05/01	33.8
Durango CIT	16/03/01	33.2
Durango CIT	19/03/01	40.7
Durango CIT	19/03/01	31.6
Durango CIT	19/03/01	33.9
Durango CIT	20/03/01	38.8
Durango CIT	20/03/01	31.4
Durango CIT	20/03/01	36.6
Durango CIT	21/03/01	33.7
Durango CIT	26/03/01	33.3
Durango CIT	28/03/01	41
Durango CIT	28/03/01	33.6
Durango CIT	29/03/01	33.4
Durango CIT	29/03/01	31.4
Durango CIT	04/05/01	33.3
Durango CIT	04/06/01	28.8
Durango CIT	27/06/01	33
Durango CIT	30/06/01	32.9
Durango CIT	09/07/01	24.2
Durango CIT	14/08/01	31.9
Durango CIT	16/08/01	32.5
Durango CIT	11/09/01	31.9
Durango CIT	20/09/01	32.2
Durango CIT	12/12/01	32.3
Average		32.8
St. dev. (±1σ)		2.3
St. dev. (%)		2.6

Table 2.3: Durango ages obtained during this project.

reproducibility of the samples measured at SUERC may be due to the large number of crystals analysed for each aliquot, which increases the possibility of zircon and fluid inclusions.

2.3.8 He extraction using a CO_2 laser

He extraction from apatite in a furnace is time-consuming. Each extraction – clean-up cycle takes approximately 60 minutes and the blank associated with such extraction is usually significant enough to require the analysis of multi-grain aliquots, especially for young samples. Sufficiently large aliquots of inclusion-free apatite crystals (sometimes as many as 40 in this study) are difficult and time-consuming to acquire, requiring up to two to three days of hand-picking for each such sample or aliquot. Where He abundances are low, e.g. in samples with young (U-Th)/He ages and/or low U concentrations (less than 5 ppm), the number of apatite grains necessary to maintain the blank to <1% of the total ^{4}He is large. Laser heating offers a way forward (e.g. Balogh & Simonits, 1998). The laser pan in which samples can be loaded may contain more than 200 capsules, so many samples could be loaded at the same time, reducing the re-loading down-time. The extraction time can be reduced to few minutes, significantly decreasing the analytical time. Additionaly, the low extraction system volumes and the absence of hot metal parts can lower blank levels by an order of magnitude at least, allowing the analysis of single grain and young samples.

A series of experiments were performed aimed at determining the effects of laser melting on volatising U and Th from apatite (Stuart & Persano, 1999). The samples analysed were fragments of a single Durango apatite and two natural apatites, one from

the Ratagan granitic complex in West Scotland, and the other from a granulite facies gneiss on the Isle of Lewis. Each aliquot weighed 1 mg and was composed of transparent, inclusion-free crystals 200-300 μm in diameter. U and Th concentrations were determined in three un-melted aliquots of each sample along with As, Sr, Nd and Sm (Table 2.3). Aliquots were loaded in the laser pan and heated for 1 minute using a CO_2 laser and the trace elements were determined by ICPMS. The data in Table 2.4 show the heterogeneity of U and Th between aliquots of apatite from the same sample, although the U/Th ratio is generally constant (within 1 σ). However, when apatite crystals are heated with the laser, a significant loss of U and Th occurs (Figure 2.13) and even the ratios vary in an unpredictable way (Figure 2.14). All elements are variably lost (Table 2.3). However, when the ratio ΔNd/ΔSm (ratio between the difference of concentrations of trace elements in un-melted and melted aliquots) is considered, the 1:1 relationship suggests that the REE are lost to a similar extent. Consequently Nd is used as a "reference" element against which the loss of U and Th is measured. In Durango apatite, less U and Th is lost than Nd with the exception of one aliquot(Figure 2.15). This relationship is not verified in the other samples and U and Th appear to be as volatile as the REE.

The loss of U and Th during laser heating is significant and unpredictable and reflects the difficulty in laser heating of nude apatite crystals. A CO_2 laser is highly reflective for metals (10.6 μm wavelength) The escamotage of wrapping the apatite grains in a metal that would melt at a temperature where He is completely extracted without parent element loss cannot be used with a CO_2 laser, given its highly reflectivity (10.6 μm wavelength). The study reported by Stuart & Persano (1999) highlighted the problems

associated with laser heating and was used to develop the technique for further studies (House *et al.*, 2001). House *et al.* used a Nd-YAG laser that is only partially reflected by metals like Pt and Pd.

With this extended background to low temperature thermochronology, the next chapters describe the apatite fission track and (U-Th)/He data collected for this study and outline their interpretation.

DURANGO 2: Unheated samples									
ELEMENTS	A1	A2	A3	A4	A5	A6	A7	average	st.dev %(1σ)
As (ppm)	650.00	669.70	599.90	529.70	612.50	672.40	574.60	615.54	8.56
Sr	390.00	396.20	359.20	315.80	364.10	404.70	327.50	365.36	9.37
Nd	864.50	872.50	807.40	713.90	822.40	952.20	704.10	819.57	10.81
Sm	105.40	107.10	98.20	86.60	101.10	116.70	85.80	100.13	11.12
Th	131.30	129.30	118.70	106.40	123.10	147.20	100.70	122.39	12.85
U	7.31	7.33	6.65	5.77	6.89	8.13	5.62	6.81	13.12
Th/U	17.96	17.64	17.85	18.44	17.87	18.11	17.92	17.97	1.39
DURANG0 2: Heated-with-laser samples									
ELEMENTS	LD	LE	LF	average	st.dev %(1σ)				
As (ppm)	647.36	643.35	635.23	641.98	0.96				
Sr	419.63	430.80	439.57	430.00	2.32				
Nd	912.04	924.72	937.54	924.77	1.38				
Sm	113.31	115.23	116.41	114.98	1.36				
Th	112.32	135.54	103.16	117.01	14.26				
U	6.91	7.71	6.13	6.92	11.47				
Th/U	16.25	17.58	16.84	16.89	3.92				

Ratagan granite: unheated samples						
ELEMENTS	R5	R6	R7	R8	average	st.dev %(1σ)
As (ppm)	28.02	28.86	27.19	24.32	27.10	8.48
Sr	1607.80	1628.80	1592.30	1432.20	1565.28	6.68
Nd	956.11	984.13	930.51	833.62	926.09	8.24
Sm	95.55	96.89	91.92	82.54	91.73	7.94
Th	37.47	40.76	36.59	33.11	36.98	10.36
U	26.34	29.15	26.20	23.09	26.20	11.57
Th/U	1.42	1.40	1.40	1.43	1.41	1.50
Ratagan granite: heated-with-laser samples						
ELEMENTS	R1	R2	R3	R4	average	st.dev %(1σ)
As (ppm)	14.86	15.16	16.06	15.06	15.28	3.60
Sr	1702.60	1735.90	1820.30	1765.70	1756.13	2.44
Nd	1097.70	1145.00	116.60	1095.40	863.68	67.15
Sm	109.32	115.21	117.76	110.50	113.20	3.25
Th	43.17	44.68	48.76	44.31	45.23	5.47
U	11.77	3.06	11.82	5.47	8.03	56.35
Th/U	3.67	14.58	4.12	8.10	7.62	69.28

Lewis gneiss: unheated						
ELEMENTS	U7	PC7	PC8	PC9	average	st.dev %(1σ)
As (ppm)	22.87	4.25	4.25	4.25	4.25	0.04
Sr	871.63	287.74	287.75	293.30	289.60	1.11
Nd	331.19	378.45	342.39	364.56	361.80	5.03
Sm	79.30	83.48	77.21	80.72	80.47	3.91
Th	2.57	1.78	1.48	1.70	1.66	9.34
U	14.69	15.09	14.98	15.17	15.08	0.64
Th/U	0.17	0.12	0.10	0.11	0.11	8.89
Lewis gneiss: heated						
ELEMENTS	L7	L8	L9	average	st.dev %(1σ)	
As (ppm)	8.12	7.90	13.63	9.88	32.84	
Sr	253.63	272.28	400.99	308.97	25.97	
Nd	295.41	312.21	323.17	310.26	4.51	
Sm	68.47	72.89	78.62	73.32	6.94	
Th	1.65	1.54	1.88	1.69	10.37	
U	12.44	11.13	12.41	11.99	6.25	
Th/U	0.13	0.14	0.15	0.14	6.86	

Table 2.4: contents of U, Th and REE of Durango and two other natural samples.

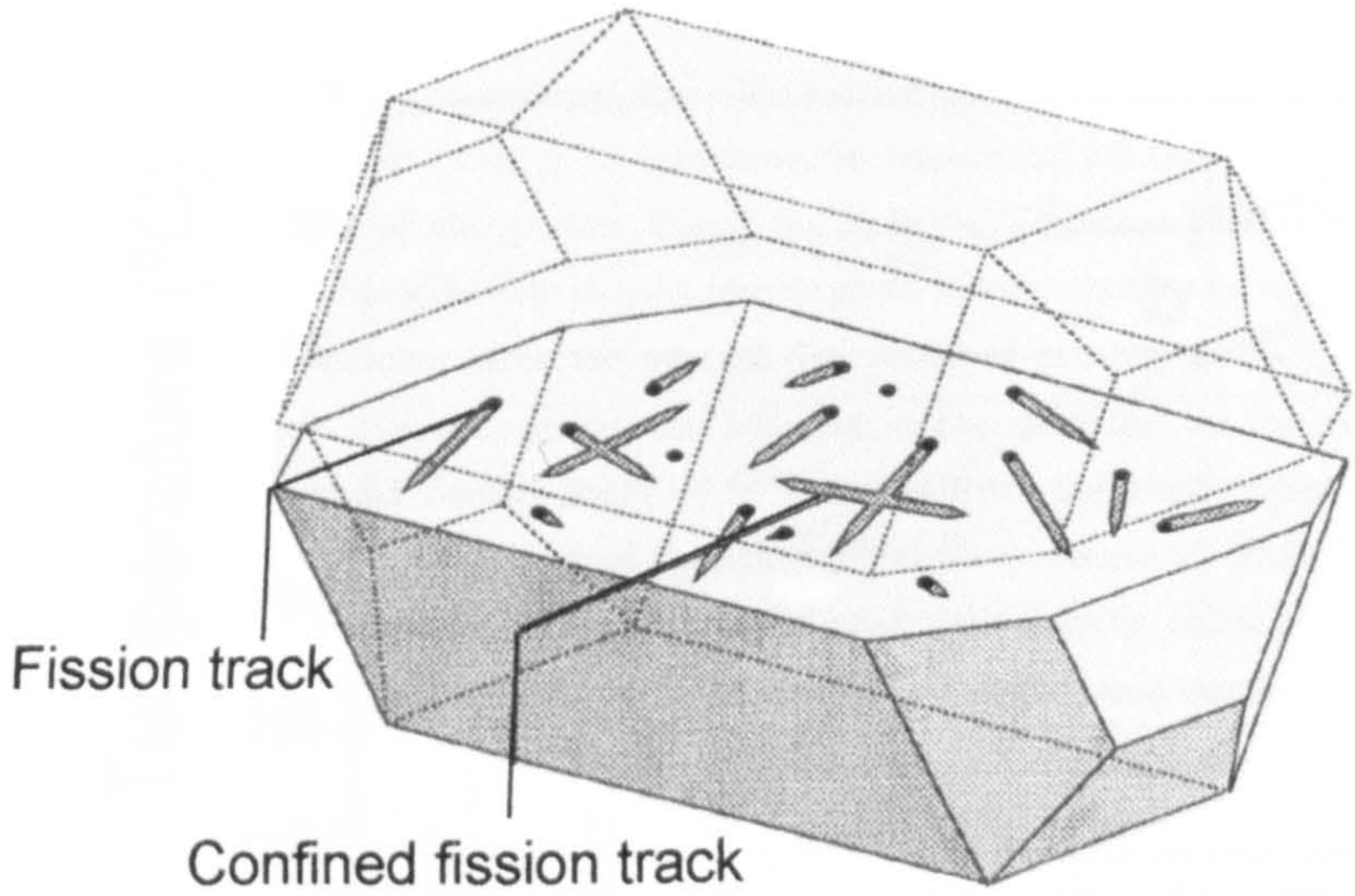

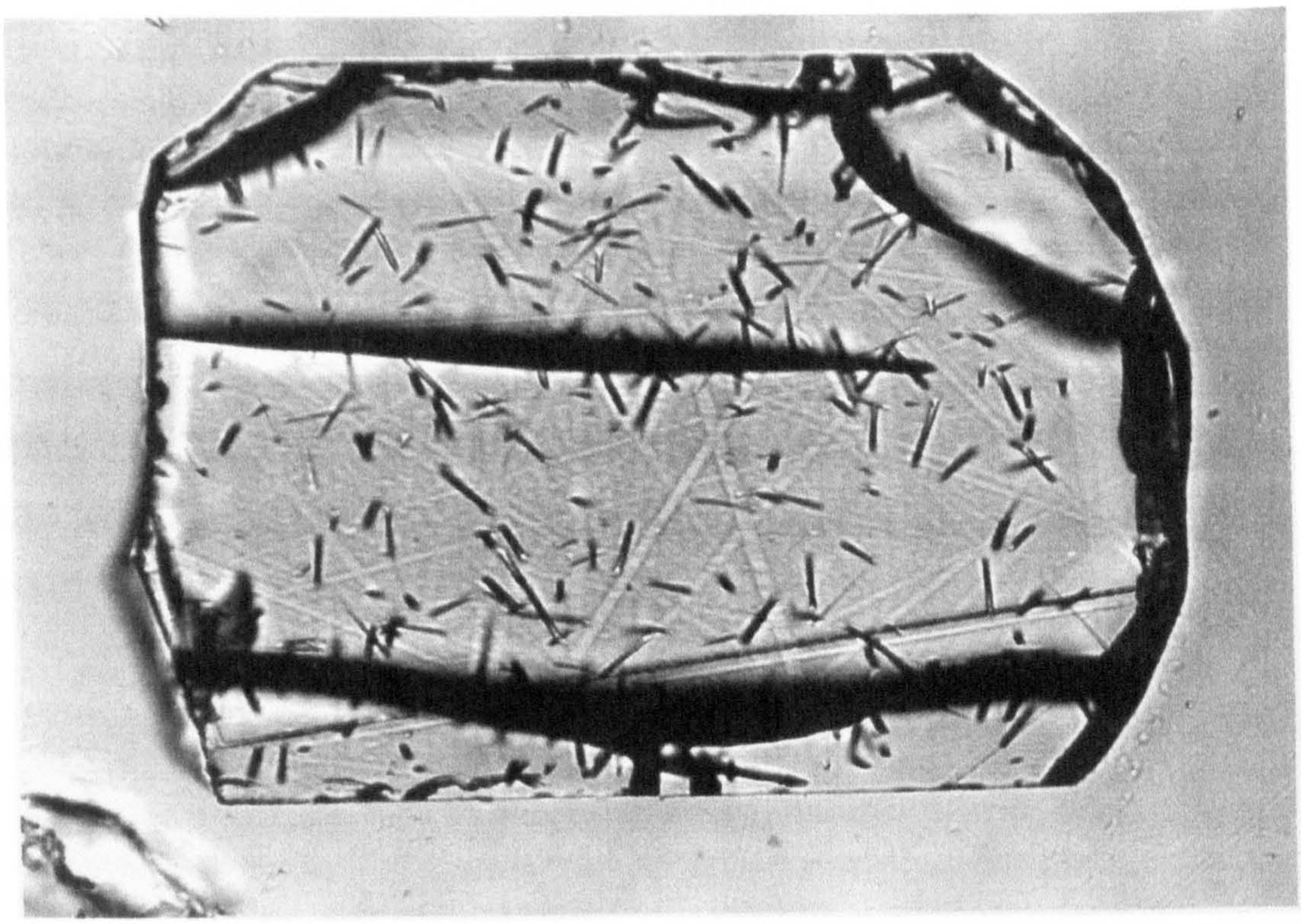

Figure 2.1: (a) Sketch of etched fission tracks as they would appear on a polished surface of an apatite crystal. (b) An apatite crystal after being etched, as observed under magnification x1000. Confined and unconfined (intersecting the surface) tracks are visible (from Brown, 1991)

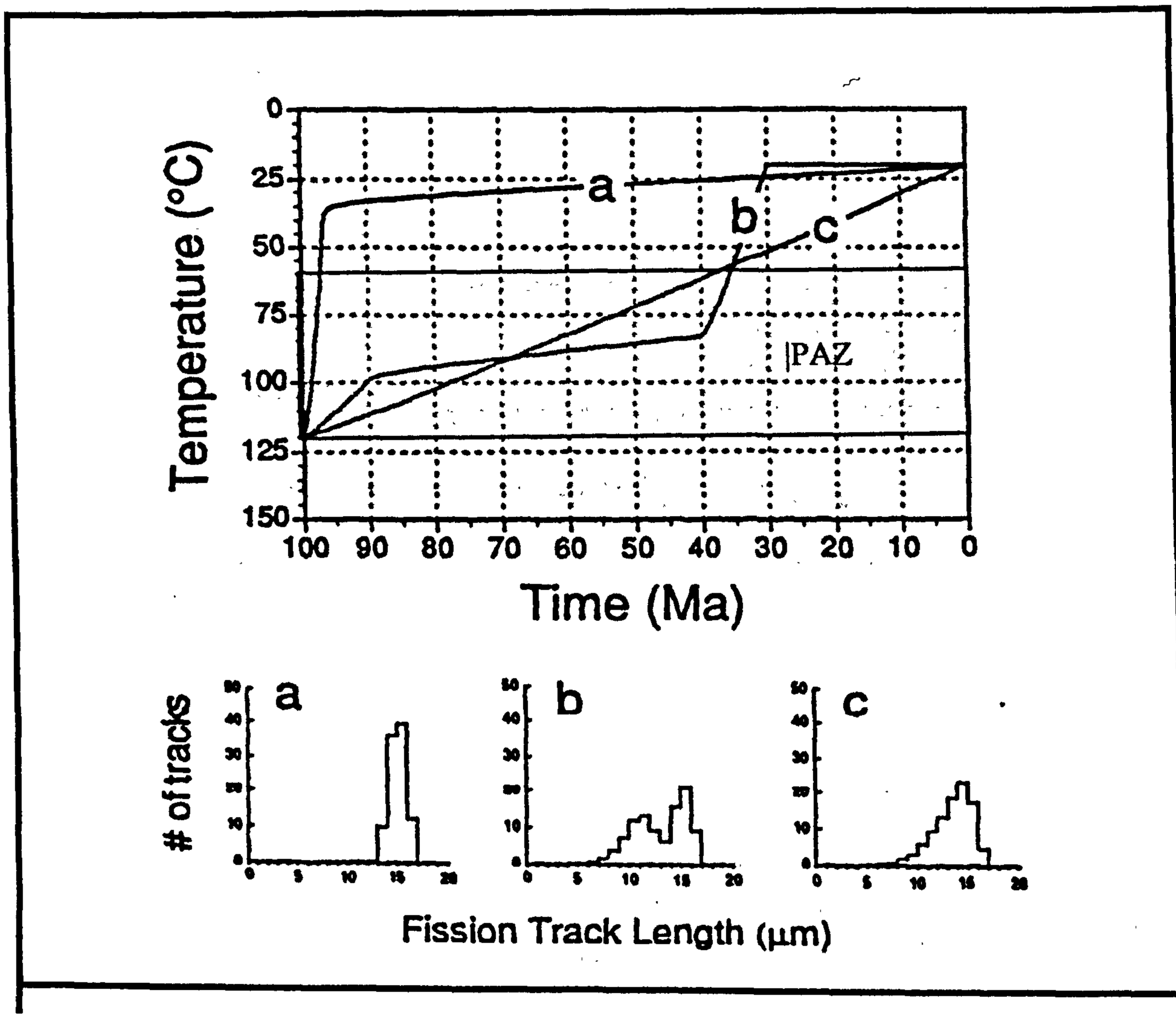

Figure 2.2: Samples that have experienced three different thermal histories are characterised by the different fission track length distributions indicated by the letters a, b and c (see text for discussion; from Brown, 1991)

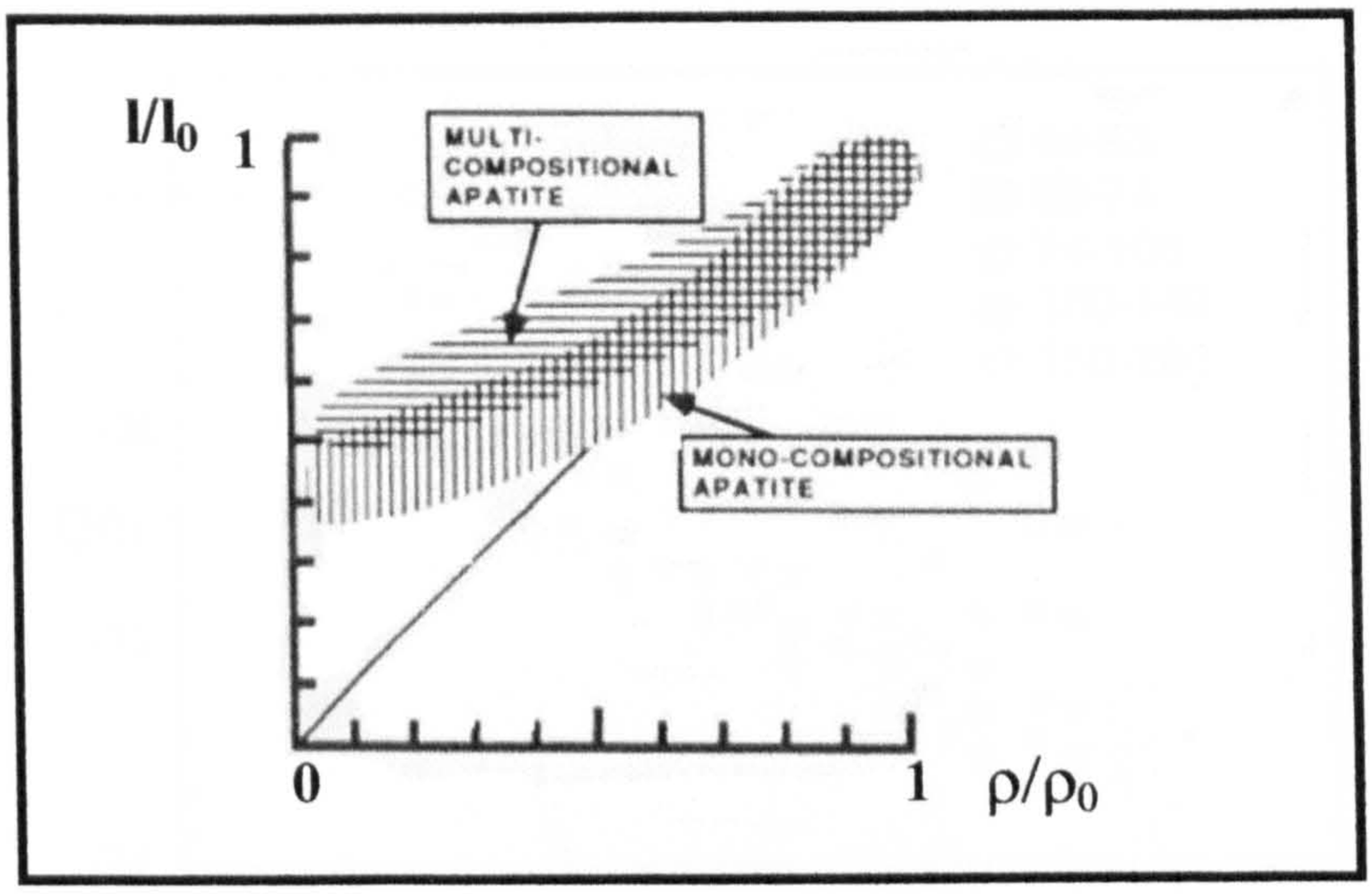

Figure 2.3: Relationship between length reduction (l/l_0) and track density reduction (ρ/ρ_0) (from Green, 1988)

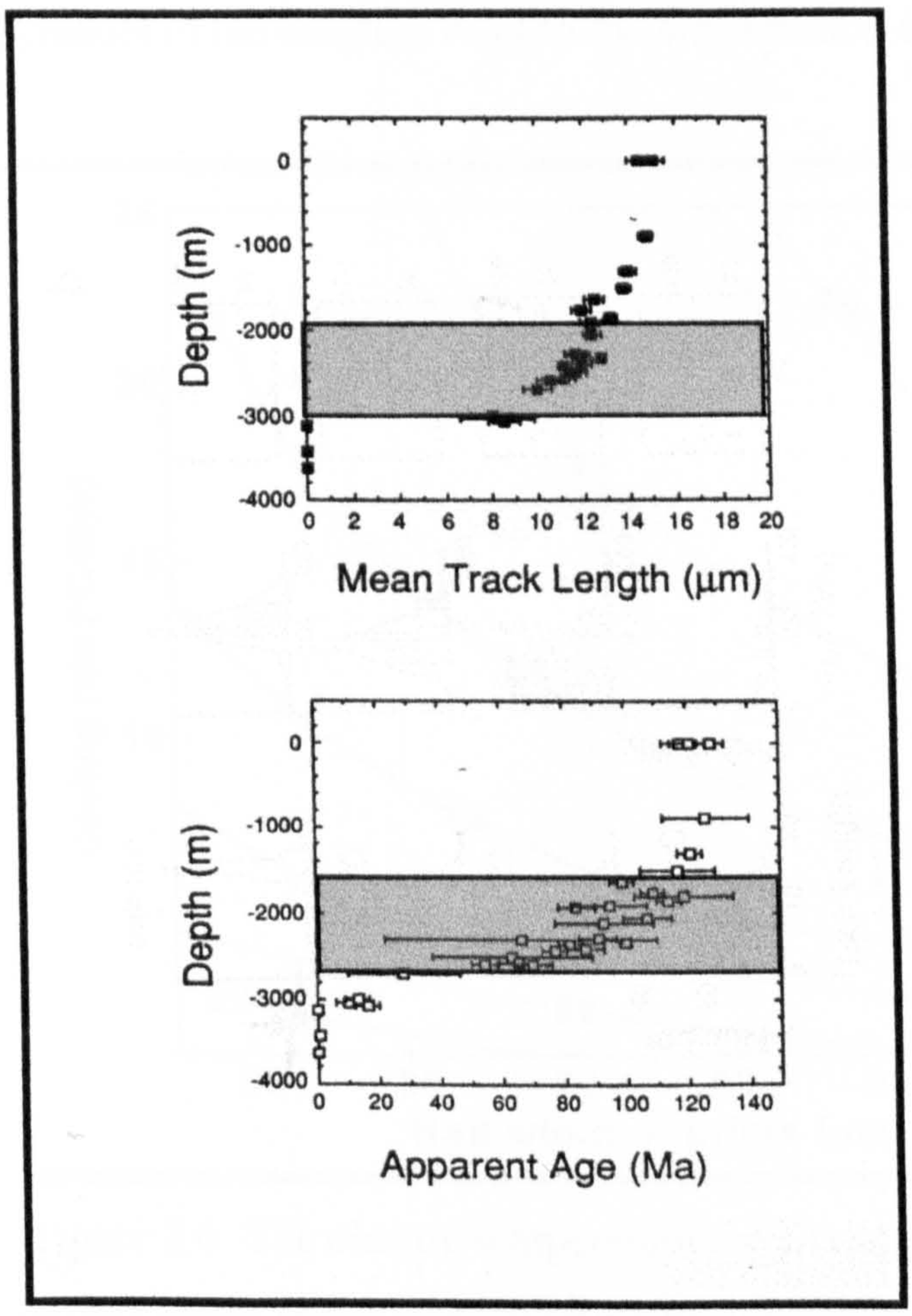

Figure 2.4: Variation of mean track length and apparent fission track ages for samples collected at different depths down a borehole (from Brown, 1991). The grey area represents the PAZ

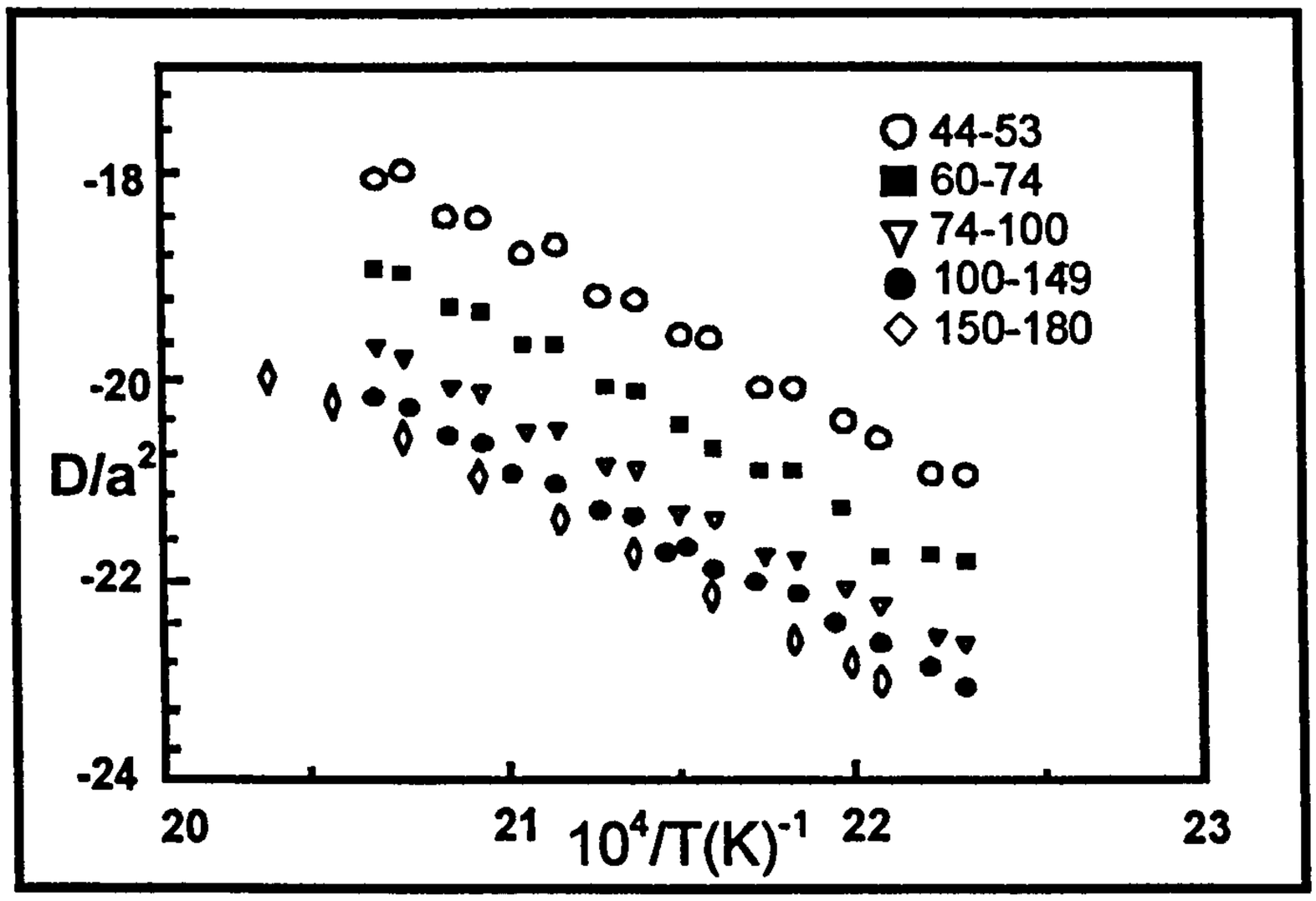

Figure 2.5: Arrenhius plot of helium diffusion in apatite (from Farley, 2000). The measurements were done on different size fractions of Durango apatite. The different symbols in the diagram refer to the size fraction in μm.

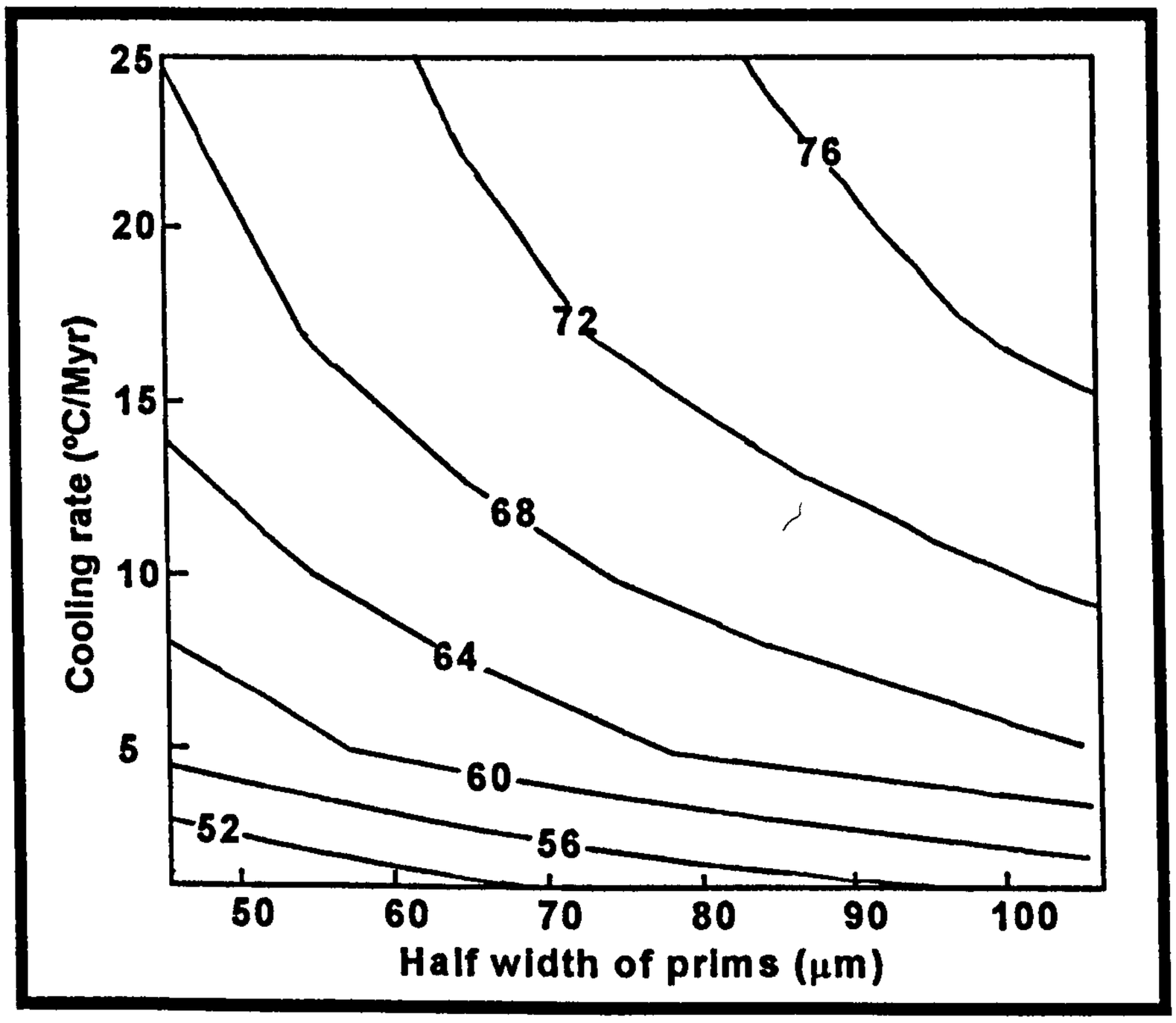

Figure 2.6: The closure temperature for Durango apatite computed as a function of the apatite prism radius and cooling rate (from Farley, 2000).

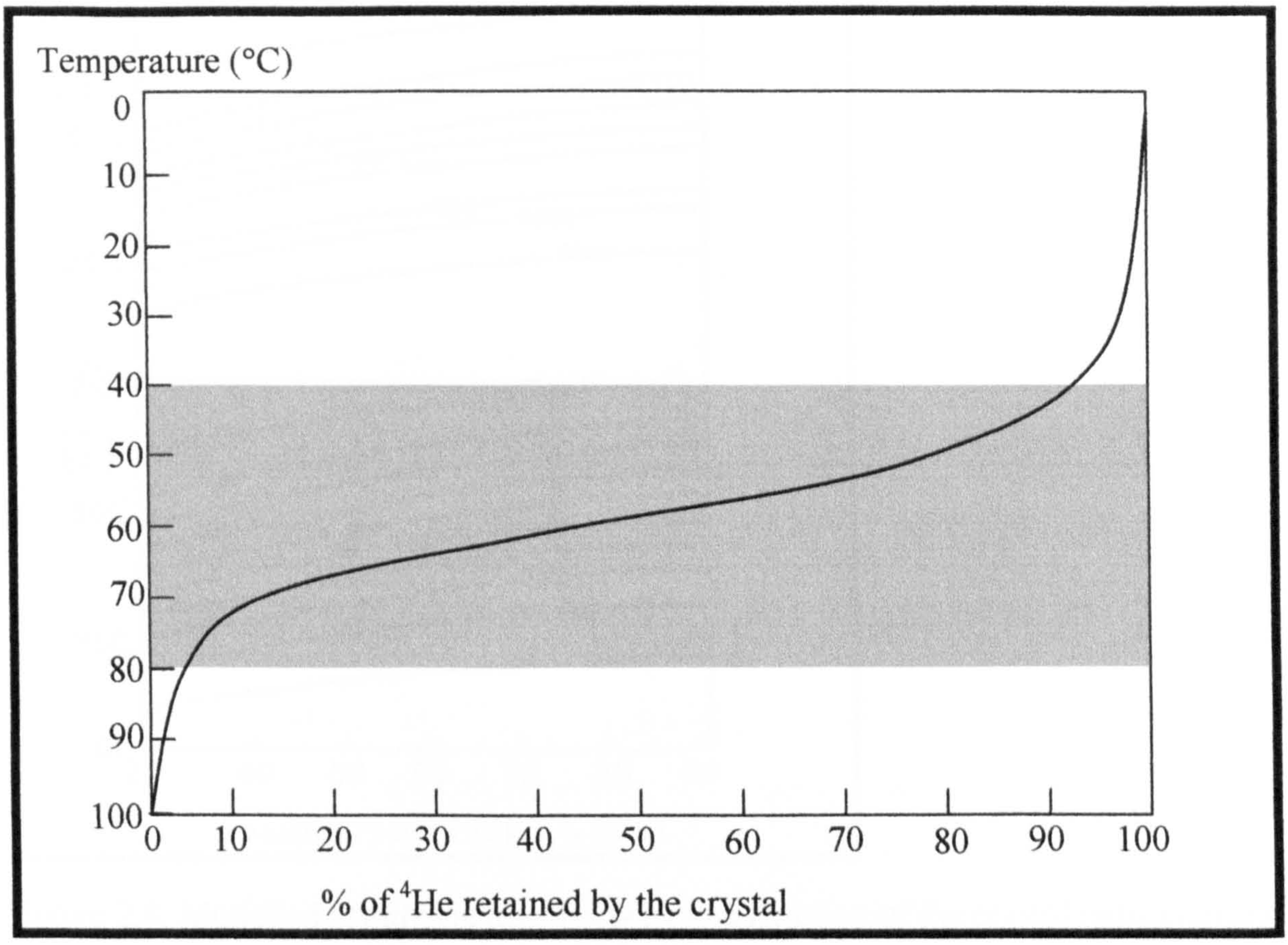

Figure 2.7: Percentage of ^{4}He retained by an apatite crystal as a function of temperature. The grey area is the Partial Retention Zone (PRZ), in this case ranging from about 80 to 40°C.

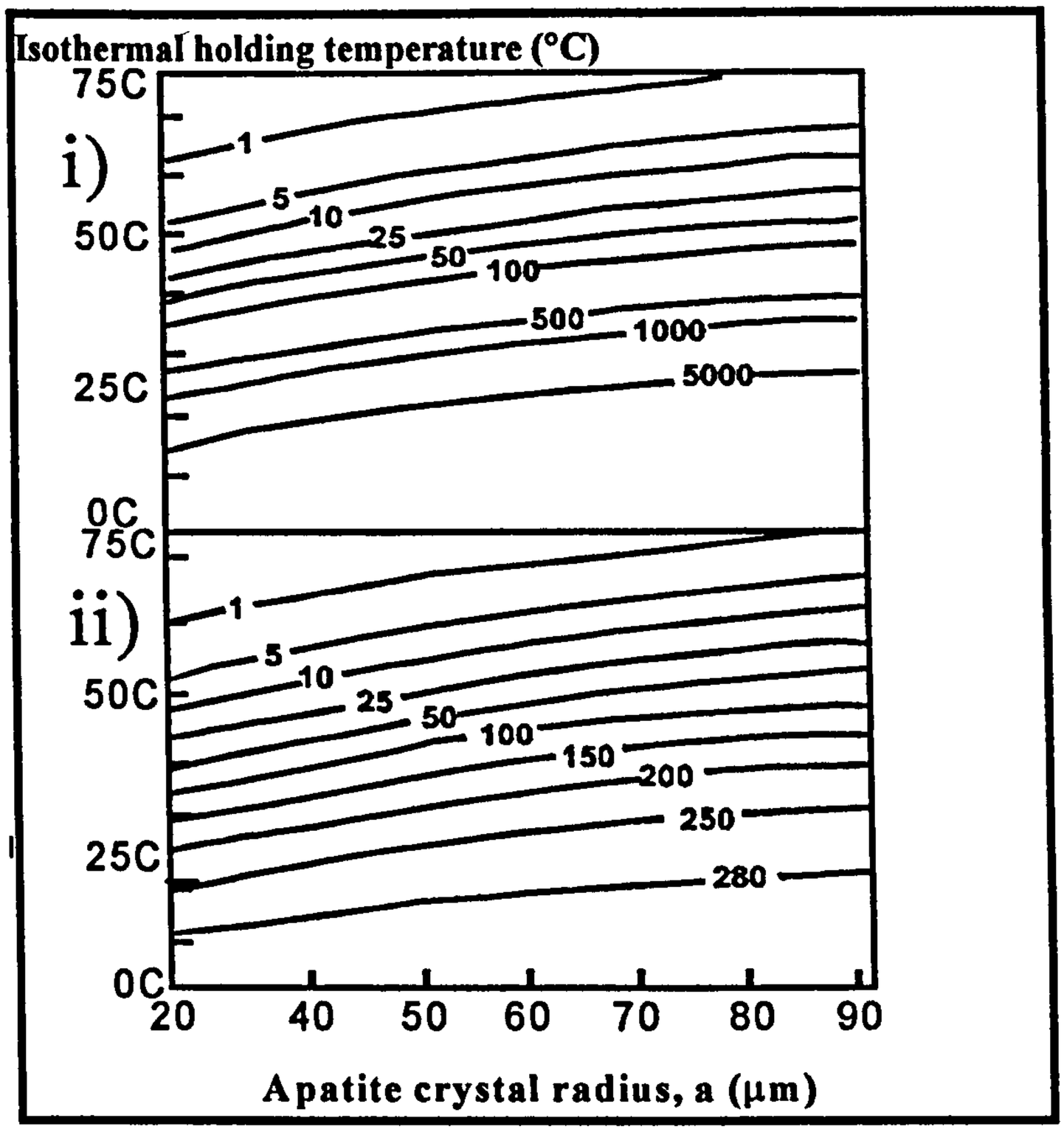

Figure 2.8: Modelled apatite He ages (in Ma) as a function of the crystal radius (*a*) and isothermal holding temperature for an infinite period (i) and a 300 Myr holding period (ii). Variations in He ages for apatite with different sizes are more pronounced at temperature below 50°C (from Reiners and Farley, 2001).

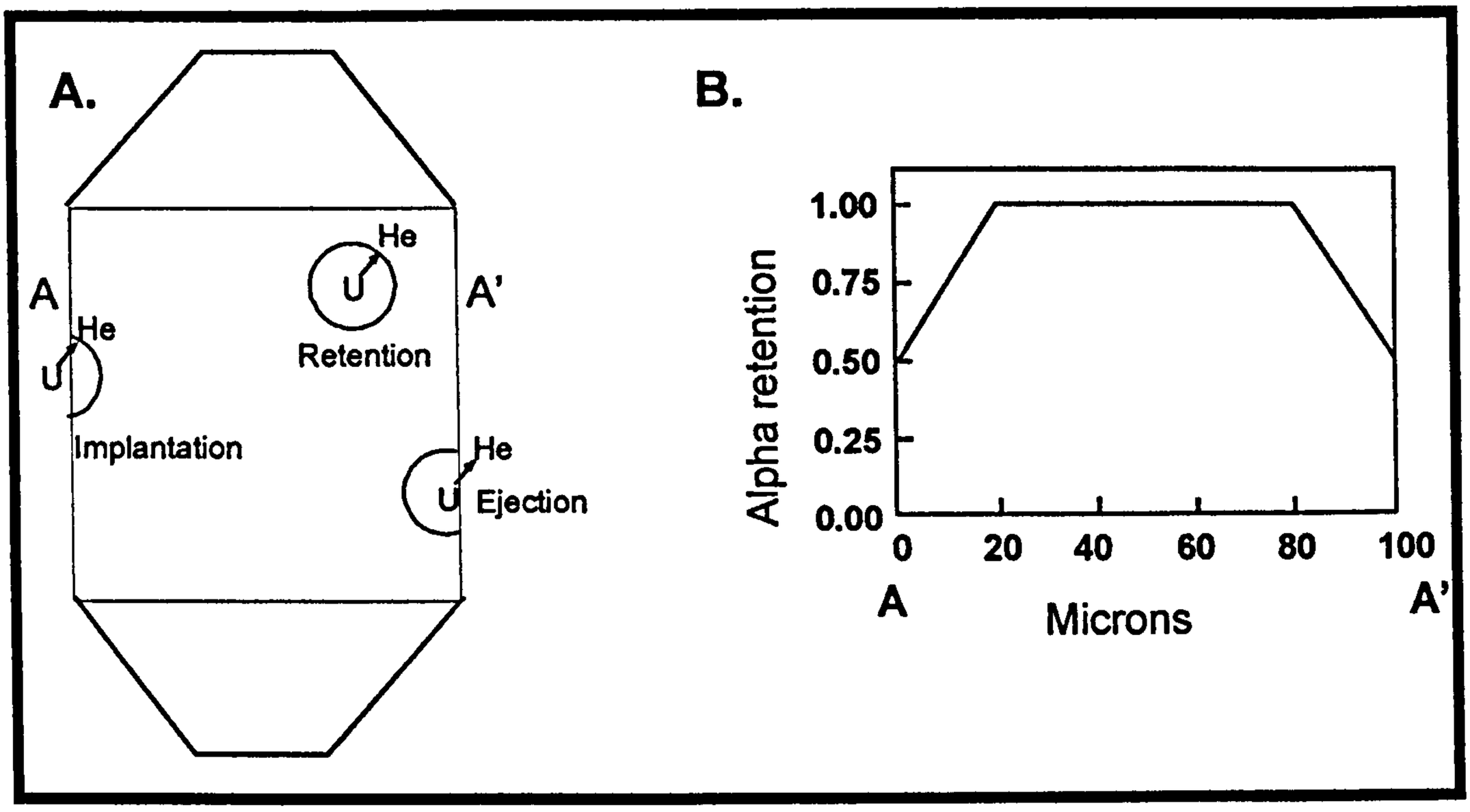

Figure 2.9: A: An illustration of the three possible cases of α recoil within a crystal: α retention, α ejection and α implantation. B: A schematic diagram of α retention changes from core to rim in a hypothetical apatite crystal (from Wolf *et al.*, 1996).

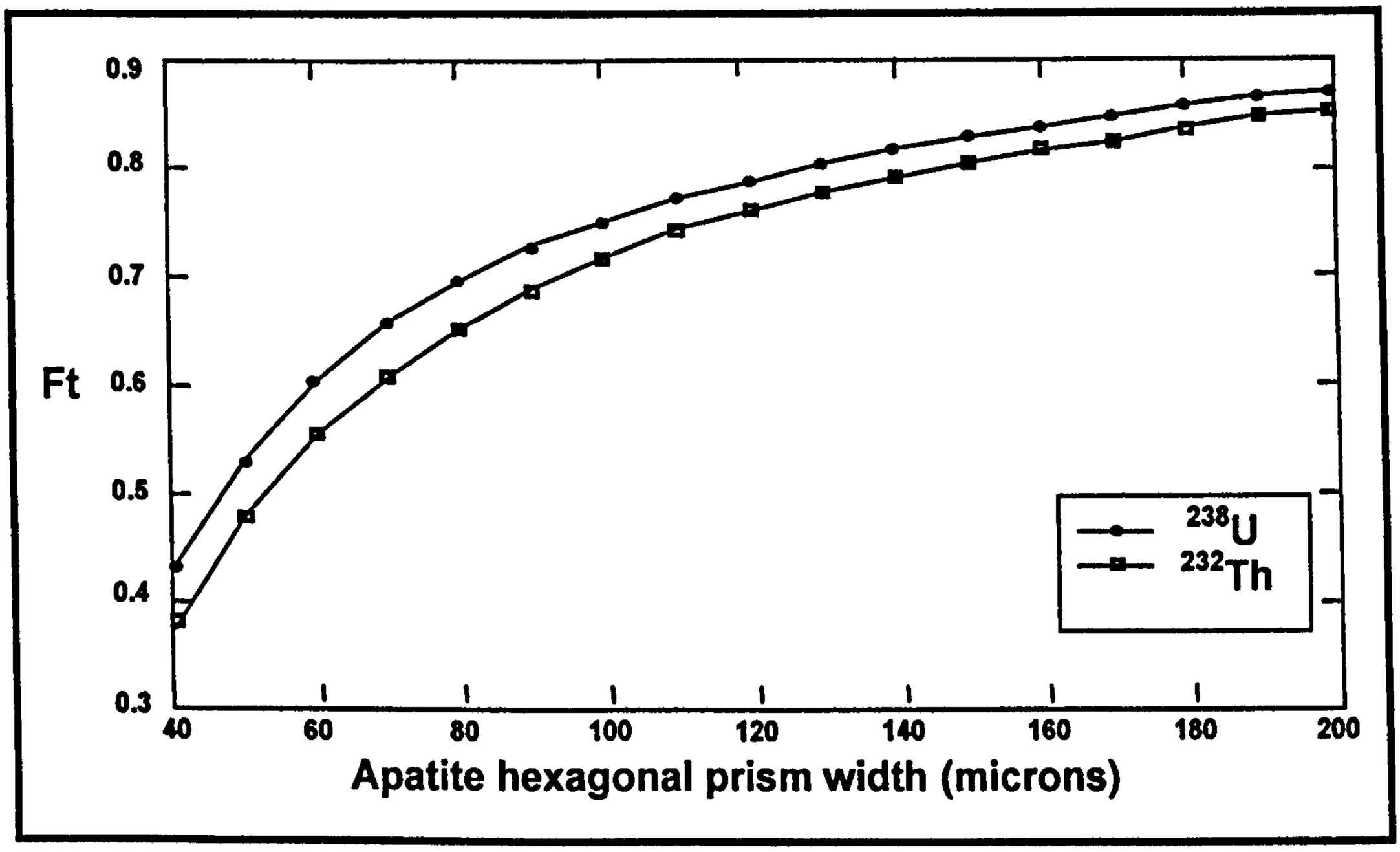

Figure 2.10: The effect of α recoil correction on apatite crystals. Ft is the total ^{4}He retained by the grain (from Farley *et al.*, 1996)

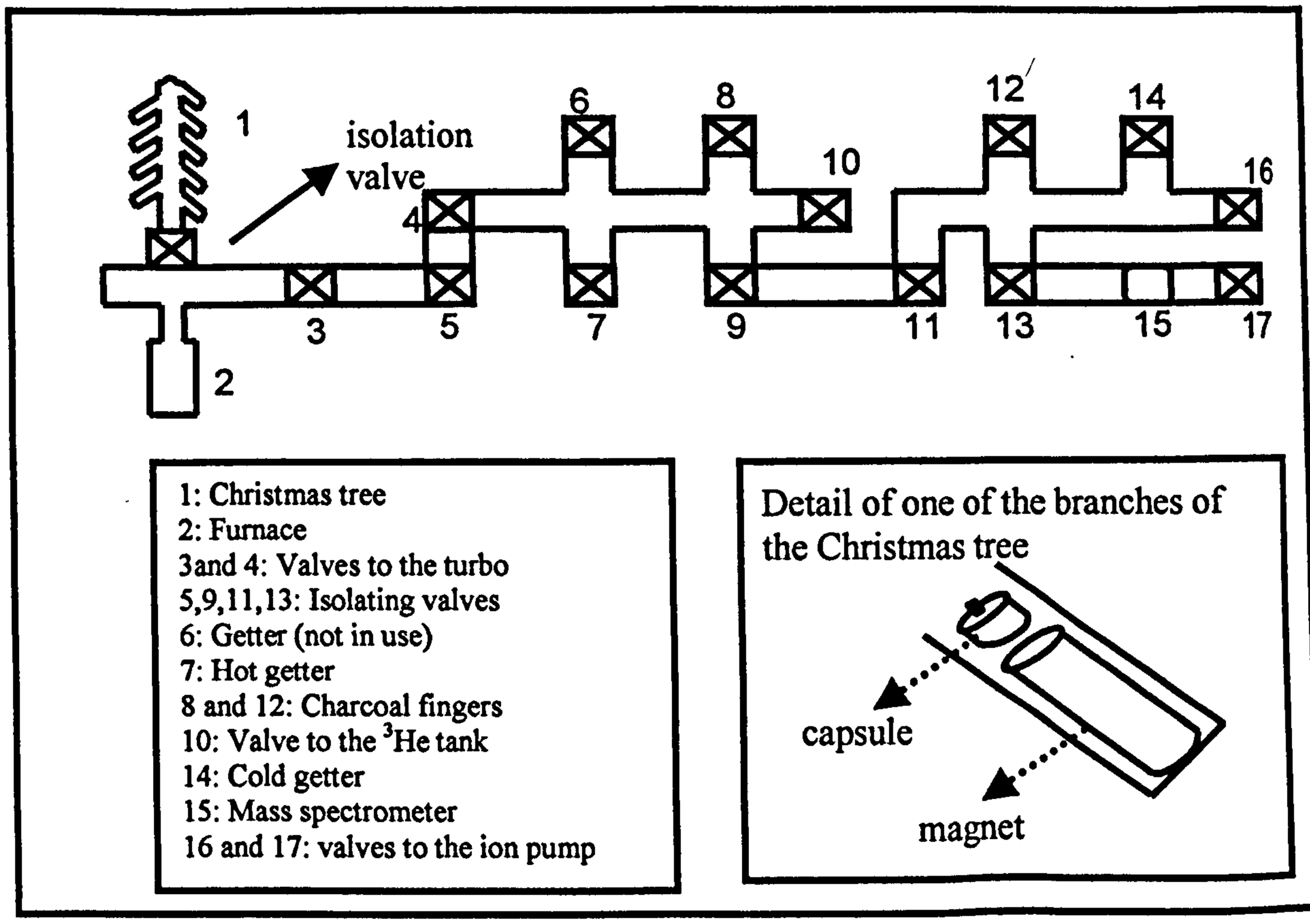

Figure 2.11: Sketch of the extraction line used for the ^{4}He analysis

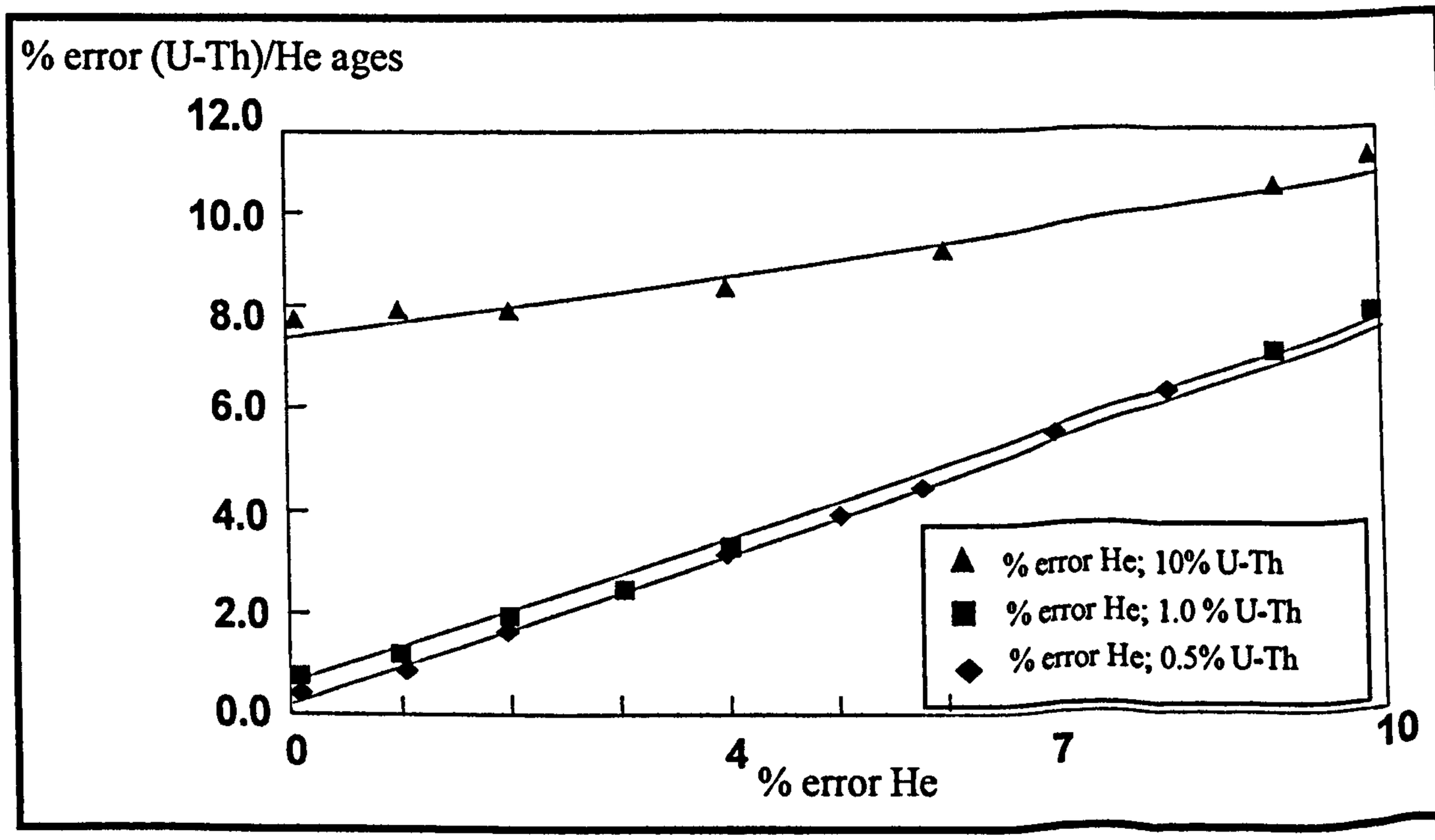

Figure 2.12: Linear error propagation (approximated) for the He versus U and Th uncertainties. The data are from experiments performed during this project.

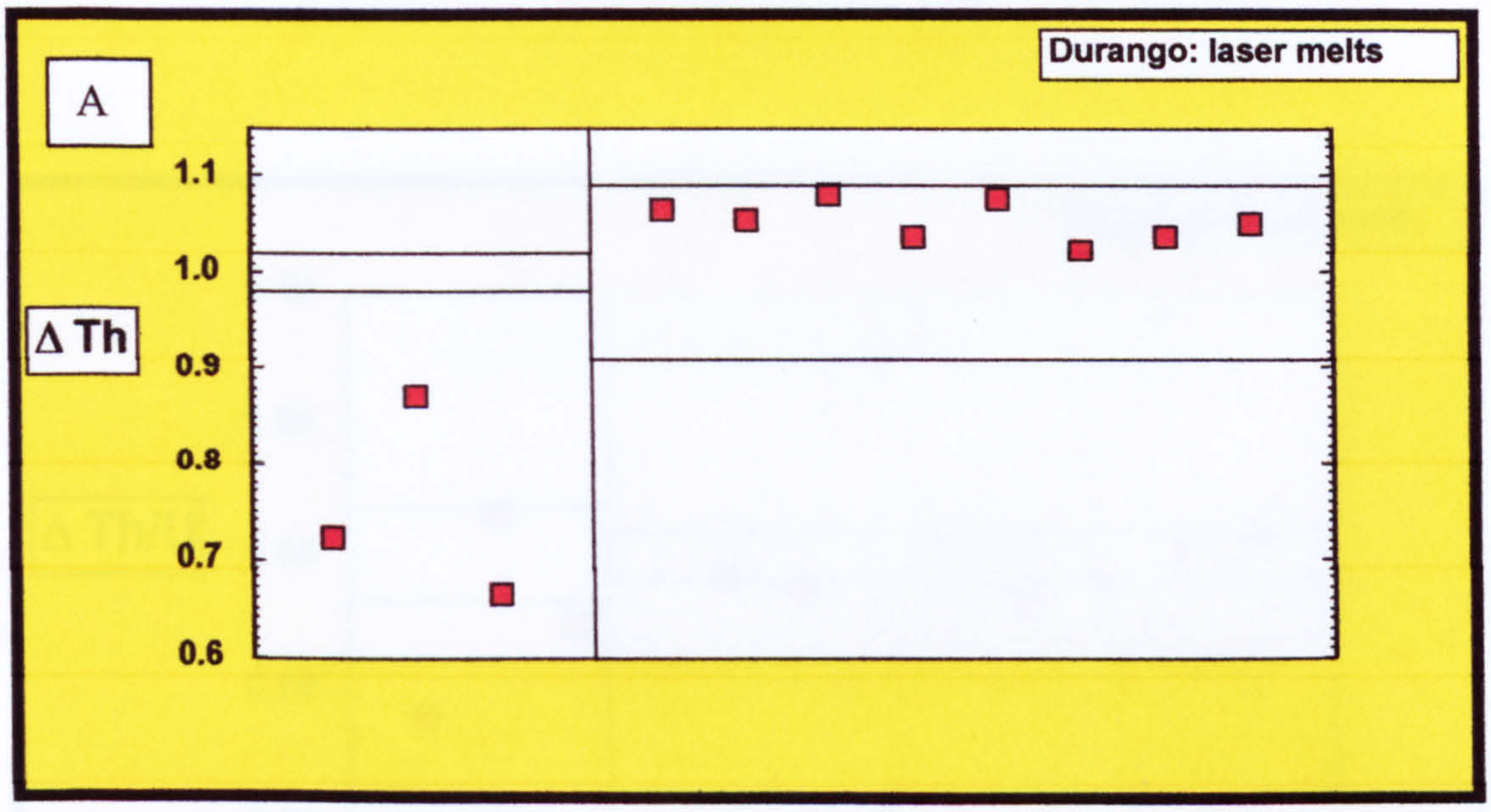

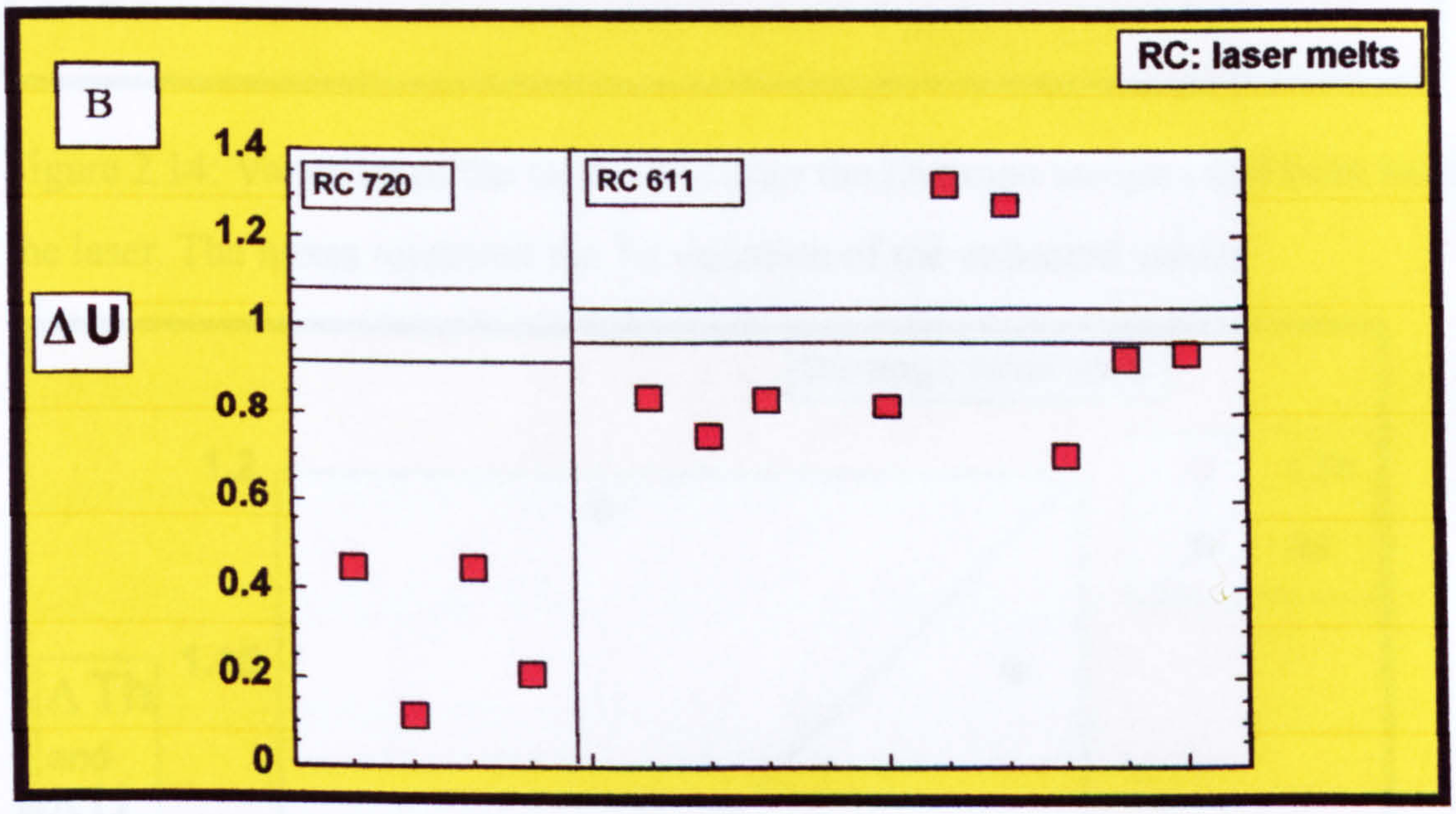

Figure 2.13: A) variation of Th content between un-heated and heated-with-laser samples of Durango apatite. The samples were heated for 1 minute (right of the vertical line) and 3 minutes (left of the vertical line) The boxes represent the 1σ variation of the unheated values.

B) variation of U content between unheated and heated-with-laser samples from the Ragatan granite (RC 720) and the Lewis gneiss (RC 611). The boxes represent the 1σ variation of the unheated values

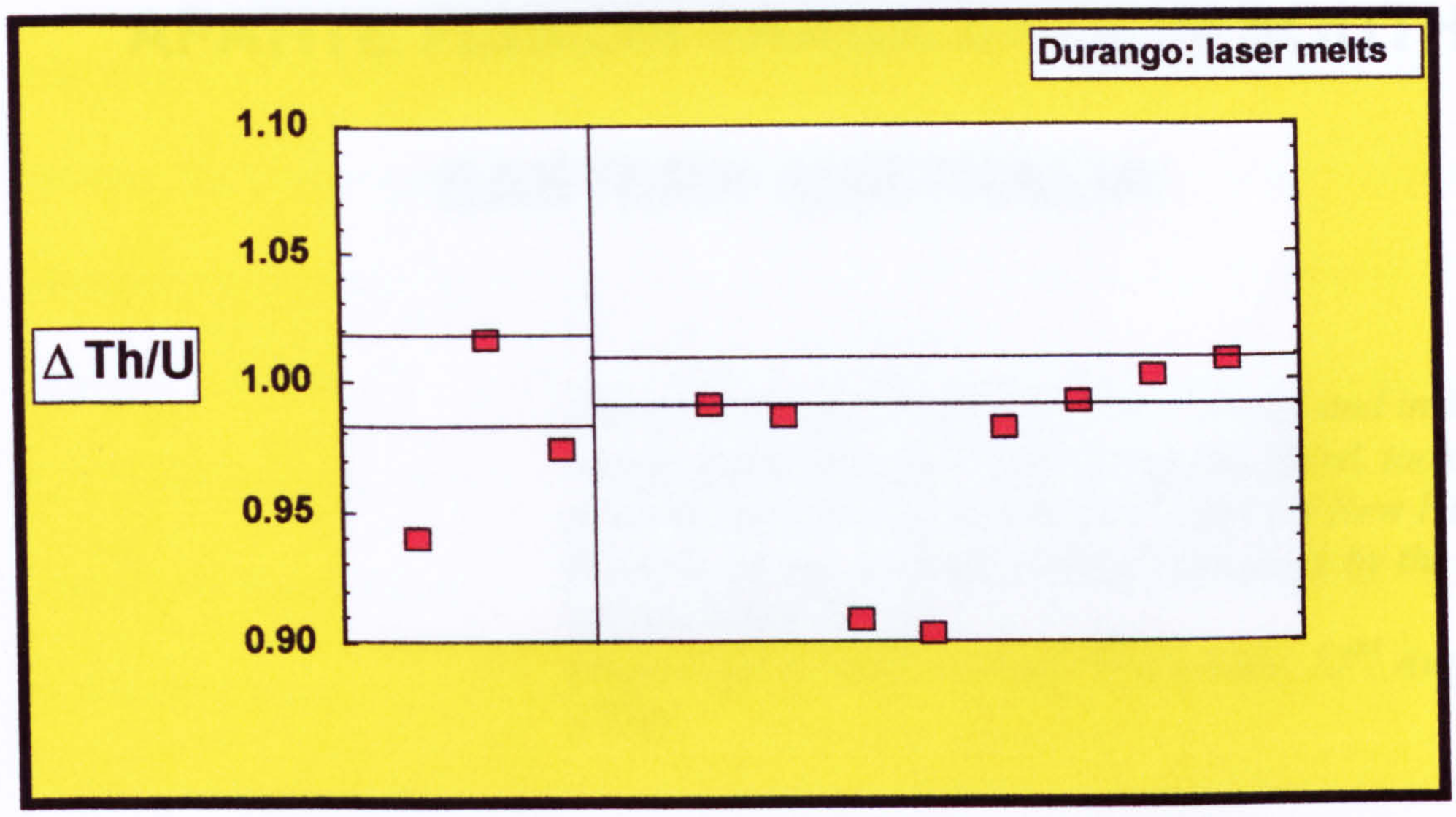

Figure 2.14: Variation of the ratio Th/U after the Durango samples had been heated with the laser. The boxes represent the 1σ variation of the unheated values

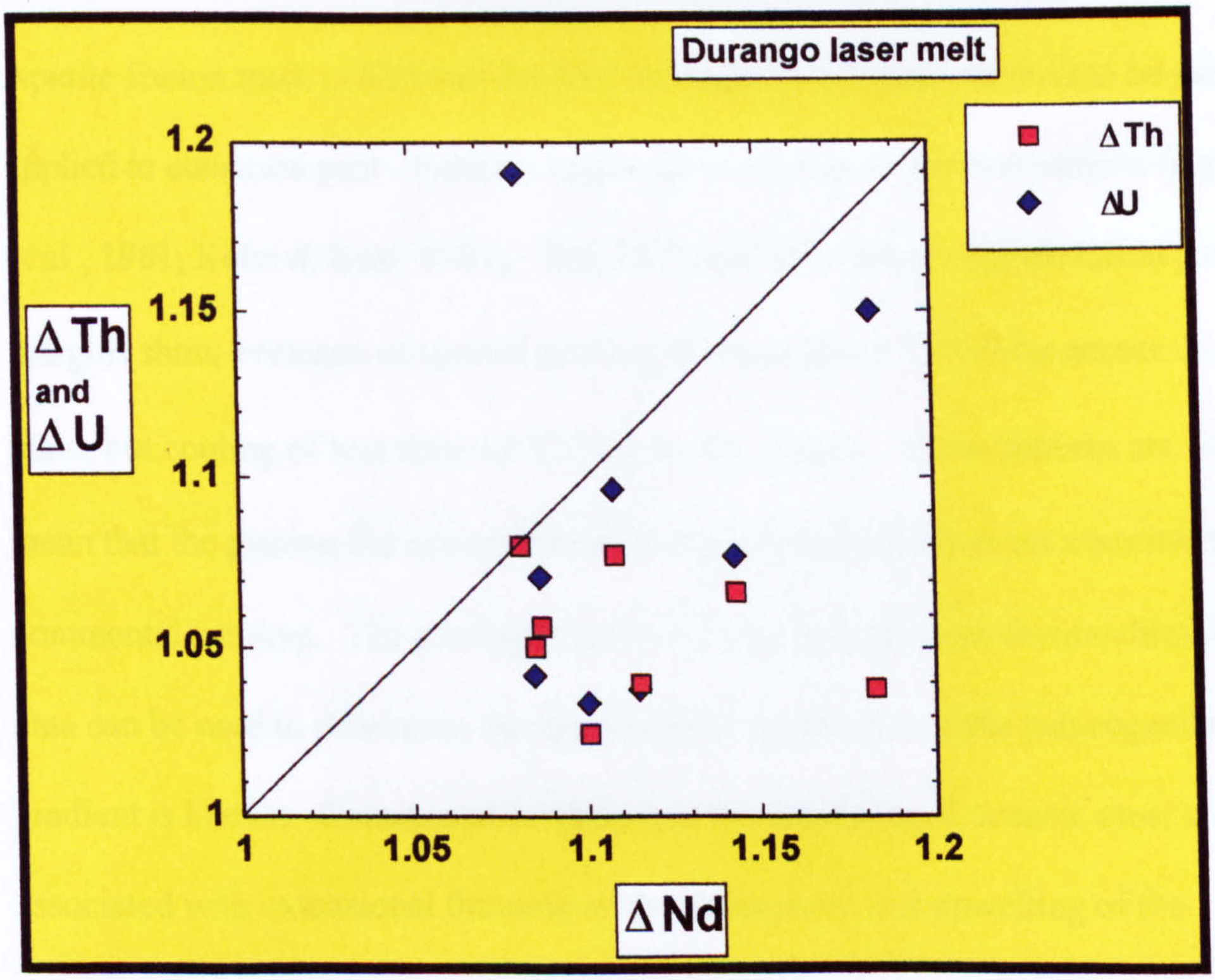

Figure 2.15: Variation of ΔTh/ ΔNd and ΔU/ ΔNd in Durango apatite that have been heated with a laser

CHAPTER THREE

APATITE FISSION TRACK DATA IN SOUTH EASTERN AUSTRALIA

I now once more hoisted English Colours and in the Name of His Majesty King George the Third, took possession of the whole Eastern Coast [of New Holland] from the above Latitude down to this place by the name of New South Wales.
(from Capt. Cook's Journal, Wednesday, 22nd August 1770)

3.1 Introduction

Apatite fission track (AFT) was the first thermochronological method to be successfully applied to constrain post - breakup landscape evolution at passive margins (e.g. Morley et al., 1981; Kohn & Eyal, 1981). The AFT data from many high elevation passive margins show evidence of syn-rift cooling of the order of 10°C/Myr across the coastal plain, but cooling of less than 0.5°C/Myr on the plateau. These patterns are taken to mean that the plateau did not experience a rapid denudational event associated with continental breakup. The cooling history of rocks derived from thermochronological data can be used to determine the magnitude of denudation if the palaeogeothermal gradient is known. Continental breakup and the formation of oceanic crust are associated with extensional thinning of the lithosphere and upwelling of the asthenosphere (e.g. Lister *et al.*, 1986), but lateral migration of heat from the rift and nascent ocean basin toward the sub-aerial margin and rift shoulders is considered to be

limited and, at least at some passive margins, practically insignificant (Wellman, 1987; Makris *et al.*, 1991; Al-Harthy, 2001, Brown *et al.*, 2002). Although invaluable information can be obtained by the application of AFTT to high elevation passive margins, the temperature range at which this method is sensitive (120-60°C) is usually adequate only to distinguish between extreme scenarios and, when the amount of crust removed is less than 2 km, the syn- and post-breakup rates of denudation yielded by AFTT are imprecise. Recent 3-D numerical models of high elevation passive margins have shown that landscape evolution scenarios and styles of escarpment evolution can be discriminated if rates of denudation are precisely constrained across the entire width of the coastal plain, even in areas where syn- and post-breakup erosion may not have exceeded 2 km (Brown *et al.*, 2002; van der Beek *et al.*, 2002). This Chapter describes new AFTT-derived constraints on the evolution of the eastern Australian passive margin and identifies the areas where the thermal histories are poorly constrained. Chapter 4 demonstrates the strength of combining AFT and (U-Th)/He thermochronometers to constrain precisely the evolution of the major landscape elements in south eastern Australia.

In this Chapter, the field area is introduced (3.2 and 3.3), the three most frequently applied models of landscape evolution at high elevation passive margins are described (3.4) and the possibility of using AFT data to discriminate between them is discussed (3.5). In section 3.6, new and published AFTT data are presented and interpreted in order 1) to determine the syn - and post - breakup denudational history of south eastern Australia and 2) to test the applicability of the three models of passive margins evolution to this portion of the margin. Although extremely informative, the

conclusions derived from the AFTT data highlight the limitations of the method and the need for a lower thermochronometer sensitive enough to accurately determine denudation differences between 1 and 2 km

3.2 Evolution of the Tasman Sea

Australia, New Zealand and Antarctica comprised eastern Gondwana in the late Mesozoic. A set of magnetic lineations identified on both sides of an extinct spreading centre in the Tasman Sea (Hayes & Ringis, 1973) show that break-up propagated from south to north (the Coral Sea), ceasing at 52 Ma (Gaina *et al.*, 1998).

The continental margin of eastern Australia developed by rifting and breakup of Australia and the Lord Howe Rise in the Late Cretaceous and Palaeogene, giving rise to the Tasman Sea (Hayes and Ringis, 1973) (Figure 3.1). This generated a narrow continental shelf, usually less than 50 km wide, with slopes of 20° that start at depths between 130 and 170 m (Jongsma & Mutter, 1977).

The Tasman Sea asymmetry and the narrow, unstructured and sediment-poor Australian margin (e.g. Colwell & Coffin, 1987) has been modelled as being produced by either a non-axial breaching of the rift valley that caused all of the pre-breakup rift valley to remain attached to the Lord Howe Rise (Jongsma & Mutter, 1977), or by a lower-plate/upper-plate detachment model (Lister & Etheridge, 1989). In the latter case, the Australian margin is interpreted to be an underplated upper plate, uplifted margin and the Lord Howe Rise the conjugate lower plate margin. Although underplating of the

Australian continental crust is consistent with seismic (Colwell *et* al., 1993) and geochemical data from xenoliths in Tertiary volcanic rocks (e.g Chen *et al.*, 1998), the timing of underplating has not been constrained and Lister & Etherigde's model still needs to be tested. The Australian is considered to be a non-volcanic rift margin and syn-breakup magmatic extrusions are limited to the Mt Dromedary (98 Ma) and a few others igneous complex offshore 101 Ma (Colwell *et al.*, 1993). The widespread volcanism present along all the Australian margin is Cenozoic and its relation with the Tasman Sea sea-floor spreading is still under discussion (e.g. Sun *et al.*, 1989; Bryan *et al.*, 1997).

3.3 Geology of southeastern Australia

Southeastern Australia consists mainly of Palaeozoic rocks of the Lachlan Fold Belt (LFB) overlain between 32° and 36°S by Permo-Triassic sediments of the Sydney Basin. The LFB is a complex orogenic belt of sedimentary and igneous rocks that crops out in central, western and southern New South Wales and extends into Victoria and Tasmania with a total area of exposure of close to 300,000 km^2 (Chappell & Stephens, 1988). The LFB was the site of extensive igneous activity during late Silurian and Devonian times when abundant granites and related volcanic rocks were produced. Usually the plutons form batholiths with a north-south elongated shape, approximately parallel to the present continental margin. Approximately half of the granites of the LFB are S-type (i.e. with a Sedimentary source) ; the others are I-type (i.e. with a Igneous source) with less than 1% of all granites being Alkali-type (White & Chappell, 1988). In the study area only I- and A-type granites are present.

Radiometric ages of the granites of the LFB are sparse, but most of the data indicate that the granites were emplaced between 440 and 390 Ma (Chappell & Stephens, 1988; Williams, 2001).

Since the Carboniferous, the surface of the LFB has been largely sub-aerial and, although the Early to Middle Cretaceous was a period of worldwide marine transgression, the LFB and the Sydney Basin were part of a large island surrounded by depositional basins (Twidale, 1994). Deep mantles of weathered bedrock developed (Hill, 1999). Bird & Chivas (1988, 1989, 1993) have argued that the oxygen-isotope signature of kaolinite in these deeply weathered palaeosols reflects the timing of formation of this secondary mineral. This age determination is based on Australia's northward drift from polar latitudes in the Mesozoic to lower latitudes and warmer climate in the Cenozoic, causing the $\delta^{18}O$ of meteoric water to become progressively higher. Based on the fact that two palaeosols in South Australia overlain by Jurassic rocks exhibit $\delta^{18}O$ of +10.3 and 12.3‰, values of $\delta^{18}O$ less than 15‰ are considered to indicate weathering profiles formed in periods prior to the late Cretaceous (Bird & Chivas, 1989). On this base, ten weathering profiles in southern New South Wales were produced during the Late Mesozoic (Bird & Chivas, 1989). Of these, nine are from the highlands and one is from the coast near Ulladulla (Figure 3.2) at 20 m a.s.l., overlain by 30 Ma basalts (Wellman & McDougall, 1974). Bird & Chivas (1993) and Nott & Purvis (1995) have used these weathering profiles to support the notion that at least part of the coastal plain in southern New South Wales was already developed in the late Cretaceous, and certainly by the Mid Tertiary. Moreover, the Eocene basalts near

Ulladulla have been used to support the hypothesis that the coastal plain must be at least 50 million years old (Young & McDougall, 1985).

In the following section a description of the most important models of high elevation passive margin evolution is presented and it is shown that, although highly informative, the geological and geomorphological evidences are not able to distinguish between different evolutionary scenarios.

3.4 Models of high elevation passive margins evolution

3.4.1 Introduction

The frequent association between escarpments and continental margins has been taken to mean that escarpments are formed through one or more of the following: erosion of a pre-existing high elevation plateau (e.g. van der Beek & Braun, 1999), base level lowering following breakup (e.g. Ollier, 1985) and marginal surface uplift during rifting and subsequent erosion of the high shoulder (e.g. Gilchrist & Summerfield, 1994). The long-term persistence of escarpments up to 200 km inland of coastlines, has been variously explained by rift-related uplift due to magmatic underplating (e.g. Lister *et al.*, 1991; O'Sullivan *et al.*, 2000), flexural isostatic uplift in response to denudation and offshore loading (Gilchrist & Summerfield, 1990; Summerfield, 1991) or a combination of the two (e.g. Kohn *et al.*, 2002).

Three main models of escarpment formation and evolution at high elevation passive margins have been developed (Gallagher et al., 1998). They are schematically illustrated in Figure 3.3. These models are predominantly qualitative and differ in the nature of the syn- and post-breakup tectonics, and the style and rates of escarpment evolution. These models are referred as:

a) Escarpment retreat across a downwarped rift shoulder;

b) Escarpment retreat across a high elevation rift shoulder;

c) Excavation-in-place of a high elevation rift shoulder.

3.4.2 Escarpment retreat across a downwarped rift shoulder model

This model was proposed by King (1950, 1955) to explain the formation and evolution of the series of scarps he identified along the south African margin. Ollier (1982) applied the same idea to the eastern margin of Australia. He indicated that, as a consequence of continental breakup "tectonic uplift warped a pre-existing plain, and on the steeper, eastern slopes erosion carved steep, gorge-like valleys that eventually coalesced into a continuous escarpment" (Ollier, 1982; p. 13). According to this model the tectonic uplift associated with continental breakup and opening of the Tasman Sea gave rise to the Continental Drainage Divide (CDD) and initiated a phase of deep valley incision to the east. The newly formed coastal plain was backed by an escarpment that retreats inland, toward the warp axis. In this model, the escarpment is never a drainage divide. Remnants of the pre-breakup landsurfaces are thought to be found seaward of the escarpment as high elevation plateaus surrounded by a low altitude, dissected

coastal plain (e.g. the Bulga and the Dorrigo Plateaus in New England, Figure 3.2). Based on this assumption, Seidl *et al.* (1996) reconstructed the old landsurface and concluded that the area near the present coastline in New England was about 300 m above sea level at the time of breakup. This implies a gradient of approximately 1° for the downwarped rift shoulder. Supporting evidence comes in the form of "coastal facets" (Ollier & Pain, 1997), triangular-shape coastal surfaces that are believed to be remnants of the palaeosurface, the pre-breakup plateau surface that was warped during rifting. A few of these coastal facets are located south of Bega (Figure 3.2) at the site of sample 00-CP-36 (Chapter 4). In some areas near the coast (e.g. Ulladulla, Figure 3.2), late Cretaceous and early Tertiary igneous rocks have been recognized (Nott & Purvis, 1995; Young & McDougall, 1985). Although Nott & Purvis (1995) and Young & McDougall (1985) considered these igneous rocks to be an indication of a very early formation of the coastal plain and retreat of the escarpment, Ollier & Pain (1997) interpreted the basalts as remnants of the downwarped palaeosurface, bypassed by the erosion.

According to the downwarped model, denudation was at a minimum, possibly less than 500 m at the present coastline, reaching a maximum equal to the elevation of the escarpment (up to 1200 m) at the foot of the escarpment (Seidl *et al.*, 1996). Although the model implies that the lithosphere has some elasticity, in order to allow downwarping of the margin, isostastic rebound is not included, claiming that the amount of denudation is not enough to cause significant passive uplift, a somehow circular argument. Erosion on the plateau is considered to be negligible.

3.4.3 Escarpment retreat across a high elevation rift shoulder

Escarpment retreat models (e.g. Gilchrist *et al.*, 1994; Kooi & Beaumont, 1994; Tucker & Slingerland, 1994) incorporate a steep (10°-30°) escarpment formed at a new continental margin either by differential vertical displacement across normal faults (e.g. Brown, 1991) or by the drop of the base level due to continental breakup (e.g. van der Beek *et al*, 1999). Large scale (up to 1000 km^2) numerical surface process models predicting long-term lanscape evolution indicate that for escarpment retreat to occur the top of the escarpment must be a drainage divide, a necessary, but not sufficient condition, as other requirements need to be met (Kooi & Beaumont, 1994). The presence of high relief between the plateau surface and the base level, and a poorly developed drainage net favour steepening (and so slope failure processes) and lateral migrations of the channels (Tucker & Slingerland, 1994). Escarpment retreat is also favoured by flexural isostasy which produces continuous backtilting of the escarpment, preserving the slope, increasing the relief between the plateau and the base level, and significantly enhancing the amount of denudation as channels cut into an isostatically uplifted crust (Kooi & Beaumont, 1994).

Figure 3.4 shows a 1-D model prediction of the evolution of topography, denudation and rates of denudation for an escarpment retreat scenario. It is important to note that escarpment retreat rates in Figure 3.4 are constant through time, but that syn-rift denudation rate at the coast is at least one order of magnitude greater than at any other point across the coastal plain and it rapidly decays to the present values (<20 m/Myr). In this scenario the amount of denudation is greatest at the coastline (the value depending on the flexural isostatic rebound allowed by the chosen elastic thickness of

the lithosphere, T_e) and it decreases towards the foot of the escarpment. Syn- and post-breakup denudation is negligible on the plateau (Figure 3.4).

Estimates of escarpment retreat rates in eastern Australia are wide-ranging. Constant rates are usually calculated by dividing the width of the coastal plain by the time since breakup, and such rates vary between 1 and 2 km/Myr (e.g. Ollier & Pain, 1997; Seidl et *al.*, 1997). Three basalts a few kilometres north of Ulladulla (Figure 3.2) have K-Ar ages of between 26.6 and 30.0 Ma (Wellman & McDougall, 1974). The escarpment lies only 4.5 km beyond the westernmost dated basalt on the coastal plain (Young, 1982) providing a maximum Neogene escarpment retreat rate of about 150 m/Myr (Nott *et al.*, 1996). Extrapolating this rate back to the time of sea-floor spreading (85 Ma) gives an escarpment retreat of 13 km. Even assuming that the escarpment was formed in the early stages of continental extension (some 40 Myr before sea-floor spreading), the maximum width of the costal plain obtained using the constant value of escarpment retreat rate of 150 m/Myr is 19 km. However, in southern New South Wales the coastal lowlands range from 60 (southern New South Wales) to 200 km wide (New England) (Seidl et al., 1997). Consequently, escarpment retreat rates must vary spatially if they are assumed to be temporally constant.

Constant escarpment rates of the order of 1-2 km/Myr are one order of magnitude higher than the erosion rates calculated from cosmogenic isotopic analyses of samples collected across the escarpment, seaward of major knickpoints (Weissel & Seidl, 1998). Maximum soil production rates of 53 m/Myr have been derived from ^{10}Be and ^{26}Al analyses on the escarpment in the upper Bega valley (Heimsath *et al.*, 2000). These data seem to indicate that, at present the escarpment is a slow evolving feature. The

large discrepancy between vertical and lateral retreat rates may be an indication that knickpoints retreat may not indicative of escarpment retreat rates, as in some areas (e.g. in northern New South Wales) knickpoints lie well inland of the present escarpment.

3.4.4 Excavation in place of a high elevation rift shoulder

In this class models (also called downwearing or plateau degradation) the high elevation rift shoulder is excavated *in situ* by rivers flowing to the base level of the new ocean and the coastal plain is formed by degradation of the interfluves (e.g. Gilchrist *et al.*, 1994; van der Beek *et al.*, 2002). The evolution of the coastal plain is controlled by the presence of a well-developed, pre-breakup drainage divide inland of the newly formed escarpment. Theory predicts that the coastal plain is formed rapidly and a new escarpment develops at the location of the initial divide (e.g. Gilchrist et al., 1994; van der Beek, 2002). A numerical model based on field observations in south western Africa predicts that, when a pre-rift drainage divide lies less than 100 km inland of the new coast, escarpment retreat does not occur (Gilchrist *et al.*, 1994). "In the first 30 Myr of evolution [in the numerical model] the escarpment and the upland are strongly incised as the river heads retreat rapidly toward the divide powered by the discharge from the large upland catchment" (Gilchrist et al., 1994; p. 12,223). The model predicts that the initial river incision process occurs rapidly, but the strike-averaged denudation rate remains much lower than in the escarpment retreat model because large interfluves are still present. After 30 Myr steep-sided valleys are still dominant as the isostatic rebound due to denudation in the channels enhances the elevation of the interfluves, possibly to become higher than the initial topography. The interfluves are slowly

eroded away and denudation becomes concentrated on the escarpment that starts to retreat (Gilchrist *et al.*, 1994). These results are reproduced by the 3-D model suggested by van der Beek *et al.* (2002) (Figure 3.4). According to this model, while the coastal plain is excavated, the drainage divide does not retreat. This is due to the fact that fluvial processes dominate over hillslope diffusion and the retreat of the river-heads slows as channels collect progressively less water as they approach the divide. Drainage divides neither erode nor migrate and such models are referred to as "pinned divide" models (Kooi & Beaumont, 1994).

As flexural isostasy acts on the entire coastal plain at the same time, the amount of denudation is more constant across the lowlands than in the escarpment retreat case, although denudation propagates from the coast toward the interior, as when the escarpment retreats. The amount of denudation on the internal plateau is negligible in this model. A combination of AFT data and cosmogenic radionuclide concentrations in Namibia demonstrate that the rate of denudation seaward of the escarpment has been <20 m/Myr since the Eocene, but it has been at least one order of magnitude higher during rifting (Cockburn *et al.*, 2000). These results suggest that the data are consistent with a downwearing rift shoulder scenario, but not with an escarpment retreat model at constant pace (Cockburn *et al.*, 2000).

3.5 Testing escarpment evolution models using fission track data

Gallagher *et al.* (1998) showed that each of the models described above should be characterised by different apatite fission track age distributions across the margin (Figure 3.5). A downwarped rift shoulder model and its minimal denudation will be indicated by fission track ages at the coast and on the plateau that are considerably older than sea-floor spreading, and younger ages, but still older than oceanic crust formation, on the coastal plain at the foot of the escarpment, where denudation is at a maximum. The models of downwearing and escarpment retreat are both associated with syn-rift apatite fission track ages at the coast that become progressively older toward the plateau. It is difficult, however, to differentiate between the two scenarios (e.g. Abbate *et al.* 2002.). In the case presented by Gallagher *et al.* (1998) the difference between the two models is only evident on the inland plateau, where the amount of denudation is more pronounced in the case of a downwearing scenario (Figure 3.3 and 3.5). This predicted variation of apatite fission track ages assumes that a syn-rift lowering of the base level occurs both sides of the drainage net. The difference between predicted apatite fission track ages across the coastal plain for the two models is modest and it may be masked by the uncertainties in the data. Moreover these predictions are quite simplistic, as they assume a constant and normal (25-30°C/km) geothermal gradient across the margin, and they do not take in consideration the timing of escarpment evolution.

Apatite fission track data from five high elevation passive margins are summarized in Figure 3.6. Despite the complexity and variations within and among the different datasets, the youngest ages are generally confined to the present coastline (e.g. eastern Australia and western India), or across the coastal plain (e.g. south western Africa and south eastern Brazil), whereas the oldest ages characterise the inland, high elevation plateau. Moreover, the youngest ages are similar to, or slightly younger than the time of breakup, indicating that AFT dating records the drop in base level. These trends are inconsistent with the downwarped rift shoulder model, and are compatible with both other scenarios.

Another typical feature of the apatite fission track data at passive margins is the "boomerang pattern" (Green, 1986). This shows that samples collected along a traverse from the present coastline, across the coastal plain and escarpment, on to the plateau have experienced different amounts of syn- and post-breakup cooling, and therefore different amount of denudation. In Figure 3.7 fission track ages are plotted versus the mean track length. The young fission track ages are characterised by long mean track length indicative of rapid cooling through the PAZ at the time of continental breakup. As ages increase across the coastal plain, the mean track length decreases, indicating that these samples have experienced syn-rift cooling from successively lower maximum temperatures. On the plateau, the oldest ages are associated with track length distributions dominated by long track lengths, indicating that the samples left the PAZ a long time before the samples now on the coastal plain. The "boomerang plot" is not always obvious and a large number of data is often necessary to show the trend convincingly.

3.6 Apatite fission track data in eastern Australia

Hundreds of apatite fission track data have been published from the eastern Australian margin (Morley et al., 1981; Moore et al., 1986; Dumitru et al., 1991; O'Sullivan *et al.*, 1995; Kohn *et al.*, 2002). The apparent ages range from ~350 Ma on the plateau to ~100 Ma near the coast (Figure 3.8). The mean track lengths tend to be longer (up to 14 μm) near the coast and on the plateau top, whereas across the coastal lowland they are variable between 13.5 and 11 μm (Figure 3.9). The young fission track ages and long track lengths suggest that, at time of continental extension and breakup, the samples now at the coast were at or above 110-120°C. Based on vitrinite reflectance data from the Sydney Basin, Moore *et al.* (1986) considered a moderately high palaeogeothermal gradient (38-53°C/km) and suggested removal of crustal section of 2-2.5 km at the coast and less erosion (1.5-2 km) at the foot of the escarpment. They considered that the pattern of the apatite fission data across the eastern highlands is due to differential post-breakup erosion rather than to any component of differential uplift. They also suggested that the thermal effects of continental rifting extended into the continental interior, increasing the palaeogeothermal gradient across the coastal plain up to the present foot of the escarpment, some 50 km inland of the coast. Although Moore *et al.* (1986) were unable to constrain the palaeogeothermal gradient at the time of breakup, Dumitru *et al.* (1991) used vitrinite reflectance data from the Sydney Basin of Middleton & Schmidt (1982) to suggest that high geothermal gradients were also present in southern New South Wales and constrained the amount of denudation at the present coastline to 1.5-3 km. Numerical thermal models, however, predict that the geothermal gradient in the rift flanks orthogonal to the spreading axis is unlikely to be

affected by rifting (van der Beek et al., 1995; Gallagher & Brown, 1997). Normal geothermal gradients (25-30°C/km) combined with the AFT data constrain the amount of denudation in south eastern Australia during rifting and breakup to up to 4 km at the present coastline, but to less than 2 km at the foot of the escarpment. However, the sedimentary sequences in the Sydney Basin are horizontal (Herbert & Helby, 1980), indicating that upwarping of the margin did not occur, at least in this area.

Despite these insights, the syn- and post-breakup landscape evolution derived from the AFT data in southern New South Wales is still confused. AFT ages of more than 150 Ma from the Palaeozoic basement of the coastal plain (Figure 3.8) can be taken to indicate that rifting did not enhance denudation and that the young AFT ages found on or just south of the Sydney Basin are due to local high geothermal gradients and/or removal of sedimentary cover. In this case, the downwarped rift shoulder model cannot be ruled out with certainty. In the next section new fission track data from 14 samples collected in southern New South Wales are presented and interpreted. These samples are a sub-set of the apatite samples that were used for (U-Th)/He age determinations (Chapter 4).

3.6.1 Apatite fission tracks results

All the samples for apatite fission track analyses were collected from granites from the Bega Batholith, at elevations from sea level up to 1140 m on the plateau top along traverses close to the Towamba River and seaward of Brown Mt. (Figure 3.10, 3.11). The sampling aimed to collect a suite of samples over the maximum possible range of

elevations that encompasses the main geomorphological features of the margin and the escarpment in particular. Samples 00-CP-04, 00-CP-05 (Towamba River traverse) and 00-CP-33, 00-CP-36 (Brown Mt. traverse) are from A-type granites, the others from I-type granites (section 3.2).

Apatite fission track ages and confined track lengths and Dpar measurements are reported in Table 3.1. Dpar were measured to account for the chemical composition of the apatites, which affects the fission track ages (Chapter 2). Ages were determined using the external detector method (Gleadow, 1981) and the zeta calibration technique (Hurford & Green, 1983). Details of the zeta calibration measurements, and sample preparation procedures are reported in Appendix 2. Between 4 and 20 grains for each sample were identified for fission track age determinations. None of the fission track ages failed the χ^2 test, indicating that within a single sample the apatite composition does not vary.

3.6.1.1. Brown Mt. traverse

The apatite fission track ages of the eight samples from the Brown Mt. traverse range from 90 ± 4 Ma (1σ) at sea level to 262 ± 28 Ma on the plateau at an elevation of 1140 m. Only the coastal plain sample 99-OZ-13 yields an AFT age (90 ± 4 Ma) that is statistically indistinguishable from the time of breakup. All the other samples are older, increasing towards the foot of the escarpment. Samples 00-CP-36 and 00-CP-33 on the coastal plain yield AFT ages of 188 ± 10 and 246 ± 22 Ma respectively, which are over 100 Myr older than sea-floor spreading (85 Ma). These are supported by similar ages reported by Moore *et al.* (1986) in the same location. The Dpar measurements of these

two samples show that tracks consistently have etch pits with a diameter larger than 2.5 μm, indicative of an apatite chemical composition more resistant to annealing than a standard Durango (Dpar = 1.8 μm). The Dpar measurement has been included in the AFTSolve model, so that the effect of the chemical composition of the apatite has been taken in consideration. On the escarpment face (99-OZ-08) and on the plateau (99-OZ-10 and 99-OZ-09), AFT ages are statistically undistinguishable, and vary between 252±15 (99-OZ-08) and 261±28 (99-OZ-10). The Dpar indicate that the chemical

Sample name (N° crystals)	ρ_D (N_D)	ρ_s (N_s)	ρ_i (N_i)	χ^2	AFT age (±1σ) (Ma)	Mean track length(±σ) (μm) (N° tracks)	Dpar (±1σ) (μm)
Brown Mt. traverse							
99-OZ-13 (20)	12.6 (7887)	0.051 (866)	0.13 (2226)	72.83	90±4	14.2±1.2 (118)	1.87±0.05
99-OZ-12 (14)	17.4 (7887)	5.815 (296)	13.438 (684)	14.86	137±5	13.7±1.31 (107)	1.85±0.05
00-CP-36 (19)	16.6 (7745)	13.055 (718)	20.873 (1148)	16.05	188±10	13.08±1.9 (80)	2.54±0.04
00-CP-35 (11)	14.9 (7745)	3.302 (282)	7.4 (632)	6.7	121±9	13.6±1.94 (80)	1.91±0.05
00-CP-33 (12)	16.4 (7745)	10.35 (296)	11.783 (337)	12.45	246±22	12.03±2.66 (44)	2.61±0.07
99-OZ-08 (4)	16.9 (7745)	4.945 (90)	6.429 (117)	7.08	251±42	13.1±1.63 (31)	1.87±0.05
99-OZ-09 (12)	17.1 (7745)	11.042 (636)	13.924 (802)	5.12	262±28	12.34±1.85 (67)	1.82±0.05
99-OZ-10 (20)	10.5 (7745)	4.205 (841)	3.115 (623)	22.85	252±15	12.9±2.1 (62)	1.82±0.05
Towamba River traverse							
00-CP-02 (14)	17.4 (7745)	5.344 (272)	13.438 (684)	12.76	127±10	13.8±2.05 (68)	1.88±0.05
00-CP-03 (14)	14.1 (7745)	5.142 (343)	9.535 (636)	19.91	135±10	13.45±1.94 (71)	1.87±0.07
00-CP-04 (16)	16.5 (7887)	4.958 (354)	13.002 (817)	8.57	195±21	13.25±2.41 (71)	2.8±0.05
00-CP-05 (19)	14.8 (7745)	3.643 (402)	8.124 (1181)	24.35	193±19	12.20±2.84 (84)	2.6±0.03
00-CP-11 (11)	14.6 (7745)	11.433 (726)	14.63 (929)	11.26	207±11	12.65±2.27 (77)	1.93±0.05
00-CP-10 (20)	14.4 (7745)	4.789 (704)	4.238 (623)	13.78	301±18	13.5±1.68 (99)	1.89±0.04

Table 3.1: AFT data from the 14 samples collected in southern New South Wales.

composition of these samples is similar to Durango, suggesting that their old AFT ages are the result of slow Mesozoic and Cenozoic cooling, the rate of which can be determined by using a thermal model (see below).

The track length distribution of 99-OZ-13 is strongly unimodal with a mean confined track length of 14.2 ± 1.2 μm (Figure 3.12). The mean track length of samples across the coastal plain decreases to 12.03 μm (00-CP-33) toward the foot of the escarpment, whereas the standard deviation of the mean increases up to 2.66 μm, as the confined tracks have a bimodal distribution of lengths between 8 and 15 μm (Figure 3.12). The samples on the plateau and escarpment face have mean track lengths similar to those at lower elevations, but the standard deviation of the mean is smaller (up to 1.85 μm), as the track length distribution is negatively skewed toward long tracks (Figure 3.12)

3.6.1.2 Towamba River traverse

Along the Towamba River traverse the AFT ages are young near the coast (127±10 Ma), increasing to 301±18 Ma on the plateau, showing the same trend as that of the Brown Mt. traverse (Figure 3.10, 3.11). The lowest elevation sample is from 23 km inland of coast and it yields 127±10 Ma AFT age, which is older than breakup time, but is comparable to the AFT age of sample 00-CP-35 (121±9 Ma) which is 28 km inland of the coast along the Brown Mt. traverse. Two samples on the coastal plain (00-CP-04 and 00-CP-05) yield AFT ages of 195±21 and 193±19 Ma, respectively. These old ages reflect the samples' high Dpar value (2.8±0.05 and 2.6±0.03 μm), indicative of a stronger resistance to annealing than a Durango apatite. The samples on the escarpment

face and on the plateau yield very old ages, which are not related to apatite composition; 00-CP-10 yields the oldest measured FT age of 301± 18 Ma.

Mean track lengths of samples decrease from the coast to the foot of the escarpment from13.8 μm (00-CP-02) to 12.2 μm (00-CP-05). The standard deviation of the mean ranges between 2.05 and 2.84 μm, indicative of the fact that inland samples may have spent longer time in the PAZ than those along the coast (Figure 3.12). Sample 00-CP-10 from the plateau has a mean track length of 13.5 μm and a negatively skewed track length distribution, suggesting a time of cooling below 60°C prior to the samples at lower elevations (Figure 3.12).

3.6.2 Thermal modelling

3.6.2.1 Introduction

A thermal model has been used to identify the cooling histories that fit the apatite fission track data and to provide a semi-quantitative estimate of the denudational evolution of the margin. Rates of cooling and denudation are presented in Chapter 4, where, by combining AFT data and (U-Th)/He ages, the thermal histories are better constrained. The thermal histories for each sample presented here are derived only from the FT data. In Chapter 4 the apatite (U-Th)/He ages are included in the thermal histories. The rationale of this exercise is to separate clearly the information derived from the AFT and (U-Th)/He data, not least because a previously untested methodology has been used here to couple the two thermochronometers.

Mica K-Ar ages from the Bega Batholith indicate that the present land surface exposes rocks that had cooled to below ~300°C by ~400 Ma (Foster & Gray, 2000). $^{39}Ar/^{40}Ar$ and K/Ar ages of K-feldspars from the Cooma granodiorite, on the plateau (Figure 3.2), indicate that by 390 Ma the granite was at about 170°C (Fergusson & Phillips, 2001). These constraints can be used to determine the cooling history that have characterised different parts of the traverses. Figures 3.13 and 3.14 show the envelope of the thermal histories that best fit the data ($\chi^2 > 5\%$) along the two traverses using AFTSolve (Ketcham *et al.*, 1999). The best-fit line is also shown and closer it is to the borders of the envelope, the poorer the fit to the AFT data. The initial track length is taken to be 16.3 μm and a Monte Carlo algorithm is used (Ketcham *et al.*, 1999). The present surface temperature is taken to be 17°C (Bird & Chivas, 1993).

3.6.2.2 Brown Mt. traverse thermal histories

Samples closest to the coast (99-OZ-13; 99-OZ-12; 00-CP-36)

Some of these three thermal histories and the best-fit lines (Figure 3.13) are characterised by an episode of rapid cooling that brought the samples from more than 120°C to less than 60°C no later than 80 Ma, although constant cooling since 200 Ma cannot be discarted. The best-fit line for the three samples indicates that this rapid cooling event is likely to have started at about 120-110 Ma (99-OZ-13), although it cannot be ruled out that it started as early as 150 Ma (99-OZ-12 and 00-CP-36).

Samples across the coastal plain and on the escarpment face (00-CP-35; 00-CP-33; 99-OZ-08)

The thermal histories of these samples are complicated, as they must account for the bimodal distribution of the track lengths and the chemical composition of the apatite crystals that make 00-CP-35 and 00-CP-33 more resistant to annealing. The three samples experienced an episode of rapid cooling between 300 and 230 Ma that brought them to 60- 80°C (Figure 3.13). By 150 Ma the samples, possibly with the exception of 00-CP-35, were at less than 70°C, so that, if a late Cretaceous rapid cooling event occurred it is not recorded by the apatite fission tracks. The best-fit line for 00-CP-35 shows an increased rate of cooling between 150 and 100 Ma that brought the sample from 80°C to less than 60°C. However, the envelope does not rule out constant cooling since 200 Ma.

Samples from the plateau (99-OZ-10; 99-OZ-09)

The unimodal, negatively skewed track length distribution means that these samples were at temperature lower than 70°C by at least 200 Ma (Figure 3.13). When continental extension and breakup occurred the plateau samples had long since left the PAZ and, if erosion was enhanced, it is not recorded by the AFT data.

3.6.2.3 Towamba River traverse thermal histories

Sample from the coastal plain (00-CP-02; 00-CP-03)

The thermal histories show an episode of rapid cooling after 150 Ma, which brought the samples from more than 120°C to less than 70°C by no later than 70 Ma (Figure 3.14).

Samples from the escarpment face 00-CP-04; 00-CP-05; 00-CP-11

These samples lie on a vertical profile on the escarpment face. 00-CP-04 entered the PAZ later than the other two samples by a rapid cooling event that terminated no later than 200 Ma (Figure 3.14). By 150 Ma the three samples were at the top of the PAZ and any subsequent rapid cooling episode indicated by the best-fit lines may be an artefact of the modelling.

Sample from the plateau 00-CP-10

This sample was at the top of the PAZ by 200 Ma and the best-fit line suggests constant slow cooling to surface temperatures since then (Figure 3.14) at a rate of about 0.2°C/Myr.

3.7 Summary and conclusions

The AFTT results presented in this chapter place some important constraints on the syn- and post-breakup evolution of the south eastern Australia passive margin. The part of the continental margin less than 23 km from the present coast may have been influenced

by a widespread rapid cooling event between about 150 and 70 Ma. This cooling effect broadly coincides with the extension and opening of the Tasman Sea and probably peaked near the present coast at around 120-100 Ma, some 20-40 Myr before sea-floor spreading. It is tempting, therefore, to propose that processes associated with crustal extension rather than ocean basin formation are linked to rapid cooling on the continental margin. By the time oceanic crust formed the major cooling event had already occurred, in agreement with the fact that the 98 Ma Mt. Dromedary complex at the coast (Figure 3.10) was emplaced at depths no greater than 1-2 km (Fabel & Finlayson, 1992).

The 190-250 Ma apatite fission track ages on the coastal plain (00-CP-33, 00-CP-36, 00-CP-04, 00-CP-05) are not related to differential cooling, but to the chemical composition of the apatites derived from A-type granites (e.g. Carlson *et al.*, 1999). AFTSolve forward model predicts that a 200 Ma fission track age from apatites with Dpar $\geq$ 2.8 (e.g. 00-CP-04) corresponds to a 128 Ma age from an apatite with a Durango-like composition. AFTT indicates that the accelerated cooling lasted until at least 70 Ma. This event may have continued longer, cooling the samples out of the PAZ, but mid-Tertiary weathered profiles on the coastal plain indicate that erosion has been low since then (Bird & Chivas, 1994).

The intensity of syn-rift cooling decreases toward the escarpment and it may or not have affected the inland portion of the coastal plain. The thermal episode may have been diachronous along the margin, given the age differences between the two traverses, moving from south to north. However, latitudinal variations in intensity cannot be tested as samples at the coast were collected only from one traverse because the

lithology in the lowest part of the Towamba River did not contain apatite. Large sets of time-temperature paths are found to satisfy the AFT data and cooling rates cannot be extrapolated with the necessary precision to calculate amount and rates of denudation.

Samples now on the plateau surface were at less than 70°C by 150 Ma. A constant cooling rate of 0.35°C/Myr since the late Cretaceous is required to bring the samples to the surface. The plateau was characterised by a regional relief of up to 800 m in at least the early Tertiary (Taylor *et al.*, 1990), indicating that topography has not changed significantly in the last 60 Myr or so. Late Mesozoic palaeosols on the plateau indicate that the erosion has been locally minimal in the last 60 Myr (Bird & Chivas, 1993). Consequently, it seems likely that the plateau was not affected by continental breakup and has experienced slow, constant cooling that produced low denudation rates evolution since the Mesozoic.

When the chemical composition of the apatites is taken in account, the AFT ages from southern New South Wales are clearly inconsistent with the downwarped rift shoulder model, but they satisfy the other two models. AFTT (compare Figure 3.5; 3.11) does not distinguish between escarpment retreat versus excavation-in-place scenarios and the syn- and post-breakup cooling across the coastal plain cannot be precisely determined. In the next Chapter the advantages of coupling fission track and (U-Th)/He ages are highlighted in terms of addressing the questions about escarpment formation and evolution that the AFTT has not answered.

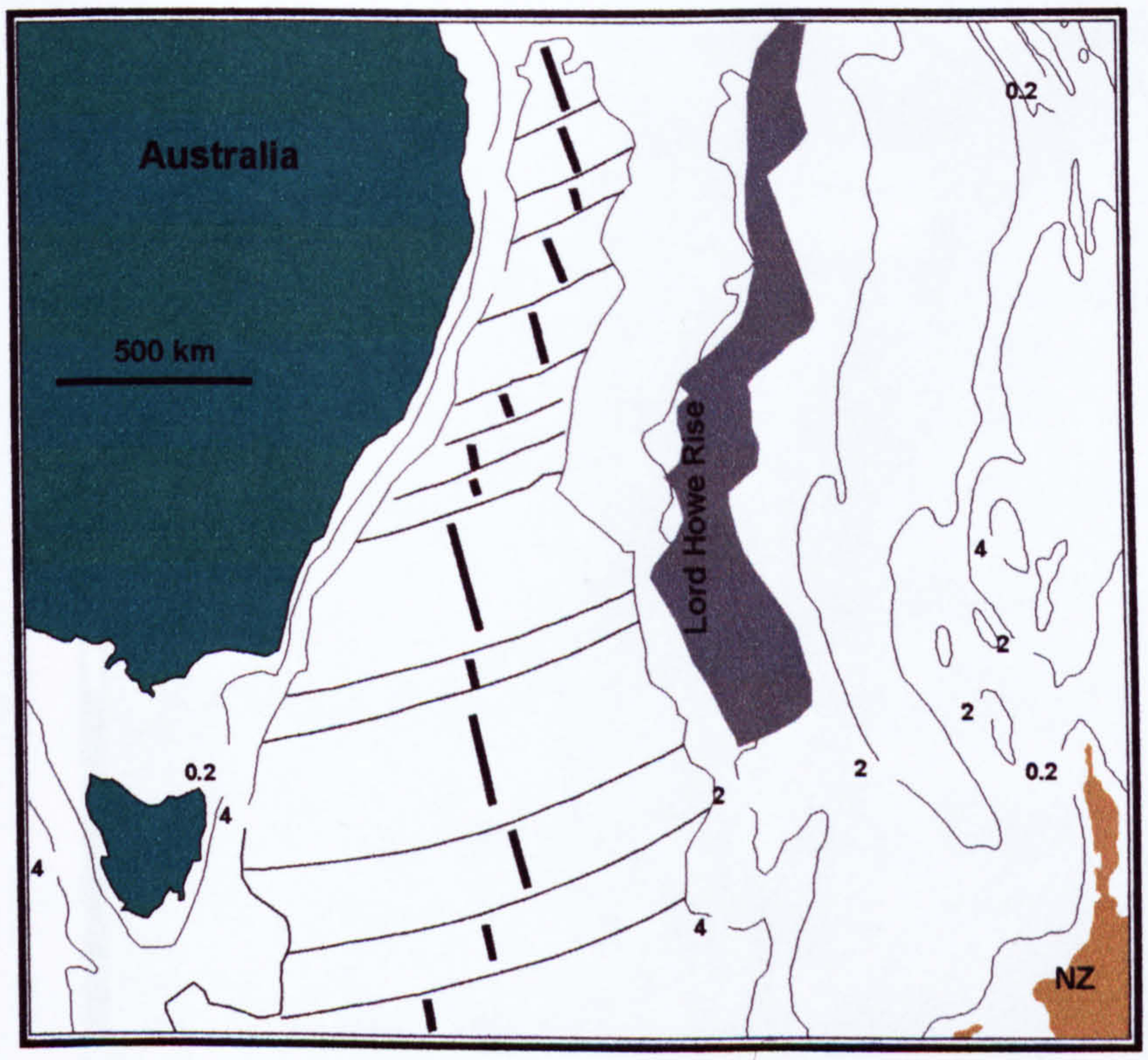

Figure 3.1: Simplified tectonic map of eastern Australia and the Tasman Sea. The thick lines represent the now-defunct mid-ocean ridge. The numbers represent depth in km (from Lister et al., 1991)

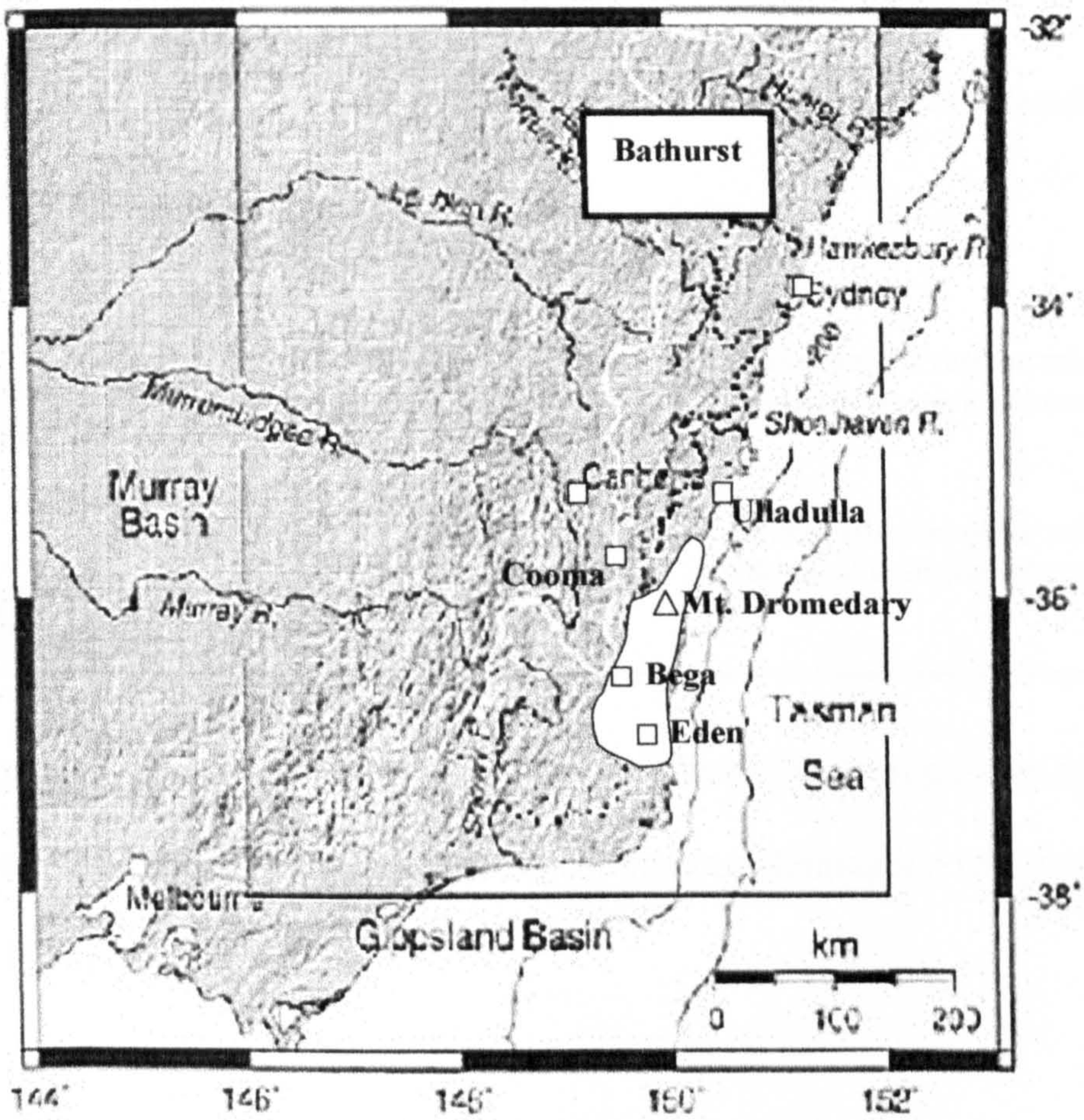

Figure 3.2: DEM image of eastern Australia with indicated the CDD (white line) and the escarpment (dashed line) (from van der Beek *et al.*, 1999). The white areas represent the two studied areas

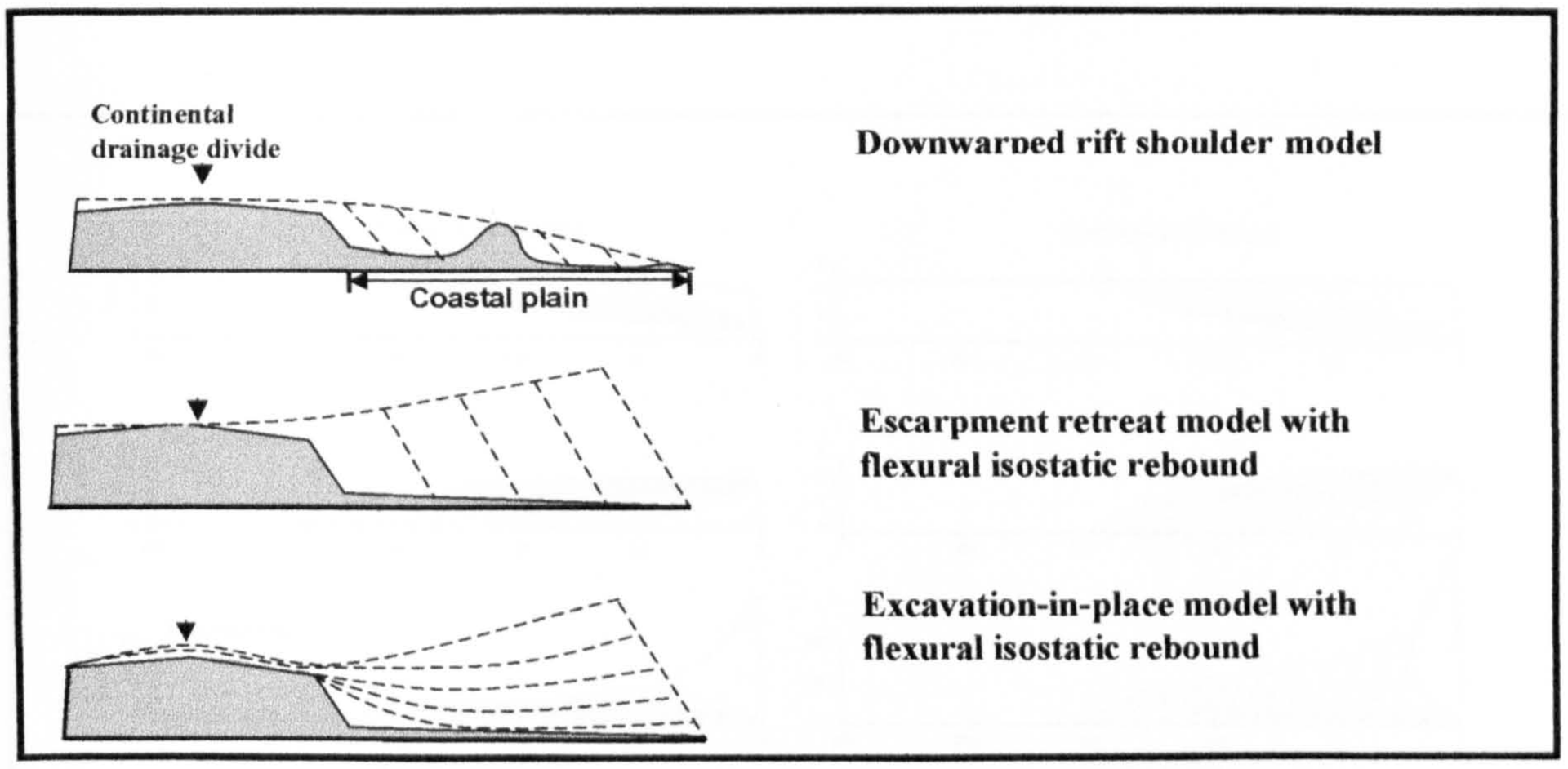

Figure 3.3: Schematic representation of the three models of passive margin evolution. The dotted lines represent the amount of post-breakup denudation (redrawn from Gallagher *et al.* 1998)

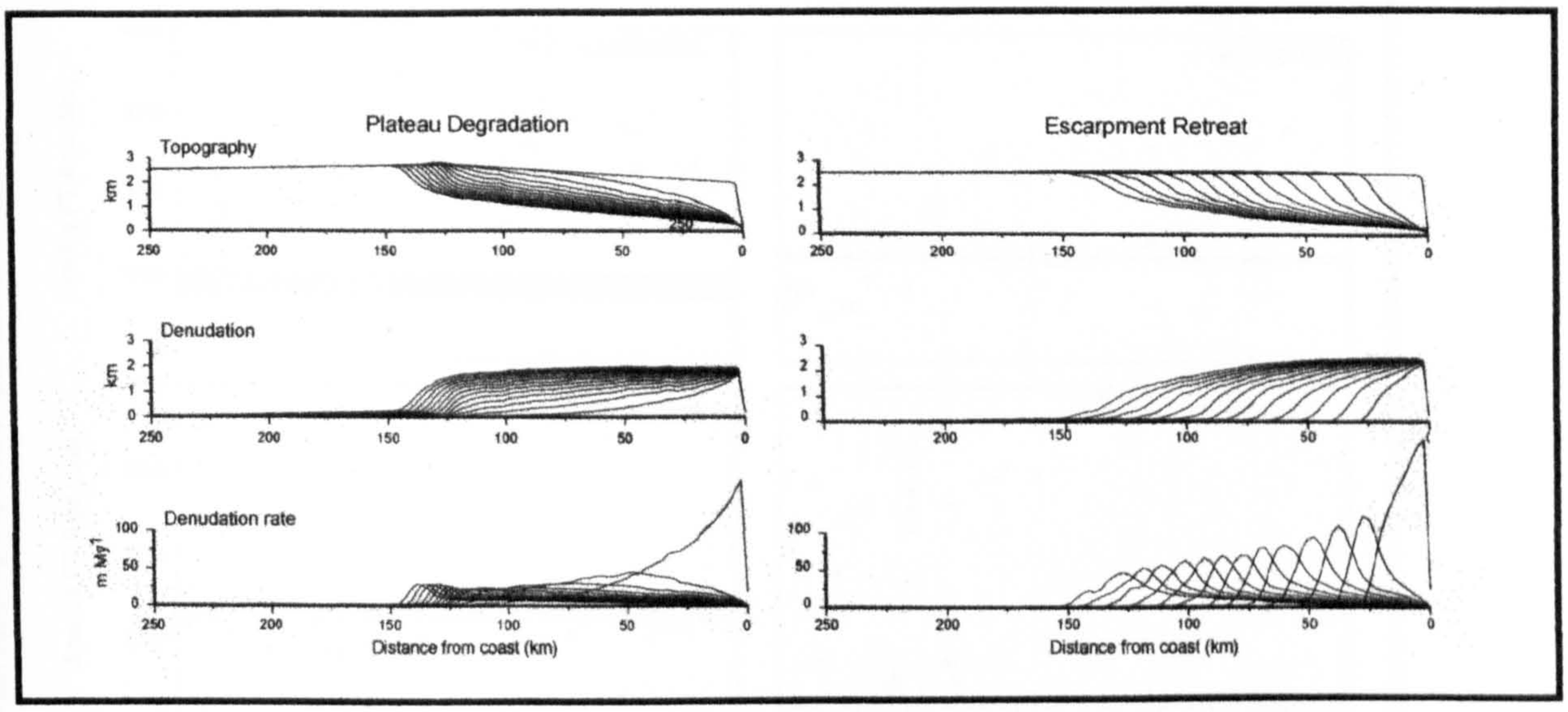

Figure 3.4: Predicted variations in topography, denudation and rates of denudation for the plateau degradation model (corresponding to the downwearing model in the text) and the escarpment retreat models across a high elevation rift shoulder. Lines are drawn every 10 Myr, from 100 Ma to the present (from van der Beek *et al.*, 2002)

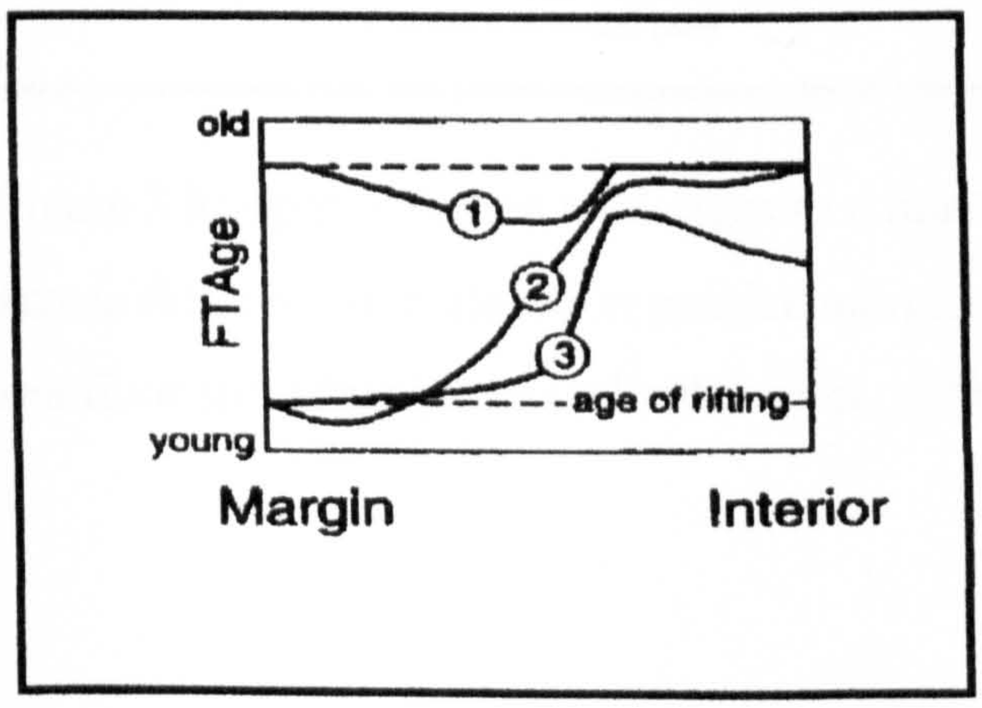

Figure 3.5: Predicted apatite fission tracks ages pattern across an hypothetical passive margin for the three models. 1) downwarped rift shoulder model; 2) escarpment retreat across a high elevation rift shoulder, and 3) excavation in place of a high elevation rift shoulder (from Gallagher *et al.*, 1998)

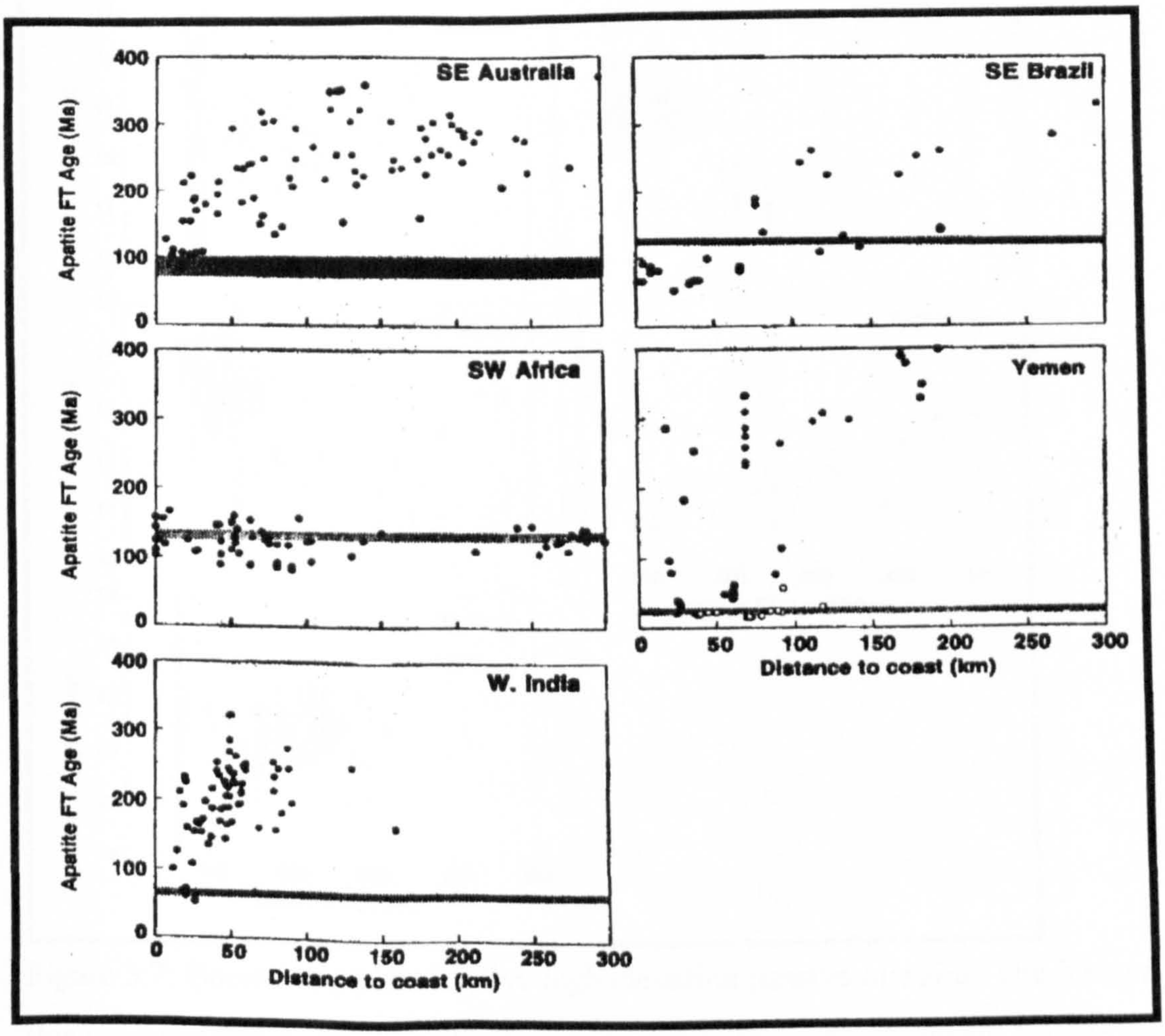

Figure 3.6: Apatite fission track ages as a function of distance from the present coastline across different high elevation passive margins. The dark bands represent time of onset of sea-floor spreading (from Gallagher *et al.*, 1998)

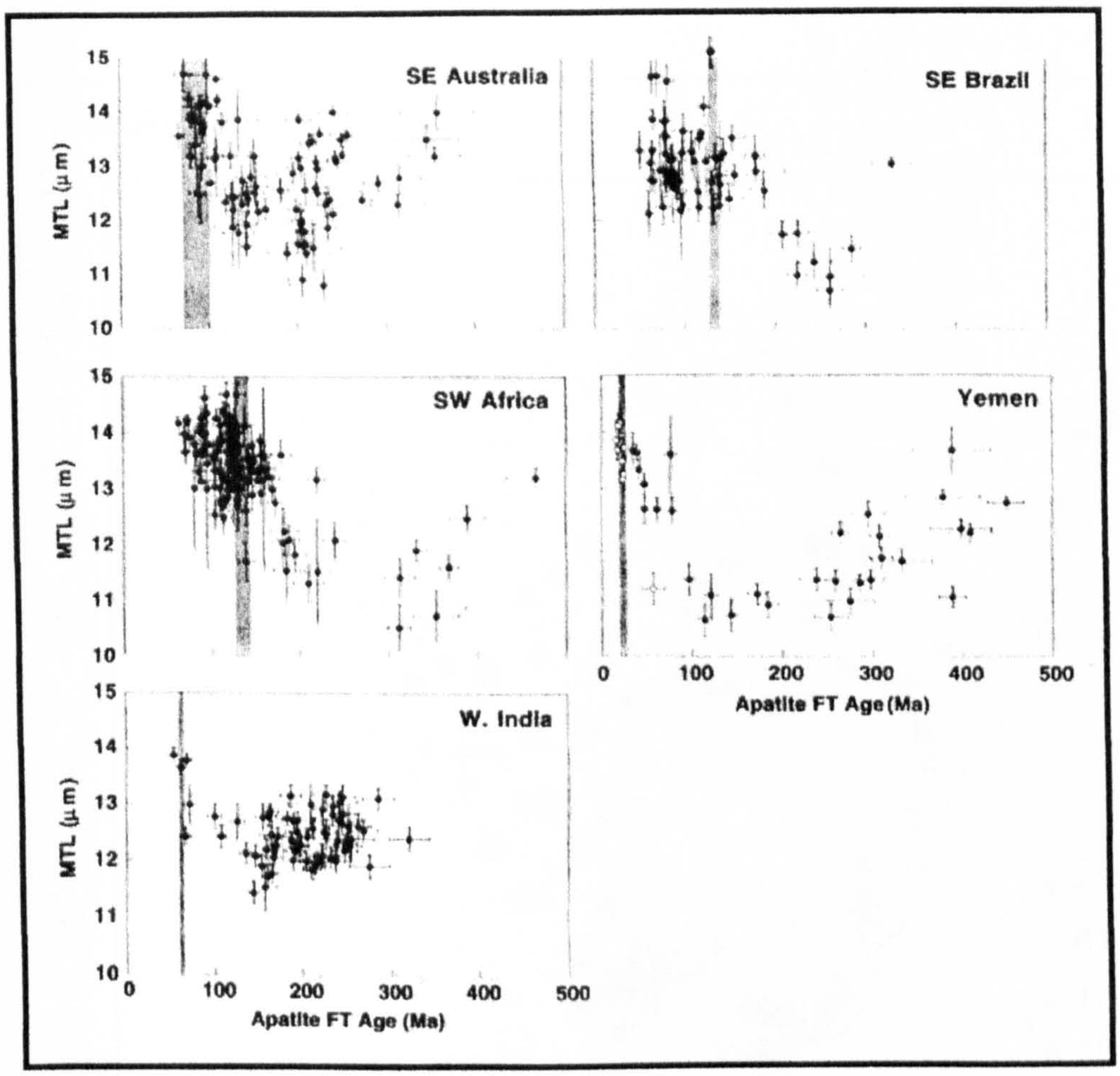

Figure 3.7: Boomerang plots for five high elevation passive margins. The Yemen data show this characteristic pattern ore clearly, whereas the other settings reveal a more complex cooling history. The dark vertical bands indicate the time of onset of sea-floor spreading (from Gallagher *et al.*, 1998)

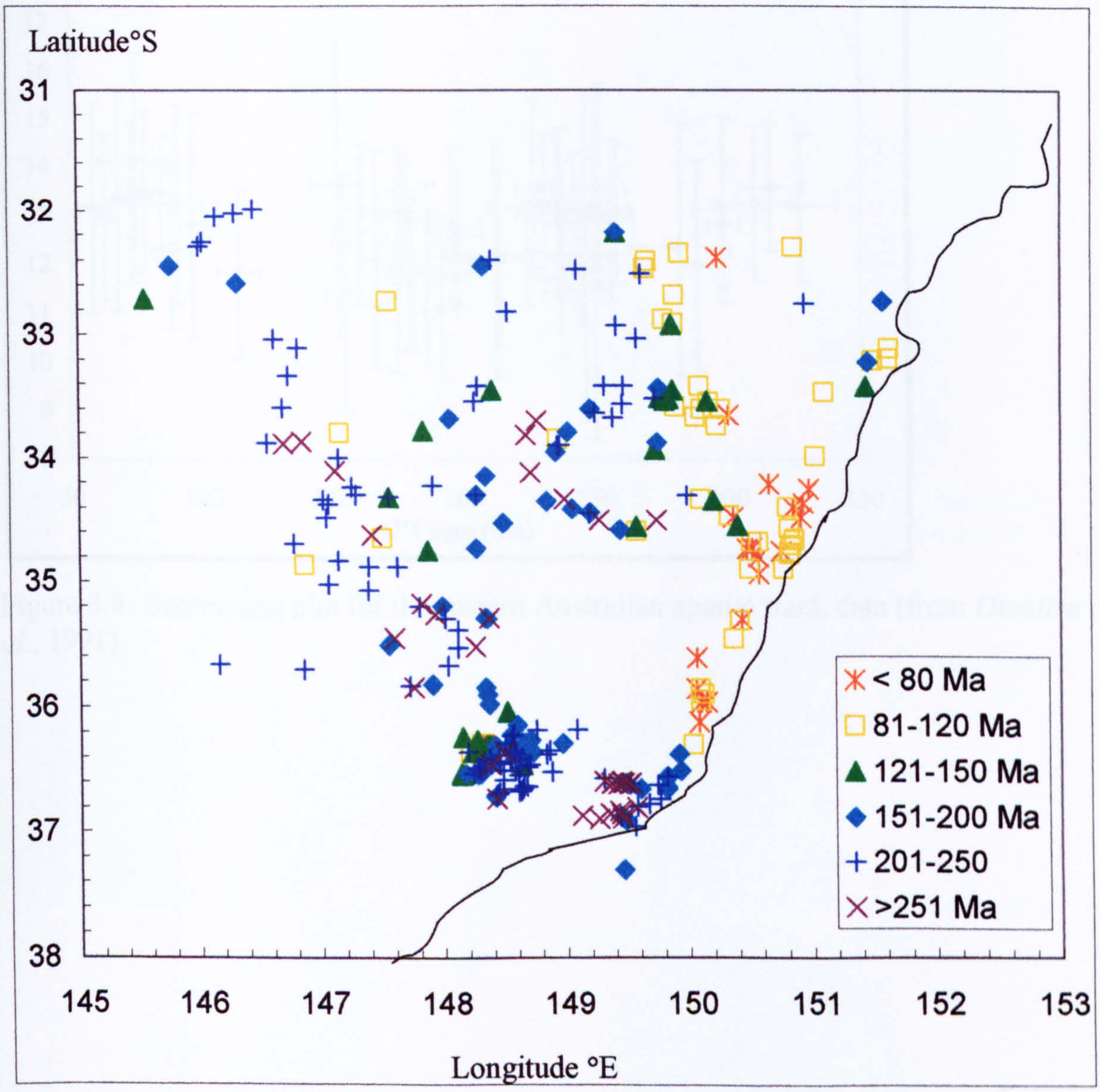

Figure 3.8: "Map" of apatite fission track ages from eastern Australia (from Gleadow *et al.*, 2002). The coastline is indicated.

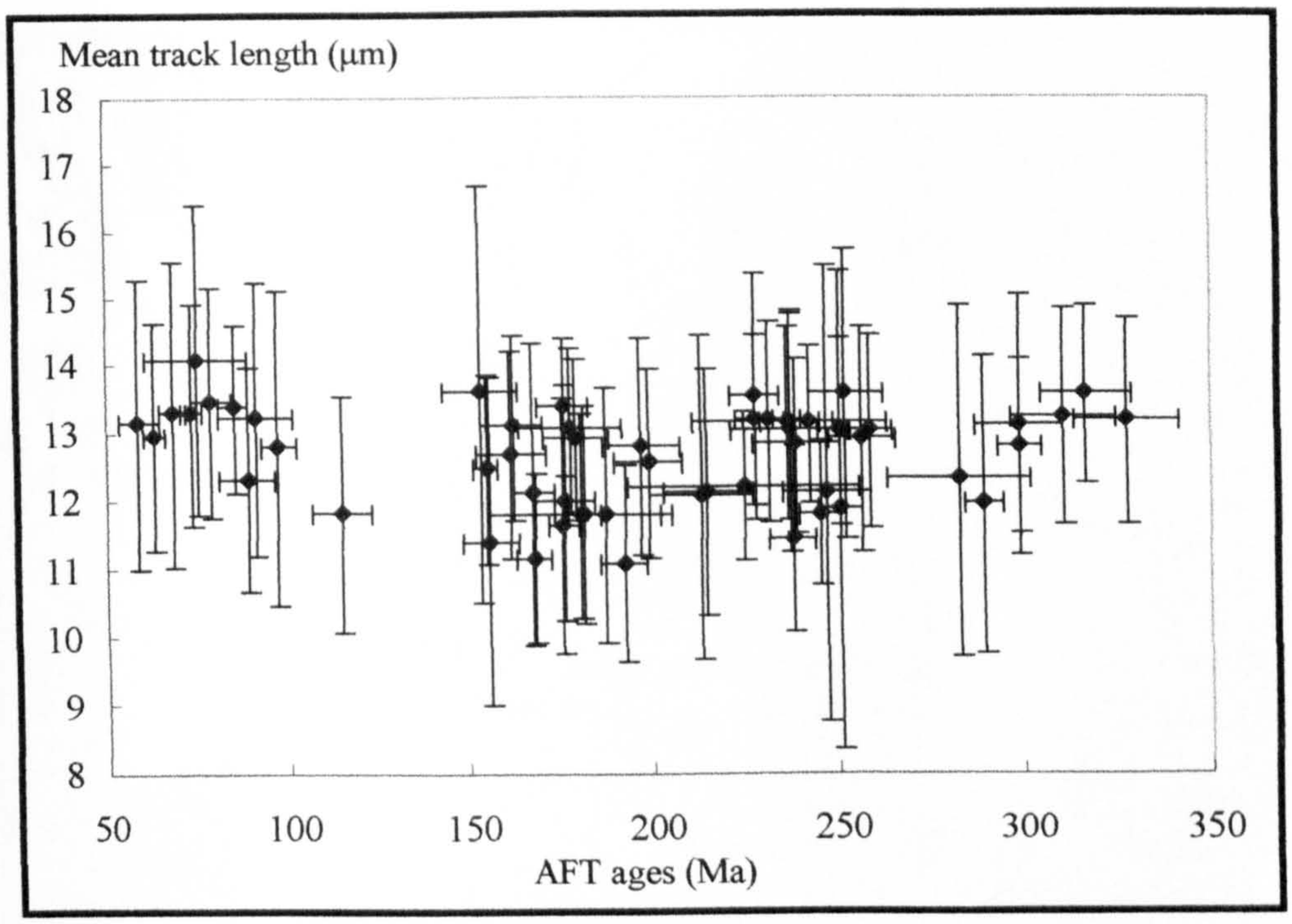

Figure 3.9: Boomerang plot for the eastern Australian apatite track data (from *Dumitru et al.*, 1991)

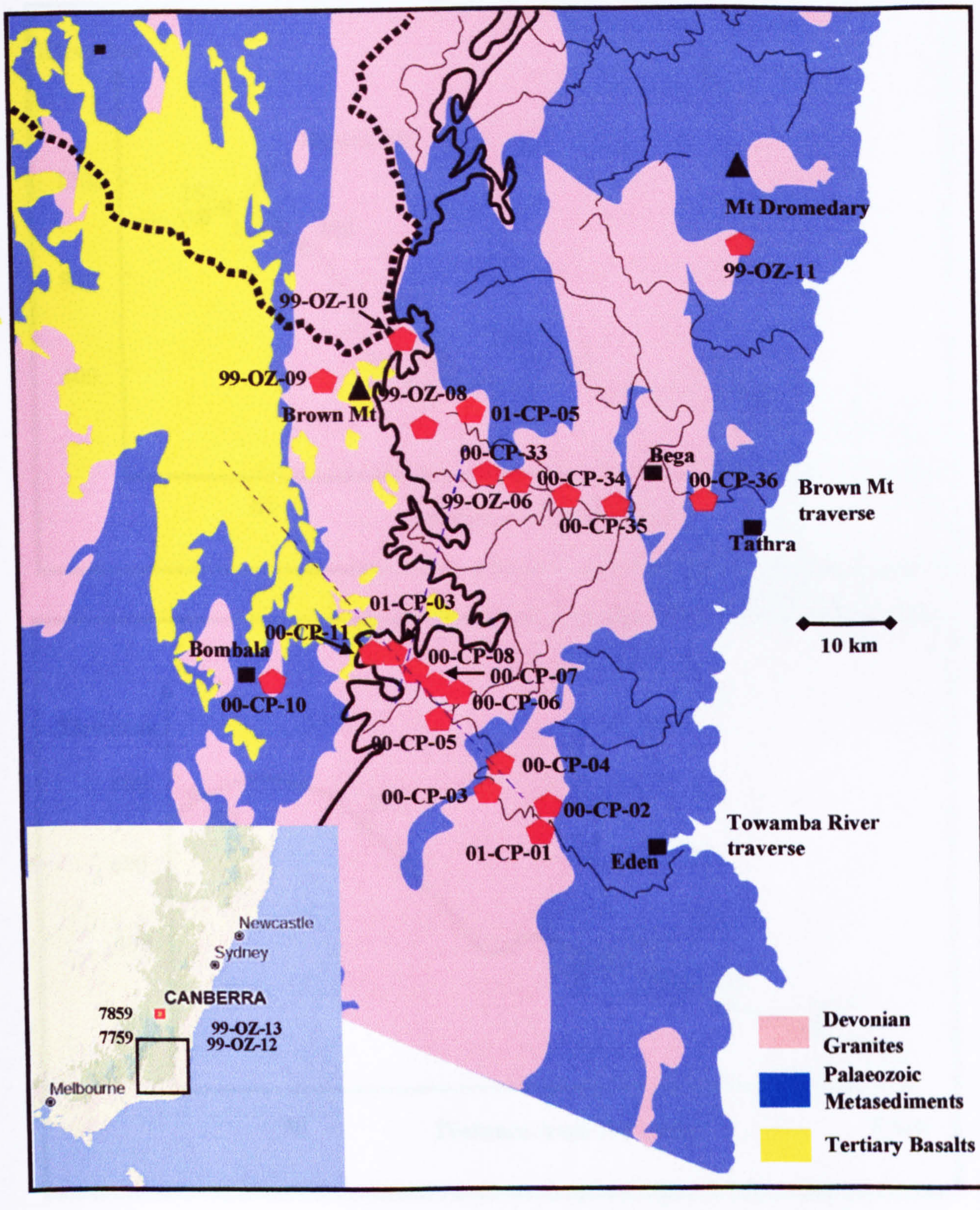

Figure 3.10: Sample location on a schematic geological map of the area. The escarpment (continuous line) and the Continental Drainage Divide (dotted line) are represented along with two faults (dashed blue lines). 7859 and 7759 are samples on the plateau, courtesy of Dr. B. Kohn

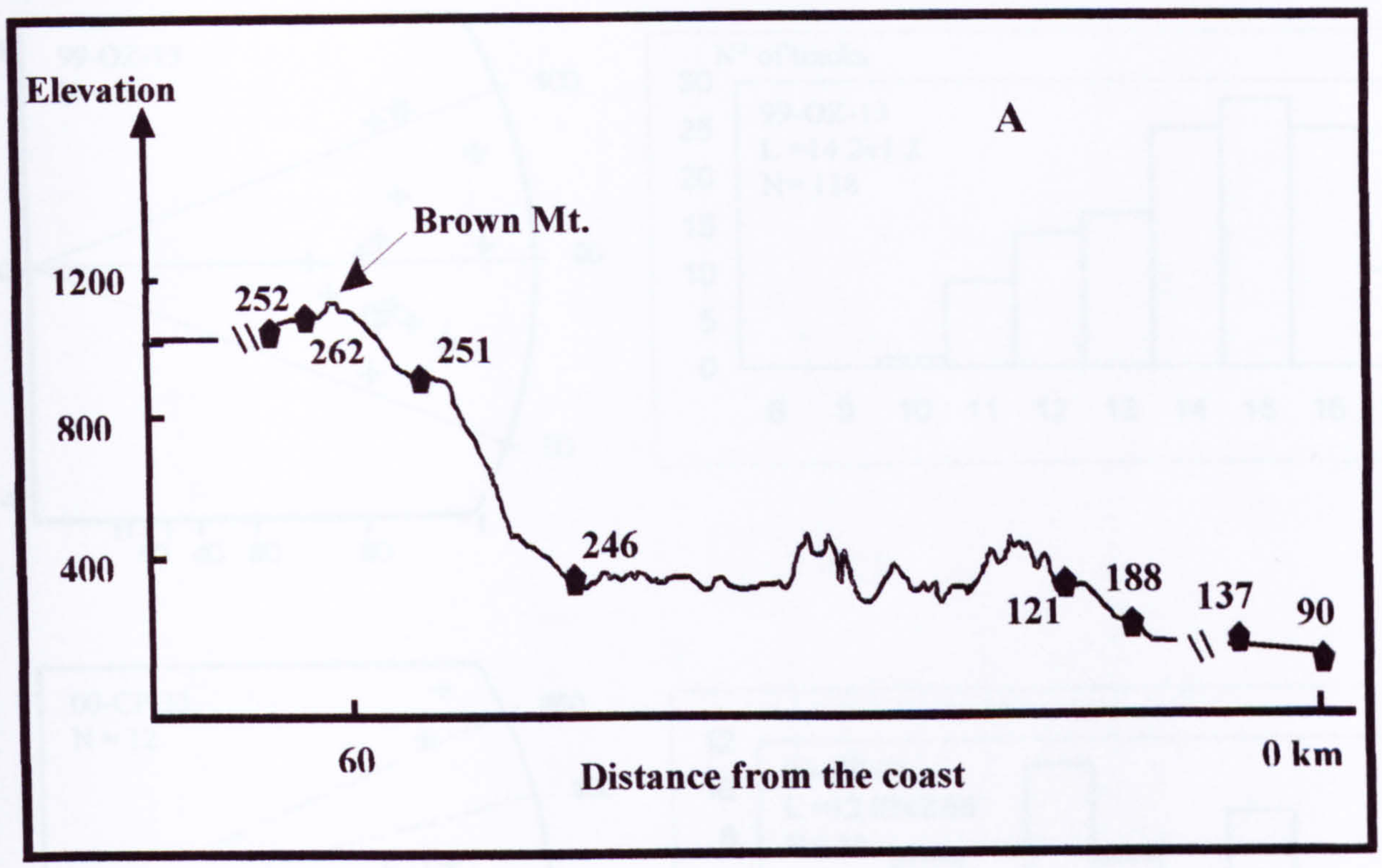

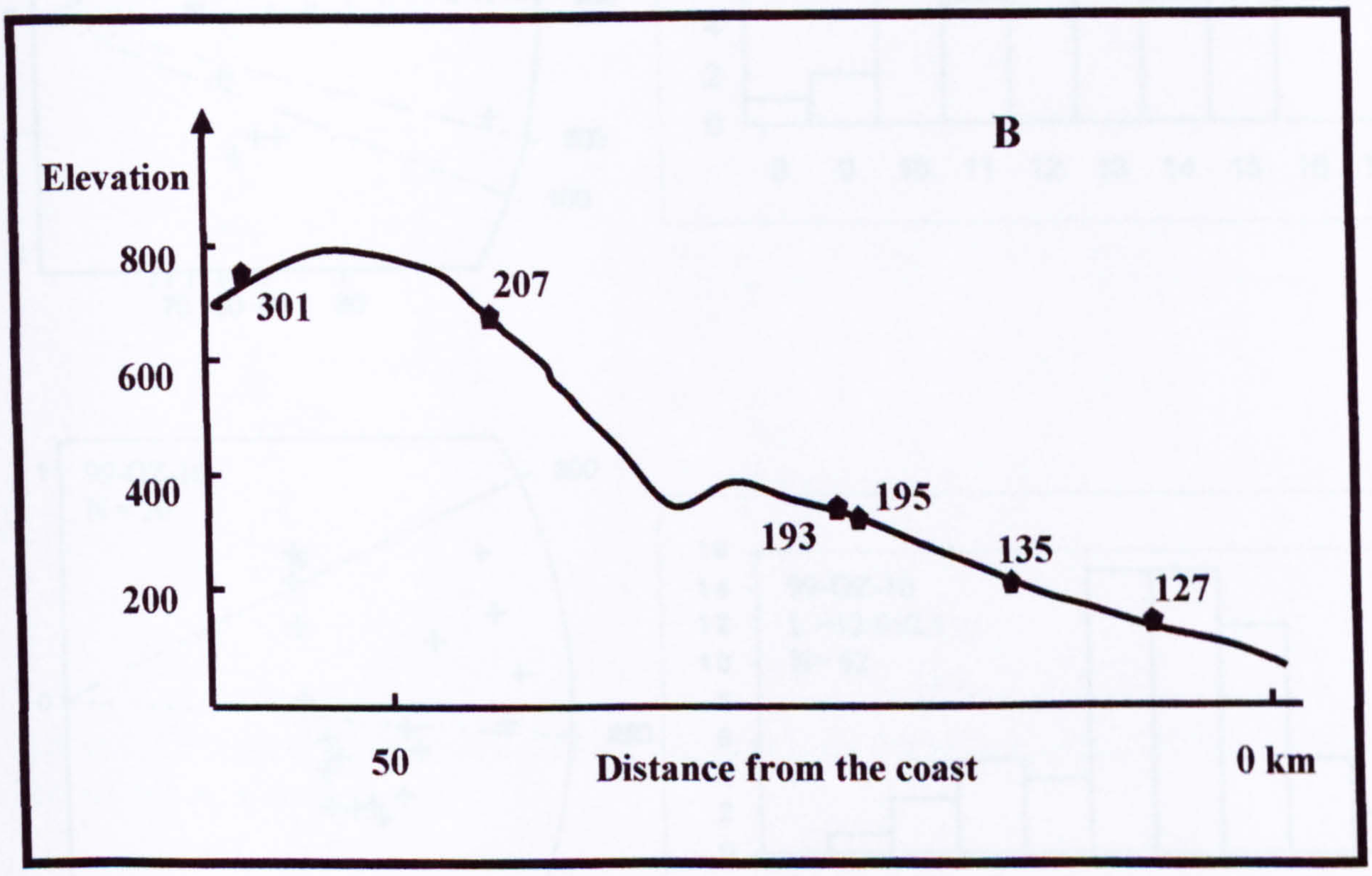

Figure 3.11: Cross sections across the Brown Mt. (A) and Towamba River (B) traverses showing the apatite fission track ages.

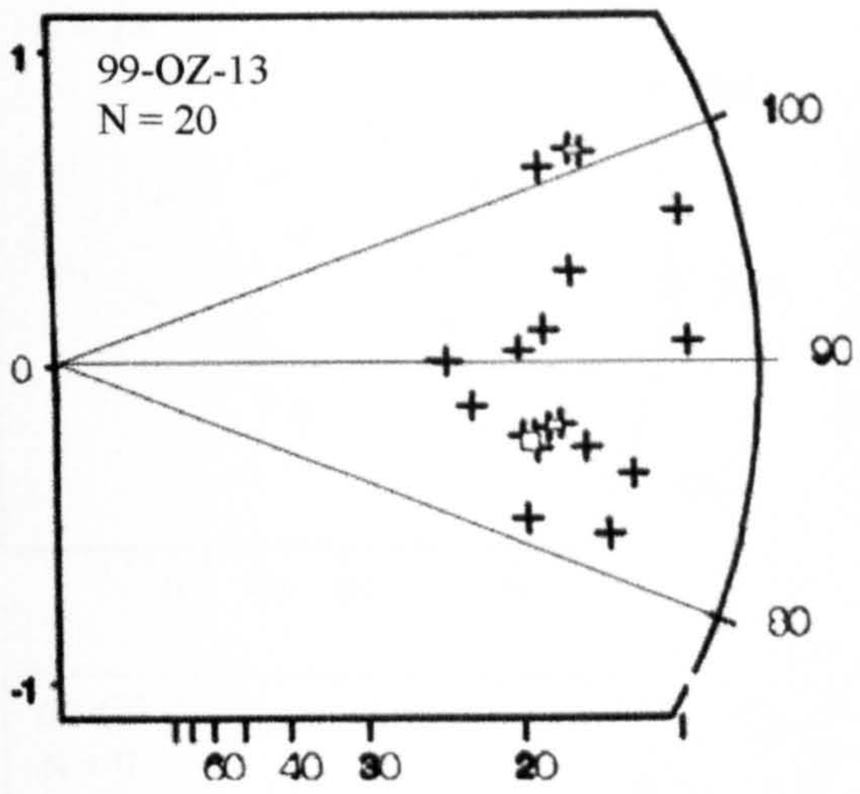
99-OZ-13
N = 20
1
0
-1
100
90
80
60
40
30
20

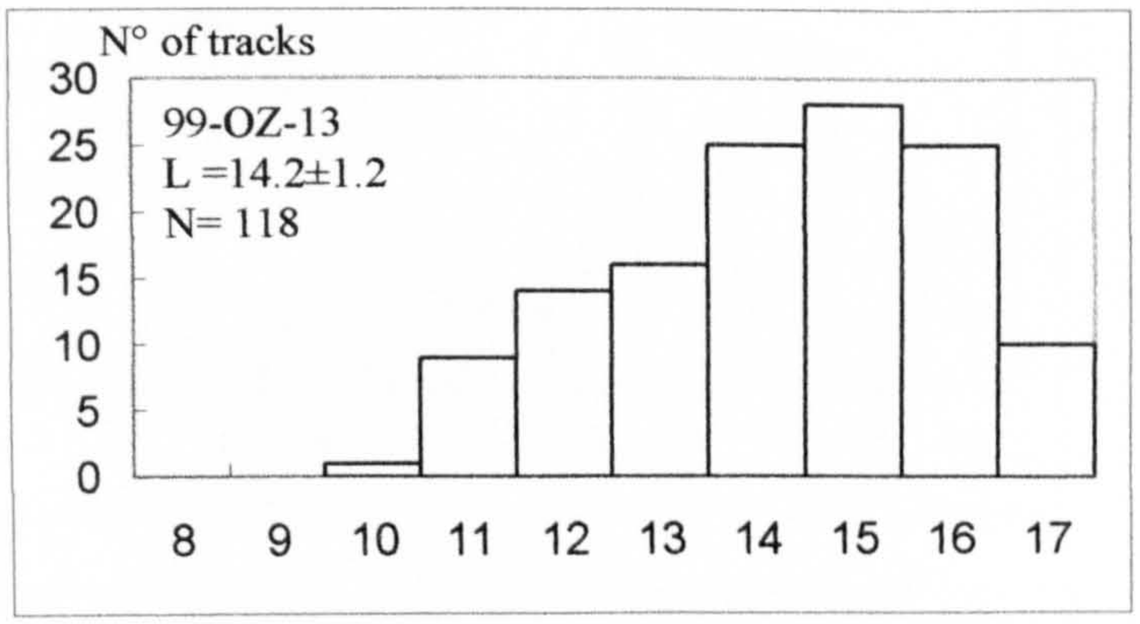
N° of tracks
99-OZ-13
L =14.2±1.2
N= 118
30
25
20
15
10
5
0
8
9
10
11
12
13
14
15
16
17

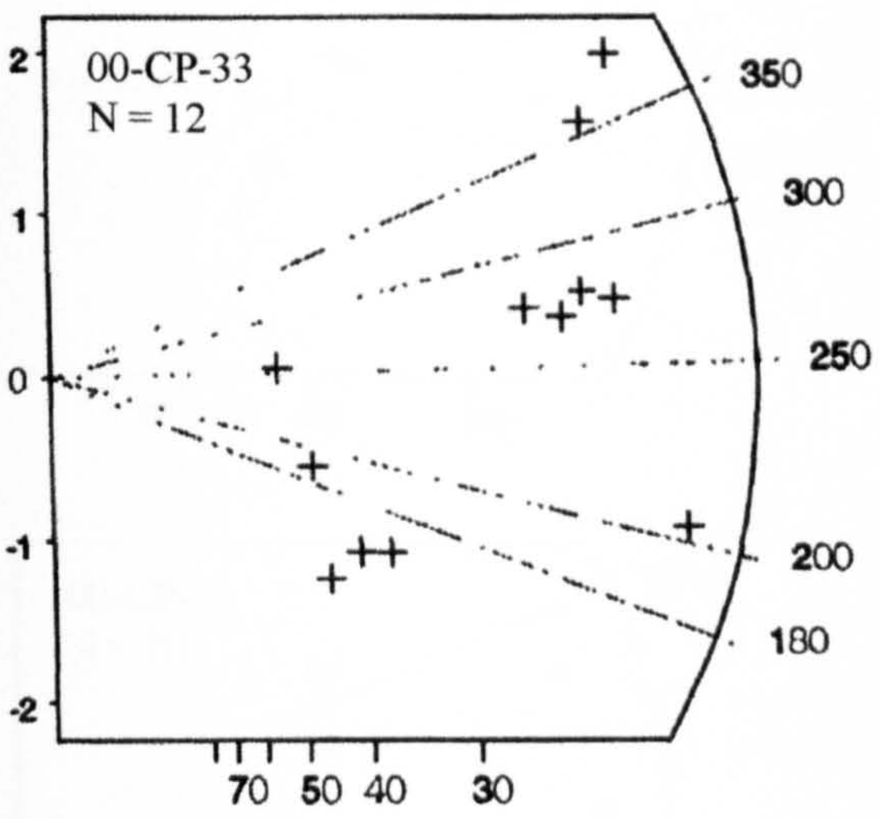
00-CP-33
N = 12
2
1
0
-1
-2
350
300
250
200
180
70
50
40
30

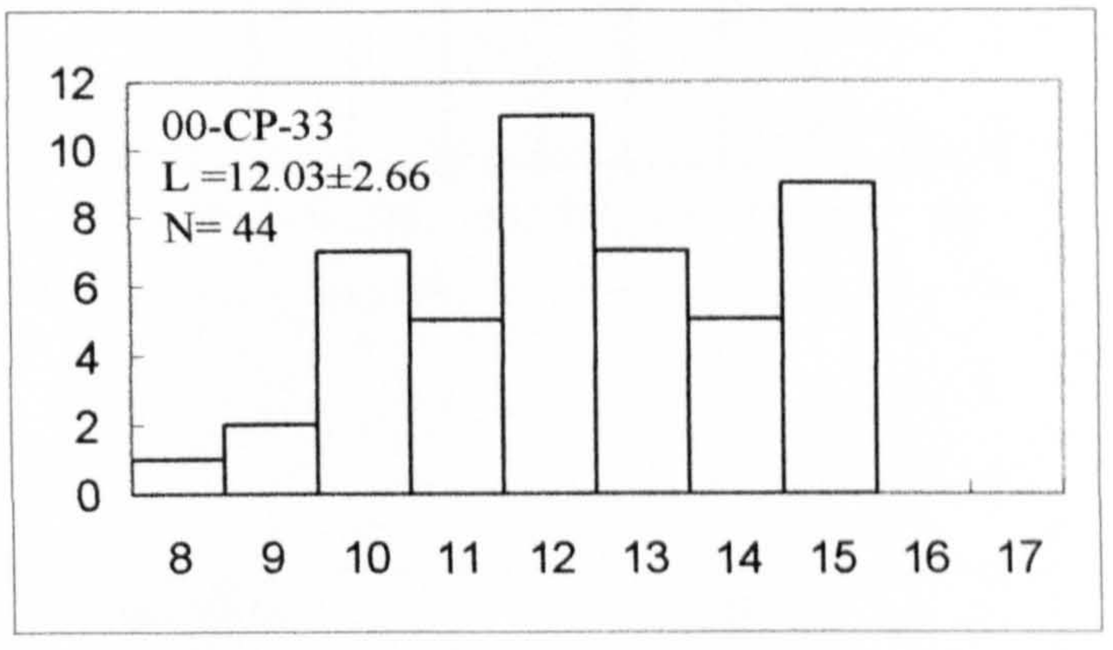
00-CP-33
L =12.03±2.66
N= 44
12
10
8
6
4
2
0
8
9
10
11
12
13
14
15
16
17

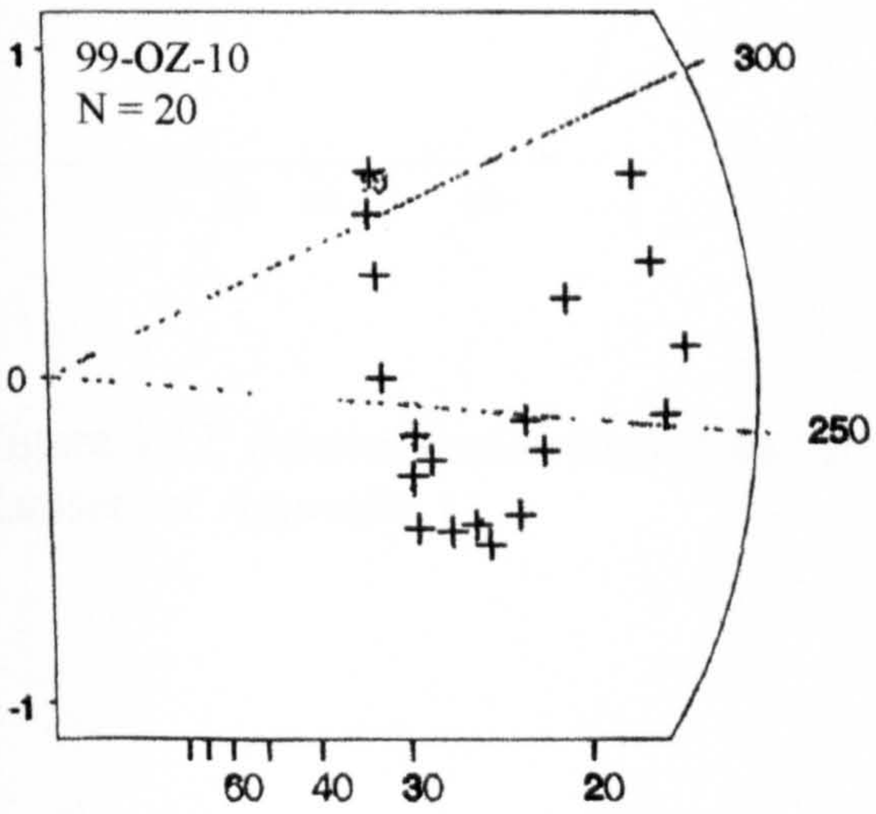
99-OZ-10
N = 20
1
0
-1
300
250
60
40
30
20

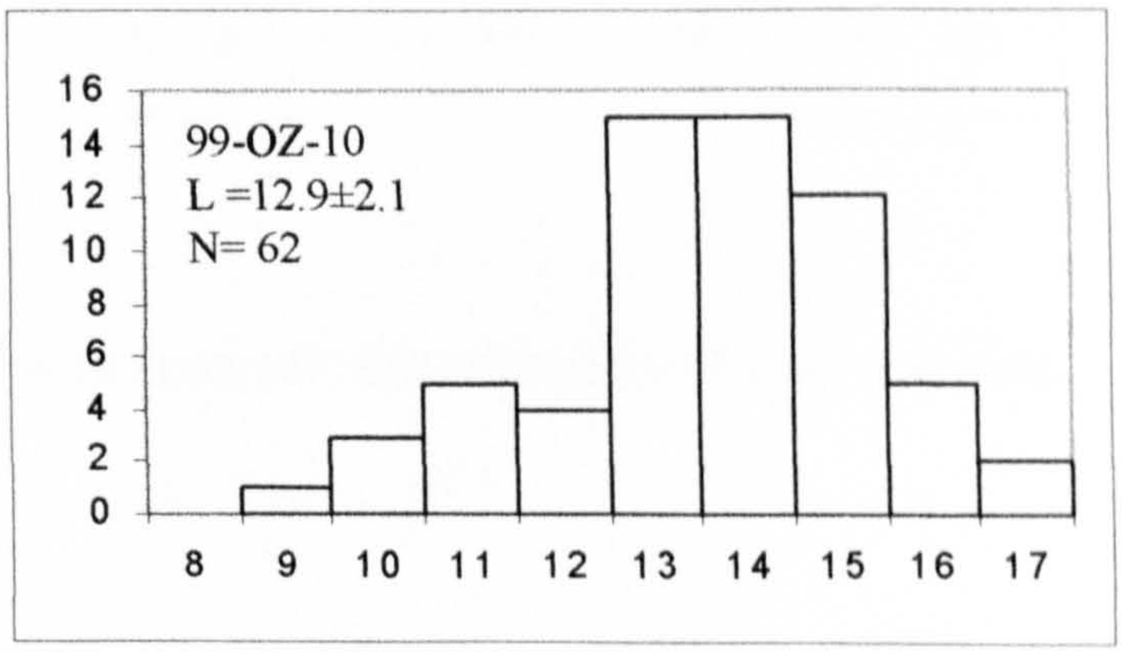
99-OZ-10
L =12.9±2.1
N= 62
16
14
12
10
8
6
4
2
0
8
9
10
11
12
13
14
15
16
17

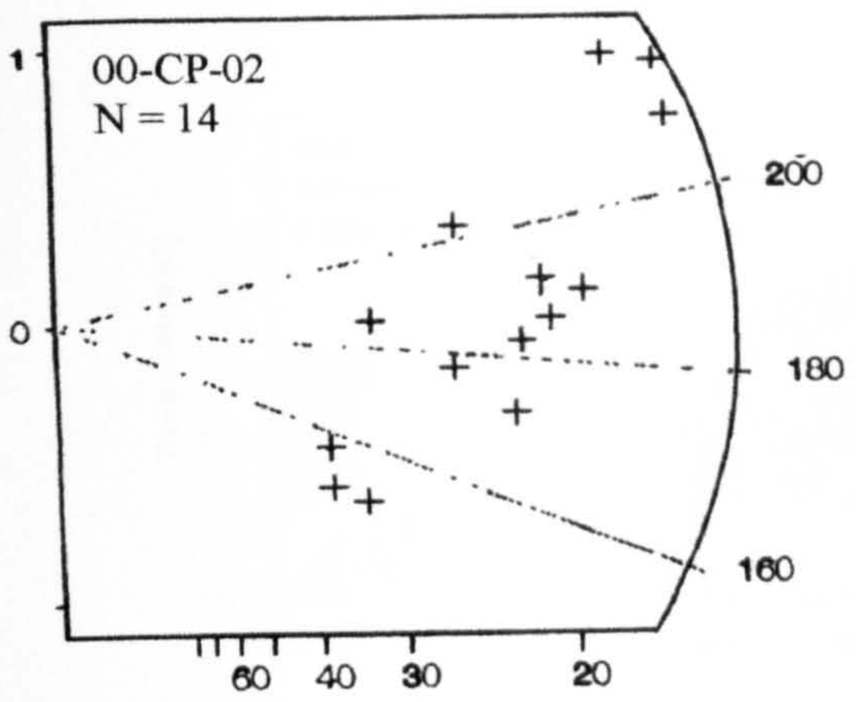

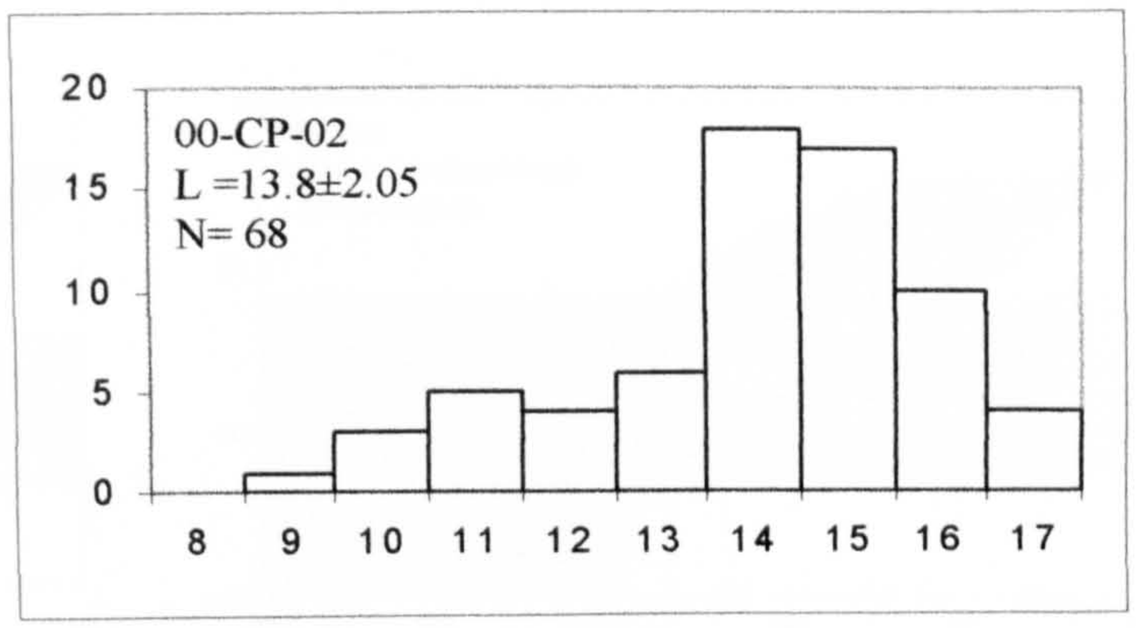

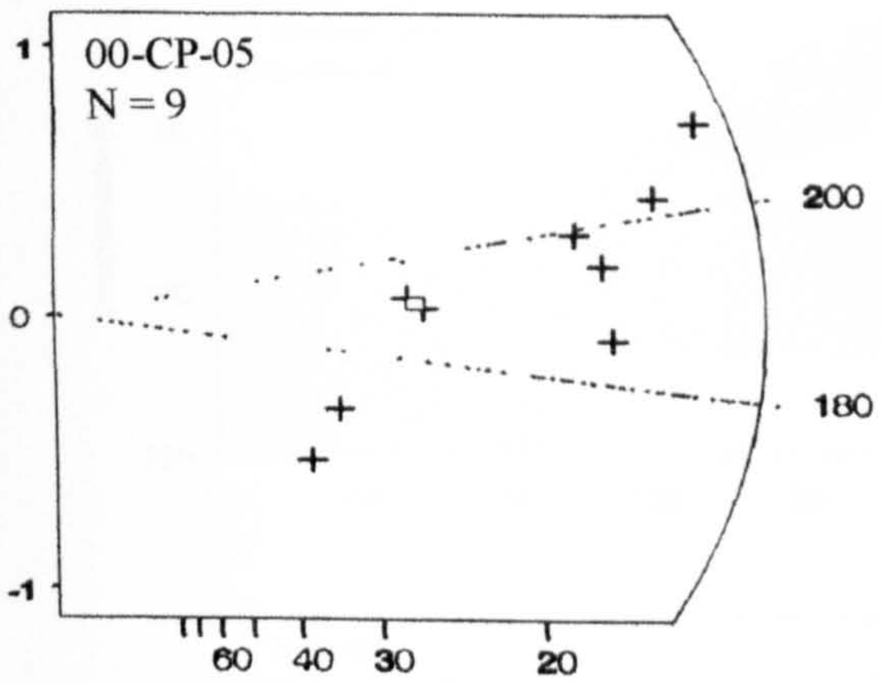

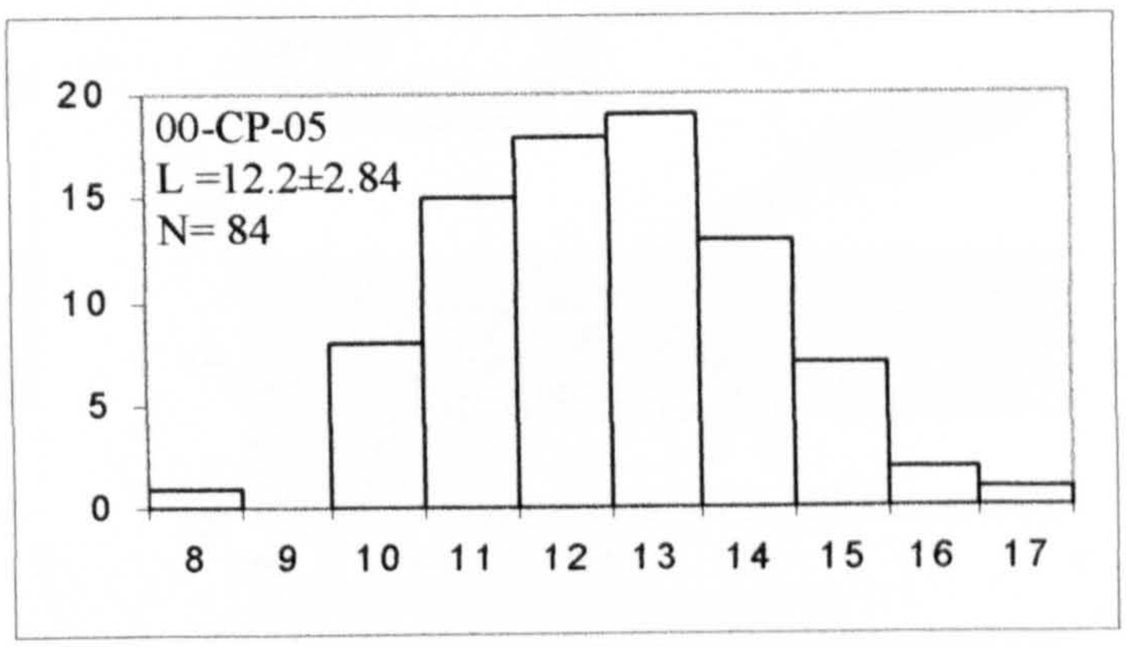

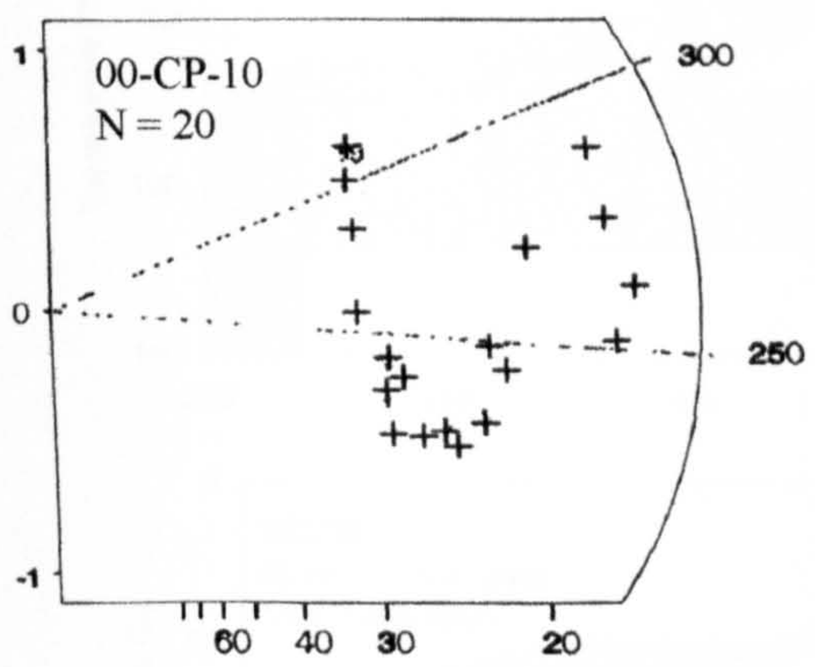

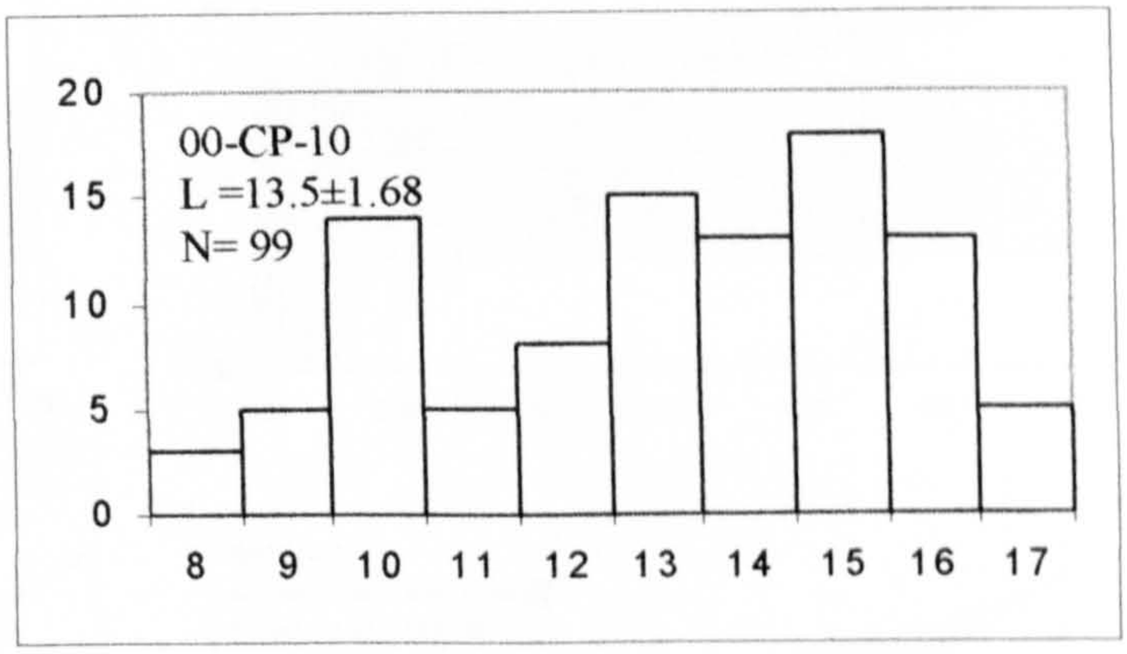

Figure 3.12: Apatite fission track data for the most representative samples (for the complete dataset see Appendix 1)

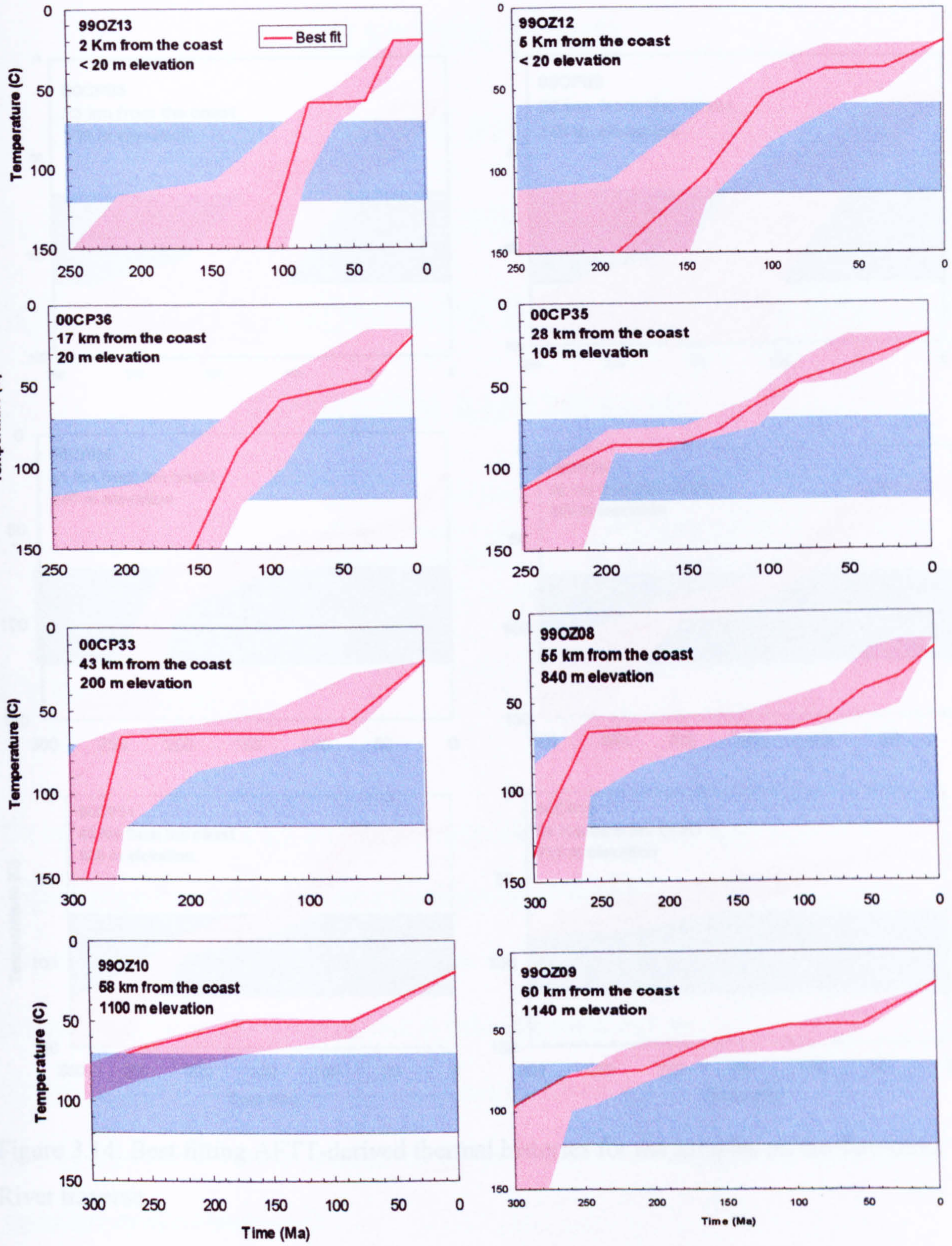

Figure 3.13: Best fitting AFTT-derived thermal histories for the samples on the Brown Mt traverse

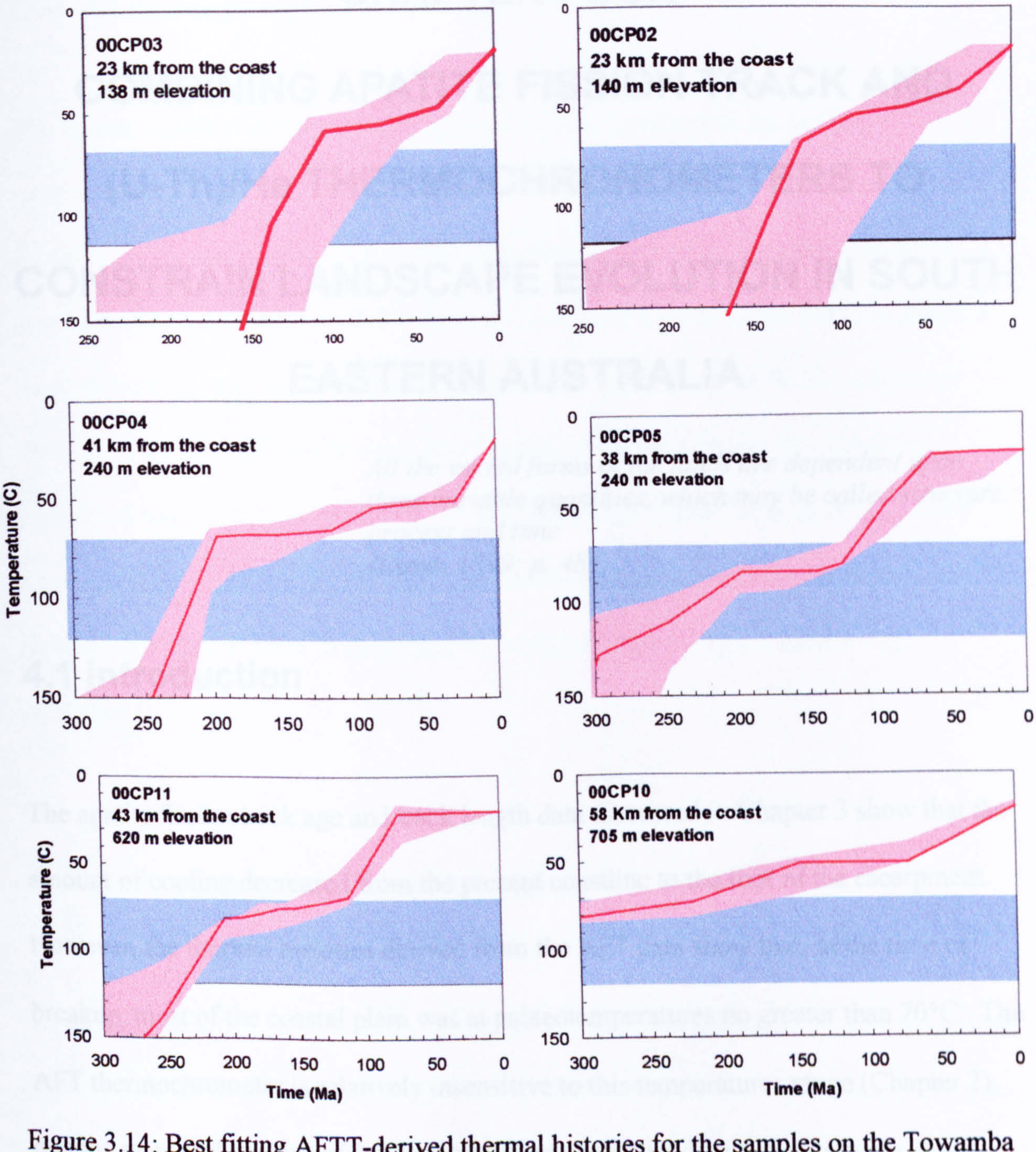

Figure 3.14: Best fitting AFTT-derived thermal histories for the samples on the Towamba River traverse

CHAPTER FOUR

COMBINING APATITE FISSION TRACK AND (U-Th)/He THERMOCHRONOMETERS TO CONSTRAIN LANDSCAPE EVOLUTION IN SOUTH EASTERN AUSTRALIA

All the varied forms of the lands are dependent upon three variable quantities, which may be called structure, process and time
(Davis, 1899; p. 481)

4.1 Introduction

The apatite fission track age and track length data discussed in Chapter 3 show that the amount of cooling decreased from the present coastline to the foot of the escarpment. However, the thermal histories derived from the AFT data show that, at the time of breakup, most of the coastal plain was at palaeotemperatures no greater than 70°C. The AFT thermochrometer is relatively insensitive to this temperatures range (Chapter 2), and the rates and amount of denudation can be constrained only qualitatively. Four questions remain unanswered:

- did the rapid cooling event that affected the present coast propagate inland and, if so, at what rates?

-what was the distribution of denudation across the coastal plain?

- what was the chronology of escarpment evolution?

- how did the escarpment form and evolve?

The apatite (U-Th)/He thermochronometer overlaps and extends the range of temperatures over which AFTT is effective. However, (U-Th)/He ages of individual samples do not constrain unique thermal histories (Chapter 2). The combination of apatite fission track and (U-Th)/He thermochronometers narrows the range of possible thermal histories and has the potential to be used to identify the style of escarpment erosion. Therefore this method can be of fundamental importance for evaluating models of passive margin evolution. In the following sections the apatite (U-Th)/He ages from southern New South Wales are presented, and then combined with the apatite fission track data in order to determine the style and chronology of escarpment evolution.

4.2 Samples and analytical procedure

Apatite (U-Th)/He ages have been determined from 25 samples collected on the Brown Mountain and Towamba River traverses (Figure 3.10). In addition, two samples on the plateau top from approximately 100 km north of Brown Mt. and about 120 km inland of the escarpment lip were analysed to test any relationship between amount and rates of denudation with distance from the escarpment lip (samples 7859, 7759; Figure 3.10).

Between 1 and 44 inclusion-free apatite crystals (Table A1.3) were handpicked from the heavy minerals separates from the granites, as outlined in Chapter 2. Prism diameters range from 60 to 260 μm, and were measured using a 10 x 10 μm division graticule. Variations in alpha recoil correction were kept to < 0.5% by selecting apatite crystals with similar dimensions. The grains from samples from the Brown Mt. traverse were packed in Cu foil, and the other samples were loaded into steel capsules (see Chapter 2 and Appendix 2). All the samples were analysed in triplicate or duplicate apart from 99-OZ-06 for which there were sufficient suitable apatite crystals for only one aliquot. Six replicates of sample 99-OZ-13 were measured to calculate the accuracy of the data produced at SUERC (Chapter 2).

4.3 Results

The U, Th and He data for all the samples are summarised in Table A1.3 and average, recoil-corrected He ages are plotted on the two cross sections in Figure 4.1. The apatite (U-Th)/He ages are always younger than the fission track ages and they exhibit the same general trend of increasing ages from the coast to the plateau top. Differences between apatite (U-Th)/He and fission track ages are within the uncertainties of the data near the coast on the Brown Mt. traverse (Figure 4.2). On the coastal lowlands and across the escarpment, the difference between AFT and (U-Th)/He ages varies between 17 Myr (99-OZ-11) and 147 Myr (99-OZ-08) and may be related to the chemical composition of the apatites rather than to differences in the amount and tempo of cooling. Apatites from A-type granites (Chapter 3) display spuriously old fission track ages due to their

Sample name	^{4}He (cc)	^{238}U (ng)	^{232}Th (ng)	Grain size (μm)	Corrected Age (Ma)$^{++}$	Average Age (Ma)
7859-09	1.4e-7	4.2	4.1	70	247.2	247.2
7759-08	6.2e-8	1.9	4.2	75	183.2	183.2
99-OZ-09	1.4e-7	4.1	3.6	70	203.7	
99-OZ-09	1.5e-7	4.2	3.9	80	217.6	
99-OZ-09	1.0e-7	2.8	3.0	60	198.4	206.6
99-OZ-10	5.0e-8	2.1	3.2	60	190.0	
99-OZ-10	1.3e-7	4.0	8.1	90	213.4	
99-OZ-10	1.1e-7	4.2	7.1	90	235.3	212.9
99-OZ-08*	4.2e-8	3.2	3.6	60	114.2	
99-OZ-08*	1.6e-8	1.7	2.6	100	92.8	
99-OZ-08*	6.2e-8	3.8	7.3	260	106.1	104.4
01-CP-05	5.3e-8	3.8	3.6	90	112	
	4.9e-8	3.2	4.1	90	113.2	
	6.0e-8	4.8	5.1	80	115.0	104
99-OZ-33	9.8e-9	0.6	1.2	60	151.6	
99-OZ-33	1.5e-8	0.8	2.3	60	138.5	
99-OZ-33	1.7e-8	1.1	2.0	60	149.2	146.4
99-OZ-33	1.2e-7	0.7	2.0	65	(777.6)	
99-OZ-06	2.0e-8	1.4	3.9	75	88.2	88.2
99-OZ-34	2.0e-8	1.6	2.5	60	125.3	
99-OZ-34	6.6e-8	7.4	6.8	60	101.1	
99-OZ-34	1.2e-8	1.0	1.8	60	109.8	112.1
99-OZ-35	1.7e-8	1.3	0.8	75	121.6	
99-OZ-35	1.1e-8	2.5	1.6	60	104.8	
99-OZ-35	1.0e-8	1.1	1.0	65	99.1	108.5
99-OZ-36	1.5e-8	1.3	1.6	70	101.5	
99-OZ-36	1.3e-8	1.0	2.1	60	100.8	
99-OZ-36	6.0e-9	0.5	1.2	60	94.9	99.1
99-OZ-11	3.9e-8	2.4	3.8	90	119.5	
99-OZ-11	8.9e-9	0.8	1.1	80	89.4	104.5
99-OZ-11	4.6e-7	1.5	19.6	80	(602.1)	
99-OZ-12	3.6e-8	3.2	4.3	70	93.1	
99-OZ-12	1.8e-8	1.8	2.7	80	79.4	
99-OZ-12		0.5	0.8	70	97.6	90.0
99-OZ-13	2.7e-8	2.9	4.8	80	77.8	
99-OZ-13	1.3e-8	1.0	2.2	90	83.7	
99-OZ-13	3.0e-8	2.5	5.8	70	82.4	
99-OZ-13	2.5e-8	1.8	3.8	80	91.8	
99-OZ-13	1.1e-8	0.9	2.1	90	83.4	
99-OZ-13	3.3e-8	2.2	4.9	90	100.8	86.6
01-CP-01	2.3e-8	2.4	5.2	90	91.8	95.1
	2.7e-8	2.9	4.7	80	98.4	
00-CP-02	2.7e-8	3.5	7.2	80	84.2	87.1
	2.9e-8	3.9	6.4	75	90.0	
	5.2e-7	2.8	7.3		(456)	
00-CP-03	1.0e-8	3.5	1.5	80	91	96
	1.2e-8	4.2	2.3	90	101	
00-CP-04	5.4e-8	3.2	5.2	80	112	117
	7.2e-8	1.8	4.1	80	112	
00-CP-05	6.0e-8	1.9	3.4	80	111.7	109
	3.2e-8	2.5	6.7	80	105.6	
00-CP-06	2.3e-8	2.9	1.9	80	98.4	105
	1.1e-8	3.5	3.2	75	111.3	
00-CP-07	3.9e-8	4.2	5.6	80	108.2	113
	1.7e-8	7.1	4.8	80	117.3	

Sample name	^{4}He (cc)	^{238}U (ng)	^{232}Th (ng)	Grain size (μm)	Corrected Age (Ma)$^{++}$	Average Age (Ma)
00-CP-08	1.5e-8	4.8	10.2	90	126.3	126
	2.1e-8	2.4	4.5	80	128.7	
01-CP-03	7.2e-8	1.6	2.0	80	151.2	153
	9.6e-8	1.3	3.9	70	155.4	
00-CP-10	1.1e-7	1.2	1.5	80	246.8	253
	8.5e-8	1.9	3.8	90	258.9	

Table 4.1: Helium ages of apatites from southeast Australia

$^{+}$ The ages in parentheses are He ages older than the crystallization age of the rock and so they are not considereed .

$^{++}$ Helium ages are corrected for α-ejection following the method of Farley et al. (1996)

- α-ejection correction is based on U zonation determined from fission track (FT) distribution. FTs are concentrated in the outer 30-40% of all crystal, in a rim that is always > 20 μm wide – while the core contains virtually no U. The total ejection He loss is determined by comparison of core and total crystal volume.

high D-par, whereas the (U-Th)/He ages are not affected by the chemical composition.

Differences between apatite fission track and He ages on the plateau range between 39 (99-OZ-09) and 54 Myr (99-OZ-10).

On the Brown Mt. traverse all the samples (with the exception of 00-CP-33) from the coastal plain and escarpment face yield (U-Th)/He ages corresponding to the early stages of the Tasman Sea break-up (120-80 Ma) (Figure 4.3). The (U-Th)/He ages across the traverse are not correlated with elevation or with distance from the present coastline, although older samples are concentrated towards the foot of the escarpment. Samples (99-OZ-08 and 01-CP-05) from the escarpment face (530 and 840 m a.s.l.), have similar (U-Th)/He ages to samples from the coastal plain. The samples on the plateau (99-OZ-09 and 99-OZ-10) yield much older He ages (207 ± 17 and 213 ±17, respectively).

Sample 00-CP-33 from the foot of the escarpment yields a (U-Th)/He age (147±17 Ma), that is clearly older than the time of early rifting. This is not the result of grain size variation (Reiners & Farley, 2001) as the grains have a diameter similar to those of the

other samples collected across the coastal plain. Optical inspection of fission track distributions in 100 crystals and their external detector mica "prints" revealed that more than 90% of the apatites have zircon inclusions up to 10 μm long, that may have gone undetected during the hand-picking process, shifting the (U-Th)/He age toward spurious old values. However the three replicate of sample 00-CP-33 yielded similar ages, with a standard deviation of the mean of 12%. This is slightly higher than the 8% determined on six replicates of sample 99-OZ-13. Random U-rich mineral inclusions are expected to result in He ages that do not reproduce well; therefore there is a strong probability that the old He age of sample 00-CP-33 reflects its cooling history.

All the samples on the coastal plain on the Towamba River traverse have He ages corresponding to the early stages of the Tasman Sea breakup (120-80 Ma), as recorded by the Brown Mt. traverse. Along the Towamba River, however, the samples from the escarpment face (00-CP-07; 00-CP-08; 00-CP11) yield ages that are older than the rifting event and get increasingly older towards the escarpment lip (Figure 4.1B). The sample from the plateau (00-CP-10) yields a He age of 253±20 Ma. This is indistinguishable from plateau ages on the Brown Mt. traverse. The (U-Th)/He ages from the coastal plain are indistinguishable from each other, within 1σ analytical uncertainty, apart for 00-CP-04 and 00-CP-06 which are similar to the lowermost two samples from the escarpment face. Nonetheless, the (U-Th)/He ages from the escarpment show a positive correlation with elevation that is consistent with these samples having experienced the same amount of denudation since 120-110 Ma (Figure 4.3C).

The samples from the western flank of the Continental Drainage Divide (7859 and 7759) yield old (U-Th)/He ages (247±20 and 182±15 Ma) that are indistinguishable from the ages on the plateau near the escarpment lip. There is no clear correlation between elevation and/or distance from the escarpment lip for the samples collected on the plateau top.

Three aliquots from three different samples yielded (U-Th)/He ages that are older than the time of crystallisation of the rock (Table A1.3). The blank run performed after each of these aliquots (Chapter 2) was characterised by between 0.5 and 1% of the He released by the sample. These ages are considered to be spurious, possibly due to the presence of He-bearing fluid inclusions. They are not considered in the following discussion.

4.4 Discussion

The (U-Th)/He age variation across the coastal plain (Figure 4.3B) indicates that breakup-related cooling was highest at the present coast and minimum at the foot of the present escarpment, as suggested by the apatite fission track data. The positive correlation between elevation and (U-Th)/He ages on the escarpment face along the Towamba River traverse indicates that the average rate of denudation at the time of cooling through the PRZ in this area was about 8 m/Myr (Figure 4.3C). The (U-Th)/He ages–elevation plot (Figure 4.3C) does not show a break in slope, so neither the fossil PRZ nor the onset of the denudational event can be determined. This suggests that the sample 00-CP-06 from the foot of the escarpment (elevation 295 m) was at temperatures

< 80°C at 110-120 Ma. The lack of correlation between elevation and (U-Th)/He ages across the coastal plain indicates that the amount of cooling was locally variable. The traverses are not vertical profiles through the crust, i.e. they do not approximate to boreholes. Consequently rates of denudation cannot be calculated by the slope of the trend of the (U-Th)/He ages versus elevation. The variable amount of cooling indicated by the He ages across the coastal plain is indicative of differences in the amount of denudation and geothermal gradient and/or to post-late-Mesozoic fault movements, or some combination of the three. The 1:250,000 geological map of this region (Dpt. Mineral Resources, 1995) shows a single NNW-SSE fault crossing the Brown Mt. traverse west of sample 00-CP-33 (Figure 3.10). However, no correlation can be drawn between the position of this fault and the He age trend across the coastal plain. Very few other faults are mapped, but the area is characterised by granites where faults are not easily detected. Overall, it is likely that the variation in the (U-Th)/He ages on the coastal plain is due to a decrease in the amount of denudation towards the foot of the escarpment and/or an elevated palaeogeothermal gradient at the present coastline, but brittle tectonics may have played a role locally. Distinguishing between these factors is of fundamental importance not only to determining the evolution of the escarpment, but also to constraining the pre-rift topography (section 4.5.1).

The (U-Th)/He ages on the plateau are consistent with slow cooling from late Mesozoic palaeotemperatures that were lower than those experienced by the samples from the coastal plain and escarpment face. The lack of correlation between the plateau (U-Th)/He ages and elevation and/or distance from the escarpment lip suggest that the present highlands were not significantly affected by the continental break-up.

In summary, the apatite (U-Th)/He ages from both traverses provide the following information:

1) The region that is currently at the foot of the escarpment was at temperature < 80°C in the late Mesozoic;

2) at around 100-90 Ma the area near the present coastline was at >80°C;

3) the plateau samples show no evidence of thermal effects associated with the opening of the Tasman Sea.

The two samples from the escarpment face on the Brown Mt. traverse (99-OZ-08; 01-CP-05) do not fit this interpretation. They yield ages of 104±8 Ma and 113± 9 Ma, respectively. Despite their proximity to the plateau top, these ages are indistinguishable from the ages found across the coastal plain. The low age is unrelated to apatite grain size variation (Reiners & Farley, 2001), as the three replicates for each sample yielded similar ages, despite significant variation of grain size among the single aliquots (between 60 and 260 μm in diameter). However, optical observation of fission track distribution in 99-OZ-08 apatites and their mica prints show that all the 80 grains observed are characterised by zoned U distribution. Fission tracks are concentrated in the outer 30-40% of the crystals, in a rim that is always wider than 20 μm, while the core has virtually no U. Although the recoil correction has been modified to take account of this U distribution (see note to Table A1.3), the correction may not account for the total recoil loss of He occurred in this sample. Meester and Dunai (2002) demonstrated that a non-uniform distribution of U (and subsequently Th) in the apatite crystal can account for a variation in (U-Th)/He age of up to 33 %. These young He

ages could reflect later denudation of this area, with the samples residing in the PRZ until more recent times than the samples now on the coastal plain. To check this hypothesis, a forward model has been used to predict He ages for a given thermal history. A 60 μm apatite grain entering the PRZ at 180 Ma and reaching 40°C at 60 Ma will yield an age of 110 Ma, very similar to the He ages of 99-OZ-08 and 01-CP-05. It is important to point out that this is one of the many thermal histories that predicts this He age. Nonetheless, it indicates that the escarpment face experienced erosion later than the coastal plain, when the rapid cooling event had already terminated, in agreement with the low denudational rate (8m/Myr) derived from the samples on the escarpment along the Towamba River traverse.

The (U-Th)/He age of 99-OZ-06 (88±7 Ma), from near the foot of the escarpment, could indicate either a rapid cooling from higher temperatures than the other samples nearby, suggesting a localised high geothermal gradient, or fault-controlled exhumation, or a longer residence in the PRZ prior to denudation at 90-100 Ma. The sample was collected on an interfluve (220 m a.s.l.), which may have been denuded more slowly than the streams beds with the sample thus residing in the PRZ for longer.

Sample 00-CP-36, 17 km from the present coastline was collected on a "facet" considered to be a remnant of a pre-rift palaeosurface (Ollier & Pain, 1998). The 99±8 Ma (U-Th)/He age is inconsistent with the presumed antiquity of this area, however, and demonstrates that the coastal plain must have been denuded of several km since the late Mesozoic.

4.4.1 Combining apatite fission track and (U-Th)/He data

A simple way to combine apatite fission track and (U-Th)/He data is to use the "good" (χ^2>0.5) AFTT-derived thermal histories from AFT-Solve (Chapter 3) as parameters for forward modelling of (U-Th)/He ages (e.g. Wolf et al., 1998). A sub-set of AFT-derived thermal histories generate the (U-Th)/He ages obtained in the laboratory. DECOMP sofware determines (U-Th)/He ages for selected time-temperature paths for given grain size and U distribution within minerals (Meester & Dunai, 2002a, 2002b). DECOMP uses an algorithm that takes into account the combined effects of α-recoil, heterogeneous distribution of the parent elements, and diffusion. Prediction of (U-Th)/He ages for different time-temperature paths shows that the age difference between this method and the recoil correction technique (e.g. Farley, 2002) can be 20%, for a homogeneous distribution of the parent elements (Meester & Dunai, 2002). This is especially important when samples have been in the PRZ for long times relative to the time since cooling.

A general result of predicting (U-Th)/He ages using the AFT-derived thermal histories is that at least 50% of the possible time-temperature paths that fit the fission track data do not reproduce the measured (U-Th)/He age. The AFT-derived thermal histories that satisfy the He age define narrower envelopes than the fission track data alone. Consequently, the number of acceptable time-temperature paths is decreased and the precision of the denudation history is improved.

Figure 4.4 shows the thermal histories that satisfy the (U-Th)/He and fission track data for all samples. A maximum of 50 paths are shown for each sample: the continuous

lines represent thermal histories that fit the (U-Th)/He ages by 1σ, the dotted lines by 2σ. The description and interpretation of the thermal histories obtained for the samples collected along the two traverses (Figure 4.4) are reported in the following sections. Samples 99-OZ-13 and 99-OZ-08 from the Brown Mt. traverse have no AFT-derived thermal histories that satisfy the He ages and they will be discussed below.

4.4.1.1 Brown Mt. traverse

Samples closest to the coast (99-OZ-13 and 99-OZ-12)

These samples are characterised by a rapid cooling episode that occurred at, or near, the time of break-up. At about 120 Ma the samples were at more than 120°C, so it is not possible to determine precisely when the cooling event started. The (U-Th)/He ages are consistent with a rapid cooling event which reached the lower limit of the He PRZ (~40°C) at 70±10 Ma. The fission track-derived thermal histories reproduce (U-Th)/He ages that are always 10-15% younger than the measured age. The misfit may be due to the difficulty in measuring annealing of fission track in apatite and it suggests that even when samples cool rapidly, annealing occurs over geological times.

Assuming that samples 99-OZ-12 and 99-OZ-13 were at 40°C at 80 to 60 Ma, minimum cooling rates of 2.0-1.3°C/Myr occurred during rifting and continental breakup.

Sample from the coastal plain (00-CP- 35)

The AFT data require this sample to be in the PAZ at 200 Ma or earlier and that at 120 Ma it was at 60-65°C. Of the eight thermal histories that fit the fission track data, only

three predict the measured (U-Th)/He age. These time-temperature paths show a rapid cooling event (0.6°C/Myr) starting at about 100 Ma that cooled the sample to below 40°C no later than 65 Ma. These data indicate that, although rapid, the cooling rate was at least three times lower than that experienced by the coast samples. When seafloor spreading ceased at 65 Ma, the sample was at approximately 40°C.

Sample from the escarpment foot (00-CP-33)

The sample now at the foot of the escarpment was at 55±8°C at 120 Ma and it had cooled to 40°C by 50 Ma. The time-temperature paths do not show the c. 100 Ma rapid cooling event, but are consistent with a constant cooling rate of about 0.3°C/Myr since 120 Ma. At these low temperatures, however, both two thermochronometers are too insensitive to show differences in cooling rates. Although the (U-Th)/He age is old (146 Ma), it is consistent with the fission track data that indicate that this area was in the PRZ before the other coastal plain samples.

Sample on the escarpment face (99-OZ-08)

All the 1070 "good" thermal histories produced by AFTSolve result in (U-Th)/He ages that are older than the measured age by 30-50%, even when a U-rich rim is considered. The young (U-Th)/He age may indicate that the sample was in the PRZ for longer (see above) than predicted by the fission track data.

Samples from the plateau top (99-OZ-09 and 99-OZ-10)

The AFTT-derived thermal histories that are consistent with the measured (U-Th)/He ages show that at 120 Ma the samples were below 60°C and that prior to this they had cooled slowly through the PRZ at approximately 0.15°C/Myr. At this rate they reached the surface in the last 65 Myr. Although AFTT provides only vague constraints for the thermal histories cooler than 60°C, the measured (U-Th)/He ages are obtained only if the samples were between 55 and 35°C at 120 Ma.

4.4.1.2 Towamba River traverse

Samples from the coastal plain (01-CP-01 and 00-CP-02)

At approximately 120 Ma, these samples were at different temperatures, indicating that, although the samples yielded similar fission track and (U-Th)/He ages they experienced different thermal histories. 00-CP-02 is from the north bank of the Towamba River and has a cooling history similar to the samples near the coast from the Brown Mt. traverse. At the time of continental extension it was at about 110-120°C, while sample 01-CP-01, from the southern bank, was at least 30°C cooler. Nonetheless, by 65 Ma the two samples were both at 50-40°C. The cooling rate of 01-CP-01 was approximately 1.4°C/Myr compared to 0.6°C/Myr for 00-CP-02. The thermal histories derived from the latter sample shows that the rapid cooling event started at about 120 Ma, confirming the conclusion derived from the AFT data that the onset of the rapid cooling event occurred some 30-40 Myr before sea-floor spreading.

Sample from the foot of the escarpment (00-CP-04 and 00-CP-05)

Samples 00-CP-05 and 00-CP-04 were collected at the foot of the escarpment at 240 m. The main difference between the thermal histories derived from the two samples lies before 120 Ma. At 150 Ma 00-CP-04 was at approximately 60°C, whereas 00-CP-08 was at 75±5°C. However by 100 Ma both were at the top of the He PRZ, the thermal histories being consistent with a constant cooling between 150 and 100 Ma, at different rates for each sample. Since 100 Ma the time - temperatures paths of the two samples are indistinguishable within the uncertainties of the methods, and they reached 40°C at around 65 Ma. This results in cooling rates of 0.5-0.4°C/Myr between 120 Ma and 65 Ma. None of the thermal histories for sample 00-CP-04 show a rapid cooling event, whereas two of the time - temperature paths for 00-CP-04 show a rapid cooling from 75 to 45°C at 110-90 Ma.

Sample from the plateau top (00-CP-10)

The sample collected inland of the escarpment lip shows no indication of rapid cooling associated with the time of breakup. The time-temperatures paths for this sample are characterised by slow and constant cooling of 0.15-0.2°C/Myr since 200 Ma. This is similar to the thermal histories derived for the two samples on the plateau on the Brown Mt. traverse, for which cooling rates of about 0.15°C/Myr were obtained. The plateau in this region may have experienced a common post-breakup evolutionary history dominated by low rates of denudation. Relief was probably already quite subdued in the Late Mesozoic and local geomorphological features were not significant enough to affect the He-thermochronological data.

4.5 Interpretation

On both traverses the cooling rates decrease from the coastline to the plateau top (Figure 4.5). This trend indicates that differences in palaeotemperatures between samples collected at the same distance from the continental shelf are related to local difference in denudation and/or palaeogeothermal gradient, but the area was affected by the same denudational and/or thermal event. Between 120 and 80 Ma relatively rapid (up to 2°C/Myr) cooling affected the coastal region. The ability to identify the rapid cooling event is lost near the foot of the escarpment, because by 120 Ma the samples were already above 60°C. Constant cooling rates of 0.3°C/Myr (00-CP-33) and 0.5-0.4°C/Myr (00-CP-08 and 00-CP-04 respectively) between 120 and 65 Ma may be continued to the present time. On the plateau the cooling rates of 0.15°C/Myr for the last 200 Myr are at least half of those calculated for the foot of the escarpment, indicating that denudation everywhere on the coastal plain occurred more rapidly than it did on the plateau. Constant cooling rates on the plateau are also indicative of the fact that the geothermal gradient may have remained constant over the last 120 Ma at least.

4.5.1 Denudation across the coastal plain

Cooling rates can be converted to denudation rates if the palaeogeothermal gradient is known (or estimated) (e.g. Gleadow & Brown, 2000). At its most extreme, the different rates of cooling recorded across the south eastern Australian margin can be due to differences in geothermal gradient, with the amount of denudation remaining constant.

If a geothermal gradient of 25°C/km (consistent with present values of heat flow; Beardsmore & Cull, 2001) is assumed then the foot of the escarpment has endured 1.8 km of denudation since 120 Ma. In order to achieve the same amount of denudation across the coastal plain a variable post-extensional geothermal gradient of 55-60°C/km must be invoked at the present coastline. Assuming a geothermal gradient that increased linearly from 40 to 60°C/km, within a 50-km wide coastal plain, van der Beek (2002) suggests that the eastern Australian margin has evolved by passive denudation with associated flexural isostatic rebound of a pre-existing ~2.5 km high plateau. Using the PECUBE numerical model, (U-Th)/He ages ranging from 20 to 150 Ma (coast to escarpment) were predicted for constant escarpment retreat, and from 70 to 150 Ma for the plateau downwearing scenario (Figure 4.6). The trend of the He age data that is common to both traverses is not reflected in the model prediction. More importantly, the model does not reproduce the ~90 Ma ages at the present coastline found along the Brown Mt. traverse, however the age taken for the initiation of rifting is not reported.

The amounts of denudation in Figure 4.7 are calculated for two end-member cases:

(i) A geothermal gradient that increases exponentially from 25°C/km (current value) at the escarpment base to 60°C/km (maximum value measured in rifts, eg. Makris *et al.*, 1991) at the present coastline from 120 to 80 Ma;

(ii) A constant geothermal gradient of 25°C/km through time and across the coastal plain.

The amount of denudation shown in Figure 4.7 is calculated from the averaged palaeotemperature experienced by the sample at 120, 80 and 40 Ma according to the

thermal histories derived from the AFT-He thermochronological data. Samples either side of the Towamba River are plotted separately, as near the present coastline they have experienced different amounts of cooling since 120 Ma. In the case of a variable geothermal gradient (Figure 4.7), the total denudation since 120 Ma along the traverses is of approximately 3 km at the coast and 1.8 km a the foot of the escarpment, implying an isostatic rebound and/or rock uplift of a maximum of only 1 km.

In the constant geothermal gradient case (Figure 4.7), the total denudation at the coast is in excess of 4 km for both traverses, while it may be of the order of 2-3 km at the foot of the present escarpment. Considerable rock uplift possibly due to isostatic rebound, need to be accounted for. Both sides of the Towamba River have experienced the same amount of denudation near the escarpment, within the uncertainties of the method, but, near the coast, total erosion on either side of the river is different. This may indicate that the syn- or post-breakup tectonics of the area is complex and that margin-parallel faults were active in the early stages of continental break-up. The Brown Mt. area appears to have experienced less denudation than the Towamba River, although the difference is difficult to resolve accurately with the analytical techniques.

Denudation of the region more than 40 km inland of the coast is unaffected by the change in geothermal gradient at the coastline. For a constant 25°C/km geothermal gradient, the difference in the amount of denudation is in excess of 2500 m within a 50 km-wide strip of the coastal plain. A 3-D numerical surface process model employed in south east Africa (van der Beek et al., 2002; Brown et al., 2002) show that a similar pattern of denudation can be explained by assuming an elastic thickness of the lithosphere (T_e) of about 10 km, a lower, but still realistic value, similar to the ~15 km

suggested by McKenzie & Fairhead (1997) for continental regions, but it is higher than the values of ≤ 5 km typical of oceanic crust. A similar estimate could be employed in eastern Australia to invoke a constant geothermal scenario and explain the observed pattern of denudation derived from the thermochronological data. A higher T_e would reduce the amount of isostatic flexure as the 25 km value assumed by van der Beek *et al.*'s model (1999); however, they invoke a higher geothermal gradient at the coast. The relationship between geothermal gradient and elastic thickness is, however, complex, because an increase of heat flow would decrease T_e (e.g. Watts, 2001). Alternatively, syn- and post-breakup brittle movements along faults need to be invoked to account for differential denudation between adjacent areas

4.5.1.1 Pre-rift topography

The backstacking technique allows the calculation of the initial elevation and the amount of surface uplift before denudation, knowing the present elevation and the amount of denudation experienced by a region (Brown, 1992). In the model suggested by Brown (1992), Airy isostatic rebound is used so that unloading is locally compensated.

Backstacking is calculated from:

$$U_s + H_i + \Delta Hsl = (H_o + \Delta E) - (\Delta E\ \rho_c/\rho_m)$$

where: Us is the surface uplift; H_i and H_o are the initial and present elevations, respectively; ΔE is the amount of denudation; ρ_c and ρ_m are the density of crust and mantle and ΔHsl is the change in sea level.

Figure 4. 9 shows the sum of Us + Hi + ΔHsl for each point across the two traverses through time. As the variation in sea level is the same for all samples, this can be ignored and the profiles indicate the topographic evolution of the margin since 120 Ma. Thermochronological data cannot distinguish between pre-denudational event topography and surface uplift. When the geothermal gradient is constant, an upwarp (about 1° slope) of the topography near the coast along the Brown Mt. traverse is visible. However, the difference in topography between the constant versus variable geothermal scenarios could be in response to thermal buoyancy due to the change in palaeogeothermal gradient (e.g. Brown *et al.*, 2002). In any case, the predicted pre-rift topography strongly resembles the present situation with a significant change in elevation at the present position of the escarpment. The plateau top was possibly at about 1200 m at Brown Mt. and about 800 m at the head of the Towamba River, whereas the present coastline was between 400 and 600 m in elevation. Employing flexural isostasy instead of Airy isostasy would provide a more precise reconstruction of the landscape and the palaeorelief may result attenuated, but Airy isostasy allows first order morphological features to be detected. Consequently, the position of the present escarpment pre-dates the breakup and the escarpment has been "pinned" to its position as predicted by the downwearing scenario for passive margins evolution (e.g. Kooi & Beaumont, 1994).

4.5.2 Chronology of escarpment evolution

The amounts of denudation from the coastal plain to the plateau top are calculated from the average palaeotemperatures experienced by the samples at 120; 80 and 40 Ma.

Figure 4.7 shows that erosion was diachronous across the coastal plain and, although a regional pattern can be identified, the areas covered by the two traverses may have evolved slightly differently. Near the present coastline denudation was rapid between 120 and 80 Ma and less than 1 km of crust has been removed since sea-floor spreading (85 Ma). Obviously, in the case of constant geothermal gradient, the amount of crust removed is higher as are the rates of erosion. Between 120 and 80 Ma rates of Denudation rates at the coast were 100 to 60 m/Myr (constant and variable geothermal gradient scenarios, respectively) between 120 and 80 Ma. At approximately 80 Ma erosion rates decreased to values of 10 m/Myr, similar to the rates indicated by cosmogenic isotope studies for the last 2 Myr (Heimsath et al., 2000) and the average value calculated from the vertical profile on the escarpment face along the Towamba River traverse (see section 4.3).

Rates of erosion crucial for determining mechanisms and times of escarpment evolution. In Chapter 3 the three models of escarpment evolution were described and the inconsistency of the fission track data with the downwarped rift shoulder model was noted. The ~90 Ma (U-Th)/He ages at the coast, even on one of the "facets" (see section 4.3), provides strong evidence that the downwarped rift shoulder model is not applicable to this region. In order to distinguish between the remaining two scenarios and to clarify time of escarpment evolution, (U-Th)/He ages have been predicted for time-temperatures paths that are characteristic of the escarpment retreat and downwearingof a rift shoulder mechanisms, using DECOMP. The predicted ages are from apatite crystals 60 μm in diameter and at least 180 μm long. For both scenarios constant (25°C/km) and variable (from 25 to 60°C/km) geothermal gradients are

considered. To define times of escarpment evolution 4 different options that satisfy the thermochronological data are considered:

(i) The escarpment was at its present position at 115 Ma

(ii) The escarpment was at its present position at 90 Ma

(iii) The escarpment was at its present position at 60 Ma

(iv) The escarpment evolved at constant pace and it reached its present position at present times.

The time frames are chosen based on experimental (Cockburn et al., 2000) and theoretical (Gilchrist et al., 1994) studies for the south eastern African margin. In Figure 4.9, (U-Th)/He ages are referred to the removal of 4.5, 4.0, 3.5, 3.0, 2.5, 2.0 and 1.5 km of crust in the case of a constant geothermal gradient and 2.5, 2.3, 2.0, 1.8 and 1.5 km in the case of a variable geothermal gradient. The same amount of crust is predicted to be removed by each mechanism. In the downwearing rift shoulder scenario denudation has acted upon all the coastal plain after 120 Ma. In the escarpment retreat scenario denudation is propagated inland as the escarpment moves towards the continental interior. (U-Th)/He ages from 120 to 80 Ma indicates that erosion of more than 2.5 km was completed by 50 Ma. Prolonged denudation would produce (U-Th)/He ages that are younger than the time of breakup (see for instance Figure 4.9c). Erosion of less than 2.5 km brings to the surface material that was in or above the PRZ prior to 120 Ma. In order to predict the thermal histories of these samples, it was assumed that the samples were at approximately 120°C at 240 Ma, as indicated by fission track data from

the plateau top (Chapter 3). Comparing the measured (U-Th)/He data with the predicted ages allows a number of erosional scenarios to be ruled out.

A constant retreat of the escarpment from the present coastline would produce (U-Th)/He ages across the coastal plain, that are younger than 80 Ma which are inconsistent with the measured ages (Figure 4.9C and 4.9D). Rapid retreat of the escarpment does not predict the ~90 Ma old ages found at the coast. Generally the escarpment retreat scenarios are inconsistent with the (U-Th)/He data for both traverses.

Constant downwearing produces 70-50 Ma (U-Th)/He ages at the present coastline, which are not reflected by the data (Figure 4.9C and 4.9D). Predicted He ages at the coast are closest to the measured age when the degradation of the plateau is completed within 30 to 60 Myr. A close match between the measured and predicted (U-Th)/He ages does not occur, probably because of local geomorphological and geological features, such as fault movements. However, the constant geothermal gradient and denudation occurring between 90 and 60 Ma matches most measured He ages, apart those from few kilometres from the escarpment foot (99-OZ-06 and 01-CP-03). The coastal plain close to the foot of the escarpment may have evolved less rapidly than the rest of the coastal plain. The downwearing scenario is also consistent with the reconstruction of the pre-rift topography obtained by backstacking the amount of crust removed, suggesting that the escarpment marks the location of a pre-rift, possibly minor, drainage divide. A similar scenario for the evolution of the south west and south east African passive margins has been proposed from AFTT and cosmogenic isotopes studies (Cockburn *et al.*, 2000; Brown *et al.*, 2002).

4.6 Conclusions

The combination of apatite fission track and apatite (U-Th)/He data has allowed the reconstruction of the syn- and post-breakup denudational history of the south eastern Australian margin and has provided strong constraints on the style and tempo of the escarpment formation and evolution. The thermochronological data are inconsistent with a downwarped rift shoulder model and the (U-Th)/He ages suggest that the escarpment formed by rapid river incision seaward of a pre-existing drainage divide located at the present escarpment. The seaward portion of the coastal plain was the first to be eroded well before the onset of sea-floor spreading. The development and preservation of Late Mesozoic weathered profiles attests to the early formation of the coastal strip and it may be not just a coincidence that they are limited to few kilometres inland of the coast, whereas in other part of the coastal lowlands they are mid to late Tertiary age (Bird & Chivas, 1993). Their preservation also indicates that erosion related to continental breakup was not pronounced and that the formation of an ocean basin did not have any relevant repercussion in the development of the continental margin. River erosion propagated inland but the present topography was established no later than 60 Ma. Across this landscape basalts were extruded in the Tertiary, filling valleys on the plateau and occupying depressions in the lowlands.

A similar pattern of thermochronological data across other high elevation passive margins (e.g. Cockburn *et al.*, 2000; Brown *et al.*, 2002) have been employed to suggest that the escarpment has developed by downwearing of a high altitude plateau rather than by constant retreat. North of study area in the Sydney Basin, syn and post-breakup

apatite fission track ages indicate that a major portion of the eastern Australia margin has evolved by excavation in place (Kohn et al., 2002). However some high altitude area on the plateau are characterised by syn-rift fission track ages (e.g. O'Sullivan *et al.*, 1996). The next chapter takes in consideration one of these regions in the attempt to use new (U-Th)/He ages to identify the denudational history of the area seen as part of the evolution of the entire margin.

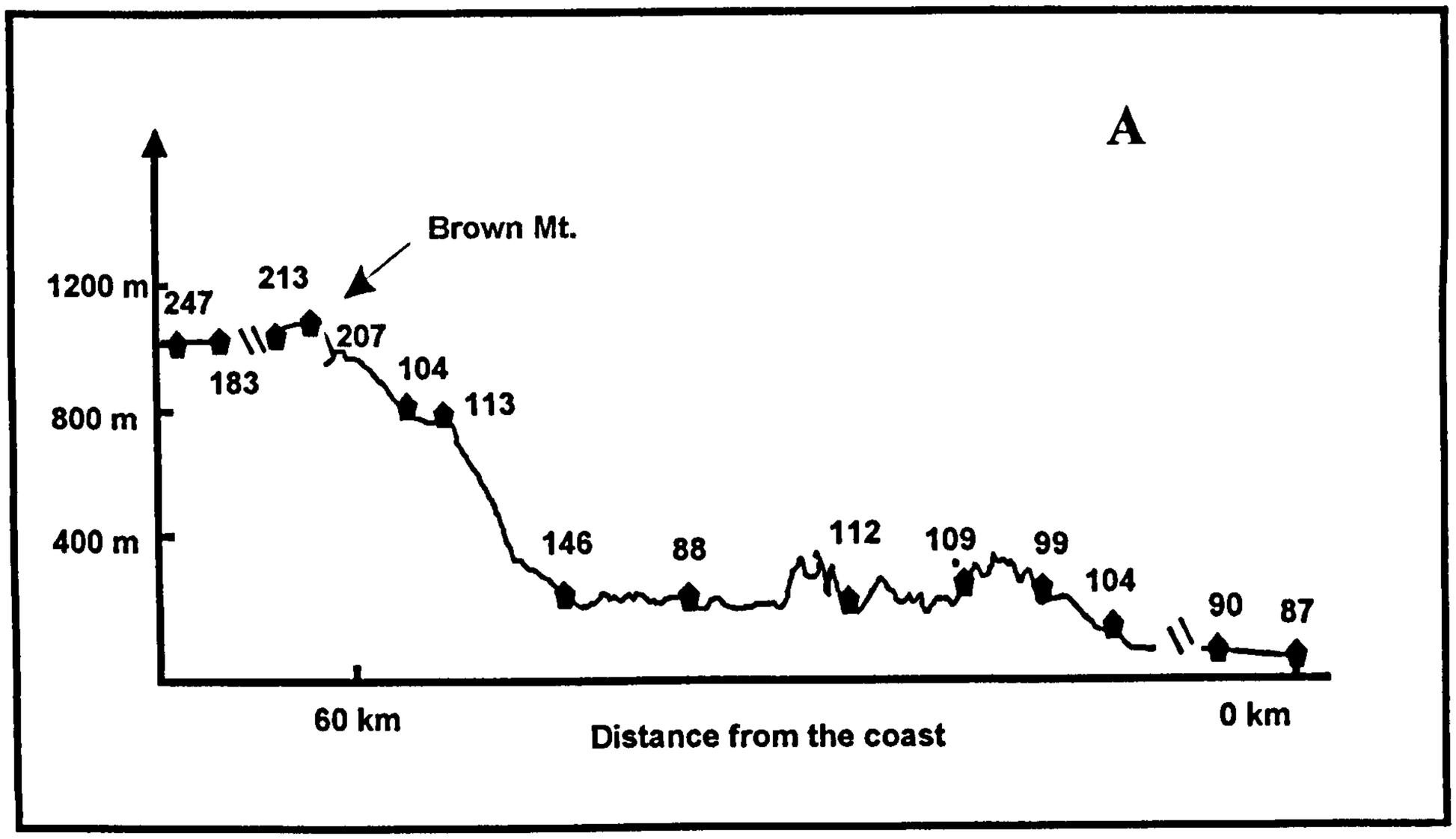

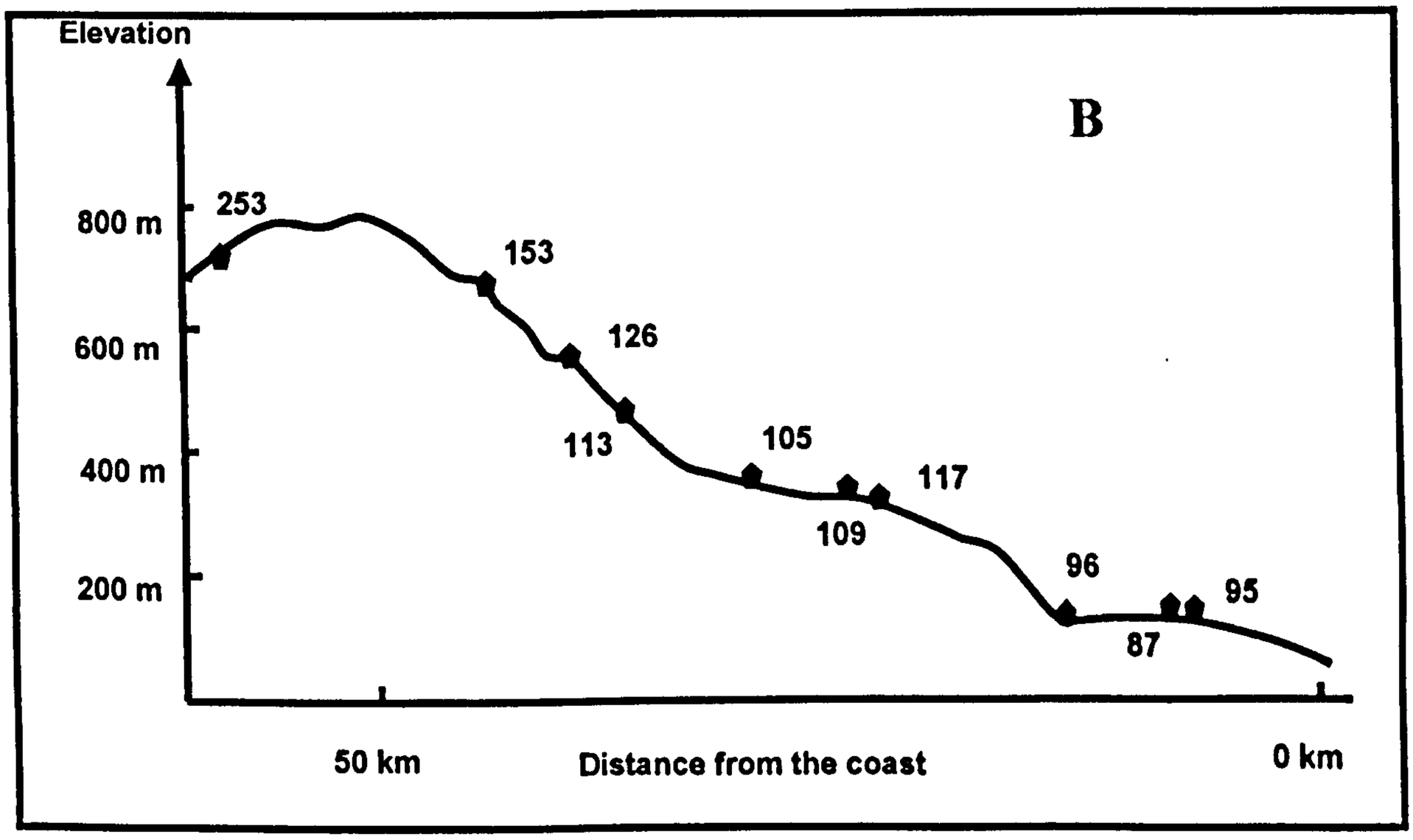

Figure 4.1: Apatite (U-Th)/He ages in Ma for (A) the Brown Mt. traverse and (B) the Towamba River traverse

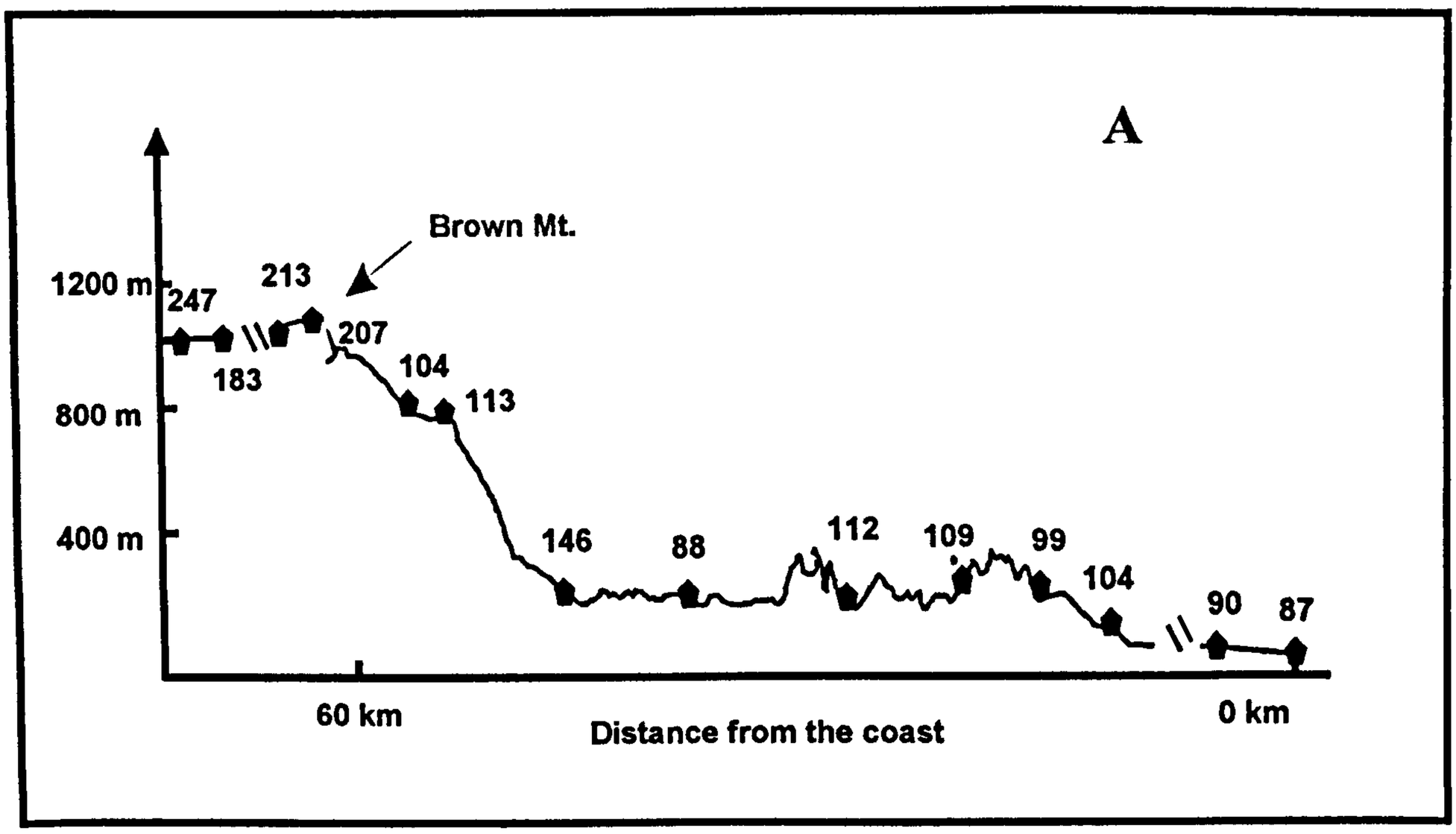

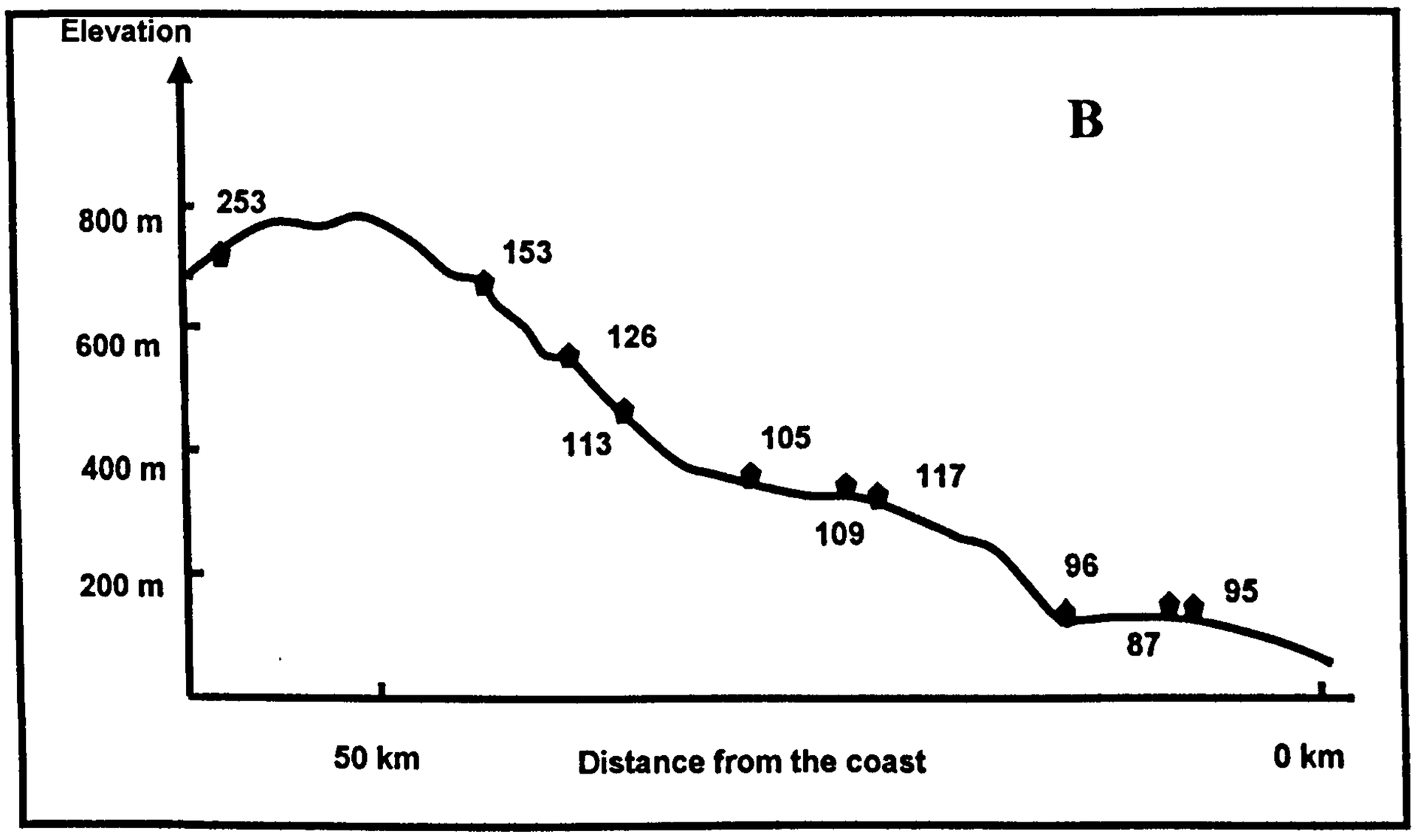

Figure 4.1: Apatite (U-Th)/He ages in Ma for (A) the Brown Mt. traverse and (B) the Towamba River traverse

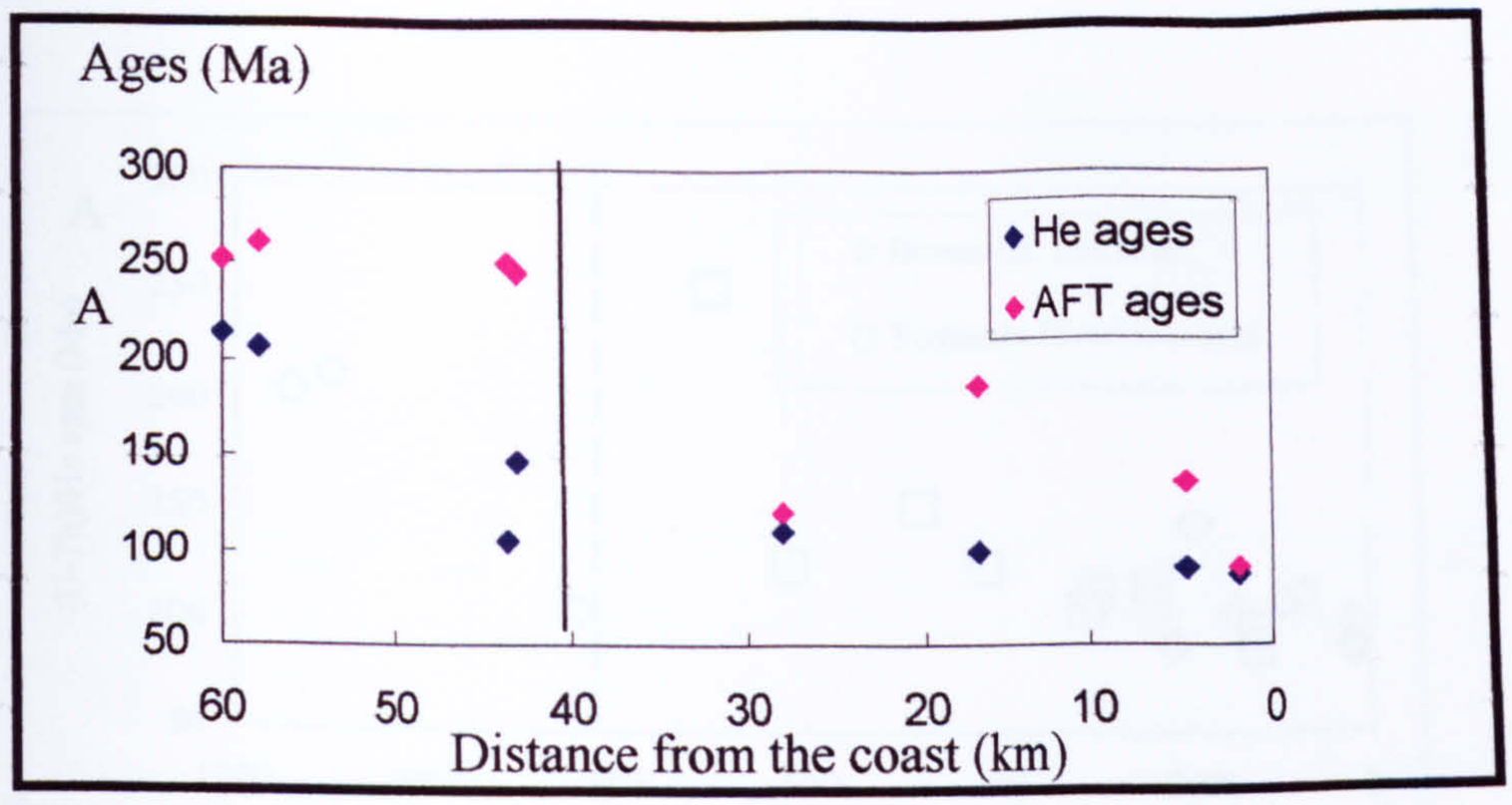

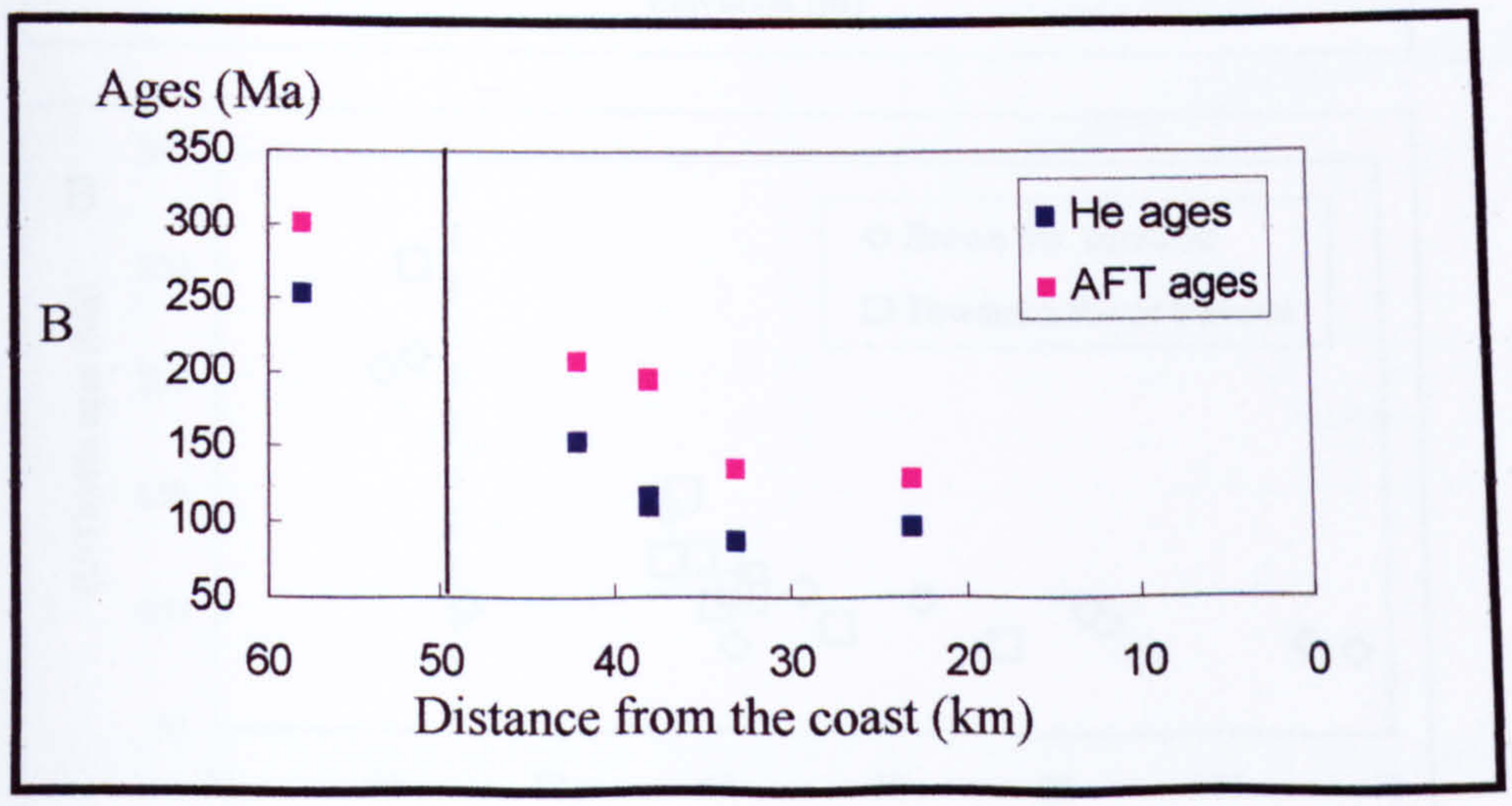

Figure 4.2: Apatite (U-Th)/He versus apatite fission track ages across the eastern Australia margin for the (A) Brown Mt. and (B) the Towamba River traverse. The vertical line represents the position of the escarpment on both traverses.

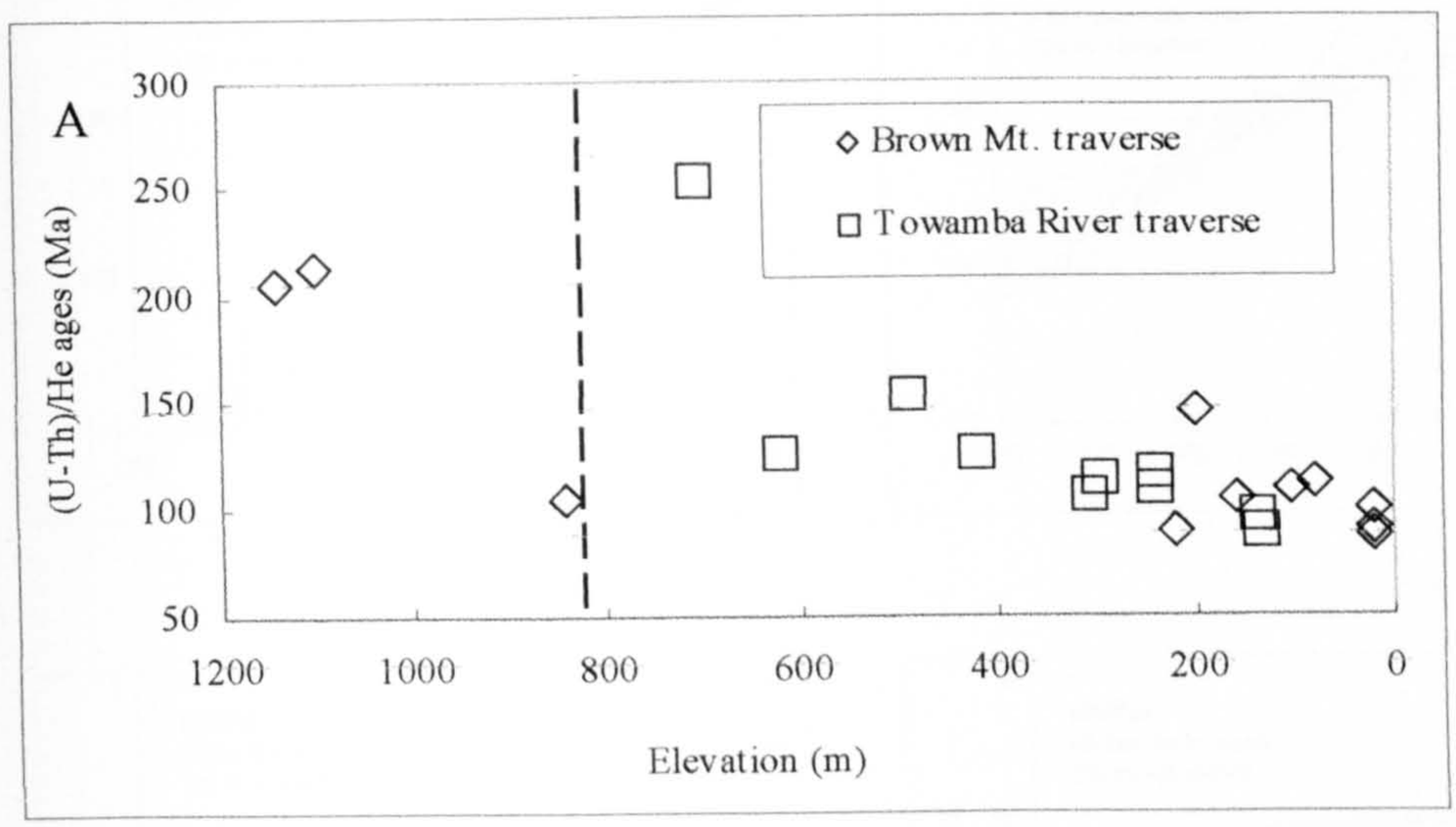

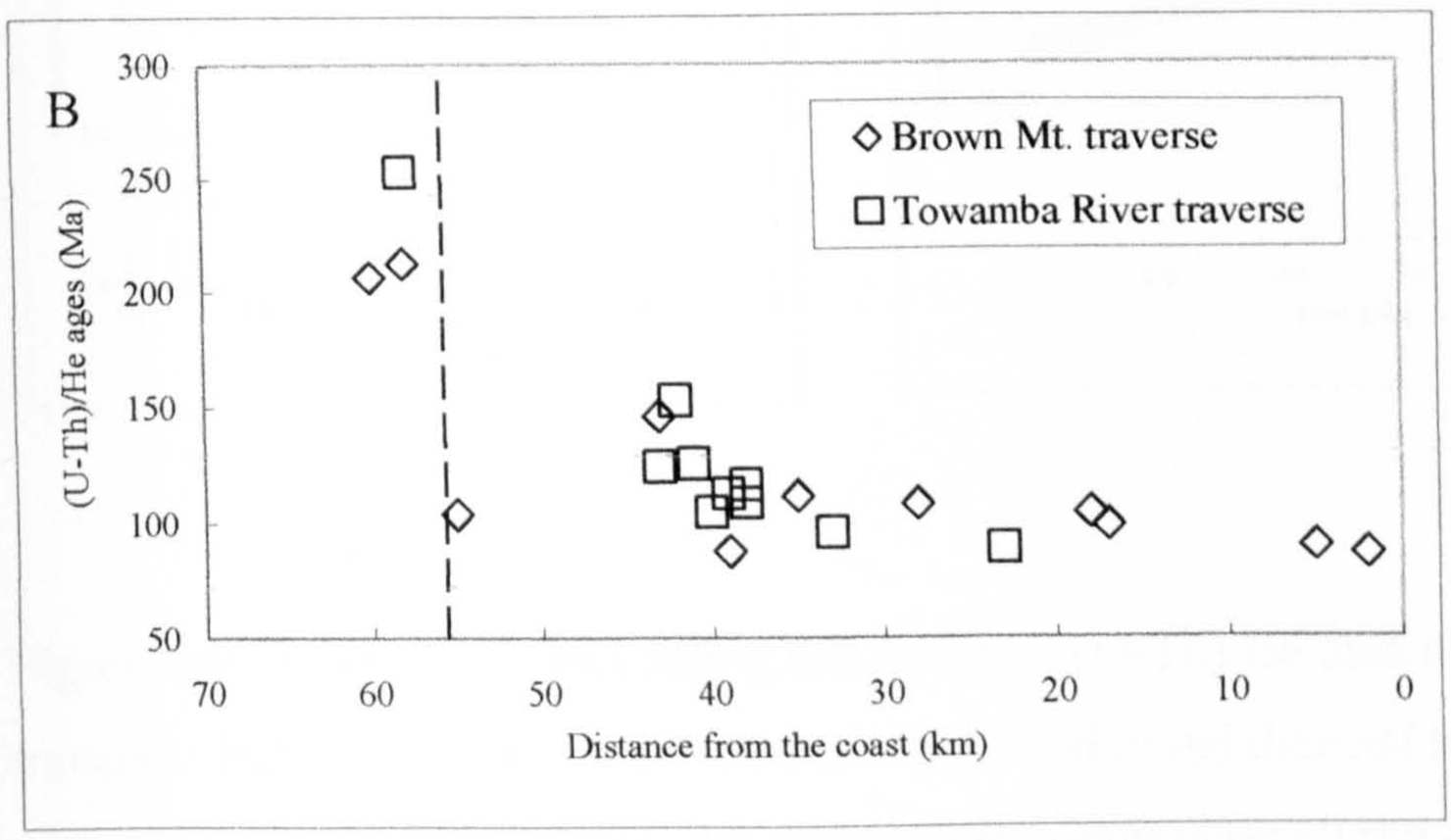

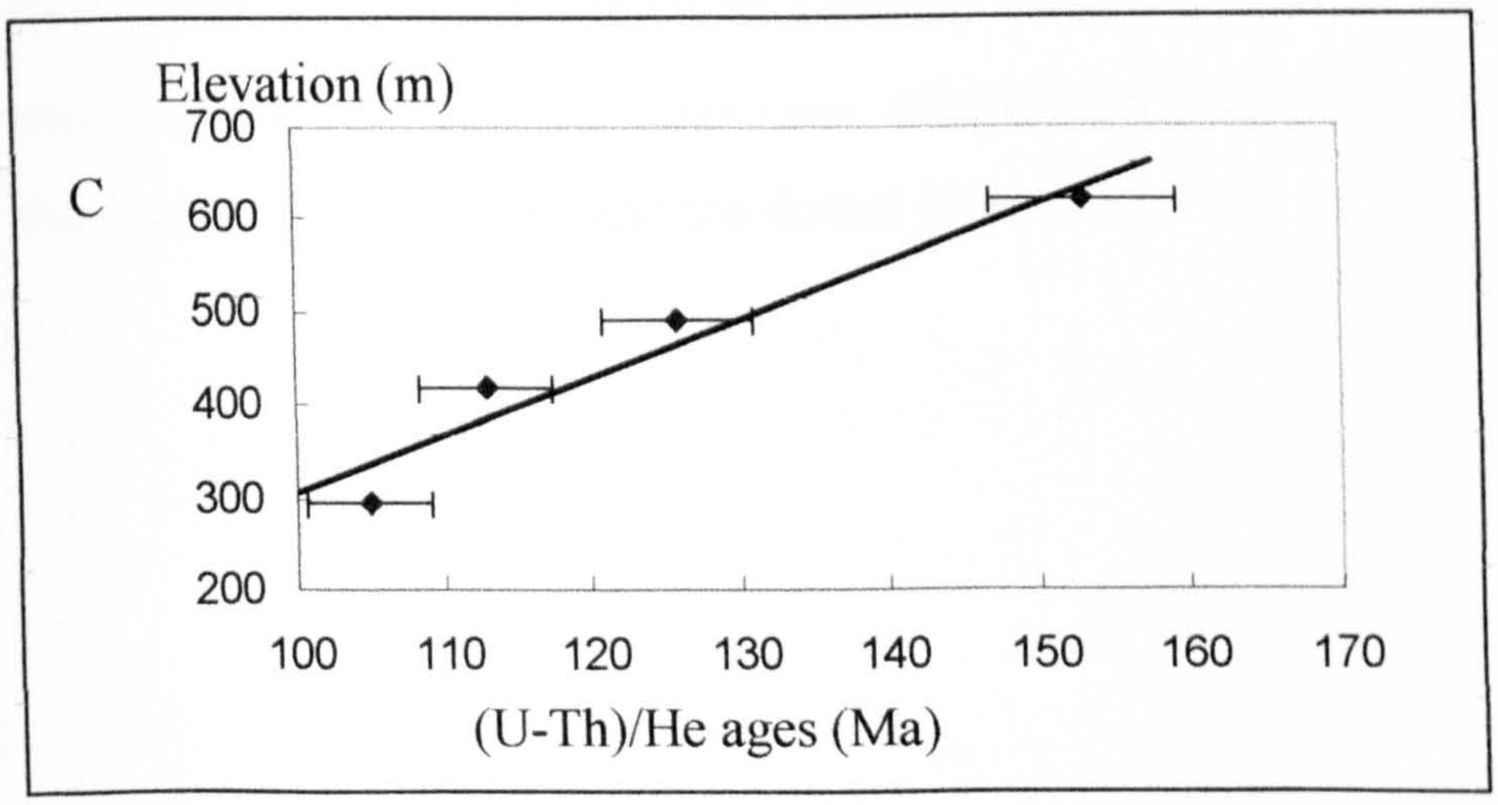

Figure 4.3: Apatite (U-Th)/He ages versus elevation (A) and distance from the coast (B) across the two traverses. The dashed line represents the position of the escarpment. (U-Th)/He ages of samples on the escarpment face at Towamba River (C) define a slope that gives a denudation rate of 8m/Myr.

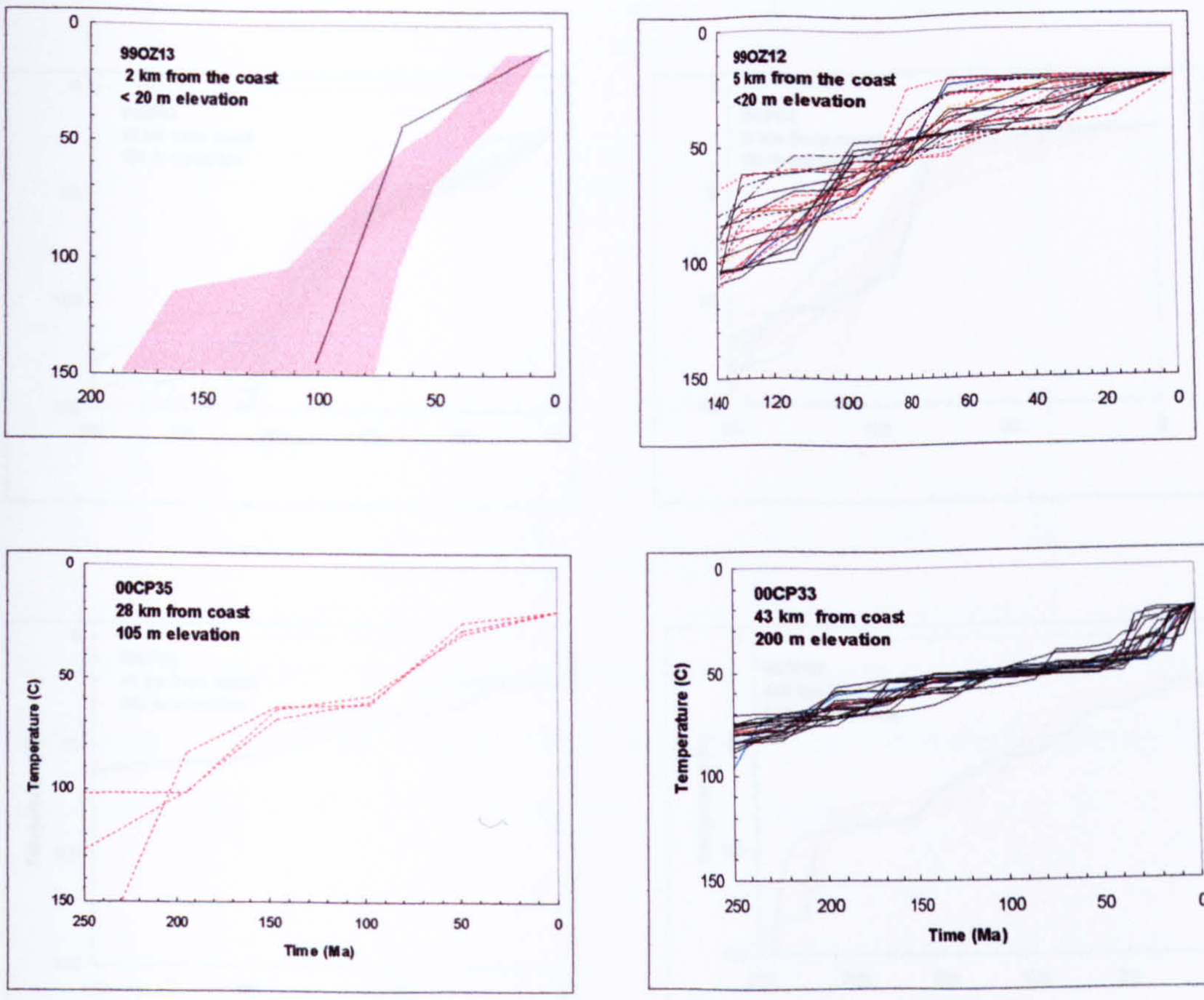

Figure 4.4: Thermal histories fitting the AFT and (U-Th)/He data along the Brown Mt. traverse. For sample 99-OZ-13 none of the AFT-derived thermal histories predicts the measured He age. In this case, the envelope encompassing all the cooling histories that fit the AFT is presented along with a thermal history (solid line) that predicts the measured He age. In all the other case, solid lines represent thermal histories predicting the measured He age (1σ) and the dotted lines (2 σ).

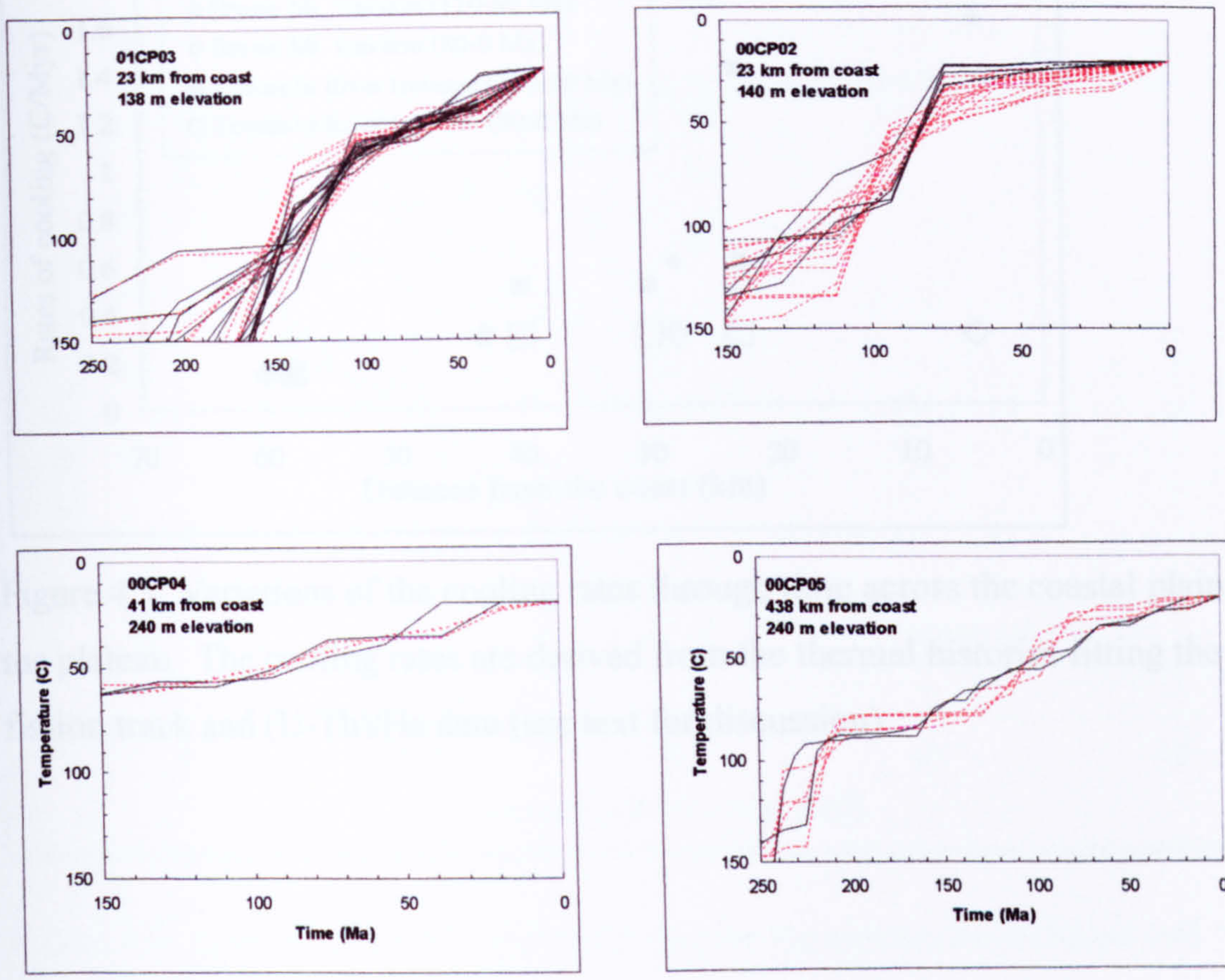

Figure 4.4(cont.): Thermal histories fitting the AFT and (U-Th)/He data along the Towamba R. traverse.

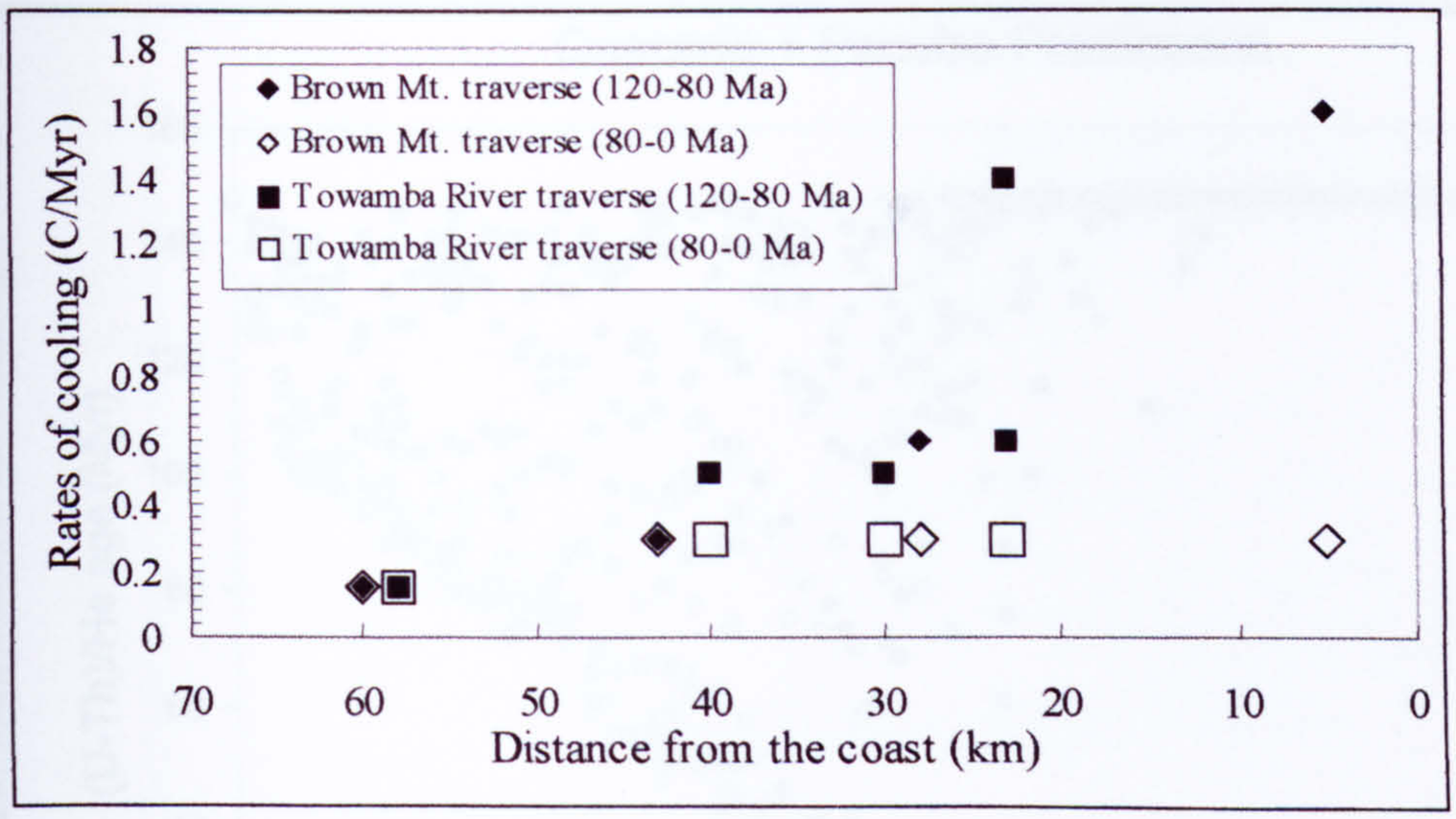

Figure 4.5: Variations of the cooling rates through time across the coastal plain and on the plateau. The cooling rates are derived from the thermal histories fitting the apatite fission track and (U-Th)/He data (see text for discussion)

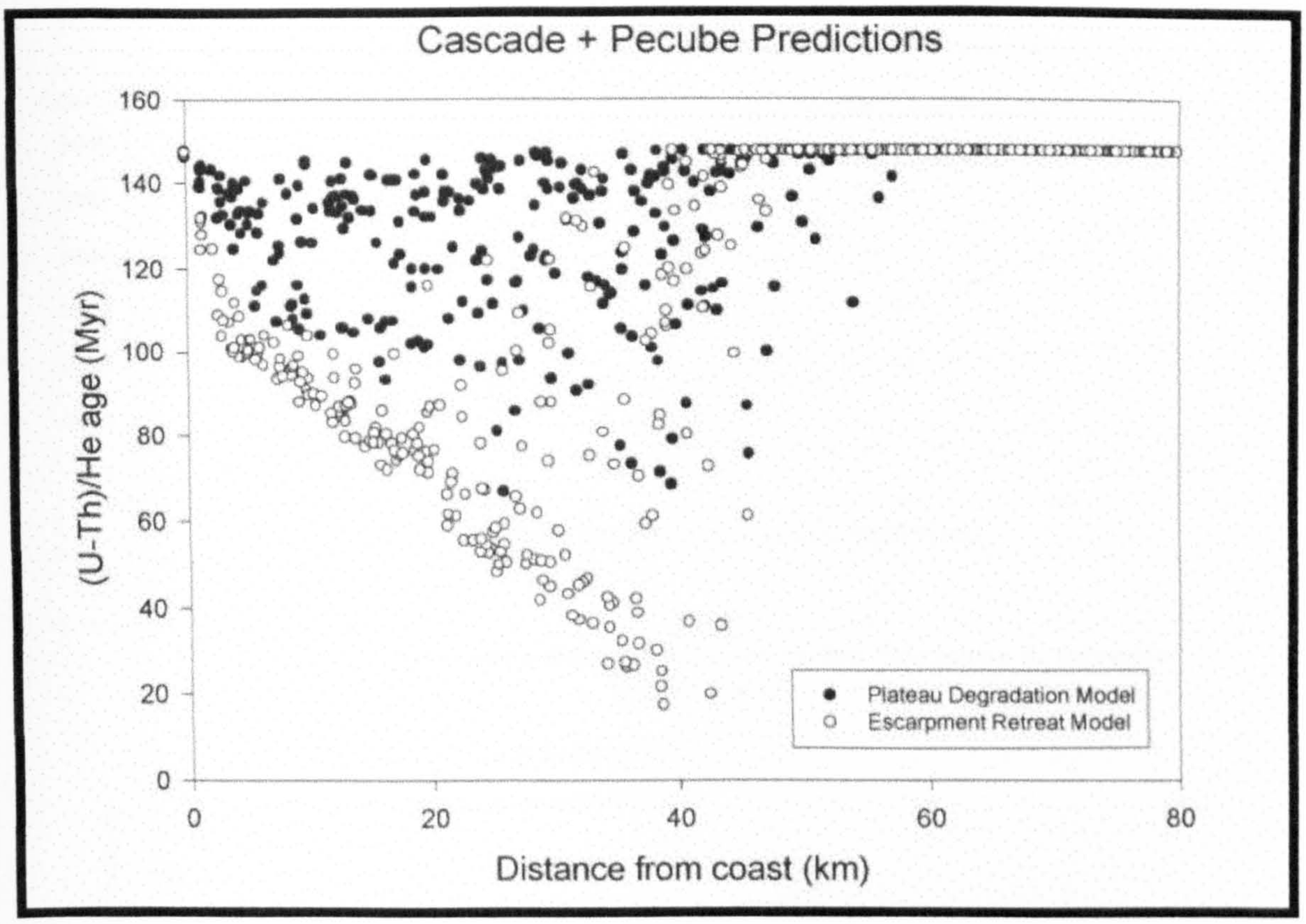

Figure 4.6: Apatite (U-Th)/He ages predicted for the plateau degradation and escarpment retreat scenarios (from van der Beek *et al.*, 2002)

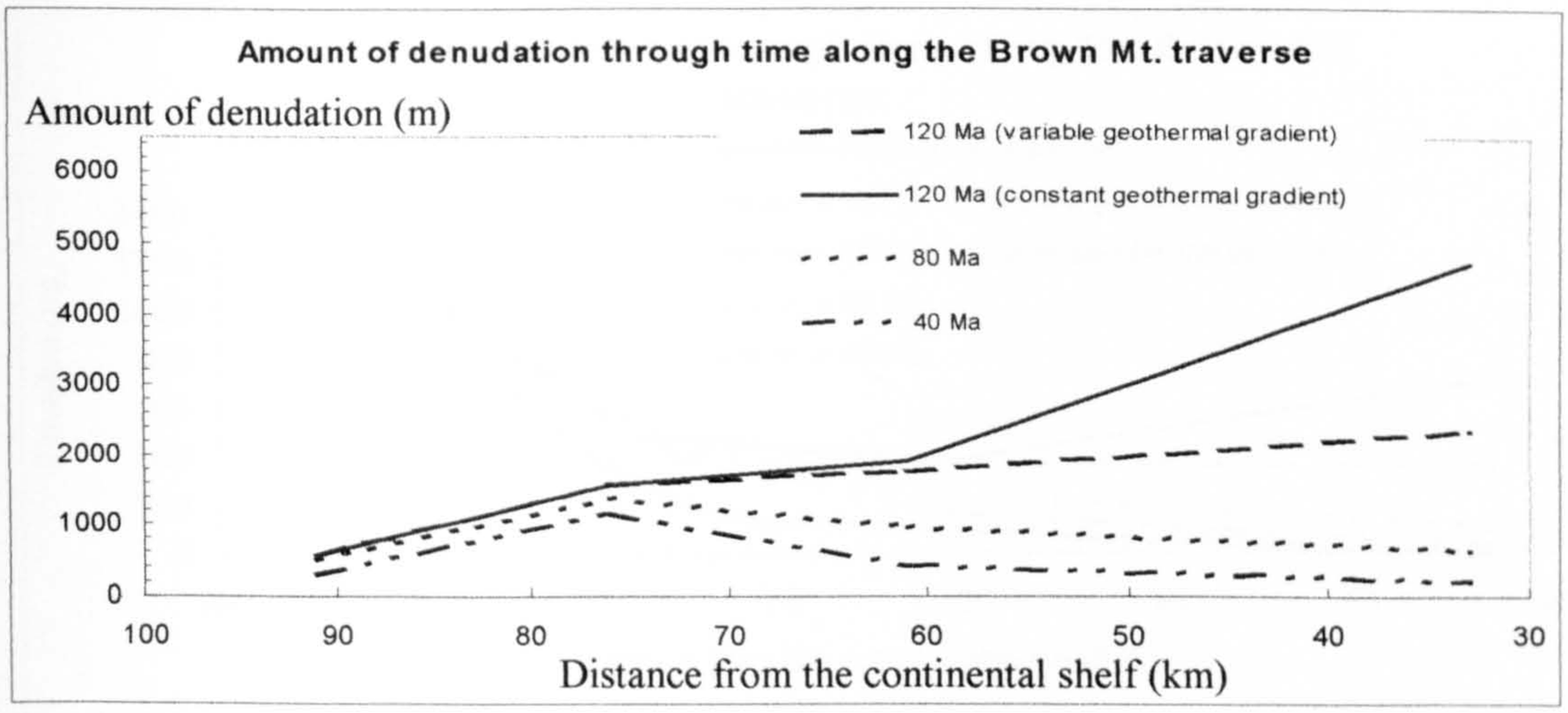

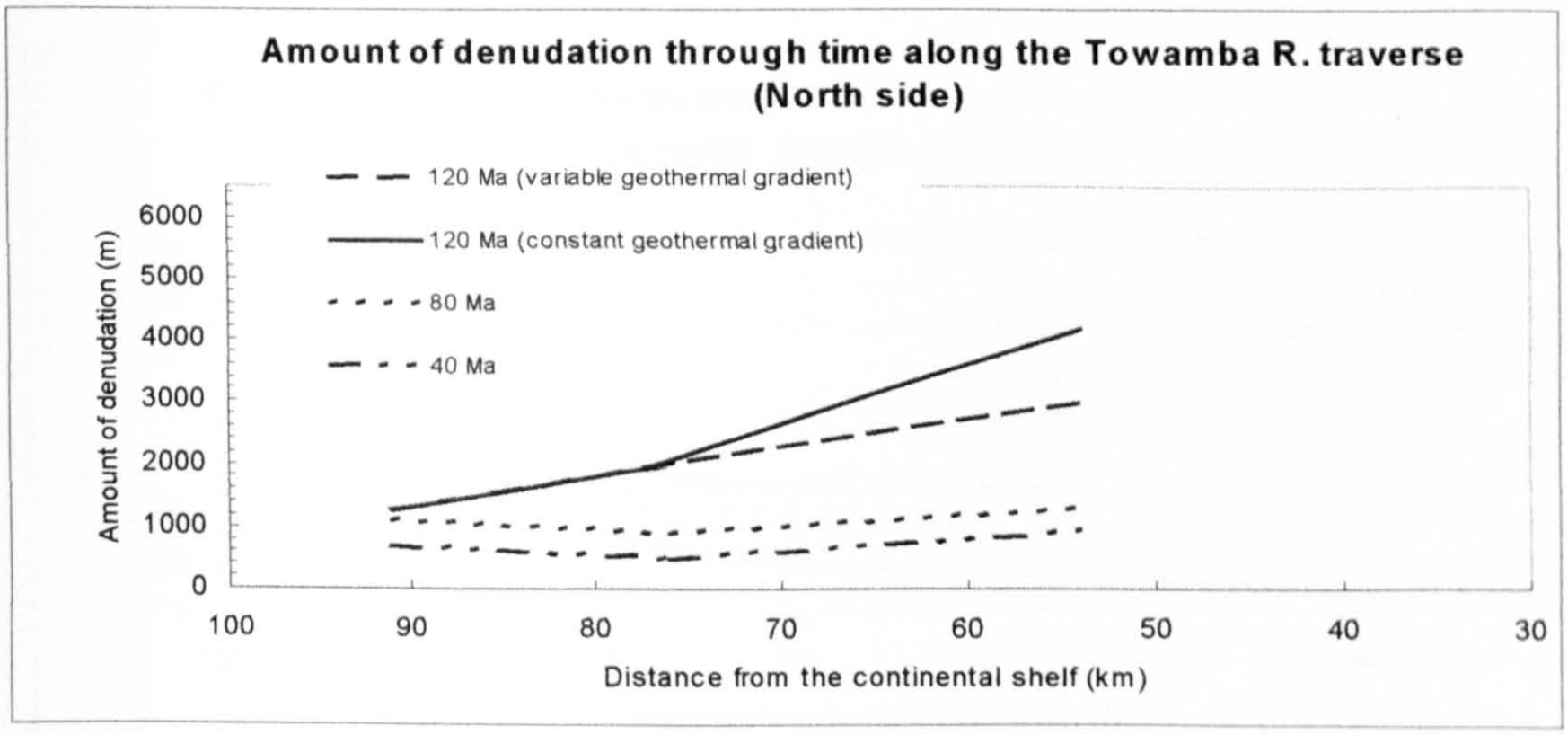

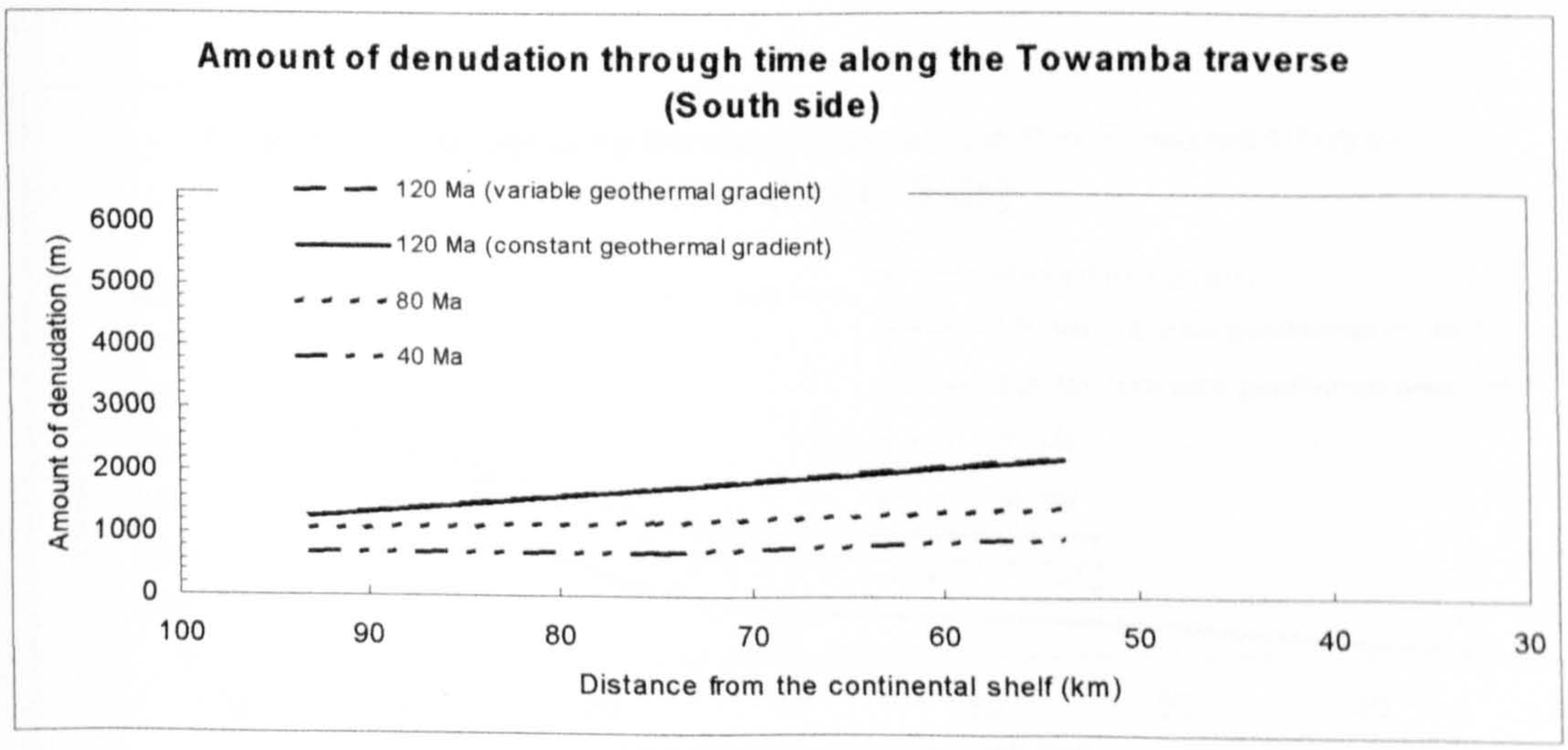

Figure 4.7: Amounts of denudation at different time intervals across the Brown Mt. and Towamba River traverses (see text for discussion)

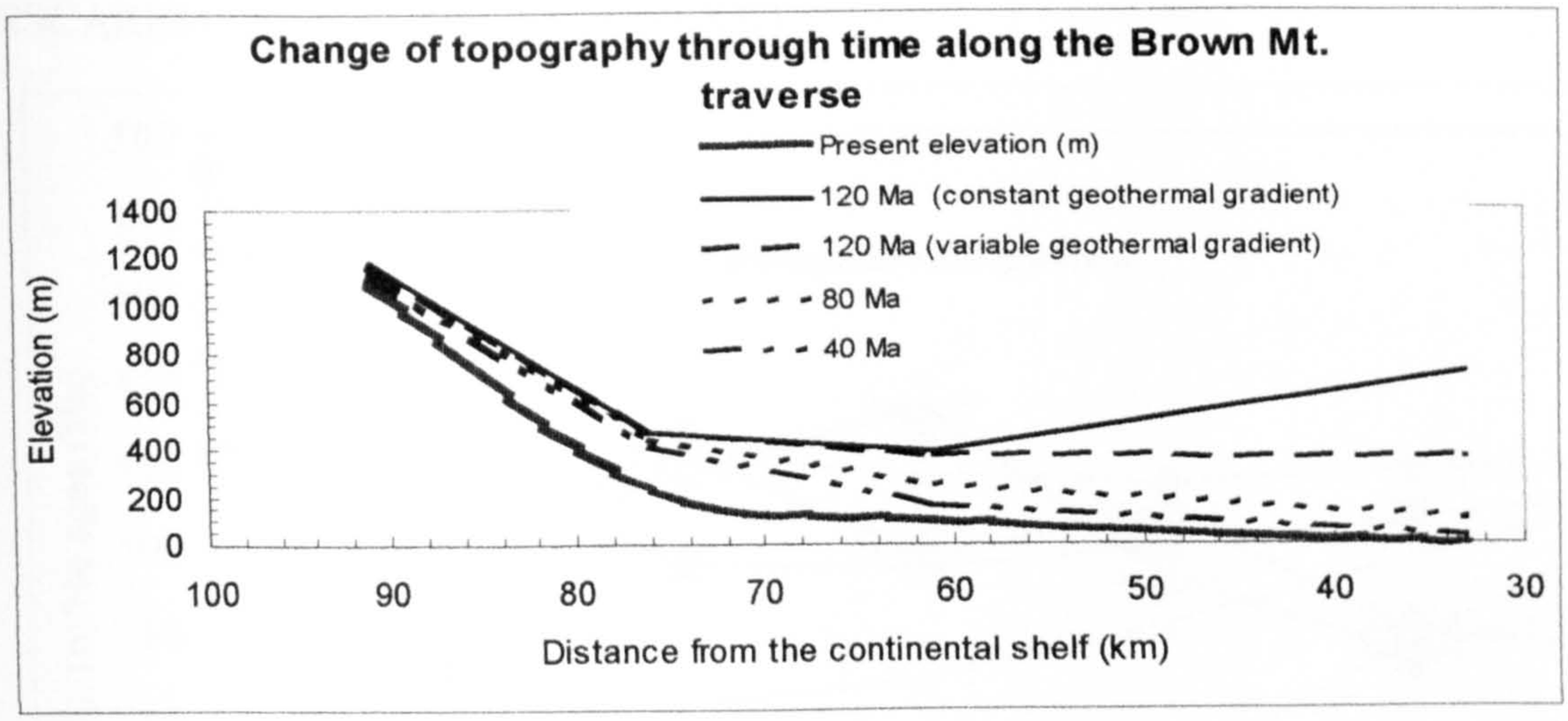

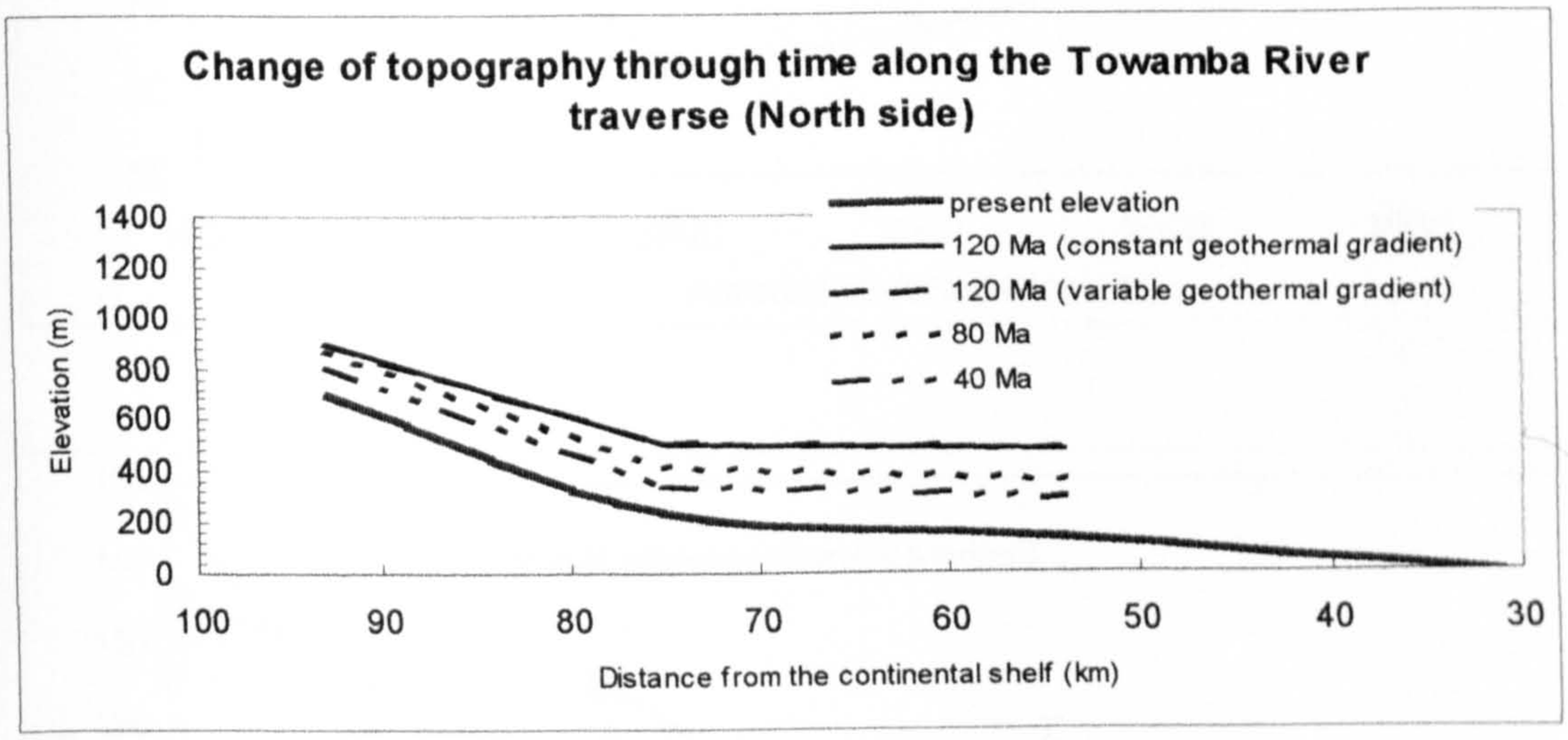

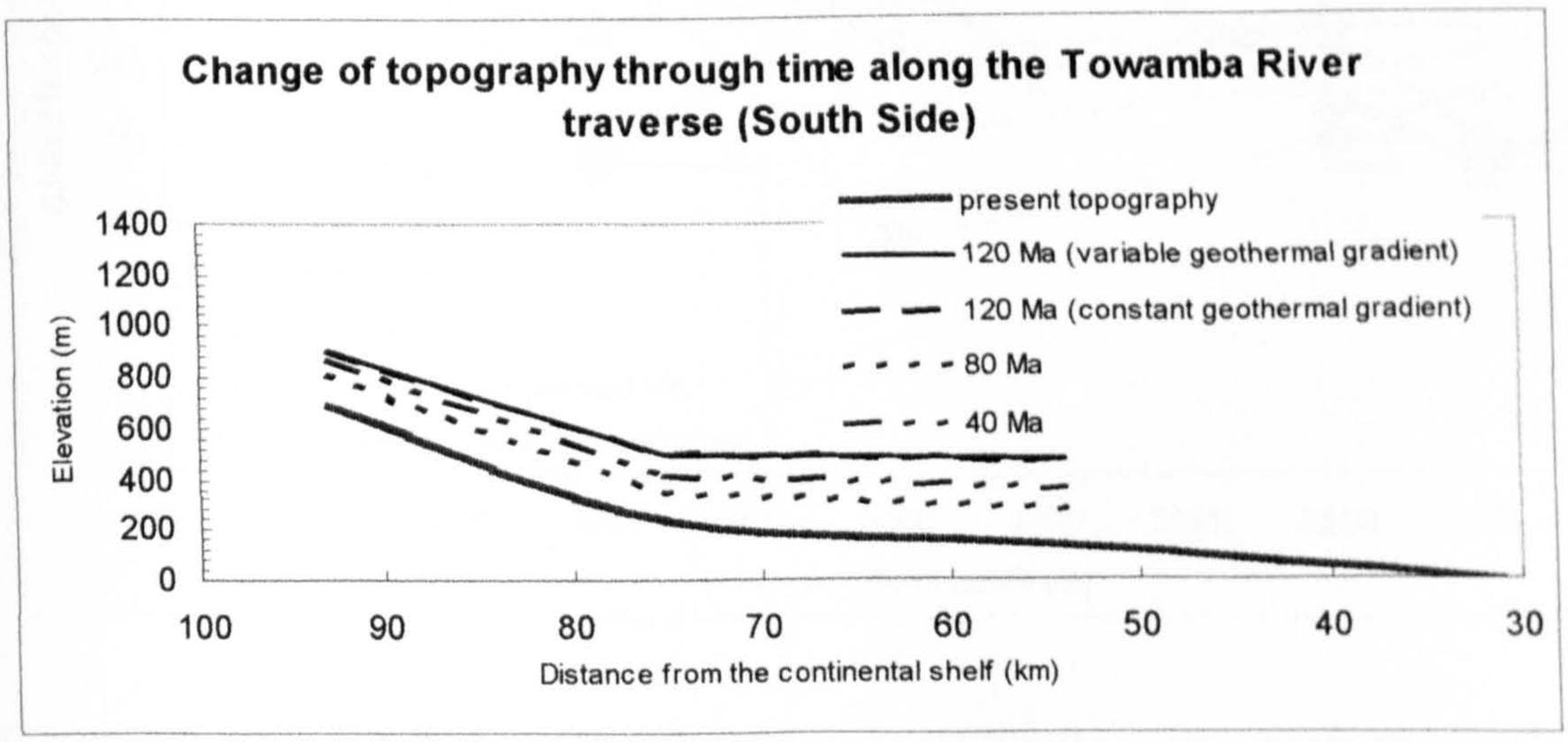

Figure 4.8: Palaeotopography is reconstructed using the backstacking technique (see text for discussion) along the Brown Mt. and Towamba River traverses. The present topography is indicated for comparison

ESCARPMENT RETREAT SCENARIO

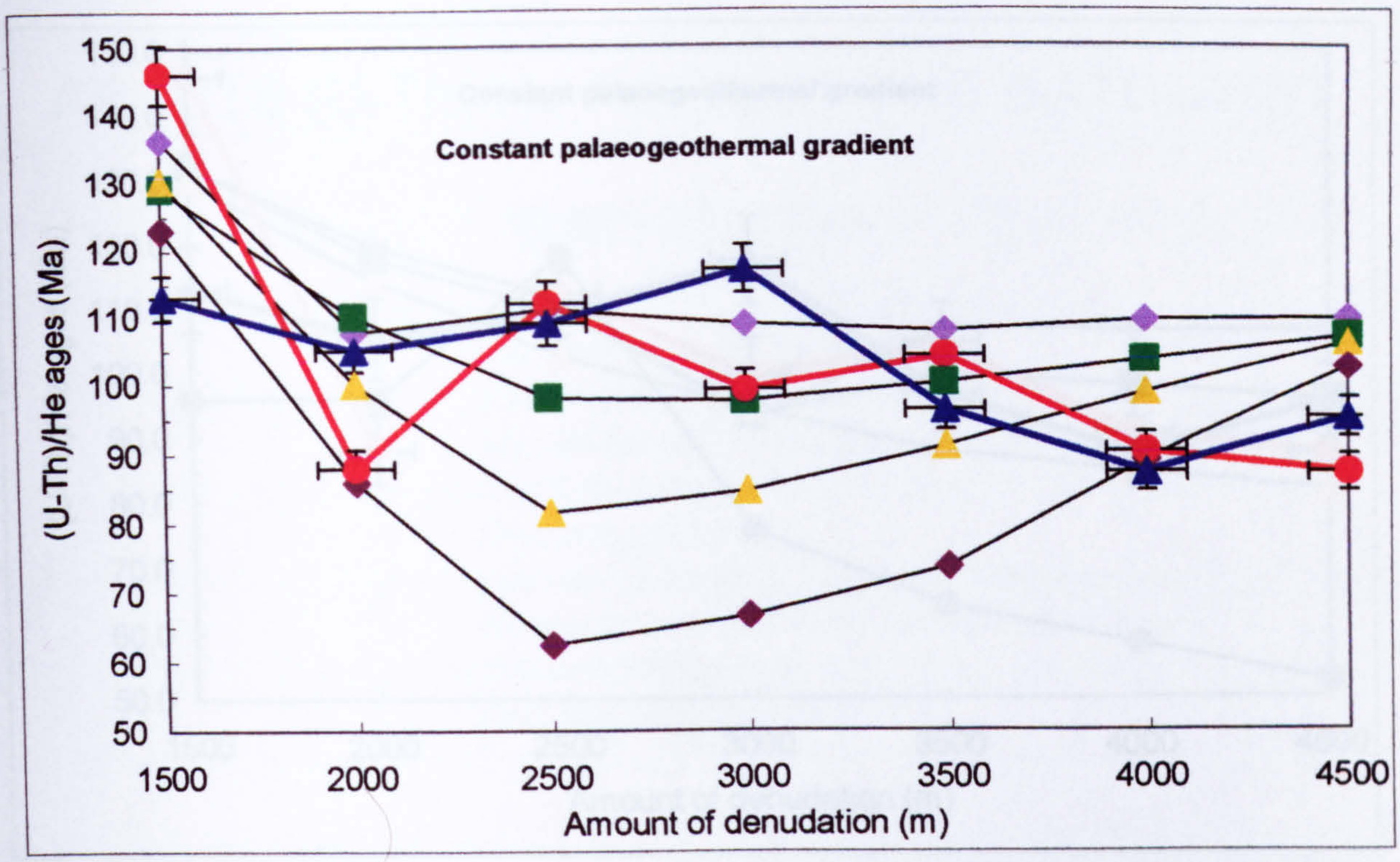

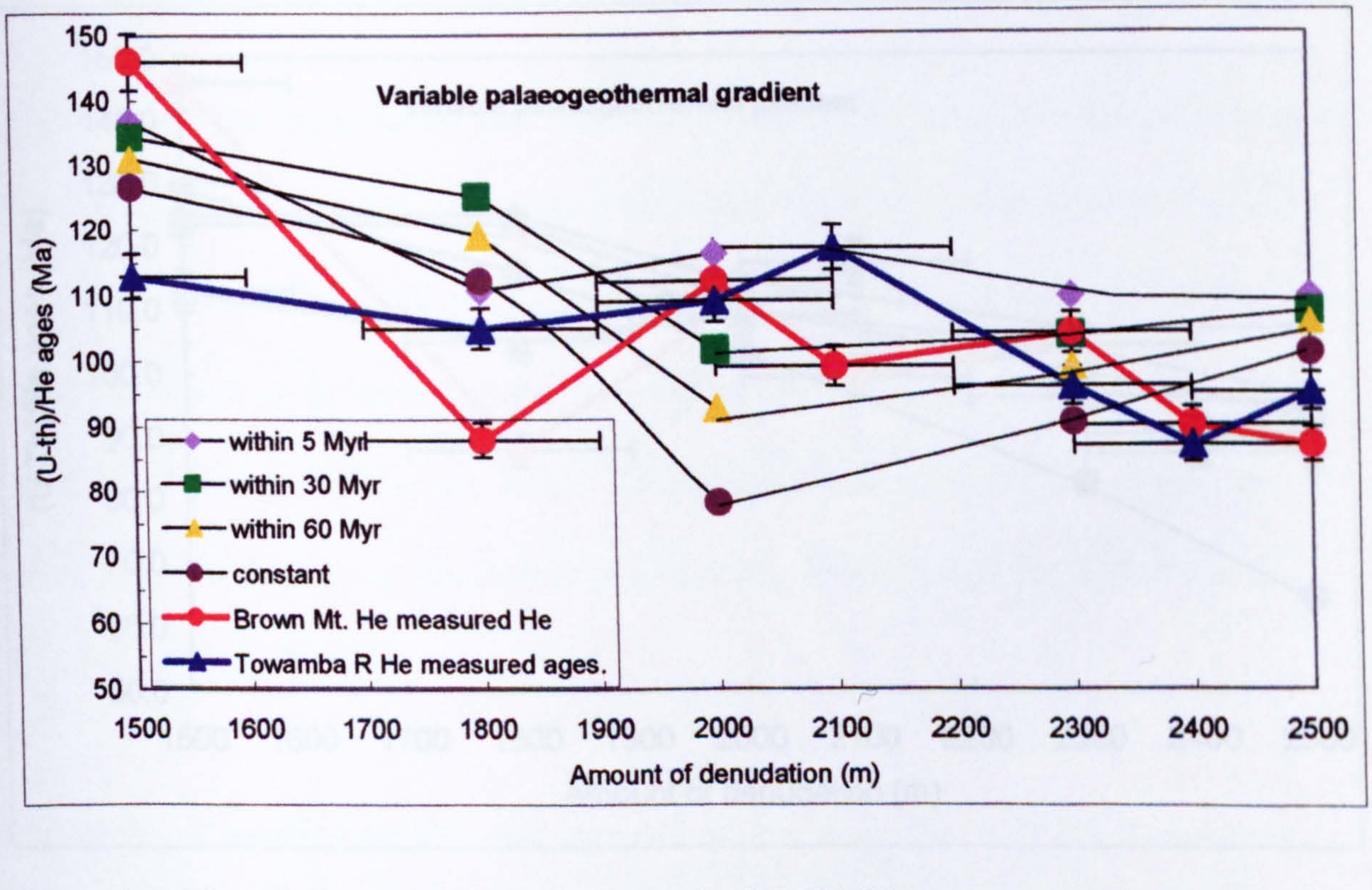

Figure 4.9: The predicted and measured apatite (U-Th)/He ages across the south eastern Australian continental margin. The He ages are predicted for an escarpment retreat rate scenario across a rift shoulder for (A) constant and (B) variable palaeogeothermal gradients.

EXCAVATION IN PLACE SCENARIO

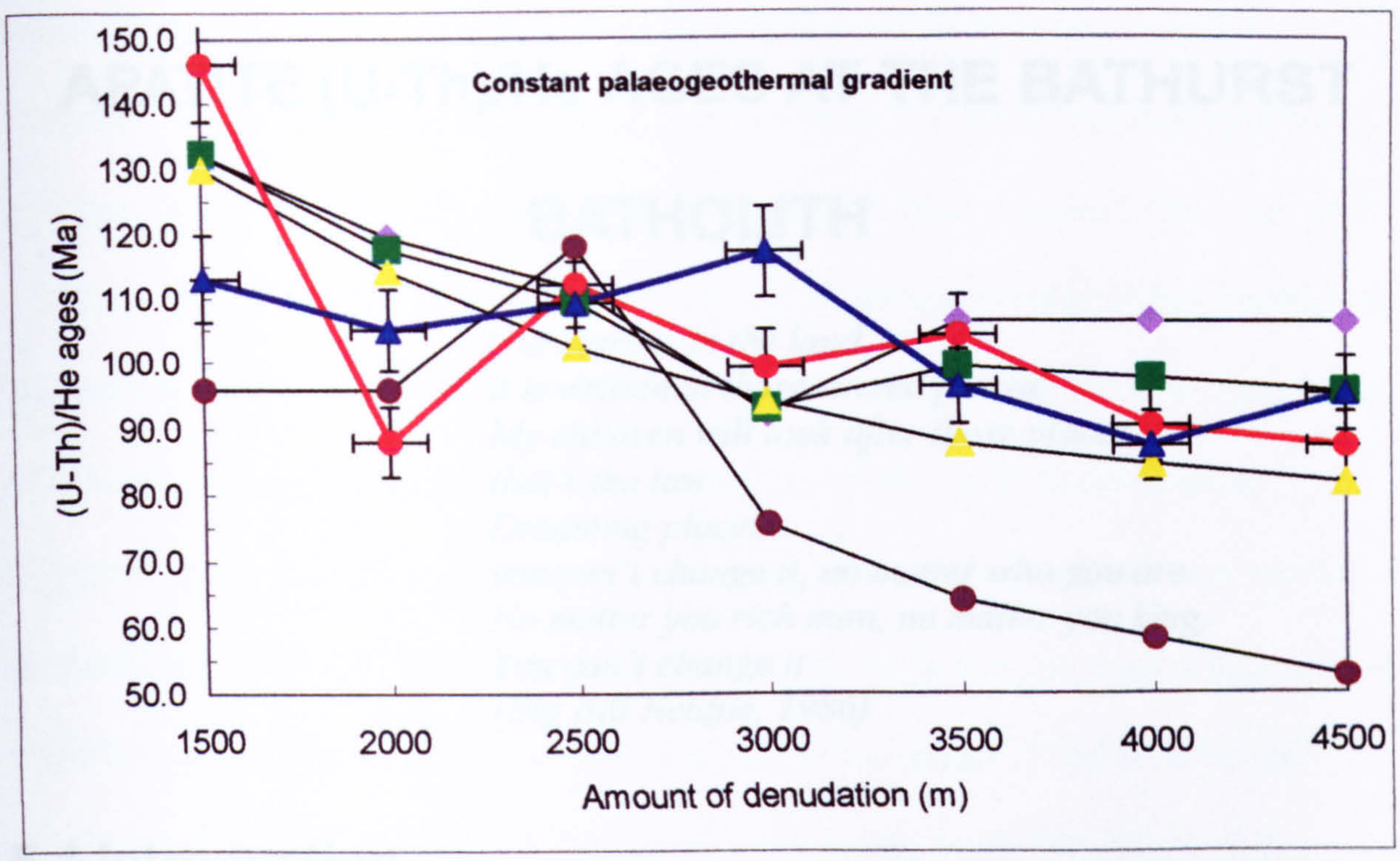

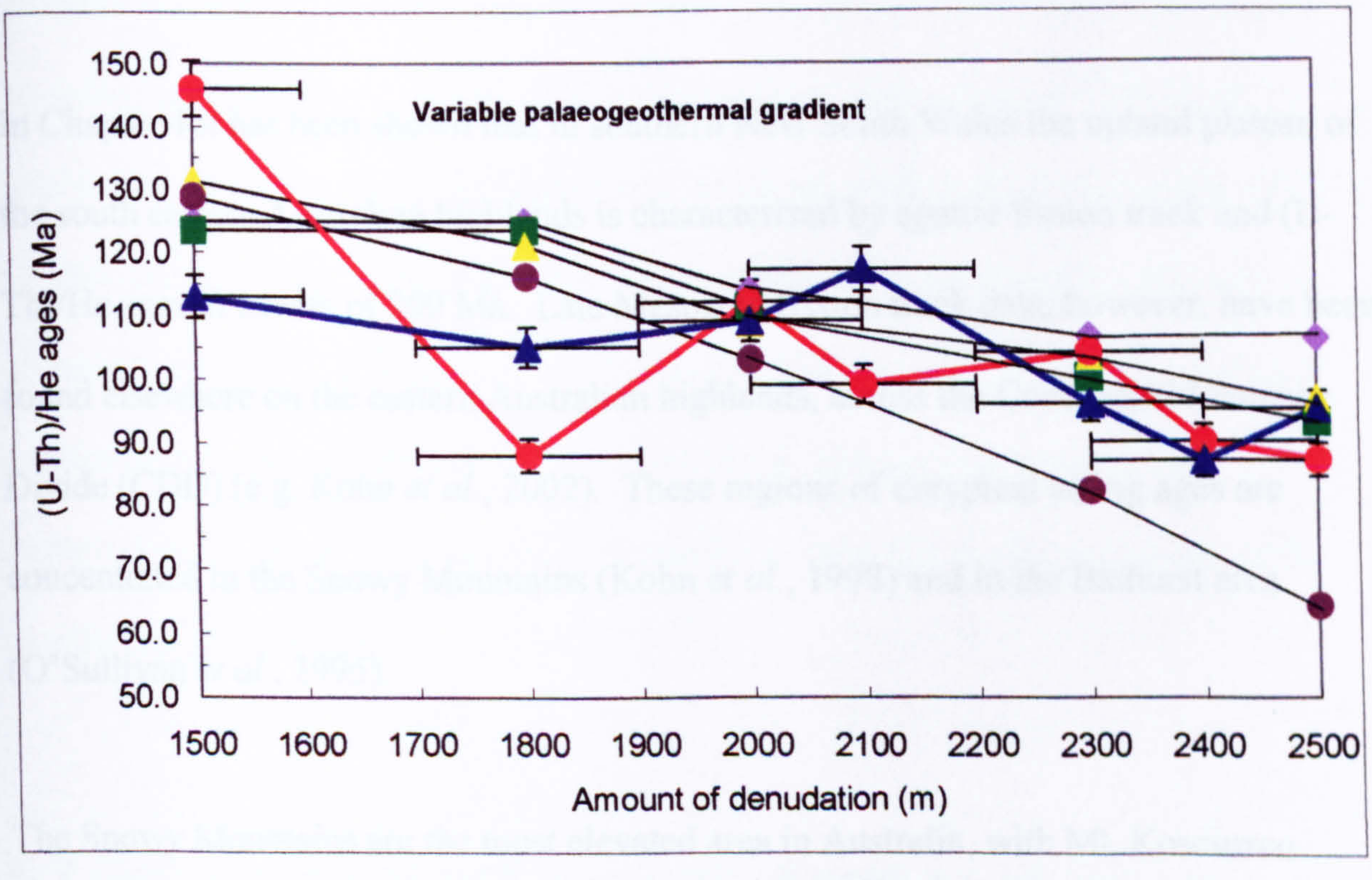

Figure 4.9 (cont): The predicted apatite (U-Th)/He ages are shown compared to the measured ages across the continental margin. The He ages are predicted for excavation in place across a rift shoulder for C) a constant or (D) variable at the coast palaeogeothermal gradients (see text for discussion)

CHAPTER FIVE

APATITE (U-Th)/He AGES AT THE BATHURST BATHOLITH

Our story is in the land... ...
it is written in those sacred places.
My children will look after those places,
that's the law
Dreaming places... ....
you can't change it, no matter who you are.
No matter you rich man, no matter you king.
You can't change it
(Big Bill Neidjie, 1986)

5.1 Introduction

In Chapter 4 it has been shown that in southern New South Wales the upland plateau of the south eastern Australian highlands is characterised by apatite fission track and (U-Th)/He ages in excess of 200 Ma. Late Mesozoic fission track data, however, have been found elsewhere on the eastern Australian highlands, across the Continental Drainage Divide (CDD) (e.g. Kohn *et al.*, 2002). These regions of untypical young ages are concentrated in the Snowy Mountains (Kohn *et al.*, 1998) and in the Bathurst area (O'Sullivan *et al.*, 1995).

The Snowy Mountains are the most elevated area in Australia, with Mt. Kosciuzco reaching an altitude of 2228 m. The peculiar topography of this region, characterised by an impressive relief is considered to be a local feature reflected in the AFT data, possibly related to reactivation of faults in the Mesozoic and Cenozoic (e.g. Kohn *et al.*,

2002). In constrast, the Bathurst landscape is not exceptional to the highlands across the CDD: the relief is subdued and rarely the area reaches 1200 m in elevation. However, apatite fission track ages on the eastern flank of the CDD at Bathurst are between 73 and 100 Ma, very similar to the ones on the coastal plain. O'Sullivan *et al.* (1995) suggested that the coincidence of these ages with the opening of the Tasman Sea indicates that the eastern flank of the Bathurst region has experienced more than 2 km of denudation since continental breakup, unlike the other regions of the eastern highlands across the CDD. A more detailed study of the eastern and western regions of the Lachlan Fold Belt (LFB) has highlighted that apatite fission track ages younger than 150 Ma (but older than 100 Ma) are also present on the western flank of the CDD (O'Sullivan *et al.*, 1996; 2000). In section 5.3, following a brief introduction about the geographical and geological setting of the area (5.2), the apatite fission track data are presented and discussed in terms of their correlation to the evolution of the CDD. In section 5.4 six apatite (U-Th)/He ages for three samples taken either side of the CDD in the Bathurst region are presented and possible evolutionary scenarios for this area are discussed, taking into consideration all the available thermochronological, geological and geomorphological information. The aim of this chapter is to identify the importance of local-scale evolutionary scenarios in the context of a continental-scale passive margin evolution.

5.2 Geographical and geological setting of the area

The Bathurst region is an elevated area across the CDD comprised between 33-34°S and 149-150°E (Figure 5.1and Figure 3.2). It is dominated by the Bathurst Batholith, a

Carboniferous granitic complex, surrounded by the Palaeozoic metasediments of the Lachlan Fold Belt and overlain by the Permian - Triassic deposits of the Sydney Basin to the east (Chapter 3). The escarpment is about 60 km seaward of the CDD in this area. It has been suggested that the escarpment's evolution is either lithologically (Pickett & Bishop, 1992) or tectonically controlled (e.g. Branagan & Pedram, 1990; van der Beek *et al.*, 2001) and the escarpment may not represent the continuation of the prominent erosional escarpment that run alongside the rest of the eastern Australian margin.

Sediments outtiers in and around the Bathurst region suggest that the area was once covered by Permian to Mesozoic deposits of the Sydney Basin (Dulhunty, 1964). The extent of the sedimentary cover and the time of erosion are poorly constrained. Mass balance determinations of the volume of offshore sediments (Shaw, 1979) and sediment sources studies for the Sydney Basin, suggest that the maximum thickness of cover which was eroded was no more than 1 km, even along the present coastal plain (Branagan, 1983). Vitrinite reflectance data from boreholes, palaeomagnetic data from magnetite in authigenic illite and apatite fission track data in the Sydney Basin all suggest that the eroded cover could not have exceeded 2 km (O'Sullivan *et al.*, 1996; Haltry, 2000). By extension, it is unlikely that the Permian and Mesozoic sediments over the Bathurst region exceeded more than a few hundreds metres. The removal of this is not enough to significantly perturb the apatite fission track or (U-Th)/He systematics.

On and around the Bathurst Batholith 51 and 12 Ma dated basalts are present (Dulhunty, 1973): they indicate that post-Eocene erosion has been of the order of 2-10 m\Myr. .

5.3 Apatite fission track results and interpretation

Eleven fission track ages are reported from the Bathurst area (O'Sullivan *et al.*, 1995, O'Sullivan *et al.*, 1996; Figure 5.1 and Table 5.1); in this section they are used to provide information about the evolution of the CDD. The samples are divided here into three groups according to their geographical position.

Eastern flank of the CDD. The two samples (94POS42, 94POS43) yielded indistinguishable fission track ages of 94±6 and 93±6 Ma, although they were collected across a relief of about 500 m. The mean track length is 13.0 and 13.8 μm with a standard deviation of 2.5 and 1.5 μm, respectively, indicating relatively rapid cooling at around 100-90 Ma.

Western flank of CDD, less than 20 km from the crest. The five samples have fission track ages ranging from 121±6 (95POS25) to 179±15 (94POS44) and they show a positive correlation with altitude (Figure 5.2). The mean track length is between 12.3 and 12.6 μm and the standard deviation is between 2.3 and 3.2 μm, suggesting that the samples resided in the PAZ for an exented period and that they have been cooled to temperatures lower than 60°C less than 100 Ma. Four of the five samples failed the χ^2 test, suggesting variations in the chemical composition of the apatite grains.

Western flank of CDD, more than 20 km west of the crest. The fission track ages are in excess of 200 Ma and they do not show any correlation with elevation (Figure 5.2). The mean track length varies between 11.5 and 12.4 μm, and the standard deviation between

1.7 and 3.2 μm, indicating that the samples have resided in the PAZ for a longer time than those closer to the CDD and that they have reached temperatures below 60°C less than 100 Ma. Although the fission track ages of these samples are indistinguishable from others found in other parts of the high elevated plateau, their track length distribution is different, indicating that in this area the samples reached the surface later than in other parts of the highlands. This finding suggests that, even on the western flank of the CDD, post-100 Ma denudation was more pronounced than in other areas of the plateau (Chapter 3, 4). Indeed, O'Sullivan *et al.* (1995) concluded that in the mid-Cretaceous the western flank experienced temperatures of about 80-90°C. The AFT and (U-Th)/He data from the plateau in southern New South Wales, however, indicate that samples now at the surface were at temperature of ~50°C at time of continental breakup.

In the next sections new apatite (U-Th)/He data from the Bathurst Batholith are reported and an evolution of the area is attempted.

5.4 Apatite (U-Th)/He ages

Results

The six (U-Th)/He ages are reported in Figure 5.3 and the U, Th and He data are summarised in Table 5.2 and Appendix 2. The procedure used to prepare and analyse the samples is described in Chapter 2 and Appendix 2. Five of the samples were analysed in duplicate or triplicate, 99-OZB-02 had suitable apatites for only one aliquot.

The three samples on the eastern flank of the CDD (99-OZB-02, 99-OZB-03, 99-OZB-04) were collected at elevations between 767 m (99-OZB-02) and 1040 m (99-OZB-04) on the crest of the highlands. They yielded (U-Th)/He ages ranging from 88 ± 7 Ma (1 σ, 99–OZB–02) and 114 ± 9 Ma (99-OZB-04), showing a positive correlation with elevation that provides a denudation rate of about 14 m/Myr (Figure 5.3). The He ages yielded by 99-OZB-02 and 99-OZB-03 are indistinguishable from the AFT ages from the same area, whereas 99-OZB-04 yielded an older He age. AFT and He ages, however, are not from the same sample, so small differences as seen for 99-OZB-04, may be due to local tectonic or geomorphological variations. In general, the similarity between AFT and He ages indicates Late Cretaceous rapid denudation, inconsistent with the erosion rate derived from the He ages versus elevation profile.

The other three samples on the western flank of the CDD (99-OZB-05, 99-OZB-06, 99-OZB-07) were collected at elevations between 600 m (99-OZB-07) and 1140 m (99-OZB-05) and they yielded (U-Th)/He ages ranging from 95 ± 8 Ma (99-OZB-05) to 109 ± 9 Ma (99-OZB-07), showing a positive correlation with elevation that provides a denudation rate of about 40 m/Myr, more rapid than that indicated by the age-elevation profile on the eastern flank. Samples 99-OZB-05 and 99-OZB-06 are from within 20 km of the crest of the CDD; AFT ages from this area are less than 200 Ma, but significantly older than the He ages, suggesting that these samples cooled less rapidly than the ones from the eastern flank of the CDD. 99-OZB-07 is from an area about 60 km from the CDD where AFT ages in excess of 200 Ma have been found. In this case, the gap between AFT and He ages is greater than 100 Myr and it indicates that the region experienced slow Mesozoic and Cenozoic cooling. The He age, however, shows

that the sample was still in the PRZ at at least 95 Ma, suggesting that, although slow, post-breakup denudation in this area was more rapid than in other regions of the plateau where He ages are between 150 and 250 Ma (Chapter 4).

Discussion

The age-elevation relationship of the three samples on the eastern flank of the CDD does not show a break in slope (Chapter 2), precluding the possibility of determining the base of the fossil PRZ and, consequently, the onset of the rapid denudational event. In these terms, the slope-derived ~ 14 m/Myr denudation rate cannot be taken as a reliable value, as the profile may represent only a portion of the PRZ. The three replicates of 99-OZB-04 (Table 5.2) shows a reproducibility of 0.2% (1σ), well below the 8% taken as 1σ variation in this study, the rounding up being due to the effect of the recoil loss. The lack of relationship between grain size (i.e. recoil correction, Chapter 2) and (U-Th)/He ages suggests that the sample was rapidly denuded at the time indicated by the He age (Wolf *et al.*, 1996). This suggests that 99-OZB-04 was at the bottom of the PRZ at around 114 Ma and samples at lower elevations entered the PRZ only a few Myr later.

Variations in grain sizes amongst the aliquots of samples from the western flank are not pronounced and, within a sample, uncorrected He ages are within the 8% uncertainty of the method. The age-elevation profile does not show any break so the slope cannot be taken as indicative of the post-Cretaceous denudation rate.

If the elevation of the samples from the eastern flank is shifted 200 m below, the two profiles either side of the CDD converge and the He ages between 700 and 600 m ("corrected" elevation) are indistinguishable from each other (Figure 5.4). It is tempting to suggest that these ages reflect the bottom of the PRZ and they indicate the time of the onset of the rapid denudational event, between 90 and 100 Ma. According to this hypothesis, either side of the CDD experienced a similar Late Cretaceous evolution and a post-90 Ma tectonic movement caused the fossil PRZ (hence the He ages profile) to be disrupted of about 200 m.

In the next section this hypothesis, and the more general landscape evolution scenarios for the Bathurst region are discussed, taking in consideration all the available information.

5.5 Evolutionary scenarios

Constraints on the thermal history of the regions either side of the CDD can be derived from different sources:

A 51 Ma basalt rests on a granite erosional remnant rising some 120 m from the surrounding country (Figure 5.1; Dulhunty, 1973): its location constrains the average rate of denudation for the last 50 Myr to 2 m/Myr. A 12 Ma old basalt flow lies at the bottom of a palaeovalley, forming an erosion surface 60 m above the bed of the present river; in this case, the rate of denudation for the last 12 Myr is 5 m/Myr. In both events, the calculated rates of denudation are very low, in agreement with values calculated for other areas of the plateau (e.g.Bishop, 1985).

The AFT signal is complicated by the fact that of the 11 data presented before, six failed the χ^2 test and they cannot be modelled to derive thermal histories. Moreover the χ^2 test failure indicates that samples contain apatites of different composition, suggesting that AFT ages are affected by Cl-rich apatite crystals more resistant to annealing and hence returning spuriously old ages (Chapter 4). The conclusions drawn from the AFT data are therefore only qualitative and poorly constrained. The eastern flank of the CDD experienced rapid denudation at around 100-90 Ma. On the western flank AFT ages become older westward, with the oldest ages being associated with the shortest mean track length, suggesting that samples left the PAZ no earlier than 100 Ma (because long fission tracks had not had the time to accumulate).

Apatite (U-Th)/He ages are all Late Cretaceous. They can be make lying on the same profile is the eastern flank of the CDD is shifted 200 m down.

To reconstruct the evolutionary history of the Bathurst region, the two flanks are kept separate to highlight any difference that could reveal information about the evolution of the CDD.

Eastern flank

If slow present rates of denudation of the order of 5 m/Myr are projected into the past to 100 Ma (the time when, according to the AFT record, the samples were at around 90°C), a section of 500 m of crust is removed. For a normal geothermal gradient of 25°C/km and a surface temperature of 10°C, a removal of 500 m section indicates that

the samples were at about 27°C 100 Ma, inconsistent with the AFT data. Un unlikely geothermal gradient of more than 100°C/km needs to be assumed to reach a temperature of 90°C at only 500 m depth. Therefore, the rates of cooling (and hence the rates of denudation) must have remained higher for longer than predicted by the AFTT.

Forward modelling of the AFT data from 94POS43, which did not fail the χ^2 test, indicates that the sample experienced rapid cooling at around 100 ± 10 Ma. Using this information, time-temperature paths can be defined to predict the measured He ages from the same region. The thermal history producing the uncorrected He ages of different size aliquots of the same sample is the most likely to have occurred. Figure 5.5 show with a thicker line the time-temperature path that predicts the measured (U-Th)/He ages for two replicates of 99-OZB-04. This thermal history indicates that the area experienced a 120-90 Ma period characterised by relatively rapid cooling rates of 1.2°C/Myr, followed by much lower rates of 0.3°C/Myr. For a normal geothermal gradient of 25-30°C/km, denudation rates of 47-39 m/Myr and 13-11 m/Myr (estimates for 25 and 30°C/km palaeogeothermal gradient) are obtained for the high and low cooling rates periods.

Western flank

Among the samples with intermediate ages, only 95POS26 can be used to constrain possible thermal histories, as the others failed the χ^2 test. Forward modelling of the AFT data predicts a complicated thermal history according to which at around 120 Ma the sample was lying at temperatures of 90-100°C, cooling to 60-80°C at about 90 Ma. Using these constraints, He ages are predicted for different time-temperature paths to reveal the unique thermal history reproducing the measured He ages for the two aliquots

of 99-OZB-06 of different grain sizes. Figure 5.6 shows that, within the thermal constraints derived from the AFT data, the only thermal history producing the uncorrected He ages for both aliquots is characterised by a 1.2°C/Myr cooling rate event between 120 and 90 Ma, followed by a 0.5°C/Myr constant rate. These values can be translated to average erosion rates of 47 and 20 m/Myr, respectively (geothermal gradient of 25°C/km) and 39-17 m/Myr (geothermal gradient of 30°C/km). The 120-90 Ma cooling rate is the same as on the eastern flank, but it is at least twice the rates calculated for the plateau in southern New South Wales for the same period (Chapter 4).

The two replicates of samples 99-OZB-07 have the same grain size, so that a unique solution cannot be found. Measured He ages, however, can be predicted assuming that the sample was at 90°C 120 Ma, 65°C at 90 Ma and it constantly reached the surface. This thermal history provides estimates of the cooling rates of 0.8°C/Myr in the 120-90 Ma period and of 0.6°C/Myr thereafter.

The combination of AFTT and He ages, although not powerful as in the study about southern New South Wales because the two set of data do not come from the same samples, provides new, important constraints about the evolution of the margin. Cooling rates were enhanced in the whole Bathurst region at about 120 Ma and remained high until about 90 Ma, when they started to decay, reaching the present value of 5-10 m/Myr as early as 50 Ma. In this sense, the eastern and western side of the CDD experienced the same thermal history, although rates of cooling (and hence of denudation) rapidly decay moving westward. The east and west regions experienced tectonic movements sometimes after 90 Ma as shown by the disrupted apatite He ages profiles. Late Cretaceous and possibly Palaeocene tectonic movements in the area are

demonstrated by palaeomagnetic data from the Lapstone Monocline, less than 100 km seaward of the the Bathurst area (e.g. Schmidt *et al.*, 1995).

5.6 Conclusions

The combination of AFTT and (U-Th)/He ages provides the conclusions that at Bathurst the samples near the crest of the highlands, either side of the CDD experienced the same thermal history since, at least 120 Ma. In the period between 120 and 90 Ma, rates of denudation were of the order of 40-50 m/Myr, one order of magnitude higher than those calculated on the southern New South Wales plateau. The disruption of the He ages versus elevation profiles can be explained by a post-Mesozoic tectonic movement of only 200 m, which disrupted the fossil PRZ.

Moving westward, away from the CDD, the AFT and (U-Th)/He data show that this region was characterised by Late Mesozoic rates of denudation of 20-30 m/Myr, slower than in the area around the CDD crest, but still higher than the values constrained for the most part of the plateau (Chapter 4). This indicates that the separation between the two regions at Bathurst is not the CDD, but a line about 20 km west of it, likely a not mapped fault roughly running north-south across the batholith. The coincidence of some AFT and He ages with the continental extension and opening of the Tasman Sea suggests that the activation of this fault was possibly associated to the formation of the passive margin, but the data are not correlated to the evolution of the CDD.

The Bathurst region is a good example of the way local features such as faults can play a fundamental role in determining the evolutionary history of a small area and in obliterating the overall signal given by continental scale phenomena. The importance of the spatial and temporal scale at which the processes responsible for the landscape evolution occur and are effective is discussed in the next chapter.

Sample name	Elevation (m)	χ^2 probability	AFT age (1σ) (Ma)	Mean track length (1σ) (μm)
94POS42	1113	1.3	94±6	13.0±2.5
94POS43	747	23.3	93±6	13.8±1.5
95POS24	685	2.0	125±7	12.4±2.7
95POS25	730	0.8	121±6	12.3±2.5
95POS26	710	87.6	128±6	12.4±2.9
94POS37	808	0.2	145±11	12.3±3.2
94POS44	1052	0.0	179±15	12.6±2.3
95POS23	606	0.0	226±23	12.4±1.7
94POS46	756	23.3	207±6	11.5±3.2
94POS47	1083	48.3	235±9	11.9±2.3
94POS49	904	98.3	206±12	12.0±1.9

Table 5.1: AFT data from O'Sullivan *et al.* (1996)

Sample name	Elevation (m)	Average grain radius (μm)	Uncorrected (U-Th)/He ages (Ma)	Corrected (U-Th)/He ages (Ma)
99-OZB-02	767	90	75	88
99-OZB-03	860	80	69	83
		55	84	108
99-OZB-04	1040	120	102	114
		70	94	114
		70	94	114
99-OZB-05	1140	90	92	107
		70	92	111
99-OZB-06	650	80	81	97
		80	82	98
		100	84	97
99-OZB-07	600	60	72	91
		60	70	91

Table 5.2: resume' of the apatite (U-Th)/He ages in the Bathurst region. Complete data are reported in Appendix 2

CHAPTER SIX

O muse, o alto ingegno, or m'aiutate;

o mente che scrivesti ciò ch'io vidi,

qui si parrà la tua nobilitate

(Dante Alighieri, Canto II ,Inferno)

6.1 Introduction

The idea that long term, continental scale landscape development is strongly linked to the macroscale, global tectonic phenomena is very old in geomorphology (e.g. Lyell, 1830-1833), but it has not been extensively studied (Summerfield, 2000). The lack of tools able to provide data on the mechanisms, chronology and magnitude of surface processes at the temporal and spatial scales at which major tectonic processes occur made the attempt of testing the classical models of landscape development practically impossible. The development of a new range of techniques, coupled with modelling of complex landscape systems, had provided new opportunities to address long standing questions in landscape evolution. Recent works (Cockburn *et al.*, 2000; Brown *et al.*, 2002; Persano *et al.*, 2002, van der Beek *et al.*, 2002) have explored these possibilities and have shown that when rates and amounts of denudation can be constrained, the long term evolution of the landscape can be revealed.

The combination of apatite fission track and (U-Th)/He thermochronologies used in this project has allowed timing and styles of denudation to be determined in a more precise

way than previously. Both sets of data point to substantial denudation across the coastal plain in eastern Australian associated with the early stages of the Gondwana breakup, strongly arguing against ideas of long-term survival of pre-rift, erosional surfaces in this area. Constraining the time of rapid denudation to 120 to 80 Ma has now solved the apparent conundrum of kilometric-scale denudation indicated by the fission track data and the presence of Late Mesozoic surfaces on the coastal plain (e.g. Bishop & Goldrick, 2000). Thermochronological data have shown that these surfaces may have well developed on the newly formed lowland region, shifting, therefore, the time of the rapid denudation from syn-rift to syn-continental extension, some 40 Myr before sea floor spreading. In the next section the links between denudation and tectonism are explored. The conclusion that the denudational pulse occurred well before the formation of the passive margin is very important because it highlights that the landscape responded very rapidly to changes in the tectonic regime. First order topographical features, such as the escarpment, rapidly evolved, following styles and timings that have been revealed here for the first time. The rapidly evolving scenario does not affect the region inland of the escarpment. On the plateau the landscape continued to evolve unaffected by the Gondwana breakup and rates of denudation remained low and constant as they had been since the Lachlan Fold Belt ceased its tectonic activity.

However, when focus is shifted from a continental to a smaller scale, local features can become important and may control the evolution of the landscape, obliterating the overall signal. This is the case in the Bathurst area, where regional tectonic activity has disrupted the evolution of the plateau and it provides a clear example of the importance

of considering the problem of of long term, continental landscape evolution at the appropriate scale. It also focuses the attention on the risks of extending models to other regions or to inappropriate time intervals.

In the following sections the main points of landscape evolution in eastern Australia, as derived by the combination of apatite fission track and (U-Th)/He thermochronometers are highlighted and the importance of local versus continental scales is discussed. The final section compares the Australian example with other high elevation passive margins and attempt to define features in passive margin evolution common to all models of continental break-up scenarios.

6.2 Linking denudation with tectonism

How and why did the pulses of denudation recorded by the AFT and (U-Th)/He data occur? Most reviews in eastern Australia have correlated the major Late Mesozoic landscape change to the opening of the Tasman Sea (e.g. Ollier, 1982; Seidl *et al.*, 1996; Bishop & Goldrick, 2000) and the coincidence of the youngest fission track ages with sea-floor spreading are considered to be a further evidence of this correlation (e.g. Dimitru *et al.*, 1991; Kohn *et al.*, 2002). The combination of AFT and (U-Th)/He data, however, shows that the denudational pulse started at least 120 Ma, some 40 Myr before the onset of sea-floor spreading. Most generalized geophysical models of continental breakup envisage a long, up to 50 Myr, history of epi-continental tectonism, culminating in the final rupture (e.g. Falvey, 1974; Kearey & Vine, 1990). These pre-breakup phases usually result in the formation of a rift system, like in the Red Sea (e.g.

Camp & Roobol, 1992), however this is not evident in eastern Australia. Reflection profiles across the Lord Howe Rise, however, have revealed a zone of host and graben some 200 km wide (Shaw, 1979), which is taken to indicate a pre-breakup rift valley that remained attached to the Lord Howe Rise margin (Jongsma and Mutter, 1978). The time of formation of these pre-breakup structures is not constrained, but it must precede the volcanism at 101 Ma on the eastern Australian margin (Colwell *et al.*, 1993). Continental extension may have been accompanied by lateral heat flow and/or magmatic underplating causing an increase in the palaeogeothermal gradient that would be associated with surface uplift of the rift flanks (e.g. Lister *et al.*, 1991; Brown, 1991; Beaumont *et al.*, 2000). There is no evidence to constrain the geothermal gradient at time of breakup, but geophysical models have demonstrated that, unless widespread volcanism occurs, heat flow by conduction between the hotter deep crust (or the underplated material) and the shallower crust is inefficient (e.g. Watts, 2001). Rift flank uplift arises from the mechanical unloading of one side of the crustal block by faulting or denudation and it is enhance by low value of T_e (Vening & Meinesz, 1950; Watts, 2001). Thermochronological data do not necessarily require surface uplift, but the several kilometres of denudation constrained at the coast (also in a case of a high palaeogeothermal gradient) strongly argue for the occurrence of rock uplift.

The fundamental conclusion that the denudational pulse was practically extinguished at the time of the onset of sea-floor spreading has important implications. It indicates that the escarpment in eastern Australia predates the formation of the passive margin *sensu strictu*, suggesting that escarpments are features of continental extension rather than breakup. It also suggests that the landscape responded rapidly to the first changes in the

tectonic regime, reaching a sort of equilibrium that was not disrupted by the ocean basin formation. These important implications may be strictly related to south eastern Australia or may be valid for other high elevation margins. It is also possible that in eastern Australia the pre-breakup phases lasted longer than is typical of other margins, enabling the clear distinction between pre- and syn-rift denudation. In this case, the south eastern Australian margin provides an excellent natural laboratory where to test hypotheses of passive margins formation and evolution.

6.3 Mechanisms and tempo of escarpment evolution

The erosional nature of the escarpment indicates that it fromed when the highlands were a topographically elevated region. Evidence from sedimentary basins around the highlands has shown that the plateau was subaerial even during the Cretaceous high sea-level times (Colwell et al., 1993). In their model of landscape evolution, van der Beek *et al.* (1999) reproduced the present landscape starting from an erosional escarpment cutting through a plateau originally 2 km high. Using the syn- and post-breakup amounts of denudation derived from the AFT and (U-Th)/He data and the backstacking technique (Brown, 1991), a first order approximation of the pre-rift topography has been obtained (Chapter 4). According to this reconstruction, at 120 Ma substantial relief was present broadly in the same area now occupied by the escarpment, joining a high elevated plateau to a lowland region. This recostruction points out two important conclusions:

(i) The highlands were already an elevated region at 120 Ma. The elevation could be related to surface uplift caused during pre-120 Ma extensional phases, but there are no independent constraints on the timing of such events. Late Mesozoic volcanism in eastern Australia is limited and the Tertiary widespread magmatic activity is not related to the continental breakup (Johnson *et al.*, 1989). Geomorphological and sedimentological evidence, however, indicate that the highlands around Bathurst were an elevated region in the Permian (Dulhunty, 1964) and that in northern Queensland the CDD has remained stationary since the Middle Jurassic. Although these regions are far away from the study area (thousand of kilometres in the case of Queensland), such surface uplift is likey to have been a large-scale phenomenon, unlikely to have remained restricted to south eastern Australia.

(ii) The position of the present escarpment corresponds to a pre-breakup relief, possibly a long-lived drainage divide. The conclusion that the escarpment did not retreat across the coastal plain, but it was "pinned" to its present position is also strongly backed by the variations of apatite (U-Th)/He ages across the coastal plain in southern New South Wales. Different denudation histories can be ruled out by comparing the measured and the predicted He ages across the coastal plain (Chapter 4). The best match is obtained by degrading a pre-rift high elevation plateau at rates decreasing from the present coast to the foot of the escarpment, so that by 60 Ma the landscape approached its present state with rates of denudation of the order of 5-10

m/Myr since then. This conclusion has fundamental implications for the evolution of the south eastern Australia passive margin. It indicates that the portion of the coastal plain closest to the continental margin (including areas 20 km inland of the present coastline) has experienced maximum and most rapid denudation, whereas the amount and rates of denudation on the rest of the coastal plain have rapidly decreased, moving toward the escarpment. Rates and amounts of denudation can be quantified assuming a value for the palaeogeothermal gradient. The debate about the possibility of a high geothermal gradient on the continental margin during extension is ongoing. The problem, however, can be tackle from another point of view: what maximum values of lateral variations in denudation can be assumed given reasonable values of elastic thickness? van der Beek *et al.* (1999) assumed a normal value of elastic thickness for the continental crust of 25 km, but they also assumed that the geothermal gradient was as high as 60°C/km at the coast, which should favour lower T_e (Watts, 2001). An elastic thickness of 10 km has been used in southwestern Africa to account for lateral differences in amount of denudation comparable to the ones seen in eastern Australia in the case of a constant geothermal gradient of 25-30°C/km (van der Beek *et al.*, 2002). Clearly more work is needed: there is the intention to use a 3-D numerical models to test the different geothermal gradients scenarios and also incorporate the effects of thermal subsidence.

The continental extension and breakup did not affect either the basins inland of the escarpment, or the Continental Drainage Divide; the base level did not change and erosion was not enhanced.

Amongst others, a question remains open: how is the escarpment evolving now? Although impressive, the escarpment in most part of eastern Australia seems degraded, especially when compared to other high elevation passiv margins (Figure 1.2). The predominance of landslide processes over river incision in some portions of the escarpment in northern New South Wales seems to indicate that the escarpment is not evolving by slow retreat (Seidl et al., 1996); however more investigations are needed. The thermochronological data are unable to answer this question, but an "ad hoc" sampling on the escarpment face for cosmogenic isotope analysis, as it has been done in southern Africa (Cockburn et al., 2000; Fleming et al., 2000; Brown et al., 2002) may represent a further development of this project.

6.3 The continental versus local scale issue: the Bathurst example

Continental breakup and the formation of new margins is a global tectonic process and the escarpment, whose formation and evolution is strictly related to it, is a first order geomorphological feature that needs to be studied at a continental scale. Clearly characteristics, such as the geology and the geomorphology of the area, also play a role in determining the landscape evolution, but, when interpreting thermochronological

data, it is important to be able to identify the "local noises" that may mask the longer scale signal. The presence of local-scale features, able to affect the thermochronological data, may be revealed by single data points that do not fit in the regional trend and some of these cases have been discussed in Chapter 4. Sometimes the effects of such local processes are so strong that they may completely obscure the regional pattern. It is believed that the Bathurst area is one of such cases. It lies across the CDD, well inland of the escarpment, in an area where, according to the landscape evolution scenario discussed before, rates of denudation should have been of the order of 5-10 m/Myr for at least the last 200 Ma. However, syn-rift AFT ages are found on the eastern flank of the CDD (O'Sullivan *et al.*, 1996). Careful analysis of the existing AFT data from the Bathurst Batholith shows that Late Mesozoic ages are also present on the western flank of the CDD and apatite (U-Th)/He here presented indicate that this region experienced at least 2 km of post-Cretaceous denudation. AFT ages of 200 Ma associated with ~100 Ma (U-Th)/He ages occur some 20 km west of the Drainage Divide, indicating that this area, although it experienced more denudation than other portions of the eastern highlands, was eroded less (enough to affect the He data, but not to AFT ages) than the eastern part of the Bathurst Batholith. This area does not coincide with any first order geomorphological feature, and it is thought that the differences in denudation may be associated with Late Mesozoic tectonic movements. The metasediments surrounding the Bathurst Batholith are affected by many faults and, although not mapped across the granite, they may be present. The coincidence of the thermochronological ages with the opening of the Tasman Sea leads to the conclusion that these tectonic movements may have been related to the change in the tectonic

regime, causing the reactivation of Palaeozoic faults. However, these movements are not important to determine the overall evolution of the margin.

The fact that the evolution of the Bathurst region is at odds with the scenario described in Chapter 4, does not argue against a plateau degradation model, on the contrary, it highlights the importance of identifying local scale features, when dealing with continental scale phenomena.

6.4 Comparison with other high elevation passive margins: toward a global model?

Thermochronological data have been obtained from many high elevation passive margins in the last two decades or so (Chapter 3), but those of eastern Australia and south Africa are perhaps the most extensively studied. A combination of AFTT and cosmogenic isotope data point toward a downwearing model of escarpment evolution in eastern and western south Africa (Cockburn et al., 2000; Brown et al., 2002). AFT data combined with unpublished (U-Th)/He ages from the Eritrean margin (Balestrieri, pers. Comm.) suggest that, although tectonic movements played an important role in the evolution of this margin, more than 4 km of crust was rapidly removed from the portion of the coastal plain nearest to the sea and that denudation, and possibly rates of denudation, decreased approaching the foot of the escarpment (Balestrieri *et al.*, in prep.). In the case of south eastern Australia, the combination of AFT and (U-Th)/He ages strongly argues in favour of a downwearing scenario with the chronology and

magnitude very similar to that predicted by a 3-D numerical model (van der Beek *et al.*, 2002). It is tempting to suggest that the downwearing scenario is the way high elevation passive margins evolve. However, there are other cases where, because of the lack of data, the landscape evolution is not so well constrained. In Northern New South Wales, for instance, remnants of the pre-rift palaeosurface are believed to be two small plateaus now raising from the coastal plain (Chapter 3): in this case, the downwarped rift shoulder scenario seems to be more appropriate. An escarpment retreat scenario is invoked for the evolution of the escarpment in western India (Gunnell & Fleitout, 2000) and the southeastern margin of Brazil (Gallagher et al., 1994).

Until more data are available and the correlation between global and local scale geomorphology is better constrained, it is highly speculative to emphasise the dominance of the downwearing scenario over the others. Moreover, variables that may be not important in the eastern Australia case, such as lithological or climatic controls, may play a fundamental role in determining the evolution of the escarpment in other margins (e.g. Beaumont et al., 1994; Tucker et al., 1994). Other factors, often ignored, as the nature and thickness of the continental crust, the presence of absence of underplating and/or volcanic activity, the tectonic causes of continental extension may also affect the denudational history of the landscape. However, from this study it is clear that the combination of AFT and (U-Th)/He thermochronologies is a unique way to 1) determine pre-rift topography, 2) constrain amounts and rates of pre-, syn- and post-breakup denudation; 3) distinguish between different landscape evolution scenarios.

References

Abbate E., Balestrieri M.L. & Bigazzi G. 2002 Morphostructural development of the Eritrean rift flank (southern Red Sea) inferred from apatite fission track analysis *J. Geophys. Res.*, **107**, 2319, doi:10.1029/2001JB001009

Al-Harthy F.A.H. 2001 *Quantifying epeirogenic uplift and denudation across eastern Australia* Unpublished PhD thesis, King's College, Cambridge; 242 p

Balogh K. & Simonits A. 1998 Improvements in experimental techniques of conventional K/Ar and Ar/Ar geochronological methods Rapid Commun Mass Sp., 12; 1769-1770

Beardsmore G.R. & Cull J.P. 2001 *Crustal heat flow – a guide to measurement and modelling* Cambridge University Press, 301 p

Beaumont C., Kooi H. & Willett S. 2000 Coupled tectonic-surface process models with applications to rifted margins and collisional orogens In: Summerfield M.A. (Ed.) – *Geomorphology and Global Tectonics* – John Wiley & Sons Ltd, Chichester; 28-55

Bellot-Gurlet L., Bigazzi G., Dorighel O.,Oddone M.,Poupeau G. & Yegingil Z 1999 The fission-track analysis: an alternative technique for provenance studies of prehistoric obsidian artefacts *Radiat. Meas.*, **31**; 639-644

Bender M.L. 1973 Helium-uranium dating of corals *Geochim. Cosmochim. Acta*, **37**; 1229-1247

Bird M.I. & Chivas A.R. 1988 Oxygen isotope dating of the Australian regolith *Nature*, **331**; 513-516

Bird M.I. & Chivas A.R. 1989 Stable-isotope geochronology of the Australian regolith *Geochim. Cosmochim. Acta*, **53**; 3239-3256

Bird M.I. & Chivas A.R. 1993 Geomorphic an palaeoclimatic implications of an oxygen-isotope chronology for Australian deeply weathered profiles *Australian J. Earth Sci.*, **40**; 345-358

Bishop P. 1985 Southeast Australian late Mesozoic and Cenozoic denudation rates: a test for late Tertiary increases in continental denudation *Geology*, **13**; 479-482

Bishop P., Young R.W. & McDougall I. 1985 Stream profile change and longterm landscape evolution: early Miocene and modern rivers of the east Australian highlands crest, central New South Wales, Australia *J. Geology*, **93**; 455-474

Bishop P. 1986 Horizontal stability of the Australian continental drainage divide in south central New South Wales during the Cainozoic Australian *J. Earth Sci.*, **33**; 295-307

Bishop P. 1988 The eastern highlands of Australia: the evolution of an intraplate highland belt *Prog. Phys. Geogr.*, **12**; 159-182

Bishop P. 1989 Geomorphology and evolution of the eastern highlands In: Johnson R.W. (Ed.) – *Intraplate volcanism in Eastern Australia and New Zeland* – Cambridge University Press, Cambridge; 21-28

Bishop P. & Goldrick G. 2000 Geomorphological evolution of the East Australian continental margin In: Summerfield M.A. (Ed.) – *Geomorphology and Global Tectonics* – John Wiley & Sons, Chichester; 227-235

Blythe A.E., Burbank D.W., Farley K.A. & Fielding E.J. 2000 Structural and topographic evolution of the central Transverse Ranges, California, from apatite fission-track, (U-Th)/He and digital elevation model analyses *Basin Res.*, **12**; 97-114

Branagan D.F. 1983 The Sydney Basin and its vanished *J. Geol. Soc. Aust.*, **30**; 75-84

Branagan D.F. & Pedram H. 1990 The Lapstone structural complex, New South Wales. *Aust. J. Earth Sci.*, **37**; 23-36

Brown R.W. 1991 *A fission track thermochronology study of the tectonic and geomorphic development of the sub-aerial continental margins of southern Africa* Unpublished PhD thesis, La Trobe University, Bundoora, Victoria, Australia, 407 p

Brown R.W. 1991 Backstacking apatite fission track "stratigraphy": a method for resolving the erosional and isostatic rebound components of tectonic uplift history *Geology*, **19**; 74-77

Brown R.W., Rust D.J., Summerfield M.A., Gleadow A.J.W. & De Wit M.C.J. 1990 An Early Cretaceous phase of accelerated erosion on the south-western margin of Africa: evidence from apatite fission track analysis and the offshore sedimentary record *Nucl. Tracks Radiat. Meas.*, **17**; 339-350

Brown R.W., Summerfield M.A. & Gleadow A.J.W. 1994 Apatite fission track analysis: its potential for the estimation of denudation rates and implications for models of long-term landscape development. In - *Process models and theoretical geomorphology* - Kirkby M.J. (Ed.), Wiley, Chichester; 23-54

Brown R.W., Summerfield M.A. & Gleadow A.J.W. 2002 Denudational history along a transect across the Drakensberg Escarpment of southern Africa derived from apatite fission track thermochronology *J. Geophys. Res.*, **107 (B12)**, 2350, doi: 10.1029/2001JB000745

Bryan S.E., Constantine A.E., Stephens C.J. Ewart A., Schon R.W. & Parianos J. 1997 Early Cretaceous volcano-sedimentary succession along the eastern Australian continental margin: implications for the break-up of eastern Gondwana *Earth Planet. Sci. Letts.*, **153**; 85-102

CarlsonW.D., Donelick R.A. & Ketcham R.A. 1999 Variability of apatite fission-track annealing kinetics: I. Experimental results *Am. Mineral.*, **84**; 1213-

Cederbom C., Larson S.Å. Tullborg E-L. & Stiberg J-P. 2000 Fission track thermochronology applied to Phanerozoic thermotectonic events in central and southern Sweden *Tectonophysics*, **316**; 153-167

Chen Y.D., O'Reilly S.Y. & Griffin W.L. 1998 Combined U-Pb dating and Sm-Nd studies on lower crustal and mantle xenoliths from the Delegate basaltic pipes, southeastern Australia *Contrib. Mineral. Petrol.*, **130**; 154-161

Ciubotariu M. 2001 On the Th internal contamination by ingestion using the fission track method Radiat. Meas., 34; 533-535

Chappell B.W. & Stephens W.E. 1988 Origin of infracrustal (I-type) granite magmas *Trans. Royal Soc. Edinburgh: Earth Sci.*, **79**; 71-86

Clarke S.P & Jäger E. 1969 Denudation rate in the Alps from geochronologic and heat flow data *American J. Science*, **267**; 1143-1160

Cockburn H.A.P., Brown R.W., Summerfield M.A. & Seidl M.A. 2000 Quantifying passive margin denudation and landscape development using a combined fission-track thermochronology and cosmogenic isotope analysis approach *Earth Planet. Sci. Lett.*, **179**; 429-435

Colwell J.B. & Coffin M.F. 1987 Rig seismic research cruise 13: structure and stratigraphy of the northeast Gippsland Basin and southern New South Wales margin. Initial report *Bureau of Mineral Resources, geology and geophysics*, 1-36

Colwell J.B., Coffin M.F. & Spencer R.A. 1993 Structure of the southern New South Wales continental margin, southeastern Australia *Bureau of Mineral Resources, J. Austr. Geol. Geophys.*, **13**; 333-343

Crank J. 1975 *The mathematics of diffusion* Clarendon Press, Oxford; 414p

Crawford E., Herbert C., Taylor G., Helby R., Morgan R. & Ferguson J. 1980 Diatremes in the Sydney Basin In: Herbert C. & Helby R. (Eds.) - *A guide to the Sydney Basin* – Geol. Survey of New South Wales, Bull. 26; 295-323

Crowley K.D, Cameron M. & Schaefer R.L. 1991 Experimental studies of annealing of etched fission tracks in fluoroapatite *Geochim. Cosmochim. Acta*, **55**; 1449-1465

Crowley P.D., Reiners P.W., Reuter J.M. & Kaye G.D. 2002 Laramide exhumation of the Bighorn Mountains, Wyoming: an apatite (U-Th)/He thermochronology study *Geology*, **30**; 27-30

Damon P.E.& Green W.D. 1963 Investigation of the helium age dating method by stable isotope-dilution technique. In - *radioactive dating* - Proceedings of the symposium on radioactive dating in Athens, 19-23 November 1962; 55-71

Darwin C. 1859 On the origin of species by means of natural selection, or the preservation of favoured races in the struggle for life John Murray, London

Dempster T.J., Jolivet M., Tubrett M.N. & Braithwaite C.J.R. 2003 Magmatic zoning in apatite: a monitor of porosity and permeability change in granites *Contr. Mineral. Petrol.*, **145**; 568-577

Department Mineral Resources1995 *1:250,000 Geological Map Bega* Geological Survey of New South Wales, Department of Mineral Resources, Sydney

Dickins A.P. 1995 *Radiogenic isotope geology* Cambridge University Press, Cambridge; 490 pp.

Dodson M.I. 1973 Closure temperature in cooling geochronological and petrological systems *Contri. Mineral. Petrol.*, **40**; 259-274

Donelick R.A., Roden M.K., Mooers J.D., Carpenter B.S. & Miller D.S. 1990 Etchable track length reduction of induced fission tracks in apatite at room temperature (~23°C): crystallographic orientation effects and "initial" mean lengths *Nucl. Tracks Radiat. Meas.*, **17**; 261-265

Donelick R.A. 1993 A method of fission track analysis utilizing bulk chemical etching of apatite *U.S. Patent Number 6,267,274*

Donelick R.A., Ketcham R.A. & Carlson W.D. 1999 Variability of apatite fission-track annealing kinetics:II. Crystallographic orientation effects *Am. Miner.*, **84;** 1224-1234

Duddy I.R. & Kelly P.R. 1999 Uranium in mineral sands: measurements and uses *Austr. Inst. Geoscientists Bull.*, **26**; 1-7

Duggan M.B., Sutherland F.L. & Martin D.J. 1989 Mesozoic intraplate volcanism and related intrusions In: Johnson R.W. (Ed.) – *Intraplate volcanism in Eastern Australia and New Zeland* – Cambridge University Press, Cambridge; 149-152

Dulhunty J.A. 1964 Our Permian heritage in central Eastern New South Wales *J. Proc. Royal Soc. New South Wales*, **97**; 145-155

Dulhunty J.A. 1973 Potassium-Argon basalt ages and their significance in the Macquarie valley, New South Wales *J. Proc. Royal Soc. New South Wales*, **106**; 104-110

Dumitru T.A., Hill K.C., Coyle D.A., Duddy I.R., Foster D.A., Gleadow A.J.W., Green P.F., Laslett G.M., Kohn B.P. & O'Sullivan A.B. 1991 Fission track thermochronology: application to continental rifting of southeastern Australia *APEA J.*, **31**; 131-142

England P. & Molnar P. 1990 Surface uplift, uplift of rocks, and exhumation of rocks *Geology*, **18**; 1173-1177

Fabel D. & Finlayson B.L. 1992 Constraining variability in south-east Australian long-term denudation rates using a combined geomorphological and thermochronological approach *Z. Geomorph.*, **36**; 293-305

Falvey D.A. 1974 The development of continental margins in plate tectonic theory The *APEA J.*; 95-106

Fanale F.P. & Schaeffer O.A. 1965 Helium-uranium ratios for Pleistocene and Tertiary fossil aragonites *Science*, **149**; 312-317

Farley K.A. 2002 (U-Th)/He dating: Techniques, calibrations and applications - in Porcelli D., Ballentine C.J. & Wieler R. (Eds.) - *Noble gases in cosmochemistry and geochemistry, reviews in mineralogy and geochemistry*, **47**; 819-844

Farley K.A. 2000 Helium diffusion from apatite: general behavior as illustrated by Durango fluoroapatite *J. Geophys. Res.*, **105**; 1903-2914

Farley K.A., Kohn B.P. & Pillans B. 2002 The effects of secular disequilibrium on (U-Th)/He systematics and dating of Quaternary volcanic zircon and apatite *Earth Planet. Sci. Letts.*, **201**; 117-125

Farley K.A., Wolf R.A. & Silver L.T. 1996 The effects of alpha-stopping distances on (U-Th)/He dates *Geochim. Cosmochim. Acta*, **60**; 4223-4229

Farley K.A., Reiners P.W. & Nenow V. 1999 An apparatus for high-precision helium diffusion measurements from minerals *Anal. Chem.*, **71**; 2059-2061 *Earth Planet. Sci. Lett.*, **201**; 117-125

Farley K.A., Rusmore M.E. & Bouge S.W. 2001 Post-10 Ma uplift and exhumation of the northern coast mountains, British Columbia *Geology*, **29**; 99-102

Farley K.A., Kohn B.P. & Pillans B. 2002 The effects of secular disequilibrium on (U-Th)/He systematics and dating of Quaternary volcanic zircon and apatite

Fergusson C.L. & Phillips 2001 $^{40}Ar/^{40}Ar$ and K-Ar age constraints on the timing of regional deformation, south coast of New South Wales, Lachlan Fold Belt: problems and implications *Aus. J. Earth Sci.*, **48**; 395-402

Fleischer R.L., Price P.B. & Walker R.M. 1965 Effects of temperature, pressure, and ionization on the formation and stability of fission tracks in minerals and glasses *J. Geophys. Res.*, **70**; 1497-1502

Fleischer R.L., Price P.B. & Walker R.M. 1975 *Nuclear tracks in solids; principles and applications* University of California Press, Berkeley; 605 pp

Foster D.A. & Gray D.R. 2000 Evolution and structure of the Lachlan Fold Belt (orogen) of eastern Australia *Ann. Rev. Earth Planet. Sci.*, **28**; 47-80

Gaina C., Muller D.R., Royer J-Y., Stock J., Hardebeck J. & Symonds P. 1998 The tectonic history of the Tasman Sea: a puzzle with 13 pieces *J. Geophys. Res.*, **103 (B6)**; 12,413-12,433

Galbraith R.F. 1990 The radial plot: graphical assessment of spread in ages *Nucl. Tracks Radiat. Meas.*, **17**; 207-214

Gallagher K. & Brown R.W. 1997 The onshore record of passive margin evolution *J. Geol. Soc. London*, **154**; 451-457

Gallagher K, Hawkesworth C.J. & Mantovani M.S.M. 1995 Denudation, fission track analysis and the long-term evolution of passive margin topography: application to the southeast Brazilian margin *J. South American Sci.*, **8**; 65-77

Gallagher K., Brown R.W. & Johnson C. 1998 Fission track analysis and its applications to geological problems *Ann. Rev. Earth Sci.*, **26**; 519-572

Gilchrist A.R. & Summerfield M.A. 1990 Differential denudation and flexural isostasy in formation of rifted-margin upwarps *Nature*, **346**; 739-742

Gilchrist A.R. & Summerfield M.A. 1994 Tectonic models of passive margin evolution and their implications for theories of long-term landscape development In: Kirkby M.J. (Ed.) - *Process Models and Theoretical Geomorphology* – John Wiley & Sons Ltd, Chichester, 55- 84

Gilchrist A.R., Kooi H. & Beaumont C. 1994 Post-Gondwana geomorphic evolution of southwestern Africa: implications for the controls on landscape development from observations and numerical experiments *J. Geophys. Res.*, **99**; 12,211-12,228

Gleadow A.J.W. 1981 Fission track dating methods: what are the real alternatives? *Nucl. Tracks Radiat. Meas.*, **5**; 3-14

Gleadow A.J.W. & Brown R.W. 2000 Fission-track thermochronology and the long-term denudational response to denudation In: Summerfield M.A. (Ed.) – *Geomorphology and Global Tectonics* – John Wiley & Sons, Chichester; 57-76

Gleadow A.J.W. & Duddy I.R. 1981 A natural long-term track annealing experiment for apatite *Nuclear Tracks*, **5**; 169-174

Gleadow A.J.W. & Fitzgerald P.G. 1987 Uplift evidence from fission track dating of basement apatites in the Dry Valleys area, Southern Victoria Land *Earth Planet. Sci. Lett.*, **82**; 1-14

Gleadow A.J.W., Duddy I.R., Green P.F. & Lovering J.F. 1986 Confined fission track lengths in apatite: a diagnostic tool for thermal history analysis *Contrib. Min. Petrol.*, **94**; 405-415

Green P.F. 1986 On the thermotectonic evolution of Northern England: evidence from fission track analysis *Geol. Magazine*, **123**; 493-506

Green P.F. 1988 The relationship between track shortening and fission track age reduction in apatite: combined influences of inherent instability, annealing anisotropy, length bias and system calibration *Earth Planet. Sci. Letts.*, **89**; 335-352

Green P.F., Duddy I.R., Gleadow A.J.W. & Lovering J.F. 1989 Thermal annealing of fission tracks in apatite 4. Quantitative modelling technique and extension to geological timescales *Chem. Geol.* **79**; 155-182

Gunnell Y. & Fleitout L. 1998 Shoulder uplift of the western Ghats passive margin, India: a denudational model *Earth Surf. Proc. Land*, **23**; 391-40

Gögen K. & Wagner G.A. 2000 Alpha-recoil track dating of Quaternary volcanics *Chem. Geol.*, **166**; 127-137

Hammerschmidt K., Wagner G.A. & Wagner M. 1984 Radiometric dating on research drill core Urach III: a contribution to its geothermal history *J. Geophys.*, **54**; 97-105

Hayes D.E. & Ringis J. 1973 Sea-floor spreading in the Tasman Sea *Nature*, **243**; 454

Heimsath A.M., Chappell J., Dietrich W.E., Nishiizumi K. & Finkel R.C. 2000 Soil production on a retreating escarpment in southeastern Australia *Geology*, **28**; 787-790

Herbert C. 1980 Depositional development of the Sydney Basin In: Herbert C. & Helby R. (Eds.) - *A guide to the Sydney Basin* – Geol. Survey of New South Wales, Bull. 26; 10-52

Hill S.M. 1999 Mesozoic regolith and palaeolandscape features in southeastern Australia: significance for interpretation of denudation and highland evolution *Australian J. Earth Sci.*, **46**; 217-232

House M., Wernicke B., Farley K.A. & Dumitru T. 1997 Cenozoic thermal evolution of the central Sierra Nevada from (U-Th)/He thermochronometry *Earth Planet. Sci. Lett.*, **151**; 167-179

House M., Wernicke B. & Farley K.A. 1998 Dating topography of the Sierra Nevada, California using apatite (U-Th)/He ages *Nature*, **396**; 66-69

House M., Farley K.A. & Kohn B. 1999 An empirical test of helium diffusion in apatite: borehole data from the Otway basin, Australia *Earth Planet. Sci. Lett.*, **170**; 463-474

House M.A., Farley K.A. & Stockli D. 2000 Helium chronometry of apatite andtitanite using Nd-YAG laser heating *Earth Planet. Sci. Lett.*, **183**; 365-368

Hurford A.J. & Green P.F. 1982 A users' guide to fission track dating *Earth Planet. Sci. Letts.*, **59**; 343-354

Hurford A.J. & Green P.F. 1983 The zeta age calibration of fission-track dating *Isotope Geosci.*, **1**; 285-317

Hurley P.M. 1950 Distribution of radioactivity in granites and possible relation to helium age measurement *Bull. Geol. Soc. Am.*, **61**; 1-8.

Hurley P.M. 1960 *How old is the Earth?* Heinemann, London; 160 pp.

Hutton J. 1788 Theory of the Earth *Transactions of the Royal Society of Edinburgh*, **1**; 209-305

Jongsma D. & Mutter J.C. 1978 Non-axial breaching of a rift valley: evidence from the Lord Howe Rise and the southeastern Australian margin *Earh Planet. Sci. Letts.*, **39**; 226-234

Kearey P. & Vine F.J. 1990 *Global tectonics* Blackwell Science, Oxfor; 209-247

Keevil N.B. 1941 The unreliability of the helium index in geological correlation *Univ. Toronto Geol. Ser. Studies*, **46**; 39-67.

Kelvin W. Thompson Baron 1862 On the age of the sun's heat *Macmillans Magazine*, 5; 288

Ketcham R.A., Donelick R.A. & Carlson W.D. 1999 Variability of apatite fission-track annealing kinetics: III. Extrapolation to geological time scales *Am. Mineralogist* , **84**; 1235-1255

Ketcham R.A., Donelick R.A. & Carlson W.D. 1999 Variability of apatite fission-track kinetics:III. Extrapolation to geological time scales *Am. Miner.*, **84**; 1235-1255

King L.C. 1950 *South African Scenery* Oliver & Boyd, White Plains, New York, 699 **p**

King, L.C. 1955 Pediplanation and isostasy: an example from South Africa. *Quarterly Journal of the Geological Society of London* 111; 353-359.

Kohn B.P., & Eyal M. 1981 History of uplift of the crystalline basement of Siani and its relation to opening of the Red Sea as reveadl by fission track dating of apatites *Earth Planet. Sci. Letts.*, **52**, 129-141

Kohn B.P., Gleadow A.J.W. & Cox S.J.D. 1998 Denudation history of the Snowy Mountains: constraints from apatite fission track thermochronology *Aust. J. Earth Sci.*, **46**; 181-198

Kohn B., Gleadow A.J.W., Brown R.W., Gallagher K., O'Sullivan P. & Foster D.A. 2002 Shaping the Australian crust over the last 300 million years: insights from fission track thermotectonic imaging and denudation studies of key terranes *Australian J. Earth Sci.*, **49**; 697-71

Kooi H. & Beaumont C. 1994 Escarpment evolution on high-elevation rifted margins: insights derived from a surface process model that combines diffusion, advection, and reaction *J. Geophys. Res*, **99**; 12,191-12,210

Laslett G.M., Green P.F., Duddy I.R. & Gleadow A.J.W. 1987 Thermal annealing of fission tracks in apatite 2. Quantitative analysis *Chem. geol.*, **65**; 1-13

Lee J.K.W. 2000 Empirical constraints on closure temperatures from a single diffusion coefficient *Contrib. Mineral. Petr.*, **139**; 526-540

Leventhal J.S. 1975 An evaluation of the U-Th-He method for dating young basalts *J. Geophys. Res.*, **80**; 1911-1914

Li Y.G., Shi Y.Q., Zhang Y.B. & Xia P. 2001 Reactor fission rate measurement for miniature neutron source reactor by solid state nuclear track detector *Radiat. Meas.*, **34**; 589-591

Lippolt H.J., Leitz M., Wernicke R.S. & Hagedorn B. 1994 (Uranium + thorium/helium dating of apatite: experience with samples from different geochemical environments *Chem. Geol. (Isot. Geosci. Sect)*, **112**; 179-191

Lister G.S., Etheridge M.A. & Symonds P.A. 1986 Detachment faulting and the evolution of passive continental margins *Geology*, **14**; 246-250

Lister G.S. & Etheridge M.A. 1989 Detachment model for the uplift and volcanism of the Eastern Highlands. In: Johnson W. (Ed.) - *Intraplate volcanism in eastern Australia and New Zealand* – Cambridge University Press, New York; 297-312

Lister G.S., Etheridge M.A. & Symonds P.A. 1991 Detachment models fro the formation of passive continental margins *Tectonics*, **10**; 1038-1064

Lyell C. 1830 *Principles of Geology, being an attempt to explain the former changes of the Earth's surface, by reference to causes now in operation* Vol. 1, John Murray, London

Luo X.Z., Rehkamper M., Lee D.C. & Halliday A.N. 1997 High precision Th-230/Th-232 and U-234/U-238 measurements using energy-filtered ICP magnetic sector multiple collector mass spectrometry *Int. J. Mass Spectrom.*, **171**; 105-117

Makris J., Tsironidis J. & Richter H. 1991 Heatflow density distribution in the Red Sea *Tectonophysics*, **198**; 383-393

McElhinny M.W. 1973 *Palaeomagnetism and plate tectonics* Cambridge University Press, London, 253 p

McKenzie D. & Fairhead D. 1997 Estimates of the effective elastic thickness of the continental lithosphere from Bouger and free air gravity anomalies *J. Geophys. Res.*, **102**; 17523-27552

McInnes B.I.A., Farley K.A., Sillitoe R.H. & Kohn B. 1999 Application of apatite (U-Th)/He thermochronometry to the determination of the sense and amount of vertical fault displacement at the Chuquicamata porphyry copper deposit Chile *Econ. Geol.*, **94**; 937-947

Meesters A.G.C.A. & Dunai T.J. 2002a Solving the production-diffusion equation for finite diffusion domains of various shapes (part I): implications for low-temperature (U-Th)/He thermochronology *Chem. Geol.*, **186**; 333-344

Meesters A.G.C.A. & Dunai T.J. 2002b Solving the production-diffusion equation for finite diffusion domains of various shapes (part II): application to cases with α-ejection and non-homogeneous distribution of the source *Chem. Geol.*, **186**; 347-363

Middleton M.F. & Schmidt P.W. 1982 Paloethermometry of the Sydney Basin *J. Geophys. Res.*, **87**; 5351-5359

Morley M.E., Gleadow A.J.W. & Lovering J.F. 1981 Evolution of the Tasman Rift: apatite fission track dating evidence from the southeastern Australian margin In: Cresswell M.M. & Vella P. (Eds.) – *Gondwana Five* – A.A. Balkema, Rotterdam, 289-293

Moore M.E., Gleadow A.J.W. & Lovering J.F. 1986 Thermal evolution of rifted continental margins: new evidence from fission tracks in basement apatites from southeastern Australia *Earth Planet. Sci. Letts.*, **78**; 255-270

Naeser C.W. 1979 Fission track dating and geologic annealing of fission tracks In - *Lectures in Isotope Geology* - Jaeger E. & Hunziker J.C. (Eds.), Springer-Verlag, Heidelberg, 154-169

Nott J.F. & Purvis A.C. 1995 Geomorphic and tectonic significance of Early Cretaceous lavas on the coastal plain, southern New South Wales *Aust. J. Earth Sci.*, **42**; 145-149

Nott J., Young R. & McDougall I. 1996 Wearing down, wearing back, and gorge extension in the long-term denudation of a highland mass: quantitative evidence from the Shoalhaven catchment, southeast Australia *J. Geology*, **104**; 224-232

Olive V., Ellam R.M. & Wilson L. 2001 A protocol for the determination of the rare earth elements at picomole level in rocks by ICP-MS: results on geological reference materials USGS PCC-1 and DTS-1 *Geostandard and Newslett.*, **25**; 219-228

Ollier C.D. 1982 The Great Escarpment of eastern Australia: tectonic and geomorphic significance *J. Geol. Soc. Australia*, **29**; 13-23

Ollier C.D 1985 Morphotectonics of passive continental margins: introduction. *Z. Geomporphol. Suppl. Bd. N.F.*, **54**; 1-9

Ollier C.D. & Pain C.F. 1994 Landscape evolution and tectonics in southeastern Australia *AGSO J. Austr. Geol. Geophys.*, **15**; 335-345

Ollier C.D. & Pain C.F. 1997 Equating the basal unconformity with the palaeoplain: A model for passive margins *Geomorphology*, **19**, 1–15,

O'Sullivan P.B., Kohn B.P., Foster D.A. & Gleadow A.J.W. 1995 Fission track data from the Bathurst Batholith: evidence for rapid middle Cretaceous uplift and erosion within the eastern highlands of Australia *Aust. J. Earth Sci.*, **42**; 597-607

O'Sullivan P.B., Foster D.A., Kohn B.P. & Gleadow A.J.W. 1996 Tectonic implications of Early Triassic and middle Cretaceous denudation in the eastern Lachlan Fold Belt, NSW, Australia *Geology*, **6**; 563-607

O'Sullivan P.B., Gibson D.L., Kohn B.P., Pillans B. & Pain C.F. 2000 Long-term landscape evolution of the Northparkes region of the Lachlan Fold Belt, Australia: constraints from fission track and palaeomagnetic data *J Geol.*, **108**; 1-16

Ottonello G. 1997 *Principle of geochemistry* Columbia University Press, New York; 744-745

Pain C.F. & Ollier C.D. 1986 The Comboyne and Bulga Plateaus and the evolution of the Great Escarpment in New South Wales *J. Proc. Royal Soc. New South Wales*, **119**; 123-130

Pazzaglia F.J. & Gardner T.W. 1994 Late Cenozoic flexural deformation of the middle U.S. Atlantic passive margin. *J. Geophys. Res.*, **99**; 12,143-12,157

Perelygin V.P., Bondar Y.V., Ensinger W., Fleischer R.L., Vater P. & Stetsenko S.G. 2003 On search and identification of short-lived super heavy cosmic-ray nuclei (Z>110) by fossil track study of the extraterrestrial crystals: results and perspectives *Nucl. Phys.*, **718**; 410C-412C

Persano C., Stuart F.M., Bishop P. & Barfod D.N. 2002 Apatite (U-Th)/He age constraints on the development of the Great Escarpment on the southeastern Australian passive margin *Earth Planet. Sci. Lett.*, **200**; 79-90

Pugh, J.C. 1955 Isostatic readjustment in the theory of pediplanation *Quarterly Journal of the Geological Society of London* 111; 361-369.

Reiners P., Brady R., Farley K.A., Fryxell J., Wernicke B. & Lux D. 2000 Helium and argon thermochronometry of the Gold Butte Block, south Virgin Mountains, Nevada *Earth Planet. Sci. Lett.*, **178**; 315-326

Reiners P. & Farley K.A. 2001 Influence of crystal-size on apatite U-Th/He thermochronology: an example from the Bighorn Mountains, Wyoming *Earth Planet. Sci. Lett.*, **188**; 413-420

Riley N.J. 1993 Dinantian (Lower Carboniferous) biostratigraphy chronostratigraphy in the British-Isles *J. Geol. Soc.*, **150**; 427-446

Rowley E. & White N. 1998 Inverse modelling of extension and denudation in the East Irish Sea and surrounding areas *Earth Planet. Sci. Lett.*, **161**; 57-,71

Rutherford E. 1904 *Radio-activity* Cambridge at the University Press, Cambridge; 399 p.

Rutherford E. 1906 *Radioactive transformations* New Haven: Yale University Press, London; 287 pp.

Seidl M.A., Weissel J.K. & Pratson L.F. 1996 The kinematics and pattern of escarpment retreat across the rifted continental margin of SE Australia *Basin Res.*, **12**; 301-316

Seidl M.A., Finkel R.C. Caffee M.W., Hudson G.B. & Dietrich W.E. 1997 Cosmogenic isotope analyses applied to river longitudinal profile evolution. Problems and interpretation *Earth Surf. Proc. Land.*, **22**; 195-209

Seyfert C.K. & Sirkit L.A. 1973 *Earth history and plate tectonics: an introduction to historical geology* Harper & Row, London, 504 p

Shaw R.D. 1979 On the evolution of the Tasman Sea *Aust. Soc. Explor. Geophys. Bull.*, **9**; 75-81

Schmidt P.W. Lackie M.A. & Anderson J.C. 1995 Palaeomagnetic evidence for the age of the Lapstone Monocline, NSW *Australian Coal Geology*, **10**; 14-19

Shaw R.D. 1979 Sea-floor spreading in the Tasman Sea: a Lord Howe Rise-eastern Australian reconstruction *Bull. Austr. Soc. Exploration*, **9**; 75-81

Spotila J.A., Farley K.A. & Sieh K.1998 Uplift and erosion of the San Bernardino Mountains associated with transpression along the San Andreas fault, California, as constrained by radiogenic helium thermochronometry *Tectonics*, **17**; 360-378

Spotila J.A., Farley K.A., Yule J.D. & Reiners P.W. 2001 Near-field convergence along the San Andreas fault zone in southern California, based on exhumation constrained by (U-Th)/He dating *J. Geophys. Res.*, **106 (B12)**; 30909-30922

Steckler M.S & Omar G.I. 1994 Controls on erosional retreat of the uplifted rift flanks at the Gulf of Suez and northern Red Sea *J. Geophys. Res.*, **99 (B6)**; 12,159-12,173

Stockli D.F., Farley K.A. & Dumitru T. 2000 Calibration of the apatite (U-Th)/He thermochronometer on an exhumed fault block, White Mountains, California *Geology*, **28**; 983-986

Suess E. 1904 *The face of the Earth* Claredon, Oxford, vol. 1; 604 p

Summerfield M.A. 1990 Sub-aerial denudation of passive margins: regional elevation versus local relief models *Earth Planet. Sci. Letts.*, **102**; 460-469

Sun S.S., McDonough W.F. & Ewart A. 1989 Four component model of east Australian basalts In: Johnson W. (Ed.) - *Intraplate volcanism in eastern Australia and New Zealand* – Cambridge University Press, New York; 333-347

Taylor G., Truswell E.M., McQueen K.G. & Brown M.C. 1990 Early Tertiary palaeogeography, landform evolution, and palaeoclimates of the Southern Monaro, NSW, Australia *Palaeogeog. climat. ecol.*, **78**; 109-134

Tucker G.E. & Slingerland R.L. 1994 Erosional dynamics, flexural isostasy, and long-lived escarpments: a numerical modelling study *J. Geophys. Res.*, **99**; 12,229-12,244

Twidale C.R. 1994 Gondwanan (Late Jurassice and Cretaceous) palaeosurfaces on the Australian craton *Palaeogeog., Palaeoclim., Palaeoec.*, **112**; 157-186

van der Beek P.A., Andriessen P.A.M. & Cloetingh S. 1995 Morphotectonic evolution of rifted continental margins: inferences from a coupled tectonic-surface processes model and fission-track thermochronology *Tectonics*, **14**; 406-421

van der Beek P.A & Braun J. 1999 Numerical modelling of landscape evolution on geological time-scales: a parameter analysis and comparison with the south-eastern highlands of Australia *Basin Research*, **10**; 49-68

van der Beek P.A, Braun J. & Lambeck K. 1999 The post-palaeozoic uplift of southeastern Australia revisited: results from a process-based model of landscape evolution *Aust. J. Earth Sci.*, **46**; 157-172

van der Beek P.a., Purford A. & Braun J. 2001 Cenozoic landscape development in the Blue Mountains (SE Australia): lithological and tectonic controls on rifted margin morphology *J. Geol.*, **109**; 35-56

van der Beek P. 2002 Rifted margins, fission tracks, and landscape evolution models: a happy ménage à trois? On Tracks, **24**; 4-10

van der Beek P., Summerfield M.A., Braun J., Brown R.W. & Fleming A. 2002 Modeling postbreakup landscape development and denudational history across the southeast African (Drakensberg Escarpment) margin *J. Geophys. Res.*, **107 (B12)**; doi: 10.1029/2001JB000744

Wagner G.A. 1968 Fission track dating of apatites *Earth Planet. Sci. Lett.*, **4**; 411-415

Wagner G.A. 1972 The geological interpretation of fission track ages *Trans. Amer. Nucl. Soc.*, **15**; 117

Wagner G.A. & van der Haute P. 1992 *Fission-track dating* Kluwer Academic Publishers, Dordrecht, 285 p

Warnock A.C., Zeitler P.K., Wolf R.A. & Bergman S.C. 1997 An evaluation of low-temperature apatite U-Th/He thermochronometry *Geochim. Cosmochim. Acta*, **61**; 5371-5377

Watts A.B. 2001 *Isostasy and flexure of the lithosphere* Cambridge University Press, Cambredge; 458p

Wedepehl K.H. (ed.) 1978 *Handbook of geochemistry II-5* Springer - Verlag, Berlin; Tables 39; 90-D-1; 92-D-1

Weissel J.K & Karner G.D. 1989 Flexural uplift of rift flanks due to mechanical unloading of the lithosphere during extension *J. Geophys. Res.*, **94**; 13,919-13,950

Weissel J.K. & Seidl M.A. 1997 Influence of rock strength properties on escarpment retreat across passive margins *Geology*, **25**; 631-634

Weissel J.K. & Seidl M.A. 1998 Inland propagation of erosional escarpments and river profile evolution across the southeast Australian passive continental margin In: Tinkler K.J. & Wohl E.E. (Eds.) – *Rivers over rock: fluvial processes in bedrock channels* – American Geophysical Union, Geophysical Monograph 107; 189-205

Wellman P. 1987 Eastern Highlands of Australia; their uplift and erosion *J. Austr. Geol. Geophys.*, **10**; 277-286

Wellman P. 1996 The effective elastic thickness of the Australian crust: a major control on the wavelength and shape of topography and basins *AGSO Research Newsletter*, **24**; 16

Wellman P. & McDougall I. 1974 Potassium-argon ages on the Cainozoic volcanic rocks of New South Wales, Australia *J. Geol. Austr.*, **21**; 247-272

White A.J.R. & Chappell B.W. 1988 Some supracrustal (S-type) granites of the Lachlan Fold Belt *Trans. Royal Soc. Edinburgh: Earth Sci.*, **79**; 169-181

Wieler R. & Eikenberg J. 1998 An upper limit on the spontaneous fission decay constant of ^{232}Th derived from xenon in monazites with extra high Th/U ratios *Geophys. Res. Lett.*, **26**; 107

Williams I.S. 2001 Response of detrital zircon and monazite, and their U-Pb isotopic systems, to regional metamorphism and host-rock partial melting, Cooma Complex, southeastern Australia *Aust. J. Earth Sci.*, **48**; 557-580

Wolf R.A., Farley K.A. & Silver L.T. 1996a Helium diffusion and low temperature thermochronometry of apatite *Geochim. Cosmochim. Acta*, **60**; 4231-4240

Wolf R.A., Farley K.A. & Silver L.T. 1996b Assessment of (U-Th)/He thermochronometry: the low-temperature history of the San Jacinto Mountains, California *Geology*, **25**; 65-68

Wolf R.A., Farley K.A. & Kass D. 1998 A sensitivity analysis of the apatite (U-Th)/He thermochronometer *Chem. Geol.*, **148**; 105-114

Young D.A. 1958 Etching of radiation damage in lithium fluoride *Nature*, **182**; 375-377

Young E.J., Myers A.T., Munson E.L. & Canklin N.M. 1969 Mineralogy and geochemistry of fluoroapatite from Cerro de Mercado, Durango, Mexico *U.S. Geol. Surv. Prof. Pap.* **650**, D84-D93

Young R.W. 1977 Landscape development in the Shoalhaven River catchment of southeastern New South Wales *Zeitschrift fur Geomorphologie*, **21**; 262-283

Young R.W. 1982 The tempo of geomorphological change: evidence from southeastern Australia *J. Geology*, **18**; 221-230

Young R.W. & McDougall I. 1985 The age, extent and geomorphological significance of the Sassafras basalt, south-eastern New South Wales *Australian J. Earth Sci.*, **32**; 323-331

Zeitler P.K., Herczig A.L., McDougall I. & Honda M. 1987 U-Th-He dating of apatite: a potential thermochronometer *Geochim. Cosmochim. Acta*, **51**; 2865-2868

ALL MISSING
PAGES ARE
BLANK
IN
ORIGINAL

Sample location

Sample name	Location (Lat/Long)	Altitude (m)	Distance from the coast (km)
Samples from the plateau			
7859-9	S36°37'/E 148°04'	1100	153
7759-8	C36°35'/E 148°35'	1050	135
Brown Mt. traverse			
99-OZ-13	S35°17'/E 150°27'	20	2
99-OZ-12	S35°54'/E150°06'	20	5
99-OZ-11	S36°24'/E149°52'	160	18
00-CP-36	S36°39'/E149°48'	20	17
00-CP-35	S36°38'/149°35'	105	28
00-CP-34	S36°39'/E149°43'	80	35
99-OZ-06	S36°38'/E149°37'	220	39
00-CP-33	S36°38'/E149°35'	200	43
01-CP-05	S36°36'/E149°28'	530	55
99-OZ-08	S36°37'/E149°30'	840	43
99-OZ-10	S36°36'/E149°20	1100	58
99-0Z09	S36°35'/E149°21'	1140	60
Towamba River traverse			
01-CP-01	S37°01'/E149°39'	138	23
00-CP-02	S37°01'/E149°38'	140	23
00-CP-03	S36°58'/E149°34'	135	33
00-CP-04	S36°56'/E149°28'	240	38
00-CP-05	S36°54'/E149°28'	240	38
00-CP-06	S36°54'/E149°30'	295	40
00-CP-07	S36°53'/E149°27'	420	39
00-CP-08	S36°53;/E149°27'	490	41
01-CP-03	S36°54'/E149°27'	306	43
00-CP-11	S36°52'/E149°26'	620	42
00-CP-10	S36°56'/E149°16'	705	58
Bathurst Batholith			
99-OZB-02	S33°38'/E150°05	767	
99-OZB-03	S33°37'/E150°03'	860	
99-OZB-04	S33°33'/E149°50'	1040	
99-OZB-05	S33°34'/E149°45'	1140	
99-OZB-06	S33°35'/E149°46'	650	
99-OZB-07	S33°40'/E149°18'	600	

Table A1.1: Location of all the samples analysed during this study. The distance from the coast for the Bathurst Batholith samples is not reported, as they all lie inland of the escarpment.

Zeta calibration

Standard	ρ_D (10^5 cm^{-2}) (N_D)	ρ_s (10^5 cm^{-2}) (N_s)	ρ_i (10^5 cm^{-2}) (N_i)	ζ
Durango 31.4 ± 0.5 Ma				
Durango	14.56 (4861)	7.874 (121)	6.944 (1067)	393±30
Durango	14.58 (4861)	8.234 (109)	7.682 (1017)	396±40
Durango	14.51 (4861)	9.081 (179)	7.960 (1569)	394±31
Durango	13.22 (4861)	5.705 (118)	4.743 (981)	396 ± 39
Fish Canyon Tuff 27.9 ± 0.5 Ma				
Fish Canyon Tuff	14.53 (4861)	1.223 (88)	1.170 (823)	363 ± 38
Fish Canyon Tuff	14.70 (4861)	1.115 (79)	1.048 (742)	358±43
Fish Canyon Tuff	14.45 (4861)	1.262 (118)	1.185 (1105)	365±36
Fish Canyon Tuff	14.49 (4861)	1.502 (146)	1.411 (1372)	362 ± 32
Mt. Dromedary 98.7 ± 0.6 Ma				
Mt. Dromedary	12.61 (5463)	4.616 (517)	1.111 (1244)	359 ± 20
Mt. Dromedary	12.46 (5463)	3.993 (387)	9.420 (913)	376 ± 23
Mt. Dromedary	14.52 (5463)	4.345 (342)	1.211 (953)	370 ±24
Mt. Dromedary	13.18 (5102)	4.061 (576)	0.993 (1409)	369 ± 19
Mt. Dromedary	15.72 (5102)	4.498 (436)	1.290 (1250)	363 ± 21
Weighed mean: 368 ± 8				

Appendix 2

2.1 Apatite fission track analysis

Once the apatite concentrate has been obtained by separation from the bulk of the rock, it was mounted using Petropoxy on glass microscope slides. The internal surface of the apatite crystals was exposed by grinding and polishing using a water based slurry alumina powder. Apatites were etched with 5M concentration of nitric acid for 19 seconds at 25°C. The etched mount was then cut down to 1.5x1 cm tablet and cleaned with water and alcohol. Brazil Ruby muscovite was placed on the apatite mount and sample + mica were secured within a heat shrink plastic film. All samples were irradiated by the X-7 facility of the HIFAR reactor, Lucas Heights, Australia with a nominal neutron fluence of approximately 10^{16} thermal neutrons/cm^2. Between 8 to 13 apatite grain mounts were stacked vertically between two uranium dosimeter glasses (CN5), which also had muscovite detectors secured to them. Each pack of grain mounts and standard glasses were padded with aluminium foil and expanded polystyrene foam to avoid breakage during transport and irradiation. Once back from the reactor, each pile was checked for radioactivity, and when safe, it was opened. Before separating the apatite mounts from their external detector, four pinholes were made to facilitate allineation of the section at the microscope. The micas were etched with concentrated fluoridric acid for 40 seconds and, successively, they were left in running water for two hours. Induced densities were measured on the external detectors from these standard glasses in order to monitor the fluence gradient across the pile of mounts. Each apatite grain mount and its mica print were secured to a microscope slide in a way that the images of induced tracks in the mica form a mirror image of the track in the grains.

Fission track ages were determined using the zeta calibration method described by Hurford & Green (1983). The apatite age "standard" used in this study were Fish Canyon Tuff (27.9±07 Ma; 5 measurements), Mt. Dromedary (98.7±1.1 Ma; 5 measurements) and Durango apatite (31.4±0.5 Ma; 13 measurements). The weighed mean of the 13 measurements of these standard gave a value for the zeta of 368±8. This value is used throughout the analysis performed for this study.

Counting data, track densities, statistic and fission track ages for all grains analysed are tabulated for each sample. The single grain age data are represented using radial plots, which provide an effective way of identifying grains which have fission track ages considerably different from the rest of the population (Galbraith, 1990). The radial plots are constructed by graphing a value $y = (z_i - z)/\sigma_i^2$ against a value $x = 1/\sigma_i^2$, where z_i is the fission track age of each grain, z is the mean age and σ_i the error associated with each age. In the radial plots the age of each grain is obtained by the slope of a line projected from the origin through the point representing the grain and the mean age has a slope of zero (horizontal line).

The distribution of confined track lengths within each sample is illustrated graphically by histograms for 1 μm intervals. When possible, 100 track lengths have been measured.

2.1 Apatite (U-Th)/He analysis

The data presented for this study were the first to be produced at SUERC. Chapter 2 include a comprehensive description of the equipment used for the analysis; here a step to step account of the procedure is reported.

Routine measurements always start with a "spike+standard" run during which a known amount of ^{3}He and ^{4}He standard are left in the system. This is done to check the sensitivity of the mass spectrometer and the obtain values are used to compute the amount of ^{4}He present in a sample. In succession a "hot blank" is run, to identify the background level of ^{4}He present in the system. If the 3He/^{4}He ratio is greater than 1200 (see Chapter 2), a sample is dropped in the furnace. After each sample a "hot blank" is run to check that the background of the ^{4}He level has returned to its normal value: if this does not happen, "hot blanks" are run successively until the ^{4}He background is acceptable for analysing a new sample. When "hot blanks" and samples are analysed, the furnace is heated to 950°C for 40 minutes and, successively, the system is let to cool down for 10 minutes. During this period, a known amount of 3He isotope is let into the system. The gasses are then opened to the second part of the extraction line and let to equilibrate for 5 minutes: during this period the gasses are purified by the getter and the charcoal fingers (Chapter 2). Eventually the ^{3}He and ^{4}He are let into the mass spectrometer. The analysis lasts approximately 25 minutes.

The samples are then retrieved from the furnace and the apatite crystals are dissolved and analysed for their U and Th content, according to the procedure described in Chapter 2.